INFLUENCE OF PERMAFROST EXTENT ON PHOTOCHEMICAL REACTIVITY, FUNCTIONAL GROUP COMPOSITION, AND GEOCHEMICAL CYCLING OF A SUB-ARCTIC DISCONTINUOUS PERMAFROST ALASKAN WATERSHED

BY

Kristin R. Gagné, B.S.

A Dissertation Submitted in Partial Fulfillment of the Requirements
for the Degree of

Doctor of Philosophy
in
Environmental Chemistry

University of Alaska Fairbanks
May 2020

APPROVED:

Dr. Jennifer J. Guerard, Committee Chair
Dr. William Simpson, Committee Member
Dr. Thomas P. Trainor, Committee Member
Dr. Jeremy Jones, Committee Member
Dr. Thomas K. Green, Department Chair
Department of Chemistry & Biochemistry
Dr. Kinchel C. Doerner, Dean
College of Natural Science and Mathematics
Dr. Michael Castellini
Dean of The Graduate School

Abstract

Sub-Arctic Alaskan boreal forests are currently extremely susceptible to permafrost thaw caused by increases in atmospheric temperatures in the region. Upon thaw, permafrost soil organic matter can leach out organic matter, nitrogen, and metals. It is important to observe the effects the leaching of permafrost may have on photoreactivity, functional group composition, and metal introduction. Photoproduced reactive oxygen species may affect metal fate and transport through mechanisms such as the photo-Fenton reaction. Functional group analysis allows for differences in natural organic matter source and ability to complex metals throughout a watershed. Additionally, permafrost soils may have the ability to leach in metals through lateral flow of surface waters as observed in other studies. These metals could then complex to organic matter and alter the geochemical cycling within the watershed. Organic matter is a nutrient source, and metals (e.g., As) may increase the toxicity of surface waters through the thaw of permafrost. The influx of sequestered organic matter and metals to surface waters has the potential to drastically alter ecosystem processes.

This study observes how permafrost leaching affects water composition, including its overall photoreactivity and functional group composition. The data obtained was then used to observe and deduce conclusions on how permafrost thaw influences surface water photoreactivity and functional group composition. Finally, trace metal analysis was conducted on a whole watershed scale over three years to observe how permafrost influences the geochemical composition of three main thermokarst surface waters with varying degrees of permafrost degradation.

Overall, permafrost was determined to be heterogeneous and highly photoreactive both inter- and intra- watershed. Additionally, the functional group composition of surface waters

influenced by permafrost thaw was different between summer and winter, indicating that winter is an important period to sample. Due to this change in functional group composition, the photoreactivity of winter samples was higher than summer with regard to the production of reactive oxygen species. Metal concentrations also increased during the winter for lakes identified to be undergoing active permafrost thaw. Finally, this case study found that metal concentration data combined with optical indices provided important information for resolving the possible extent of permafrost beneath thermokarst lakes.

Table of Contents

List of Figures

Page

List of Tables

Page

Acknowledgments

I would like to express my most sincere gratitude to the many people in my corner who have contributed their time and energy in this milestone. This project would not have been possible without the support of my academic committee, both current and past; Dr. J. Guerard, Dr. William Simpson, Dr. Jay Jones, Dr. Thomas Trainor, and Dr. Lisa Hoferkamp. I am also extremely grateful for the assistance and support from Karen Spaleta both in the instrumentation laboratory and in data analysis. I would also like to thank my friends, family, office family, and the Chemistry Department, for the daily support. Finally, with the warmest of sincere gratitude to Madison Ross for sticking by me and supporting me through all the ups and downs and helping me accomplish what many people have not.

General Introduction:

Northern environments, encompassing the Arctic and sub-Arctic, are more sensitive to global climate shifts, especially discontinuous permafrost (Grosse et al. 2011). Permafrost, which is soil frozen for at least two consecutive years, holds an estimated 750-950 Gt of organic carbon in the Arctic (Romanovsky et al. 2011). Permafrost regions have experienced an increase in temperatures over the past 30 years at 0.6°C per decade, which is twice as fast as the global average (Stocker et al. 2013). Sub-Arctic interior Alaska is home to the boreal forest and underlain by yedoma permafrost, which has high carbon content (Heslop et al. 2019; Strauss et al. 2017; Zimov et al. 2006). Yedoma permafrost accounts for 40% of the global organic carbon found in permafrost (Strauss et al. 2013; Walter Anthony et al. 2014) and has been called the 'sleeping giant' of carbon (Humphries 2013). This 'sleeping giant' is especially susceptible to thaw (Ulrich et al. 2014) and has increased biolability when compared to non-yedoma systems (Drake et al. 2015; Heslop et al. 2017; Mann et al. 2014; Spencer et al. 2015; Vonk et al. 2013). A warming climate causes permafrost to thaw and release organic carbon into aquatic systems (Cory et al. 2014; Frey and McClelland 2009; Heslop et al. 2017; Larouche et al. 2015; Striegl et al. 2005; Vonk et al. 2013). This organic carbon can be liberated as the active layer deepens and increases the interaction of subsurface water flow with freshly thawed permafrost soil (Battin et al. 2008; Frey and McClelland 2009; Heslop et al. 2017; Neff et al. 2006). Yedoma permafrost is believed to store up to 40%, or 210-456 Pg, of the total permafrost organic carbon (Strauss et al. 2015; Walter Anthony et al. 2014). Metals can also be exported as waters flow through the active layer soil and comes in contact with permafrost soils (Raudina et al. 2018).

In order to observe the influence permafrost may have on the surface waters, permafrost extractable natural organic matter (PENOM) must be analyzed by a multitude of analytical

techniques to obtain information on what leaches out of permafrost including metals, carbon content, and reactivity. The complex molecular composition of natural organic matter can be observed through the use of nuclear magnetic resonance (NMR). NMR provides insight on carbon and hydrogen functional groups of soil and organic matter. Carbon NMR is a non-invasive and non-destructive way to determine the functional group composition of the carbon functional groups and has proven to have powerful capabilities for characterizing natural organic matter due to advancement in spectral editing (Hertkorn et al. 2007; Leenheer et al. 2003; Mao et al. 2011; Nebbioso and Piccolo 2013; Zhou et al. 2015). Carbon NMR is powerful enough to isolate linkages between NOM chemical characterization and potential organic matter sources (Zhou et al. 2015). Hydrogen NMR is non-destructive in the sense that through additional means the NOM can be re-isolated. Hydrogen NMR with the assistance of a water suppression techniques allows for the observation of the hydrogen functional groups in-situ without the addition of common NMR solvents, which can alter the NOM structure through the substitution of deuterium for hydrogen (Diehl 2008). Lam and Simpson (2008) developed a water suppression technique that removes the pre-saturation steps (SPR-W5-WATERGATE) that can cause OH and NH to exchange with the water signal (Lam and Simpson 2008; Redfield and Gupta 1971). SPR-W5-WATERGATE can be used on natural water samples without the need for NOM isolation and thus, allows reconstitution of isolated NOM in high purity water. Knowledge of the functional group composition of the NOM provides insight on how metal complexation may alter in the surface waters as the permafrost extractable natural organic matter (PENOM) provides a difference in metal complexation sites leading too small differences in metal complexation for the NOM (Claret et al. 2003).

Many studies have used optical indices and ratios at specific wavelengths to provide insight into organic matter composition in surface waters, pore waters, and leachates. Absorbance spectra provides insight into other aspects of the organic matter through ratios; E2:E3 (A250/A365), E2:E4 (A254/A436), E2:E6 (A280/A665), E4:E6 (A465/A665), spectral slope ratio (S_R) ($S_{275-295}$:$S_{350-400}$), and specific ultraviolet absorbance at 254nm ($SUVA_{254}$). E2:E3 (Guo and Chorover 2003; Helms et al. 2008; Peuravuori and Pihlaja 1997; Rodríguez et al. 2016; Santos et al. 2016) and S_R (Helms et al. 2008; Li and Hur 2017; Rodríguez et al. 2016) have negative correlations with NOM molecular weight. S_R also increases upon irradiation (Helms et al. 2008). $SUVA_{254}$ is the absorbance at 254 nm normalized to the carbon concentration and typically has a positive relationship with aromatic content due to absorbance of 254 nm is mainly caused by electron-rich sites such as double bonded carbons (Chin et al. 1994; Kim et al. 2006; Peuravuori and Pihlaja 1997; Rodríguez et al. 2016; Uyguner and Bekbolet 2005; Weishaar et al. 2003) and has been related to molecular weight (Chin et al. 1994; Imai et al. 2002; Pernet-Coudrier et al. 2011; Rodríguez et al. 2016; Świetlik and Sikorska 2006). These indices provide insight on the composition of NOM for comparison without using destructive and expensive techniques. Different optical indices are used to interpret qualities of the chromophoric natural organic matter composition in solution. Fluorescence index (FI) shows the relative contribution from common NOM sources, such as microbial and terrestrial (Cory et al. 2010; Hansen et al. 2016; McKnight et al. 2001), humification index (HIX) is an indicator of humification extent of NOM (Gabor et al. 2015; Hansen et al. 2016; Ohno 2002), freshness index (β:α) (Hansen et al. 2016; Parlanti et al. 2000; Wilson and Xenopoulos 2009) and biological index (BIX) (Hansen et al. 2016; Huguet et al. 2009) allows for the interpretation of how recently the NOM was produced through the degradation process.

Reactive oxygen species (ROS) are reactive intermediates that are produced when chromophoric natural organic matter composition interacts with ultraviolet rays (Cory et al. 2013; Scully et al. 2003). ROS include singlet oxygen ($^1O_2$), hydroxyl radicals (•OH), and hydrogen peroxide (H_2O_2). These ROS are important factors for the transportation and processing of contaminants in the water system (Blough and Zepp 1995; Page et al. 2011), for the participation in environmental geochemistry reactions (Cawley et al. 2009; Dimou et al. 2005; Packer et al. 2003; Tixier et al. 2002; Werner et al. 2005), for the reduction of complexed metals (Cawley et al. 2009; Maloney et al. 2005; Meunier et al. 2005; Voelker et al. 2000) and the alteration of NOM in surface waters (Brinkmann et al. 2003; Cawley et al. 2009; Moran et al. 2000; Del Vecchio and Blough 2004). These ROS are highly reactive (Croot et al. 2004; Wolf et al. 2018) with •OH being the most reactive (Buxton et al. 1988; Yuan et al. 2018) and thus, ROS reactivity is essential to understand the reactivity of PENOM. •OH is important to observe in PENOM due to the ability of •OH to react with recalcitrant material found in permafrost soil that is resistant to decomposition by chemical, biological, and photolysis (Buxton et al. 1988; Choi et al. 2017; Southworth and Voelker 2003). Thus, PENOM with high reactivity to •OH would assist in further decomposition of surface water recalcitrant NOM. •OH has multiple potential mechanisms for formation in surface waters; (1) through the photo-Fenton reaction in the presence of UV light or (2) nitrate/nitrite photolysis (Vaughan and Blough 1998; Vione et al. 2014; Yuan et al. 2018; Zepp et al. 1992). The hypothesized main mechanism for PENOM •OH production is through the photo-Fenton reaction. Experiments conducted with a neutral pH for the Fe-mediated photo-Fenton reaction favor the photoreactivity of terrestrially derived NOM (Yuan et al. 2018). Along with ROS, NOM in the presence of sunlight can produce triplet state NOM (^{3}NOM*). ^{3}NOM* has been observed to be an important intermediate in indirect

photolytic transformation of other compounds in the waters (Aguer et al. 2005; Canonica et al. 1995; Canonica and Freiburghaus 2001; Canonica and Hoigné 1995; Cawley et al. 2009; Chin et al. 2004; Halladja et al. 2007; McNeill and Canonica 2016; Vione et al. 2014), degradation of pharmaceuticals (Boreen et al. 2003; Cawley et al. 2009; Challis et al. 2014; McNeill and Canonica 2016; Werner et al. 2005; Yan and Song 2014), and the oxidation of antimony (III) (Buschmann and Sigg 2004; Cawley et al. 2009). ^{3}NOM* reactivity is dependent upon the functional group composition and isolation method used for the collection of NOM (Cawley et al. 2009) as phenol (McNeill and Canonica 2016) and ketone (Cawley et al. 2009) composition alters the reactivity towards ^{3}NOM*. Minimal research has been conducted on permafrost region ^{3}NOM* reactivity and thus, it is important to analyze for ^{3}NOM* reactivity of PENOM (Cavani et al. 2009; Cory and McKnight 2005).

Elemental composition of the leachate and surface waters is important as metals can complex to the NOM (Li and Hur 2017) and thus, impact the reactivity of the NOM being introduced into the modern surface waters. For example, Fe is an important metal found in natural surface waters and in the presence of sunlight or simulated sunlight the Fe complexed to the NOM can participate in a rapid reaction of Fe (II) with hydrogen peroxide to Fe (III) and hydroxyl radicals (Grannas et al. 2006; Pérez et al. 2002; Voelker and Sulzberger 1996). Although, less reactive to the photo Fenton-like processes Cu (II), Cr (III), and Mn (II) can participate similarly to Fe (II) (Cieśla et al. 2004; Wan et al. 2019). Additional metals that have the ability to complex to NOM and affect the NOM's photoreactivity and thus, should also be monitored in the leachate include; Mg, Ca, Al, Cr, Mn, Fe, Cu, and Zn (Lang et al. 1997; Wan et al. 2019). Of these metals Fe, Al, Cu, and Cr are known to affect the absorbance ability of surface water when complexed to NOM so there is an added importance to observe these

concentrations in the leachate for insight on the absorbance behavior of the sample (Li and Hur 2017; Poulin et al. 2014; Yan et al. 2013b; a, 2016). Elemental composition (Fe (II), Al (III), and Cu (II)) impacts the transformation of pollutants in the waters through increasing the pollutants solubility (Rodríguez et al. 2016). While metal complexation can increase photoreactivity of hydroxyl radical and pollutant transformation, metals can also quench the reactivity to excited triplet state NOM with the formation of counter complexes, specifically Cu (II) and Fe (III) had the strongest inhibition of ^{3}NOM* (Binet et al. 1968; Linschitz and Pekkarinen 1960; Ogawa et al. 2009; Wan et al. 2019). The use of multiple thermokarst lakes with varying degrees of known permafrost degradation allows for the observation of how optical indices, functional group composition, photoreactivity, and metal concentrations are influenced by the extent of permafrost degradation.

Chapter 1 Composition and Photoreactivity of Natural Organic Matter Leached from Discontinuous Permafrost in sub-Arctic Alaska[1]

1.1. Abstract:

Carbon-rich yedoma permafrost soils in sub-Arctic Alaska is highly susceptible to thaw with rising temperatures in the discontinuous permafrost zone. This thaw has the potential to leach carbon moieties and trace metals. The carbon moieties are classified as natural organic matter (NOM) that are formed through the breakdown of plant and microbial life. The functional group composition of this natural organic matter is poorly understood. Impacts of this NOM infiltration include changes in pH, micronutrients, metal cycling, and photoreactivity of the natural organic matter. Photoreactivity occurs when natural organic matter comes into contact with UV-rays and reactive species are produced, such as hydroxyl radical (•OH) and triplet excited state natural organic matter (^{3}NOM*). These species have the ability to alter the fate and transport of natural organic molecules, trace metals, and contaminants within the surface waters of the watershed. However, the functional group composition and photoreactivity is relatively unknown for sub-Arctic, boreal forest, Alaskan permafrost and thus, this addresses questions of 1) what is the functional group composition of permafrost organic matter that leaches upon thaw, and 2) what is the photoreactivity potential for •OH and ^{3}NOM* from this ancient organic matter. This study utilizes many analytical and experimental techniques to address these questions from ICP-MS to characterize trace metals leached from permafrost soils to NMR to identify the chemical functional group composition of organic matter. The use of analytical and experimental protocols provided insight that permafrost natural organic matter is heterogeneous between watersheds, within the same watershed, and down the collected soil core. This thawed

[1] Gagné, K.R., Murphy, C.J., and Guerard, J.J. Composition and Photoreactivity of Natural Organic Matter Leached from Discontinuous Permafrost in sub-Arctic Alaska. Prepared for submission in Biogeosciences.

natural organic matter is also dependent upon the pH and ionic strength of the water as different leaching media leached out a statistically different composition of organic matter which altered the photoreactivity ability of the organic matter.

1.2. Introduction:

Permafrost thaw releases natural organic matter (NOM), thereby enriching the carbon and inorganic content of the active layer, soils with an annual freeze-thaw cycle, and surface waters following rainfall events (Lamhonwah et al. 2017). NOM is a complex heterogeneous mixture for which the composition and reactivity depends on the source material of microbial (autochthonous) or terrestrial (allochthonous) sources and contains various functional groups composed of majority carbon, hydrogen, oxygen, sulfur, and nitrogen (Aiken et al. 1992; Guerard et al. 2009; Page et al. 2011). While NOM is a small portion of the total soil organic matter (Seifert et al. 2016), it is the most labile (Han et al. 2019; Zsolnay, 2003). The permafrost NOM reservoir has increased susceptibility to biotic (i.e. bacterial respiration) (Han et al. 2019; Luster et al. 1996; Qualls and Haines, 1992), abiotic transformation processes (i.e. photolysis) (Cory et al. 2014), and affects biogeochemical processes (Han et al. 2019; Luster et al. 1996; Qualls and Haines, 1992). Thus, it is hypothesized that as permafrost extractable natural organic matter (PENOM) leaches into the water column, this fossil carbon composition influences the reactivity of modern surface water dissolved organic matter in the context of reactive oxygen species (ROS) generation and biogeochemical cycling. This alteration in reactivity and biogeochemical cycling could cause an increase in the production of greenhouse gases such as carbon dioxide and methane, causing further increases in temperature, destabilization of soil, and further thermokarst lake production releasing more carbon dioxide and methane (Heslop et al. 2019; Walter Anthony et al. 2016).

The molecular composition, variability, and reactivity of permafrost organic carbon are relatively unexplored in sub-Arctic Alaska. Predictions indicate that by the end of the 21st century sub-Arctic discontinuous permafrost with a current soil temperature between 0 to -2.5°C will begin to actively thaw (Romanovsky et al. 2011). This thawing will introduce PENOM into the sub-Arctic surface waters (Lamhonwah et al. 2017). The thawed materials functional group composition is important to understanding how metal complexation may change with thaw, thereby affecting photoreactivity of the surface waters (Lang et al. 1997; Wan et al. 2019). Characterizing the potential influence PENOM has on ROS production in surface waters NOM is essential to understanding the future reactivity of NOM brought on by increasing soil temperatures thawing and releasing permafrost carbon (Romanovsky et al. 2011).

In order to understand what leaches from permafrost, laboratory experiments can be used to minimize other environmental variables that could complicate the leaching processes, but these procedures are not standardized throughout the literature. This complicates comparison across studies or environments as different carbon fractions may be analyzed. Variations in protocols include soil to water ratio, leaching medium, temperature, time, etc. For example, some studies used pre-thawed material and room temperature leaching in high purity (resistivity = 18 MΩ) water without pH adjustment at a 1:4 and 1:20 soil to water ratio for active layer and permafrost layer respectively (Ward and Cory, 2015). However, another study did proceed in a manner that allowed the observation of natural thaw, which included using natural pH, cool temperatures, and thawing the core in water (Waldrop et al. 2010). Both Ward and Cory (2015) and Waldrop et al. (2010) methods leached for only 24 hours. So, currently it is not clear how long leaching periods may impact functional group composition from the released PENOM pool. The isolation of PENOM out of leach material requires increased concentrations or large

volumes, these above-mentioned methods did not produce high enough concentrations or large enough volumes for PENOM isolation and thus, would need to be scaled up for both photoreactive experiments and chemical functional group determination. In addition, different leaching conditions will release different carbon pool fractions of NOM; pH 10 removes humic acids (Beckett et al. 1987), and K_2SO_4 extracts the most water-soluble organic matter compared to other salt solutions (Gabor et al. 2015). However, these media choices are at the extreme ends of natural water pH and ionic strength and may not represent realistic leaching conditions for environmental thaw.

Sub-Arctic Alaska permafrost soils have been analyzed for a multitude of data including biological incubations for the analysis of greenhouse gases such as CO_2 and CH_4 (Belshe et al. 2012; Bracho et al. 2016; Hicks Pries et al. 2016; Pegoraro et al. 2019; Schadel et al. 2018; Taş et al. 2014; Waldrop et al. 2010), functional group composition via ^{13}C NMR (Holden et al. 2015; Plaza et al. 2019; Waldrop et al. 2010), and functional group composition via FT-ICR-MS (Choi et al. 2017; Heslop et al. 2019). However, limited analysis has been completed on Alaskan sub-Arctic optical indices and metals (Herndon et al. 2019; Wickland et al. 2018), which may be useful and efficient tools for analysis of composition and reactivity. A few more studies were conducted on metal concentrations and photochemical indices in Arctic systems, but few in sub-Arctic Alaska (Barker et al. 2014; Ward and Cory, 2015, 2016).

This current study utilizes functional group composition, metal composition, and optical properties in two locations for an in-depth analysis of how functional group composition in both functional groups and metals can interact with the photochemical properties of the leachates in sub-Arctic Alaska. The purpose of this study was to (1) determine a leaching method to capture enough carbon concentration for isolation and analysis, as well as obtain a more holistic

understanding of how differences in leaching media may alter what PENOM is leached off of the soils. This isolated PENOM was then analyzed in order to (2) determine the functional group composition of PENOM in a sub-Arctic boreal forest and (3) determine the photoreactivity PENOM has towards •OH and ^{3}NOM*. In order to obtain an increased understanding of how PENOM may influence surface water functional group composition and photochemical reactivity upon thaw. In addition, this study utilized different leaching media to observe how different factors (pH and ionic strength) may influence PENOM composition leachability. These results provide an in-depth characterization of permafrost soil NOM and an expanded foundation for understanding its biogeochemical role upon thaw.

1.3. Methods:

1.3.1. Sample Site:

Soil cores were collected in March 2016 from Bonanza Creek Experimental Forest (BNZ) (64.70°N, -148.30°W) in a discontinuous permafrost boreal forest alongside the Tanana River in Fairbanks, Alaska (Figure 1.1). Vegetation is majority tussock cotton grass (*Eriophorum vaginatum*), white spruce (*Picea glauca)* and black spruce (*Picae mariana)* (Bonanza Creek Long-Term Ecological Research Program, http://www.lter.uaf.edu/boreal-forest/vegetation). BNZ has low annual precipitation with an annual precipitation of 283 mm, of which approximately 34% falls as snow, while air temperatures average 15.8°C in July and January averages -21.1°C (2010 – 2016; Bonanza Creek LTER Climate Database). Additional soil cores were also collected from Caribou-Poker Creeks Research Watershed (CPC) (65.15°N, 147.50°W) (Figure 1.1). This watershed is a boreal forest with vegetation of black spruce (*Picae mariana*), moss (*hylocomium et al.)*, alder (*Alnus viridis*) (Caribou-Poker Creek Long-Term

Ecological Research Program, https://www.lter.uaf.edu/research/study-sites-cpcrw). CPC has low annual precipitation with an average of 460 mm, of which approximately 38% falls as snow, this is due to warm summers (mean = 15.4°C in July) and cold winters (mean = - 21.1°C in January) (2010-2016; Bonanza Creek LTER Climate Database).

Four 121 cm deep permafrost core samples were collected via a SIPRE corer from each location. Soil active layer depths were determined by averaging probe depths from LTER soil temperature probe database in the immediate vicinity for 2014 during maximum thaw depth defined as the active layer. LTER soil temperature probe database indicate a 'transient layer', which thawed inconsistently over 10 years of data observations (Shur et al. 2005; Wickland et al. 2018). BNZ active layer depth was 49 ± 7 cm, while transient layer ranged from 49 to 66 cm. 66 cm was determined from the maximum depth from 2004-2014. This maximum thaw occurred in 2014 and a previous maximum thaw was 64 cm back in 2005. The top of that transient layer was determined by the average thaw depth from 2004 to 2014. CPC active layer depth was 67 ± 11 cm, while transient layer ranged from 62 to 103 cm. 103 cm was defined by the maximum depth from 2004 to 2014. This maximum occurred in 2007 and the most recent maximum thaw was 95 cm in 2014. The top of that transient layer was determined to be the average thaw depth from 2004 to 2014. Additional, cores were collected from a blueberry bog in a third watershed to be utilized for method development during March of 2015. Immediately after collection, cores were wrapped in plastic and placed in a -80°C freezer in a So-Low Ultra-Low Upright Freezer U85-22 (Environmental Equipment: Cincinnati, OH) upon return to the laboratory (Figure 1.2), until they were freeze dried on a FreeZone Plus 12 Liter Cascade Console Freeze Dry System (Labconco; Kansas City, MO) followed by storage in acid-washed plastic bags in the dark until analysis.

1.3.2. Chemicals:

Iron (III) chloride hexahydrate (99+%) was obtained from Acros Organics (New Jersey, USA). 2,4,6-Trimethylphenol (PESTANAL analytical standard) was obtained from Fluka Analytical (Mexico). Acetonitrile (ACS/HPLC Grade) was obtained from EMD Millipore Corporation (Massachusetts, USA). Methanol (ACS/HPLC Grade) was obtained from Honeywell Burdick & Jackson (Michigan, USA). Potassium sulfate was obtained from Fisher Scientific (Massachusetts, USA). Sodium hydroxide (97+%) form was obtained from EMD Chemical Inc. (Georgia, USA). Hydrochloric acid was obtained from VWR Chemicals BDH (Pennsylvania, USA). 2,2,3,3-d(4)-3-(Trimethylsilyl)propionic acid sodium salt (TSP) was obtained from Alfa Aesar (Massachusetts, USA). Deuterium oxide was obtained from Acros Organics (New Jersey, USA). Hydrofluoric Acid 48% was obtained from Mallinckrodt Baker Inc. (New Jersey, USA). Nitric acid omniTrace was obtained from EMD Chemical Inc. (Georgia, USA). All inductively coupled plasma-mass spectrometry (ICP-MS) standards were purchased from Agilent Technologies (California, USA). Potassium nitrate was obtained from FUJUFILM Wako Chemicals USA (Virginia, USA). Potassium hydrogen phthalate (99%) was obtained from Alfa Aesar (Massachusetts, USA). Suwannee River fulvic acid and Pony Lake fulvic acid were obtained from the International Humic Substances Society (Minnesota, USA). 18.2 MΩ water was obtained from a Barnstead model D11951 NANOpure Diamond filter (Iowa, USA). Poly(vinyl alcohol) (99+%) hydrolyzed was obtained from Sigma-Aldrich (Missouri, USA).

1.3.3. Leaching Method:

Leaching method testing was conducted on a separate test permafrost core collected the previous year from a residential watershed, Goldstream Valley (GSB). The goal of this

experiment was to see which ratio allowed the most carbon to leach into the media from the permafrost soil. The core was freeze dried and placed into various volumes of pH10 water; 1:10, 1:20, 1:50, 1:100, and 1:200 (soil weight/media weight) in the dark at 4°C. Aliquots were removed for total organic carbon (TOC) analysis at 1 hour, 12 hours, 36 hours, 3 days, 5 days, 8 days, 10 days. Simultaneously, a media control of 18.2 MΩ was run at a 1:200 ratio (w/w). The final leaching ratio was selected to be 1:200 (w/w) because >9 times more carbon was leached at a 1:200 (w/w) compared to all other ratios by day 8 (Figure 1.3).

Following the media ratio experiment, a 1:200 (w/w) with 18.2 MΩ water as leaching media was utilized to determine the time period of leaching for the rest of the study, according to the protocol described above over 7 days. 5 mL was removed at 0.1, 0.5, 1.0, 1.5, 2, 2.5, 4.1, 4.5, 5.1, 6.2, and 6.9 days for analysis by TOC. A large carbon concentration was necessary for an adequate isolation of organic matter. Leaching carbon content determined by TOC stabilized by day 7, carbon concentration began at 1 mg C L^{-1} and stabilized at 6 mg C L^{-1} on day 7 and 8 (Figure 1.3). Although laboratory leaching does have limitations on mobilization kinetics as the water is not flowing through, the leaching time of 7 days was consistent with permafrost soil to stream residence time, which ranged from 3 – 7 days (Heslop et al. 2017; Vonk et al. 2013). Leachable carbon concentration stabilization also occurred for Cao et al. (1999) in which they soaked Beijing soil in deionized water for 10 days and then observed that the majority of the water-soluble carbon content flushed out of pore water soil after 20 minutes. Thus, the leaching protocol was determined to be optimal for NOM isolation at 1:200 (w/w) soil to media for 7 days in the dark refrigerator.

0.5 M K_2SO_4 (high salt) (Gabor et al. 2015), pH 10 (basic), and 18.2 MΩ water (water) solutions of a 1:200 (soil to solution ratio) were prepared in acid washed 5-gallon material

buckets. All three media leachates were conducted on two cores from BNZ, which were located 5 meters apart from the transient/permafrost soil segments with similar radiocarbon ages, while the rest of the soil segments for two cores from each location were leached using 18.2 MΩ water. A 5-gallon bucket lid was placed on soil solution mixture and placed in the dark at 4°C for 7 days; manual agitation by twisting the bucket for 30 seconds occurred on a daily basis. All leachates were further filtered to isolate NOM material, which were then characterized by nuclear magnetic resonance, UV-Vis, fluorescence, and photolysis experiments.

1.3.4. NOM extraction:

At the end of 7 days, leachate was filtered with GWV high capacity groundwater sampling capsules to 0.45 um (PALL, Port Washington, New York). After 0.45 um filtration, an aliquot was removed for trace metal, total organic carbon, total nitrogen, fluorescence, and UV-Vis analyses. The remaining leachate was acidified to pH 2 with concentrated hydrochloric acid, and pumped at an 18 mL min^{-1} flow rate onto Bond-Elut PPL solid phase extraction cartridges (Agilent; Santa Clara, CA), extracted with methanol (Dittmar et al. 2008), and freeze-dried.

1.3.5. Photolysis Experiments:

Photolysis experiments were conducted at multiple time increments in an Atlas CPS+ Suntest (ATLAS; Mount Prospect, Illinois) with a 500 W Xe arc lamp set to 15°C. Samples were placed in 10 mL quartz test tubes with a 1 cm inner diameter (Robson Scientific; Hertfordshire, England). Irradiance was monitored by a PMA2100 radiometer (Solar Light Co. Inc, Glenside, PA). Isolated NOM leachates were reconstituted to approximately 10 mg C L^{-1} in aqueous solution and pH adjusted to 7.61 – 7.68 with NaOH or HCl. Circumneutral pH was chosen,

which favors the production of hydroxyl radical, (Gligorovski et al. 2015) and mimic natural pH of bulk aqueous bodies in a local sub-Arctic Alaska boreal watershed (Table 3.2). NOM solutions were irradiated for 24 hours with samples sacrificed at 1, 2, 4, 6, 12, 18, and 24 hours. Dark controls were wrapped in aluminum foil and placed in the Suntest and analyzed for all experiments simultaneously. Samples were removed from the Suntest at their respective time intervals and kept in the dark until analyzed via UV-Vis and fluorescence within 2 hours of irradiation. Rate slopes for each sample had an R^2 value greater than 0.7.

To determine the NOM reactivity from these two reactive species •OH and ^{3}NOM* chemical probes are utilized that react with these species. •OH reactivity is probed with methanol to observe •OH quenching (Chin et al. 2004; Page et al. 2011) and iron (III) to observe •OH promotion. ^{3}NOM* reactivity is probed by 2,4,6-Trimethylphenol (TMP) as electron transfer and direct hydrogen abstraction of TMP produces oxidized products that are key for the reaction of NOM and TMP to ^{3}NOM* (Cawley et al. 2009). Increased ^{3}NOM* production through photodegradation of NOM will decrease the fluorescence signal of TMP as ^{3}NOM* causes TMP to degraded into non-fluorescent byproducts. However, methanol is also used to observe hydroxylating species (Page et al. 2011) and TMP also reacts with $^1O_2$ (Cawley et al. 2009).

Spikes from stock solutions resulting in total concentrations of 10 μM TMP, 20 μM Fe(II)Cl, 12.5 μM methanol or no amendment of NOM solutions were prepped for photolysis kinetics experiments. $Fe(II)Cl_2$, methanol, and NOM time points were analyzed with UV-Vis and fluorescence and observed rates of absorbance decay were determined by collecting absorbance values from each sample over 24 hours. An average absorbance was obtained from duplicates for each time. The absorbance was fit to a log-linearized pseudo-first order kinetics model to determine the rate of absorbance loss at each wavelength. These observed rates were corrected

for PENOM light screening ability and normalized to the carbon concentration present in the sample (Equation 1). Light screening was determined by Equation 2 (Miller and Chin, 2002).

$$\bullet OH\ production\ rate = \frac{-Slope(LN(Avg_{Abs_{T(x)}})}{[Carbon]} x \frac{1}{SF}$$

Equation 1: Determination for •OH rate through UV-Vis analysis of photobleached samples with various amendments. Units are represented in hr^{-1} mg C^{-1} L.

$$SF = \frac{1 - 10^{-\alpha_\lambda l}}{2.303\alpha_\lambda l}$$

Equation 2: Screening factor equation to determine light screening ability of sample, utilizes time zero for values.

1.3.5.1. ^{3}NOM* Photoproduction:

Reconstituted 10 mg C L^{-1} NOM solutions containing 10 µM TMP were photolyzed for up to 6 hours. TMP quantitative analysis was run in duplicate with triplicate injections on an Agilent 1100 Series reverse-phase high pressure liquid chromatography (Agilent Technologies, Santa Clara, CA) via a Restek Ultra C18 5 µm column (Restek Corporation, Centre County, PA) following Cawley et al. (2009). The mobile phase comprised of 60:40 acetonitrile:water (v/v) at 1 mL min^{-1} and detected by fluorescence at λ_{ex} = 230 nm and λ_{em} = 305 nm, and calibrated against standard concentrations of TMP in aqueous solution (Cawley et al. 2009). The rate of TMP degradation was determined by taking an average area under the TMP peak in the fluorescence spectra for each time point and injection. The area was then converted to concentration using a calibration curve run at the beginning of the run. The ratio of TMP concentration at each time point to initial concentration was fit to a log-linearized pseudo-first order kinetics model to determine the rate of TMP loss. These observed rates were corrected for

PENOM light screening ability and normalized to the carbon concentration present in the sample (Equation 3). Light screening was determined by Equation 2 (Miller and Chin, 2002).

$$^{3}NOM^{*} production\ rate = -\left(\frac{LN\left({}^{[TMP]_x}/_{[TMP]_0}\right)}{[Carbon]} x \frac{1}{SF}\right)$$

Equation 3: Determination of ^{3}NOM production rate, which starts out at the rate of TMP loss. Units are represented in min^{-1} mg C^{-1} L.

1.3.6. Fluorescence/UV-Vis:

Samples were placed in 1 cm quartz cuvettes (Firefly Scientific; Staten Island, NY) and analyzed on a Jobin-Yvon Horiba Aqualog-800-C (Horiba Instruments, Edison, NJ). UV-Vis was scanned from 200 – 800 nm every 1 nm at an integration time of 0.1 seconds. Excitation-emission matrices (EEMs) were scanned λ_{ex} = 240 – 600 nm every 3 nm, λ_{em} = 240 – 800 nm every 2.33 nm with an integration time of 0.1 seconds at a medium gain. Data was corrected for instrument correction factors, inner filter effects, blank subtracted, 1st and 2nd order Rayleigh scattering removed, and normalized to Raman area before import into MATLAB (version R2015b, MathWorks).

Optical indices were obtained from both UV-Vis and fluorescence scans and equations utilized for determination can be found in Table 1.1 and Table 1.2 with references included. UV-Vis spectra were interpreted for the following indices; specific ultraviolet absorbance at 254 nm and 280 nm ($SUVA_{254}$ and $SUVA_{280}$), spectral slope ratio (S_R), E2:E4, E2:E6, E4:E6, and E2:E3 (Table 1.1). Fluorescence scans provided; fluorescence index (FI), humification index (HIX), freshness index (β:α), and biological index (BIX) (Table 1.2).

1.3.7. Nuclear Magnetic Resonance (NMR):

All NMR spectra were acquired using a Bruker Advance III Spectrometer operating at a hydrogen frequency of 600.16 MHz running TopSpin 3.5. Solid-State NOM and soil samples were run using a 4 mm Bruker H-X CP-MAS probe. NOM samples were prepared by packing approximately 20 mg isolated NOM into 12 uL rotors with Kel-F insert and drive cap. Soil samples required hydrofluoric acid wash to remove paramagnetic metals. 2 grams of freeze-dried sample were washed five times with 10% HF at a 1:10 soil to HF ratio for one hour each wash (Clark Ehlers et al. 2010). After HF treatment soil samples were rinsed with 18.2 MΩ water at a 1:10 ratio soil to water five times (Clark Ehlers et al. 2010). Samples were then frozen and freeze dried to dryness before packing in NMR rotors (Clark Ehlers et al. 2010). Approximately, 100 mg of soil sample was packed into a 50 uL rotors with Kel-F insert and drive cap. Spectra were acquired using the multi-CP MAS ^{13}C NMR (Johnson and Schmidt-Rohr, 2014). Samples were spun at 15 kHz with a 500 μs recycle delay. For all samples, 40,000 scans were collected with 2048 complex data points covering a 300 ppm spectral window. Spectra were Fourier transformed with 50 Hz of exponential line broadening, phased, and baseline corrected. Glycine was used as an external reference (176 ppm).

Solution-state samples were run using a 5 mm Bruker Smart probe with a single Z axis-gradient. Samples were prepared by dissolving 1 mg of leachate in 1 mL 18.2 MΩ water. A chemical shift reference standard of 4 mM TSP in D_2O was placed into the sample via a cylindrical insert tube. Samples were run in 5mm precision NMR tubes (Wilmad-Lab Glass, Vineland, NJ). Spectra were acquired using the SPR-W5-WATERGATE solvent suppression method (Lam and Simpson, 2008). Proton NMR spectra were acquired with 10,000 scans collecting 64,000 complex data points with a 1 us recycle delay. Spectra were Fourier

transformed with 0.3 Hz of exponential line broadening, phased, and baseline corrected using MestreNova Suite (Version 8, MestreLab Research; Santiago de Compostela, Spain).

In order to compare functional group distribution between NOM isolates, spectra were integrated over defined binning regions in both ^{1}H and ^{13}C NMR spectra. ^{13}C binning ranges include the following; 0 – 45 ppm alkyl-C, 45 – 60 ppm methoxyl, 60 – 90 ppm carbohydrates, 90 – 120 ppm proton substituted aromatics, 120 – 140 ppm carbon substituted aromatics, 140 – 160 ppm oxygen substituted aromatics, 160 – 190 ppm carboxyl/aliphatic amides, 190 – 220 ppm aldehydes and ketones (Kaiser et al. 2003; Mao et al. 2011, 2012; Zhou et al. 2015). 90 – 160 ppm is classified as total aromatics. ^{1}H binning ranges include the following; 0.6 – 1.6 ppm material derived from linear terpenoids (MDLT), 1.6 – 3.2 ppm carboxyl rich alicyclic molecules (CRAM), 3.2 – 4.5 ppm carbohydrates, and 6.5 – 8.4 ppm aromatics (Lam and Simpson, 2008). All binning regions are converted into percentages for comparison by dividing the region by the total area under the spectra.

1.3.8. Elemental Concentration:

Total non-purgeable organic carbon and total dissolved nitrogen analysis was run on a Shimadzu TOC-L CPH (Shimadzu Scientific Instruments, LOQ = 0.1 mg C L^{-1}, LOQ = 0.05 mg N L^{-1}) using non-dispersive, infrared gas analysis following combustion to determine organic carbon content of samples.

Soil samples were analyzed to determine carbon and nitrogen soil concentrations on a LECO C/N Analyzer (LECO Corporation; Saint Joseph, MI) through the University of Alaska Fairbanks Forest Soils Laboratory. Samples were ground and mixed using a SPEX 8000 mixer/mill (SPEX Sample Prep; Metuchen, NJ). Approximately 0.1 grams of soil was placed

into tear dropped aluminum foil and submitted for analysis. Soil organic carbon concentrations were obtained using a Shimadzu TOC-L CPH attached to a Shimadzu SSM-5000A (LOQ = 0.1 mg C). Inorganic carbon was determined using phosphoric acid addition and sodium carbonate for a calibration ranging from 3 to 25 mg CO_3^{-1}.

Leachate water trace metal concentrations were measured using an Agilent 7500ce (Agilent Technologies, Santa Clara, CA) inductively coupled plasma-mass spectrometer (ICP-MS) followed EPA method 300.8. Samples were filtered to 0.45 μm and diluted into a 2% HNO_3 solutions and stored in the fridge until analysis. Trace metals analyzed; Li, Na, Mg, Al, K, Ca, Ti, V, Cr, Mn, Fe, Co, Ni, Cu, Zn, As, Se, St, Mo, Ag, Cd, Sb, Ba, Pb, Bi, Th, and U. External calibration was run on each metal at the beginning of each run (0.01 – 2000 ppb). Internal standards were run in line throughout instrumentation analysis using the following metals; Ge, Y, Sc, Rh, and Ir. Calibration checks and calibration blanks were measured every 10 – 12 samples. Additional samples were analyzed included; acid blanks and reference standards (SLRS-5 riverine water and NIST 1640a trace elements in natural water systems) and were analyzed following the calibration samples.

Soil samples trace metal concentrations were measured using PanAlytical Axios four-kilowatt wavelength dispersive X-ray Fluorescence Spectrometer (Malvern, UK). Predeveloped methods, Sh.Carb(9.2t) and Protrace 27 were used to obtain trace metal concentrations based off of a set of standards; SO-4, SO-3, SO-2, and SGR-1 (standard concentrations were obtained from GEOREM database). Samples were crushed using SPEX 8000 mixer/mill (SPEX Sample Prep; Metuchen, NJ) and 10 – 12 g of sample was pressed using a 35- or 40-mm pellet die set on a SPEX SamplePrep Carver Model C Manual Press (SPEX Sample Prep; Metuchen, NJ) to 24,000 lbs of pressure using 5% polyvinyl alcohol as a binder.

1.3.9. Radiocarbon Dating:

Freeze dried and mixed soil samples were sent to Woods Hole Oceanographic Institution National Ocean Sciences Accelerator Mass Spectrometry (WHOI NOSAMS) in Woods Hole, Massachusetts for organic carbon radiocarbon dating. Samples were processed at location following WHOI NOSAMS acid fuming protocol for bulk organic carbon.

1.3.10. pH of Soil:

pH of the soil samples was determined using EPA Method 9045D and adjusted to a ratio of 2 grams of freeze-dried soil to 4 mL of MΩ water. Soil samples were crushed using SPEX 8000 mixer/mill (SPEX Sample Prep; Metuchen, NJ).

1.3.11. Statistical Analysis:

All linear regressions conducted on BNZ soil core data points were conducted using Prism8 for macOS Version 8.1.2 (GraphPad; San Diego, CA). Linear regression was determined to be statistically significant when the P-value was < 0.05. In order to answer what will leach into surface waters with increased permafrost thaw to determine correlations of leached material into surface waters.

1.4. Results and Discussion:

1.4.1. Soil:

1.4.1.1. Soil General Characterization:

In general, the moisture content of BNZ and CPC was determined to be approximately 51 ± 11%, by the difference between waterlogged soil mass and stable freeze-dried soil mass. The carbon-nitrogen mass ratio (C:N) was higher in the transient layers of the soil with a maximum of 44.41 ± 0.97 in CPC2.4, while the active layer had the smallest C:N (Table 1.3). All carbon was determined to be organic carbon, as inorganic carbon was below detection limits for all soil samples. The minimum C:N observed was in BNZ1.2 at 9.27 ± 0.63. CPC1 and CPC2 had the higher C:N between the two watersheds with an average of 25.34 ± 5.96 and 30.12 ± 12.46 respectively. BNZ1 and BNZ2 had a lower C:N, which included permafrost C:N with an average of 13.80 ± 5.84 and 18.59 ± 4.32 respectively. Overall, soil segments pH was consistent at 5.39 ± 0.25 and had below detection limits for inorganic carbon. Therefore, the carbon concentration utilized in the C:N ratio was assumed to be all organic carbon.

Overall, the carbon leachability for the soil was dependent upon soil segment and location (Equation 4). BNZ had a higher carbon leachability compared to CPC, with the highest percentage leached in the active layer. BNZ1 had a carbon leachability of 85.5 ± 1.3% (BNZ1.1) to 0.29 ± 1.8% (BNZ1.3), while BNZ2 had a carbon leachability of 15.55 ± 1.36% (BNZ2.2) to 1.24 ± 1.18% (BNZ2.4) (Table 1.3). Carbon leachability was lowest in the transient layer of BNZ. CPC1 and CPC2 carbon leachability both did not exceed 1.05% throughout the active layer and transient layer, indicating that CPC carbon was less mobilizable than BNZ.

$$\frac{C_{Leached\ (\frac{mgC}{L})} V_{Leaching\ Media\ (L)}}{C_{mg\ in\ soil}} x100 = Leached\ Carbon\ Percentage$$

Equation 4: Determination of the carbon leachability percentage. Concentrations of carbon were conducted using liquid TOC, with the units of mg C L^{-1} and solid TOC, with the units of mg C. Volume of media was obtained from the amount of volume added to the soil in order to convert mg C L^{-1} to mg C.

Radiocarbon dated samples revealed that BNZ cores provided an increased span of ages ranging from 1,500 to 7,200 years old. Meanwhile, CPC only exposed ages from 75 to 1,600 years old (Table 1.3). CPC was also all active layer based on soil temperatures relationship with thaw, while BNZ ranged from active layer to permafrost soils. Additionally, CPC was majority active layer and thus, metal concentrations are complicated by surface hydrology (Painter et al. 2013; Raudina et al. 2018; Throckmorton et al. 2016; Woo, 2012; Zhang et al. 2000). Thus, when comparing functional group composition and photoreactivity to age only BNZ samples were utilized due to the span of radiocarbon dates offered.

1.4.1.2. Soil Metal Composition:

Soil metal composition was sorted into four categories based on solid soil concentration buckets from XRF data: >1000 mg, 100 – 1000 mg, 10 – 100 mg, and <10 mg (Table 1.4). In general, BNZ soil segments >1000 mg was represented by Al, Fe, Ca (active layers), K (permafrost layers), and Si; while CPC was represented by Al, Fe, and Si. Metal classification of between 1000 mg and 100 mg was represented by Ca (permafrost layers), K (active layers), Mg, Na, Ti, and S; while CPC had Ca, K, Mg, Na, and Ti. The third tier of metals (10 – 100 mg) was represented in BNZ by P, Mn, Ba, and Sr (permafrost layers); while CPC S was added to the list and Sr only represented some of the segments. The final tier of trace metals was the same for

both BNZ and CPC and represented by V, Cr, Co, Ni, Cu, Zn, As, Se, Br, Mo, Pb, and Sr (active layers).

Metal concentrations were compared against soil radiocarbon age, revealing that some metals were positively correlated (enhancement of metals), negatively correlated (diminishment of metals), and not statistically related. Significantly zero slopes were determined where a linear regression returned a p-value greater than 0.1 and represented Ca, Mn, S, Co, Cu, Se, Br, and Pb. The majority of the other metals analyzed on BNZ were correlated with enhancement of metals with increased age, as represented by the linear regression P-value less than 0.05. These metals included; Al, K, Mg, Na, Si, Ba, Ti, V, Cr, Fe, Ni, Zn, and Sr. The enhancement of metals with age was also observed in Arctic permafrost with Al, Ba, Ti, V, and Cr (Barker et al. 2014). Cr and V specifically were interpreted to indicate the redox increasing with age and depth (Kimbrough et al. 1999). Finally, the XRF data showed that P was the only metal that presented a negative correlation with increased radio carbon age.

1.4.1.3. Soil Functional Group Composition:

Hydrofluoric Acid washed soils were analyzed using ^{13}C NMR to obtain carbon functional group composition. Some bias is introduced with HF washing although functional group composition was determined to be reproducible in literature (Sanderman et al. 2017). To minimize this bias all soils were treated simultaneously and following the same procedures. Carbon functional group analysis was conducted on BNZ1 soil segments. Over 50% of the carbon spectra were accounted for by aliphatic carbon (0 – 45 ppm) at 34.2 ± 7.7% and combined aromatic carbon (90 – 160 ppm) at 26.6 ± 3.1% (Table 1.5). Prior studies found that permafrost has a lower aromatic content when compared to the active layer both Arctic and sub-

Arctic samples from discontinuous or continuous permafrost regions (Heslop et al. 2019; Mueller et al. 2015; Waldrop et al. 2010; Ward and Cory, 2015). Additionally, two sub-Arctic boreal forest samples showed no change in aromatic content with depth (Taş et al. 2014; Waldrop et al. 2010). However, Choi et al. (2017) indicated through analysis by a FT-ICR-MS that aromatic content increases in the permafrost layer, similar to the bottom of BNZ1 which had 30.8% aromatics based on NMR. This data increase in aromatic content with depth was also observed by NMR in Arctic discontinuous and continuous permafrost regions in Alaska, Canada, and Europe (Grewer et al. 2016; Mueller et al. 2015; Pedersen et al. 2011; Pengerud et al. 2017). Meanwhile, the highest aliphatic percentage was in the transient layer at 44.83% (BNZ1.3). No pattern with depth was determined based on the functional group composition of unleached soil via ^{13}C NMR analysis, however sporadic differences in spectra were observed down the core depth based off of functional group percentages.

1.4.2. Media Leaching:

1.4.2.1. Soil Leachate Composition:

1.4.2.1.1. Optical Properties:

Fluorophoric NOM composition is only a small percentage of the overall chromophoric material (Rosario-Ortiz and Canonica, 2016). UV-Vis absorbance and fluorescence indices are used to observe correlations of molecular weight, aromaticity, source, and humification (Table 1.1/Table 1.2). Absorbance and fluorescence characteristics of aqueous solutions provide a bulk characterization of chromophoric natural organic matter composition. However, soil leachates are different pools compared to surface water samples and may exhibit changes in optical properties. The radiocarbon age of the soil introduces a potentially different ecosystem and

source material from modern material through extinct plants, animals, and microbes, which should be taken into consideration when comparing across samples from different environments and source materials. Additionally, there are limited literature values for optical indices for the comparison of soil leachates similar to this study (Claret et al. 2003; Hansen et al. 2016; Ikeya and Watanabe, 2003; Kiss et al. 2014). Finally, the UV-Vis and fluorescence spectra between literature and this study have the potential to vary depending on the instrument utilized to collect the spectra and thus, indices collected on different instruments have the potential to be shifted due to the sensitivity of various instruments (Cory et al. 2010).

Optical indices have been shown to be correlated with sample source material being more terrestrial or microbial (Hansen et al. 2016). E2:E3 was highest in high salt leachate with an average of 5.553 ± 0.050, while basic leachate had the lowest with an average of 3.567 ± 0.078 (Table 1.6). Reference material had an E2:E3 value of 4.843 for PLFA and 4.979 for SRFA, which was similar to the water leachate at an overall average of 4.604 ± 0.025. These values of E2:E3 suggest that the molecular weight of the NOM from high salt leachate may be the smallest while, basic and water leached NOM could have a larger molecular weight than reference material. E2:E4 and E2:E6 had a similar trend with the leachate as they both provide insight on the source and aromaticity of the NOM leached from the soil (Cieslewicz and Gonet, 2004; Li and Hur, 2017; Rodríguez et al. 2016). High salt leached NOM had the largest value for these two ratios, 18.607 ± 0.059 and 155.280 ± 4.525 respectively, which were lower than SRFA but higher than PLFA. Basic and water leached NOM were both below both reference materials with basic leachate having the lowest values at 8.340 ± 0.429 and 98.227 ± 7.474 (Table 1.6). Cieslewicz and Gonet (2004) determined that E2:E6 higher values were indicative of humic acids from sediments. However, this data was stated to only work well for the interpretation of

soil humic acids and thus, the high E2:E6 observed for fulvic acid from a river (SRFA) does not cause hesitation on instrumentation method techniques as SRFA is not a soil humic acid. All of the values obtained in this study were higher than Cieslewicz and Gonet (2004), E2:E4 highest value was 7.36 and E2:E6 highest value was 47.01. These differences in literature values could be due to the difference in analysis and sample type. However, this difference makes interpreting the E2:E4 and E2:E6 more difficult. E4:E6 was significantly different based on the core segment for the water leached sample at 10.254 for BNZ2.5 and 4.793 for BNZ1.4 for an average of 7.523 ± 3.861. High salt and basic leachate were more consistent with averages of 7.734 ± 0.101 and 10.836 ± 0.200 respectively (Table 1.6). Increase in ionic strength affects the absorbance of the sample through increasing the ability for the organic matter to absorb, this increase could be caused by the complexation of various metals (Gao et al. 2015). Reference materials of PLFA and SRFA had E4:E6 values of 6.089 and 8.188. Based off of Kiss and others (2014) which stated that values greater than 5 are fulvic in nature all of the organic matter leached off of the soils were fulvic acid in nature. Additionally, the higher the value the source is more sediment originated (Cieslewicz and Gonet, 2004). The average E4:E6 value found in literature on soil sample was 5.067 with a range from 2.973 – 9.380 (Ikeya and Watanabe, 2003). Slate River had the highest E4:E6 of 0.89, which is underlain by continuous permafrost and most similar to the permafrost leachate E4:E6 ratio (Mutschlecner et al. 2018b).

The three different media leachates had values above the average but within the range. The S_R of our leachates were consistent between the three leaching medias with an overall average of 0.886 ± 0.007. This value was in the middle of two-reference materials S_R for PLFA had a 1.035 and SRFA had a value of 0.812. Literature values of Alaskan rivers S_R ranged from 0.75 to 0.89, for which the leachates fall into range (Mutschlecner et al. 2018b).

$SUVA_{254}$ for water leached NOM was 3.500 ± 0.255 L mg C^{-1} m^{-1} while high salt leachate was different depending on the soil sample: BNZ1.4 had a value of 2.395 L mg C^{-1} m^{-1} and BNZ2.5 $SUVA_{254}$ was 10.086 L mg C^{-1} m^{-1}. This large difference between soil segments also occurred with the basic leachate as $SUVA_{254}$ value for BNZ1.4 was 5.034 L mg C^{-1} m^{-1} and BNZ2.5 was 15.700 L mg C^{-1} m^{-1} (Table 1.6). These large difference in $SUVA_{254}$ values is the direct result of high absorbance at 254 nm and a low carbon concentration in the high salt leachate. $SUVA_{254}$ indicates that the NOM leached and isolated from BNZ1.4 and BNZ2.5 varied specifically in aromaticity. The high $SUVA_{254}$ value of 15.7 L mg C^{-1} m^{-1} far exceeds the literature range for samples, as observed in literature, which has seen a range from 1.3 to 5.1 L mg C^{-1} m^{-1} (Cawley et al. 2013; Guerard and Chin, 2012; Hansen et al. 2016; Mutschlecner et al. 2018b; Westerhoff et al. 1999). The previous highest observed value in literature was 10.7 L mg C^{-1} m^{-1}, which was observed in SRHA (Westerhoff et al. 1999). This high value could be affected due to potential matrix interferences caused by the high pH of the basic leachate, which can cause a red shift of the peak absorbance to a longer wavelength (Mobed et al. 1996; Spencer et al. 2007) and/or an increase in the absorbance (Spencer et al. 2007) spectra depending on the carbon concentration and composition (Spencer et al. 2007). SRFA $SUVA_{254}$ was observed at 4.164 L mg C^{-1} m^{-1} and PLFA was observed at a lower value of 2.148, which were comparable to literature values of 4.2 L mg C^{-1} m^{-1} and 1.9 L mg C^{-1} m^{-1} respectively (Westerhoff et al. 1999). The water leached NOM $SUVA_{254}$ was also comparable to values from permafrost underlain river systems in northern Alaska with an average of 3.463 ± 0.278 L mg C^{-1} m^{-1} (Mutschlecner et al. 2018b). This comparison has the potential to show permafrost influencing these Arctic surface waters aromaticity. Overall, the optical indices indicated that the three different medias leach different functional group composition of NOM and provided additional

literature values for the future for soil leachate values, as the majority of the values were from surface waters. Additionally, the reference materials were different from the permafrost NOM seen in sub-Arctic Alaska.

FI, BIX, HIX, and ß:α, were chosen due to the extensive use in literature (Cory et al. 2010; Gabor et al. 2015; Hansen et al. 2016; Huguet et al. 2009; McKnight et al. 2001; Ohno, 2002; Parlanti et al. 2000; Wilson and Xenopoulos, 2009). These fluorescence indices are based off of the EEMs collected, which showed visual variation between leachate media (Figure 1.4). High salt leachate has the highest BIX index in this study with a value of 0.639 ± 0.100 followed by water leachate with a value of 0.444 ± 0.001, and basic leachate with a value of 0.383 ± 0.022 (Table 1.6). BIX values >1 correlate with NOM that is less process and thus, the high BIX value of the high salt leachate indicates the NOM is less processed in comparison to the other media leachates (Hansen et al. 2016). The ß:α values were the highest in the high salt leachate with an average of 0.581 ± 0.037 and the lowest in the basic leachate with a value average of 0.361 ± 0.017, which is consistent with BIX values correlating high salt leachate being less processed when compared to basic leachate indices values (Table 1.6). While, high salt leachate BIX correlation indicates high salt leachate is less processed than the basic leachate correlates with being more processed, which is also corroborated by the basic leachate having the largest HIX value average of 0.958 ± 0.015 (Table 1.6). As a large HIX value is correlated to increased humification of the NOM. FI values vary based on soil sample and media chosen for leaching but basic leachate values remained the lowest for both cores with an average value of 1.098 ± 0.030 (Table 1.6). Meanwhile, high salt and water leachates had FIs closer to 1.3, indication that pH 10 leaches out a different functional group composition of NOM than the other media. Optical indices with a difference greater than 0.1 has grounds for a difference in the sample on

the basis of source (McKnight et al. 2001). Basic leachate FI values were extremely low when compared to literature values that had an observed lowest FI of 1.21 from an Arctic river surface water C-18 isolate (Cawley et al. 2009). While C-18 is a different isolation method, however, Li et al. (2017) determined that C-18 is similar to other NOM extracts through principal component analysis of TOC, NMR, and FT-ICR-MS (Li et al. 2017). This low FI value observed could be due to matrix differences when compared to literature as the sample has basic behavior and high ionic strength compared to circumneutral to slightly acidic surface waters, altering the absorbance and fluorescence intensity of the leachate (Gao et al. 2015). Water leachate average FI value was 1.286 ± 0.026. This FI value is similar to Arctic river isolated NOM at 1.21-1.32 (Cawley et al. 2009). These low FIs are indicative of a more terrestrial derived organic matter, which has been classified as values around 1.3 and 1.4 in surface waters (Cory et al. 2010; McKnight et al. 2001). However, due to the limited literature values for soil leachate, the main conclusion observed that the conditions of the leaching media leaches out chemically different organic matter for isolation.

The analysis of reconstituted NOM after PPL isolation with UV-Vis and fluorescence continued to observe differences in optical indices depending upon the sample. These differences determined that the PPL did not selectively isolate identical functional group composition per sample. Optical indices continued to have variability in their values when observing UV-Vis and fluorescence optical indices for reconstituted NOM samples (Table 1.7). The percent change from leachate to reconstituted were again dependent upon the sample and optical index in question (Table 1.7). Fluorescence indices had the least amount of change between leachate and reconstituted NOM with changes less than 20% for BIX, FI, α:β, and HIX values. Meanwhile, UV-Vis indices had an increase in percentage of change from leachate to reconstituted NOM.

This high variability in optical indices between samples and within samples indicate that PPL does not isolate for a select NOM functional group composition.

1.4.2.1.2. Elemental Composition:

Carbon and nitrogen concentration of leachate was dependent upon the leaching media. Basic leachate leached the most carbon content compared to water and high salt leachates, at an average of 6.441 ± 2.866 mg C L^{-1}, water leachate leached 5.830 ± 1.833 mg C L^{-1}, and high salt leached 3.356 ± 2.323 mg C L^{-1} (Table 1.6). However, leachability of carbon was dependent upon soil segment and sample location when it came to leaching in various media (Table 1.3). The high salt leachate leached the least amount of carbon from both soil segments differing from Gabor et al. (2015). This discrepancy between the current study and Gabor et al. (2015) may be indicative of the functional group composition of Colorado soil material versus Alaska permafrost soil material. Gabor et al. (2015) only observed UV-Vis and fluorescence as an indicator for functional group composition in comparison to KCl and $CaCl_2$ leaching media without reporting values and thus, further conclusions could not be interpreted for the variability between the two soil types being compared. Although there was a difference in carbon concentration based on leachate media utilized, the overall percentage of carbon leached from the soil was not statistically different with averages of 1.10 ± 0.39% for BNZ1.4 and 1.01 ± 0.62% for BNZ2.5 (Table 1.3).

Isolate NOM carbon content was consistent between the two cores with the highest carbon percentage found in the water leachate and the lowest percentage from the high salt media leached NOM. Water leached NOM was 41.0 ± 12.7% carbon while, basic leached NOM had 18.4 ± 0.8% carbon and high salt had 11.4 ± 5.2% carbon (Table 1.6). In comparison to

reference material PLFA and SRFA had 67.0% and 56.0% carbon in their NOM isolate respectfully (Table 1.6). This carbon concentration in NOM was determined based off equation 5. Extraction efficiency of carbon was comparable to literature with a range of 71 – 88% of the carbon concentration captured by the PPL cartridges (Dittmar et al. 2008).

$$\frac{NOM_{photolysis}\ (mg) \Big/ Water_{photolysis}\ (L)}{TOC_{photolysis}\left(\frac{mg}{L}\right)} = Carbon\ in\ NOM\ \%$$

Equation 5: Determination of the carbon percentage found in the isolated NOM material.

Leachate samples were analyzed for metals to determine if different leaching media leached out different proportions of metals. Sodium, Al, and Fe had increased leachability with the high salt media and basic media when compared to the water control (Table 1.8). Meanwhile, select metals were retained on the soil when leached by the basic and high salt leaching media and had decreased concentrations in the sample. High salt media leached V and Cu out less than water and basic media leachate had decreased concentrations of Mg, K, Mn, Co, Se, Sr, and Ba than water and high salt leachate. Antimony and Bi concentrations were statistically the same for both leaching medias. Antimony leached out more than water for both high salt and basic media solutions. Bismuth concentrations were equal in both water and basic media leached samples, while high salt leached out less Bi compared to water leached sample. Antimony adsorption onto soils decreases with increased ionic strength and pH increasing the concentration in the leachate (Xi et al. 2010). Arsenic was leached equally for high salt media and water leached samples at 2.67 ± 0.01 ppb, while basic media leached more As at 3.86 ± 0.15 ppb (Table 1.8). This discrepancy was due to the pH of the solution as there was an increase in As in the pH 10

solution (Jeppu and Clement, 2012). Antimony and As clearly verified that ionic strength and pH are important factors for the adsorption and desorption of metals into leaching media.

1.4.2.2. Media Leached Functional Group Composition via NMR:

Initial functional group composition was obtained through the analysis of HF washed soil samples with solid state ^{13}C NMR. The highest percentage of carbon functional groups was found to be aliphatic with 50% for BNZ1.4 soil and 45% for BNZ2.4 soil (Table 1.9). Aliphatics were followed by aromatics with 20% and 23%, respectively, for BNZ1.4 soil and BNZ2.4 soil. Meanwhile, all other functional groups were less than 20% of the organic matter carbon composition. When comparing the two HF washed soil segments to each other, the carbon functional group composition of the two soils were similar with a standard deviation between 1% and 4% between the two spectra. Each media extracted a different percentage of functional groups from the soil for BNZ2.5, indicating the media composition is an important factor for leachate composition. Thus, the natural environment, including the pH and ionic strength of the surface waters, would impact the overall leachability of different functional groups from the permafrost soil. Most notably, high salt leached soil had less aliphatics left behind at 18% compared to the other two media types which had 33% and 28% of aliphatics still bound to soil, based off of the percent difference between the spectra (Equation 6) (Table 1.9/Figure 1.5). Overall, kinetically labile and water-soluble functional groups are expected to leach from the soil into the leachate.

$$Soil\ NMR\ \% - Leached\ Soil\ NMR\ \% = \%\ differnence$$

Equation 6: The percent difference of two NMR Spectra to observe what percentage of the chemical shift bin was left behind during the leaching process.

Both cores presented variability in functional group composition of carbon functional groups for the NOM isolated from each leaching media. High salt leaching out the highest percentage of aliphatics in both cores at 32% for BNZ1.4 and 21% for BNZ2.4 for an average of 26.2 ± 8.1% (Table 1.9). The variability of functional group composition observed in the isolated NOM leached from different media indicates that the leaching ability of metals and other material is dependent upon the solutions composition, ionic strength, pH, and concentration of other metals (Christensen, 1984; Echevarria et al. 2001; Genc and Ulupinar, 2010; Jeppu and Clement, 2012; Ter Laak et al. 2006; Lertpaitoonpan et al. 2009; Naidu et al. 1994; Pardo et al. 1992; Raven et al. 1998). The pH of the solution was deemed such an important factor for adsorption that Jeppu et al. (2012) designed a modified Langmuir-Freunlich isotherm to include a pH term as metals are pH dependent for their adsorption onto soils. For example, aliphatic sorption was disturbed by the high ionic strength leaching media. By analyzing the extreme ends of pH and ion strength scale using the media presented in this study the extreme ends of functional group composition leached from these sub-Arctic permafrost soils.

The difference between spectra functional group binning percentages between unleached soil to leached soil were determined to evaluate what functional groups were left behind on the soil from the different leaching media (Equation 6). A positive value indicates a decreased percentage in the NOM compared to bulk soil, while negative value indicates an increased percentage in the NOM signal compared to bulk soil. For example, high salt percent difference of spectra for aliphatics is 18.3% for BNZ1.4 and 24.6% for BNZ2.4, indicating a higher composition of aliphatics were leached from BNZ1.4 when compared to BNZ2.4 (Table 1.8). Thus, the overall functional group composition of aliphatics had different leachability between soil segments. Similar results were observed for basic and water leached NOM (26.2% and

27.8% respectfully for BNZ2.4) (Table 1.8/Figure 1.5). NMR spectra from unleached soil and water leached soils appeared very similar in the aliphatic range when spectra were overlaid (Figure 1.5). There was a 2.1% difference between unleached soil and leached soil aliphatic range (Table 1.8). This small difference between leached and unleached soil indicates aliphatics remain on the soil when soil is in contact with 18 MΩ water. The NMR binning percentages of leached soil appears to have higher percentage of non-aliphatic functional groups, ranging from 45 – 220 ppm, as they remain complexed onto the soils. This increased NMR signal in this region may be skewed due to the removal of leachable functional groups, such as the small percentage of aliphatics removed, as the whole area under the spectra remained 100% (Table 1.8). Further comparison of isolated NOM from water media to unleached soil shows a large discrepancy in the aliphatic ranges, as the unleached soil had a signal that was 25.74% more than the isolate water NOM, and this corroborates that aliphatics were not leached from the soils (Table 1.8/Figure 1.5). This lack of aliphatics leaching was consistent with all leaching methods, high salt had a 17.72% difference between unleached soil and NOM, while basic had 23.99% (Table 1.8). Chen et al. (2018) determined that aliphatics remained on the soil as well as this study that saw consistency of aliphatics not leaching through all ^{13}C NMR spectra of soil versus NOM conducted.

Through proton functional group analysis on isolated NOM, it was determined that carbohydrates and peptides have the largest class of functional groups binned by percentage across all leaching media extractable NOM. High salt leached out the most carbohydrate functional group at 45.55 ± 7.47% and basic leaching the least amount with 35.62 ± 6.29% (Table 1.11/Figure 1.7). Approximately 30% of the carbohydrates observed via ^{1}H NMR is suppressed due to the water suppression technique diminishing that portion of the NMR

spectrum (Lam and Simpson, 2008). Thus, the ^{1}H NMR and ^{13}C NMR spectra do not showcase similar results with leachability in carbohydrates. CRAMs were the second most extracted classification for proton functional groups ranging from 22 – 37% of the ^{1}H NMR spectra. CRAMs had an increased leachability with basic conditions representing 34.17 ± 3.35% of the ^{1}H NMR spectra compared to high salt NOM ^{1}H NMR spectra only represented by 25.98 ± 5.29% for CRAMs (Table 1.11). This CRAMs region corroborates the leachability of carboxyl groups in the carbon NMR spectra as basic conditions leached out 8.67 ± 2.40%, followed by water leached NOM at 8.43 ± 2.18% and high salt leached NOM with 8.09 ± 1.51% (Cao et al. 2018). ^{1}H aromatics constituted as the least amount present in the NOM across all leaching medias and accounted for only 7 – 12% of the ^{1}H NMR spectra (Table 1.11). This percentage is less than carbon aromatic groups indicating there are more nonprotonated aromatic carbon present in the NOM not observed in the ^{1}H NMR spectra. An ammonium triplet peak appears down field around 7 ppm (Figure 1.7) (Chalbot et al. 2016). This peak is highest in the water leachate indicating an increase in leachability of this ammonium functional group with water compared to basic and high salt NOM. Additionally, this ammonium peak may be present in NOM in this study due to the choice of NOM isolation using PPL cartridges. PPL cartridges are known to isolate more nitrogen containing NOM (Dittmar et al. 2008; Li and Hur, 2017; Perminova et al. 2014; Zherebker et al. 2019). This ammonium group can probably be attributed to microbial nitrogen mineralization occurring in the soils and being extracted upon leaching (Chantigny et al. 2010).

Overall, aliphatics remained on the soil during the leaching process and thus, the full functional group characterization found in soil is not represented in the NOM isolated. However, more complex functional groups were leached out and isolated through the NOM extraction

process (Table 1.9). High salt, basic, and water leached isolated NOM were different in their functional group composition showcasing that the leaching media does matter as to what leaches into the surface waters, and thus, surface water conditions will affect what PENOM is introduced into the watershed.

1.4.2.3. Photolysis Media Leached NOM:

1.4.2.3.1. Hydroxyl Radical:

The differences of functional group composition between different leaching media becomes apparent due to the differences in photobleaching rate for the reconstituted isolate solutions. To simplify interpretations of the photobleaching decay, the rates of decay were determined by observing rates at 254 nm for the aromatic systems; 254 nm is also a common absorbance to interpret data in the organic matter community (Figure 1.8) (Hansen et al. 2016). At 254 nm BNZ1.4 high salt NOM was more reactive to unamended rate of decay at 0.00687 ± 0.00124 L mg C^{-1} hr^{-1}, while basic and water NOM were 0.00277 ± 0.00013 L mg C^{-1} hr^{-1} and 0.002142 ± 0.000156 L mg C^{-1} hr^{-1} respectively (Table 1.12). This high reactivity of high salt NOM was not due to salt content of the NOM as the PPL extraction removes all salts present and provides even extraction efficiency no matter the salt content in the solution prior to filtration (Dittmar et al. 2008). Additionally, when methanol was added to quench the production of •OH and other radicals, the observed rate of decay decreased to 0.00540 ± 7.31E-05 L mg C^{-1} hr^{-1} for high salt NOM while, basic and water NOM rates were similar at 0.00190 ± 0.000250 L mg C^{-1} $hr^{-1}$and 0.00180 ± 0.000673 L mg C^{-1} hr^{-1} respectively (Table 1.12). In the case where iron was added to promote the production of •OH the rate of absorbance decay, high salt NOM had the highest rate of decay with 0.0121 ± 0.000799 L mg C^{-1} hr^{-1}followed by basic NOM at 0.00470 ±

0.00297 L mg C^{-1} $hr^{-1}$and water NOM at 0.00380 ± 0.000339 L mg C^{-1} hr^{-1} (Table 1.12). All iron rates of BNZ1.4 were much higher than unamended and methanol amended samples. This is an indication that •OH radical promotion significantly alters the rate of decay for the NOM (Guerard et al. 2009). With high iron concentration in the boreal forest surface waters of the area this could lead to the photo-Fenton reaction providing an increased reactivity in NOM once the PENOM mixes with modern NOM in the watershed (Figure 1.17) (Gagné, Section 3.4.3.).

When conducting the same photolysis experiments on BNZ2.5, the rates of absorbance decay varied from BNZ1.4, however high salt still remained the most reactive to photobleaching with no amendments with a decay rate of 0.00667 ± 0.000204 L mg C^{-1} hr^{-1}, which was less reactive than BNZ1.4 (Table 1.12). BNZ2.5 basic and water NOM had increased rates compared to BNZ1.4, basic and water NOM had similar rates of decay that were not statistically different from each other at 0.00197 L mg C^{-1} hr^{-1} for basic NOM and 0.00195 ± 1.78E-5 L mg C^{-1} $hr^{-1}$for water NOM (Table 1.12). Consistent with BNZ1.4, the addition of methanol to observe •OH quenching showed decreased rates of absorbance decay for all media NOM at 0.00450 ± 0.000542 L mg C^{-1} hr^{-1} for high salt NOM, 0.00164 ± 5.68E-5 L mg C^{-1} hr^{-1} for water NOM, and basic NOM had a rate of 0.00140 ± 5.01E-5 L mg C^{-1} hr^{-1} (Table 1.12). This decrease in rate of decay in methanol amended photolysis samples compared to unamended photolysis samples in both sets of cores indicates that the NOM from all three leachates are influenced by •OH naturally and when promoted by iron amendments. When the addition of iron was added to the samples to promote the production of •OH, BNZ2.5 rate of decay increased greatly similarly to BNZ1.4. High salt NOM rate of decay increased to 0.0108 ± 0.00152 L mg C^{-1} hr^{-1} while water NOM increased to 0.00757 ± 0.000230 L mg C^{-1} hr^{-1} and basic NOM at 0.00556 ± 0.000306 L mg C^{-1} hr^{-1} (Table 1.12). Overall, the rates of decay were consistently highest in the high salt

NOM across all amendments, showcasing that high salt isolated NOM was the most reactive to the ROS •OH through photolysis.

When observing the unamended photobleached samples versus the •OH quenched samples with methanol amendment a positive value indicates that the samples natural photobleaching is influenced by •OH (Equation 7). High salt NOM had the largest average positive value of 0.00182 ± 0.0005 L mg C^{-1} hr^{-1}, allowing for the interpretation that high salt NOM naturally produces more •OH upon photolysis compared to basic and water NOM (Table 1.12). Water leached NOM also had positive rates of decay (0.000310 ± 7.86x10^{-6} L mg C^{-1} hr^{-1}) which indicates that •OH radical production is an important natural product of natural photolysis for these two permafrost core segments (Table 1.12). The NOM isolated from these two segments in different media are heterogeneous in their photoreactivity.

$$k_{\bullet OH\ Plain} - k_{\bullet OH\ quenched} = Rate\ difference$$

Equation 7: •OH rate difference between unamended and quenched samples.

1.4.2.3.2. Triplet Excited State NOM:

TMP is a useful probe for ^{3}NOM* through electron transfer from the excited ketyl radical of the NOM to the TMP phenol or direct hydrogen abstraction from TMP phenol to ^{3}NOM* (Cawley et al. 2009). Literature represents ^{3}NOM* rates through apparent quantum yields through the use of a single wavelength Hg light bulb, which allows for the ease of converting a rate of ^{3}NOM* production observed into an apparent quantum yield (Bodhipaksha et al. 2015; Maizel et al. 2017). However, through this study, a broad wavelength light was utilized to mimic the effects of sun-lights UV-rays causing observations of apparent quantum yields to not be effectively utilized. High salt NOM had the highest rate of decay for TMP at -0.00777 ±

0.000591 L mg C^{-1} min^{-1} for BNZ1.4 and -0.0023 ± 0.000190 L mg C^{-1} min^{-1} for BNZ2.5, indicating ^{3}NOM* had the most production in the high salt leachate, with an average rate of -0.00505 ± 0.00143 L mg C^{-1} min^{-1} (Figure 1.9/Table 1.12). Meanwhile, water and basic NOM were less reactive to TMP decay then the high salt NOM, however the NOM did not have a unanimous rate of decay between the two core segments. BNZ1.4 basic NOM was more productive than water NOM with a decay rate of -0.00525 ± 0.000407 L mg C^{-1} min^{-1} versus -0.00384 ± 0.000225 L mg C^{-1} min^{-1} (Table 1.12). BNZ2.5 basic and water NOM rates of TMP decay were not statistically different, with a rate of approximately -0.00182 ± 0.000165 L mg C^{-1} min^{-1} (Table 1.12). Overall, BNZ1.4 was more reactive to TMP decay and thus, BNZ1.4 is more reactive to the production of ^{3}NOM* compared to BNZ2.5. Overall, high salt NOM is most susceptible to ^{3}NOM* productivity in the presence of sunlight for both core segments. This susceptibility for ^{3}NOM* production maybe an indicator of aromatic ketone content in the NOM, which when compared to NMR ketone content high salt NOM had the highest percentage of ketone functional groups at 1.8% and 1.6% for BNZ1.4 and BNZ2.4 respectfully (Table 1.10). While basic and water NOM ketone functional group composition was observed as low as 0.9% based on their respective ^{13}C NMR spectra. The controlled leached functional group composition was least susceptible for the production of TMP probed ^{3}NOM* in the presence of UV-rays.

As stated above, literature comparisons are difficult to determine as the majority of photoreactivity studies utilize one wavelength lamps and converts rates of production into apparent quantum yield. Cawley et al. (2009), whose methods were utilized in this study, also presented rates of ^{3}NOM* production in the same format as this study allowing for comparison. However, the NOM utilized by Cawley et al. (2013) were isolated by different methods including the use of XAD resin, C-18 resin and tangential flow ultrafiltration. The different

isolation techniques will imply potential differences in NOM composition causing different ^{3}NOM* production rates. The rates observed from a river located on the north slope of Arctic, Alaska ranged from 0.00125 to 0.00225 L mg C^{-1} min^{-1}, which was similar to BNZ2.5 rates and the rates observed for PLFA and SRFA (Cawley et al. 2013). BNZ1.4 had much higher rates of production compared to BNZ1.4 and Cawley et al. (2013), which is suspected to be true rates and is an indication that BNZ1.4 has an overall different functional group composition compared to BNZ2.5 and a north slope Arctic Alaskan river.

1.4.3. Water Leached Sections with Depth:

1.4.3.1. Optical Properties:

Optical indices for leachate waters values depend on the core. The cores have increased radiocarbon age with depth. This UV-Vis absorbance data allows interpretation on trends observed from molecular weight, aromaticity, source, and humification as age increases.

Overall, CPC appears to have higher values for the optical indices, E2:E3, E2:E4, E2:E6, compared to BNZ (Table 1.13). This discrepancy in optical indices between the two watershed is an additional verification that the functional group composition leached from the respective permafrost soils are different. S_R was consistent down the entire depth of all four cores with a value of 0.822 ± 0.052, which falls between PLFA (1.035) and SRFA (0.812). $SUVA_{254}$ for BNZ was 3.212 ± 1.028 for BNZ1 and 3.310 ± 0.384 for BNZ2 while, CPC was lower and less aromatic at 2.661 ± 0.163 for CPC1 and 2.246 ± 0.925 for CPC2 (Table 1.13). $SUVA_{254}$ is contradictory to literature that states permafrost is less aromatic based off of NMR spectra (Heslop et al. 2019; Mueller et al. 2015; Waldrop et al. 2010; Ward and Cory, 2015) but agree with the literature that state permafrost has increased aromatic content based off of NMR spectra

(Grewer et al. 2016; Mueller et al. 2015; Pedersen et al. 2011; Pengerud et al. 2017). BNZ has a higher overall $SUVA_{254}$ values due to the increased aromaticity at the bottom of the core and within the permafrost zone compared to CPC, which is primarily active layer and represents no permafrost. $SUVA_{254}$ values may be altered due to the Fe concentration in the leachate, as the highest Fe concentration was found in the top portions of the soil. It was also found that the leachate Fe concentrations and the $SUVA_{254}$ values had moderate correlation to each other through a linear regression with an R^2 of 0.39. This linear regression found that, as Fe concentrations in the leachate increased the $SUVA_{254}$, decreased with a slope statistically significantly non-zero. This correlation is corroborated by Poulin et al. (2014) who found that an increase in Fe caused 254 nm absorbance value to increase, thus causing an overall decrease in $SUVA_{254}$. The $SUVA_{254}$ correction value was not determined for permafrost leachate NOM and literature correction values are for the reference materials with different functional group composition to PENOM. Due to the variability in optical indices and the lack of linear trends with age, optical indices were decidedly not the preferred indicator of permafrost and age of the soil analyzed in this study.

However, the cores overall BIX, HIX, and FI indices provides insight on how each core varies in leachable carbon composition and potential reactivity. BNZ1 had a BIX average value of 0.425 ± 0.020 and BNZ2 had a higher average value of 0.450 ± 0.004. BNZ2 had less variability in BIX value with an increase in depth (Table 1.13). Meanwhile, CPC 1 and 2 had similar BIX average values to each other with values of 0.473 ± 0.012 and 0.474 ± 0.018, respectively. This higher BIX value indicates that CPC leached organic matter is closer to BIX values from stream surface waters within the boreal forest of interior Alaska ranged from 0.51 to 0.58 over both discontinuous and continuous permafrost (Mutschlecner et al. 2018b). Increased

BIX values are indicative of an increase in the level of NOM biological processing, meaning BNZ permafrost organic matter is overall less processed than CPC. This could be due to CPC cores being a majority active layer soil (Table 1.3). This active layer would be providing organic matter to the surface waters during the summer months (Schuur et al. 2015), which could be influencing the surface water BIX values seen in Alaska. The composition of this NOM has the potential to be similar to the composition of naturally leached PENOM because the residence time for leachate to get to surface waters upon leaching was discovered to be 3 to 7 days (Heslop et al. 2017; Vonk et al. 2013). However, the composition may vary in concentrations depending upon the water conditions allowing for more or less adsorption of chemical functional groups and metals (Christensen, 1984; Echevarria et al. 2001; Genc and Ulupinar, 2010; Jeppu and Clement, 2012; Ter Laak et al. 2006; Lertpaitoonpan et al. 2009; Naidu et al. 1994; Pardo et al. 1992; Raven et al. 1998). A high β:α is indicative of an increase in recently produced NOM and thus, less processed NOM by biological, photochemical, and environmental means (Hansen et al. 2016; Parlanti et al. 2000; Wilson and Xenopoulos, 2009). β:α was consistent with BIX in soil leachates at CPC with the highest values of 0.460 ± 0.017 for CPC1 and 0.459 ± 0.021 for CPC2, while BNZ had β:α lower with BNZ1 at 0.409 ± 0.019 and BNZ2 at 0.432 ± 0.007 (Table 1.13). These values were again lower than Mutschlecner et al. (2018b) stream β:α values, which had the lowest value at 0.49.

BNZ core leachates had very similar average HIX values with BNZ1 at 0.950 ± 0.061 and BNZ2 at 0.955 ± 0.024. BNZ had higher average values than CPC, which had a value of 0.910 ± 0.007 for CPC1 and 0.931 ± 0.016 (Table 1.13). These HIX values fell within the range for Alaskan streams (0.82 – 0.95) (Mutschlecner et al. 2018b) and BNZ core had similar values to a California peat soil leachate which had a BIX of 0.95 (Hansen et al. 2016).

The soil leachate had low FI values, which is indicative of organic matter derived from plant and soil material (Cory et al. 2010). BNZ1 and BNZ2 had lower average FIs at 1.319 ± 0.046 and 1.307 ± 0.035 respectively, while CPC1 and CPC2 were closer to Mutschlecner values at 1.399 ± 0.025 and 1.404 ± 0.042, respectively. BNZ FIs were observed to have a decreased correlation with increased age through a linear regression P-value of 0.0283. Alaskan streams had FI values ranging from 1.48 to 1.59 (Mutschlecner et al. 2018b), a soil leachate provided an even higher FI at 1.61 in California (Hansen et al. 2016), and when observing isolated organic matter reconstituted for fluorescence scans lower FI values were observed at 1.21 for a C-18 isolated NOM sample from an Arctic river (Cawley et al. 2009). The FI observed for the soil leachates in sub-Arctic Alaska were similar to FI values obtained from isolated reference material PLFA which had a value of 1.453 and SRFA a value of 1.300 (Guerard and Chin, 2012). However, these literature values were not consistent with PLFA during this study at 1.549 while SRFA was similar at 1.314. These differences could be due to the different instruments used to obtain the fluorescence scans as discussed in a previous section (Cory et al. 2010). Overall, the optical indices showcased that the overall composition of permafrost is heterogeneous based on the differences observed down the permafrost core and within the same watershed. However, there was no correlation between optical indices and soil age. In the end, this analysis did provide more literature values for permafrost soil leachate optical parameters, which are currently limited to a select few sites and studies.

1.4.3.2. Chemical Composition:

1.4.3.2.1. Elemental Composition:

In order to determine which set of cores was more prone to leaching carbon and nitrogen a leachability percentage was determined. BNZ and CPC had the highest percentage of carbon leachability in the active layer segment. BNZ1 had upwards of 85.53% ± 1.32% carbon leached out of the top of the core (Table 1.3). CPC had decreased carbon leachability with a maximum of 1.05% ± .0.53% carbon leached (Table 1.13). The isolated NOM from all four cores had variability within the carbon content of the NOM; BNZ1 and BNZ2 had an overall carbon percentage of 65.9 ± 20.5% and 46.4 ± 3% respectively. Meanwhile, CPC1 and CPC2 had 51.7 ± 3.7% and 62.1 ± 81.3%, the high error in CPC2 is caused by an isolation of CPC2.2 which was very light in coloration and fluffy having only a 4% carbon content. Due to this lack of carbon concentration within the CPC2.2 sample photochemical reactivity experiments were unable to occur.

Carbon and nitrogen composition of the soils were statistically the same between BNZ and CPC however, there was no correlation with carbon and nitrogen composition of the leachate with increased age. Alternatively, the average of the leached carbon for BNZ and CPC were statistically different indicating BNZ has increased leachability. BNZ active layer in this case had a much larger carbon concentration (22.358 ± 11.573 mg C L^{-1}) and nitrogen concentration (1.048 ± 0.446 mg N L^{-1}) in the leachate than CPC (4.170 ± 0.652 mg C L^{-1} and 0.168 ± 0.00112 mg N L^{-1}) (Table 1.13). BNZ permafrost statistically leached out less carbon and nitrogen compared to active layer through a linear regression compared TOC to age, while CPC did not have a linear regression for the leached carbon or nitrogen.

ICP-MS elemental metal composition analysis was conducted on the water leachate and three trends were determined statistically for the linear regression with age of the soil leached (Table 1.14). These correlation trends included; slope not significantly non-zero (p-value > 0.1), enhanced with increased age (positive slope and p-valued < 0.05), and diminished with increased age (negative slope and p-value < 0.05). The leachate metal concentrations had slopes not significantly non-zero with the exception of Sr and Ba that diminished in the leachate with increased age. Strontium and Ba are two alkaline earth elements that have been observed to complex with NOM 20 – 40% of the time and thus, are of interest when these metals influx into the surface as they have the potential to bind to NOM and alter the transport and transformation of other metals (Pokrovsky et al. 2018). Barium has been observed to increase in Arctic stream water when the subsurface flow is forced deeper, an indication of permafrost thaw (Barker et al. 2014). However, the depth of this subsurface flow was not discussed by Barker et al. (2014) thus, Ba could be concentrated on the upper portions of permafrost through freeze-thaw concentration of metals (Barker et al. 2014; McNamara et al. 1997; Petrone et al. 2006; Rember and Trefry, 2004).

1.4.3.2.2. Carbon Functional Groups:

When observing the carbon functional groups, specifically carbon aromatic functional groups BNZ1 and BNZ2 have similar percentage of carbon aromatic groups at 35%, however the standard deviation for the two cores are upwards of 4.6% (BNZ1) and 2.8% (BNZ2) when averaging the length of the cores (Table 1.15). In general, with BNZ1 and BNZ2 the carbon aromatic functional groups 90 – 160 ppm is lowest in the active layer at 27.8% and 30.3%. The transient layer tends to have the highest composition with a percentage of 40.7% in BNZ1 and

35.3% to 37.5% in BNZ2 (Table 1.15). The bottom of the core, the permafrost layer, while it does not present with the highest aromatic composition when averaged together, this layer does have a higher carbon aromatic content when compared to the active layer at 38.0% and 36.7%. When observing the aromatic content in individual ranges for statistically linear regression correlation (P-value <0.05) with percentage versus radiocarbon age the 120 – 140 ppm, carbon substituted aromatics, and 140 – 160 ppm, oxygen substituted aromatics, increased with increased age. Similarly, the carboxyl/aliphatic amides (160 – 190 ppm) also statistically correlated to increase with increasing age from 6.16% to 10.93% in BNZ2. However, carbohydrates were observed to statistically decrease with increased age from 29.69% to 28.02% for BNZ1 and 35.14% to 23.45% for BNZ2 (Table 1.15). All other carbon functional groups did not have a statistical correlation with increased age. Aliphatic content for BNZ1 was less consistent with depth compared to BNZ2. BNZ2 had 17.7 ± 1.1% aliphatic content while BNZ1 showed the highest aliphatic content in the top layer of the core with 25% and low aliphatic content in the permafrost bottom layer at 15.6%. When averaging BNZ1 for aliphatic content the standard deviation was 3.9% showing an increase in variability with depth. Methoxyl groups percentages were for the majority stable down BNZ with an average of 10.1±0.97% for BNZ1 and 9.3 ± 0.2% for BNZ2. Ketyl groups were overall the smallest percentage of functional group chemical characteristics with an average of 0.9±0.5% in BNZ1 and 1.4±0.6% in BNZ2 (Table 1.15).

CPC carbon functional group compositions were not placed into a linear regression with age to observe correlations as the core lacked the span of ages required for an accurate linear regression and thus, only observations of percentages could be interpreted. Carbon functional groups lacked variability with depth as observed in the standard deviations of all less than 0.6%.

CPC1 highest functional group composition came in at 14.7 ± 0.25% aliphatic functional group composition (0 – 45 ppm), 29.7 ± 0.62% carbon carbohydrates (60 – 90 ppm), and 34.3 ± 1.45% carbon aromatics (90 – 160 ppm) (Table 1.15). The aromatic carbons were also consistent with depth of CPC2 at 34.0±1.5%, similar to CPC1 percentages (Table 10). CPC2 aliphatics average was 18.09 ± 3.45%, however lacked a trend with increased age. Similar to aliphatics, methoxyl groups (45 – 60 ppm) composition was unable to be determined and lacked a trend with increasing age, however, the highest percentage was observed at the top of the core with 13.5%, while the remaining segments were around 9.5%. Carbon carbohydrate functional groups (60 – 90pm) had the highest percentage in the middle layer at 34.2% compared to 26% for the top and 20.4% for the bottom layer, showcasing that carbohydrate composition was not a gradient down the core (Table 1.15). Carboxyl/aliphatic amides (160 – 190 ppm) did encounter a trend with depth for CPC2, this trend indicated highest functional group composition of carboxyl/aliphatic amides in the bottom layer at 10.3% and decreasing to 7.9% in the top layer of the core, however the lack of samples proved difficult to determine if this trend was statistically significant. Ketone (190 – 220 ppm) percentages were highest in the top layer, 2.2% and lowest in the middle layer, 0.2% (Table 1.15).

Reference materials have been run by multiple studies using different ^{13}C NMR methods and magnetic strength (Cawley et al. 2013; Chin et al. 2004; Westerhoff et al. 1999). These studies share similar binning ranges, however, 90 – 120 ppm was not analyzed in two of the studies (Chin et al. 2004; Guerard, 2009). With a missing spectra range and varying methods with different NMR magnetic strength, the authors note that only observational comparisons can be made between literature and this study. Aliphatics composition was higher in PLFA compared to SRFA when both reference materials were observed using ^{13}C NMR (Chin et al. 2004;

Guerard, 2009). Meanwhile, the majority of the spectra with the exception of aliphatics were higher in SRFA compared to PLFA (Guerard, 2009). This overall comparison between reference ^{13}C NMR provides evidence that the carbon functional groups in this study were similar to other results. Additionally, while carbonyl carbons (190 – 220 ppm) were observed as lower percentage in PLFA, which was contradictory to Chin et al. (2004), the percentage observed was very similar to Cawley et al. (2013) who observed a 0.3% while, this study had 0.4% for PLFA carbonyl content. Soil samples fell in between the two reference materials for aromatic and aldehyde/ketone composition. Higher carbon functional group composition when compared to reference material occurred with carbohydrates, while the lower occurred in aliphatics and methoxy carbon content. This lower percentage could be due to these two functional groups remaining on the soil and not leaching off into the isolation media. Soil aliphatic composition was the highest percentage similar to SRFA, however the percentage was more similar to PLFA. In general, when ranking the functional group percentages, the soils ranked more closely to SRFA with the exception of carbohydrates and aromatics which were flipped in ranking when comparing SRFA and soil samples.

There is limited literature for ^{13}C NMR functional group analysis of isolated soil NOM. Polyakov et al. (2018) isolated soil NOM from volcanic soils and analyzed it using a 500 MHz CPMAS solids NMR. Although the leaching and isolated techniques were different as well as the soil utilized it is worth comparison to provide a reference point for NOM functional group composition. The binning regions were slightly different for the volcanic soils and will be denoted as such in the discussion. Aliphatic percentages from 0 – 47 ppm for the volcanic soils were observed to range from 21 – 45% with an average of 27.2%, the volcanic soil leaching protocol may have allowed for an increased leachability of aliphatic functional groups compared

to the water leached isolation of permafrost soils (Polyakov et al. 2018). When it came to the observation of aromatics Polyakov et al. (2018) binning was different from this study with aromatics being denoted as 110 – 164 ppm and thus, the aromatics have the potential to be less than this study which observed aromatics as 90 – 160 ppm. Permafrost NOM averaged 34.70% aromatics while the volcanic soil averaged 33%, which could be influenced by the smaller binning range by Polyakov et al. (2018). Polyakov et al. (2018) also included 60 – 110 ppm as aromatic in nature. If that bin was added to the permafrost NOM aromatic region and these two bins were compared permafrost NOM had a much greater average at 62.47% compared to the volcanic NOM which observed a 47.2% aromatic content. This difference in aromatic content could be caused by the ecosystem in the soils environment as boreal forest have high aromatic plants, mainly spruce trees. As well as introducing a higher aliphatic content due to the decrease in aromatic content. Additionally, Polyakov et al. (2018) only proceeded with 0 – 190 ppm range while, this study observed 0 – 220 ppm which can also alter the percentage results. This discrepancy in binning ranges is caused by variability in where the spectrum goes back to baseline and is observed as reliable values for signal to noise ratios. Overall, volcanic soil isolated NOM and permafrost soil isolated NOM were consistent in aliphatics and aromatics being the highest percentage of the NMR spectrum and on average aromatics were higher than aliphatics.

1.4.3.2.3. Hydrogen Functional Groups:

Hydrogen NMR spectra for BNZ1 and BNZ2 had variability in spectra percentages down the cores. Only one trend was observed with hydrogen functional groups statistically and this trend was an increase in CRAMs with increasing age. CRAMs were low in the active layer of

both cores at 24.2% for BNZ1.1 and 25.5% for BNZ2.1 and high in the permafrost layer of both cores at 30.68% for BNZ1.6 and 36.05% for BNZ2.6 (Table 1.16). Carbohydrates composed the highest percentage of the functional group composition determined by ^{1}H NMR at 30.9 ± 6.1% and 30.6 ± 4.1% (Table 1.16). This carbohydrate percentage has the potential to be upwards of 30% truncated due to the water suppression through the use of SPR-W5-WATERGATE method (Lam and Simpson, 2008). The highest percentage of MDLT both appeared in the active layer portion of the cores while the lowest was observed in the transient layer; 17.5% compared to 22.18% in BNZ1 and the core had an average of 20.5 ± 2.2% for BNZ1 and 22.5 ± 2.8% for BNZ2 (Table 1.16). Aromatic content was lowest in active layer presenting at 9.2% and 6.4% for BNZ1 and BNZ2, while the permafrost had approximately 15% for both cores but no statistical trend was observed (Table 1.16).

Consistent with carbon functional groups of CPC1, hydrogen functional groups were observationally consistent down the depth of the cores as statistical correlations with linear regression were not conducted due to the limited radiocarbon age span of these cores. Hydrogen functional group composition as you go down were consistent; MDLT of 18.5 ± 1.6%, CRAM section of 30 ± 1.1%, and carbohydrates were the most consistent at 43.5 ± 0.5% (Table 1.16). The main variability presented itself in the form of hydrogen aromatics, however this aromaticity did not indicate a pattern down the core. CPC1.2 had the lowest aromaticity at 4.2% and the highest percentage in CPC1.4 at 10.9%. CPC1.3 and CPC1.4 both had 8.5% hydrogen aromatic in the proton NMR (Table 1.16). Meanwhile, CPC2 from the same watershed had a different composition with depth. CPC2 decreased the percentage of carbohydrates with increased depth; 56.3%, 43.9%, and 36.4% (Table 1.16). This decrease in carbohydrates is indicative of increased productivity. This productivity probably occurred before the permafrost organic matter was

frozen in place, suggestive of increased age. Similarly, with CPC1, CPC2 hydrogen aromatic functional group was lowest at the bottom of the CPC2 at 9.8%, while the most modern active layer segment had 14.9%. CPC2.4 and CPC2.3 had similar MDLT values at 18.9% and 17.2%, while CPC2.2 was 11% (Table 1.16).

The analysis of soil isolated NOM for proton functional group assessment is limited in literature and was observed on isolated NOM resuspended in D_2O and DMSO. Along with different solvent resuspension soil NOM was leached and isolated differently from this study and thus, percentages may be skewed due to variations in methods. The use of deuterated solvents allows for running an NMR experiment without solvent suppression techniques, however, the deuterated solvents do not allow for a natural analysis of the NOM in H_2O. With that being said, the authors understand the limitations this poses for the comparison of ^1H NMR binning percentages for hydrogen functional groups. Isolated NOM by PPL, XAD-8, and water extractable organic matter from silt loam soil and peat soil were resuspended in DMSO and through the analysis minute changes between isolation method and soil type were observed (Han et al. 2019). Thus, the minute variability between soil NOM isolated in this study were reliable and represent true differences between the samples. Specific binning percentages were not observed by Han et al. (2019) however, the authors indicated obvious differences were observed through ^1H NMR analysis (Han et al. 2019). Additionally, leaching and isolation of peat soil humic acid and fulvic acid hydrogen functional groups were observed using a 500 MHz NMR with resuspension in NaOD in literature (Hertkorn et al. 2002). Due to the change in solvent difference the binning regions were shifted and binning groups have different classifications and so comparisons were only observed between aliphatic (MDLT), carbohydrate, and aromatic regions. BNZ1 (20.46%), BNZ2 (22.46%), and CPC1 (18.5%) aliphatic percentages most closely

resembled humic acid percentage from isolate peat soil, which had a percentage of 24.9% (Table 1.16). CPC2 had a percentage of 15.70% for aliphatic range which was closest in comparison to the aliphatic percentage from fulvic acid isolated from peat soil at 14.2%. The highest percentage for both soil NOM in this study and soil NOM from isolated peat soil was classified as carbohydrates. BNZ and CPC cores averaged a range from 36.67% to 45.50% carbohydrate and literature observed a carbohydrate percentage of 45% for humic acid and 35.9% fulvic acid (Table 1.16). The aromatic percentage of literature peat soils were much higher than this study with humic acid having an 18.2% and fulvic acid having 15.6% aromatic content. This dissimilarity could be caused by the aromatic region using DMSO as a solvent, which was determined to be 6.0 – 10.0 ppm, while this study only obtained a binning percentage from 6.5 – 8.4 ppm. Additionally, the peat soil could be more aromatic in nature due to the change in sampling location. The similarities provided by aliphatic and carbohydrate comparison between literature and this study allows insight in that, although leaching, isolation, and NMR methods are different, there is a common agreeance that carbohydrate hydrogen functional group dominates the isolated NOM material from soils.

1.4.3.2.4. Functional Group Discussion:

Permafrost aromatic content was higher than active layer content. Contrary to literature, the ^{13}C NMR data states that permafrost has a decreased aromatic content (Ward and Cory, 2015). Ward and Cory (2015) observed ^{13}C NMR results from Arctic Alaska soils that were pre-thawed before being leached and at a different soil to media ratios. These conditions may be the reason the aromaticity content conclusions vary between this study and the Arctic study. The increased aromatic content of permafrost is backed up by the ^{1}H NMR of these same NOM

samples which had the lowest aromatic content in the active layers and the bottom of both cores had the highest aromatic percentage. The percent composition of carbohydrates decreased with depth is indicative of more productivity in the permafrost layer. However, one would hypothesize the transient layer to have the highest productivity due to recent thawing and refreezing. This lack of productivity in transient and active layer is potentially caused by the influence of recently leached NOM from plant material during the time of thaw when the plant leachate collects in the transient layer. These findings through NMR allowed for the observation of variability between core layers, intra-watershed, and inter-watershed. Permafrost NOM should not be clumped into one bulk characteristics as the variability is observable via NMR. Additionally, permafrost NOM is not low in aromaticity as previously mentioned in literature.

1.4.3.3. Photolysis of Reconstituted PENOM Water Isolates:

1.4.3.3.1. Hydroxyl Radicals:

Hydroxyl radical production is important in these permafrost regions due to the high iron concentrations from the soils and surface (Table 1.17). Iron and NOM in the presence of sunlight form reactive hydroxyl radical for further degradation of NOM, contaminants, and metal transportation. The rates of absorbance decay for the two-different watershed's permafrost NOM have variability with depth, but the highest rate of absorbance decay is with CPC1.2 at a rate of 0.00234 ± 9.47E-05 L mg C^{-1} hr^{-1} (Table 1.18/Figure 1.10). BNZ1 highest rate of decay occurred at the transitional layer BNZ1.4 with a rate of 0.00249 ± 0.00011 L mg C^{-1} hr^{-1} at 254 nm. Contrary to CPC1, BNZ1 had the lowest rate of absorbance decay at the top of the core in the active layer with a rate of 0.00108 ± 9.09E-05 L mg C^{-1} hr^{-1}, which is a 73.4% decrease in rates between the two boreal watershed active layers (Table 1.18/Figure 1.10). In this study permafrost

sections at BNZ1 were just as reactive if not more reactive than the active layer segments, ranging from 0.00164 ± 0.000202 L mg C^{-1} hr^{-1} to 0.00214 ± 0.000156 L mg C^{-1} hr^{-1}, which is 40.5% to 65.6% faster rates respectfully (Table 1.18/Figure 1.10). CPC1 only consists of active layer and transient layer and thus has more stability in the rate of absorbance decay. The top half or the core was statistically different from the bottom half of the core but within those halves the two pieces were not statistically different from each other (Table 1.18/Figure 1.10). Quenching hydroxyl radical presented a similar trend in both cores. For CPC1, the highest rate of absorbance decay occurred in the top half of the core with a rate of 0.00181 ± 0.000107 L mg C^{-1} hr^{-1} in segment CPC1.3, which was the bottom half of the top of the core (Table 1.18/Figure 1.11). CPC1 total average for hydroxyl radical quenching absorbed rate of decay is 0.00166 ± 0.000144 L mg C^{-1} hr^{-1} (Table 1.18/Figure 1.11). For BNZ1, the slowest rate of decay still occurred at the top of the core with a rate of 0.00100 ± 9.47E-05 L mg C^{-1} hr^{-1} and the transient segment BNZ1.3 held the highest rates of decay with a rate of 0.00197 ± 0.000311 L mg C^{-1} hr^{-1}. When averaging BNZ1 the average rate came out to be 0.00149 ± 0.000365 L mg C^{-1} hr^{-1}. BNZ1 had more variability quenching of hydroxyl radicals than CPC1 (Table 1.18/Figure 1.11). Since the interest is in hydroxyl radical production, iron was added to the NOM samples during photolysis to determine the rate of decay in absorbance with the promotion of hydroxyl radicals. CPC1 continued to have the highest rate of decay at the top of the core with a rate of 0.000303 ± 0.000334 hr^{-1}, while BNZ1 had the highest rate changed to the bottom of the transient layer (BNZ1.4) with a rate of 0.00379 ± 0.000339 L mg C^{-1} hr^{-1}. Additionally, a decrease in variability in depth was observed in both cores, CPC1 averaged a rate 0.00246 ± 0.000394 L mg C^{-1} hr^{-1}. Meanwhile, BNZ1 averaged a rate of 0.00252 ± 0.000642 L mg C^{-1} hr^{-1}. CPC1 had less variability than BNZ1 in the rate of absorbance decay with promotion of hydroxyl radical, BNZ

is more sensitive to hydroxyl radical production to the NOM rate of decay through photolysis. However, these averages are not statistically different from each other (Table 1.18/Figure 1.11).

Observing the difference between unamended photolysis and amended photolysis allows for the interpretation of how •OH are playing a role in the photolysis of the NOM. Focusing on •OH quenching through the amendment of methanol positive numbers in the differences indicate that natural production of •OH is impacting the photolysis rates of the NOM, the higher the number the more impact •OH is having on the NOM. Negative numbers means the rate of observed absorbance decay is increased in the presence of methanol, so quenching •OH allows for increased photobleaching. If the error associated with the difference in rate exceeds the difference in rate, then the rates are not statistically different. When interpreting difference in rate graphs, if the error bar is larger than the difference in rate then the rate of unamended absorbance decay and methanol amended absorbance decay are not statistically different, and thus, methanol addition does not alter the rate of absorbance decay compared to the unamended photolysis rates. BNZ1 active layer top, transient/permafrost top, and permafrost bottom isolated NOM were not influenced by the addition of methanol to the NOM solutions. Meanwhile the rest of the core segments had positive values with the transient layer (BNZ1.3) and middle of the permafrost (BNZ2.5) having similar differences in rates with the difference being 0.000523 ± 0.000330 L mg C^{-1} hr^{-1} and 0.000527 ± 0.000144 L mg C^{-1} hr^{-1} respectfully (Table 1.18). The observation of differences between two cores in the same area shows the heterogeneity of permafrost NOM reactivity. Crossing over to the second core only one core was analyzed down its entirety due to lack of isolate NOM collected from CPC2 so only CPC1 underwent •OH photolysis experimentation. The difference in rates of unamended photolysis and methanol amended photolysis were greater in the positive direction with a range from 0.000237 ±

0.000135 L mg C^{-1} hr^{-1} for CPC1.5 to 0.000632 ± 0.000135 L mg C^{-1} hr^{-1} for CPC1.2 (Table 1.18). CPC1 while in the same ecosystem of the boreal forest was more susceptible to natural OH production from the active layer.

Meanwhile, when adding an •OH promoter of iron to the NOM solutions a positive number is indicative of photobleaching being slowed by the iron amendment and a negative number photobleaching is enhanced by iron amendment. Negative numbers show that •OH production is enhancing the photobleaching property of the NOM. On average, for all three cores analyzed, the difference between unamended and iron amended photolysis experiments were greater than the difference with methanol amended photolysis samples. For BNZ1, the largest difference in rate occurred in the middle of the core where the transient layer meets permafrost (BNZ1.4) with a rate difference of -0.00165 ± 0.000373 L mg C^{-1} hr^{-1}, so iron amendment enhanced the photobleaching of this segment (Table 1.18). The average rate difference for BNZ1 minus one segment that was not statistically different from the unamended photolysis was -0.000706 ± 0.000576 L mg C^{-1} hr^{-1} (Table 1.18). The percent error showcases the sporadic nature of how iron amendment influenced the rate of absorbance decay, which cannot be explained by a pattern in depth or age. Moving five meters to the second core, the largest difference and segment most influenced by the iron amendment was the top of the permafrost segments (BNZ2.5) with a rate difference of -0.00562 ± 0.000231 L mg C^{-1} hr^{-1} (Table 1.18) The bottom of the core in the permafrost region (BNZ2.6) had a positive difference of 0.000317 ± 0.000286 L mg C^{-1} hr^{-1}, so unlike the bottom of BNZ1 where photolysis was enhanced by the addition of iron, BNZ2 was slowed with the addition of iron into the solution matrix. The active layer of BNZ2 had similar difference in rates to BNZ1 with a difference of -0.000173 ± 0.00027 L mg C^{-1} hr^{-1}. BNZ2 also had variability down the core with an average difference in rate of

-0.00111 ± 0.00253 L mg C^{-1} hr^{-1} (Table 1.18). Finally, CPC1 had the smallest difference in rates however, they were all negative similar to the previous watershed. The second segment in the active layer did not have statistically different unamended rates from iron rates and the other segments had negative rates that were statistically the same as each other with an average difference in rate of -0.000632 ± 9.20E-05 L mg C^{-1} hr^{-1} (Table 1.18).

1.4.3.3.2. Triplet Excited State NOM:

Unlike the steady functional group percentages with depth on CPC1 the reactivity of these NOM isolates varies with depth in regards to ^{3}NOM*. The top of the core was most reactive to ^{3}NOM* production with a rate of 0.00275 ± 0.000194 L mg C^{-1} min^{-1} followed by the bottom or the transient layer of the core with a rate of 0.00243 ± 0.000124 L mg C^{-1} min^{-1} (Table 1.18/Figure 1.13). This variability indicates that the functional group compositions on a finite scale are different than the bulk characterization provided by NMR. While, NMR provides information on the functional group environments, reactivity studies can provide more details on how those functional group environments may vary between samples analyzed. Meanwhile, five meters away from CPC1, CPC2 had the least amount of ^{3}NOM* reactivity at the top of the core with a rate of 0.000705 ± 4.82E-05 L mg C^{-1} min^{-1}; this was the slowest rate of all the core segments (Table 1.18/Figure 1.13). The fastest rate was found in BNZ1 at a spike in the transient layer with a rate of 0.0038414 ± 0.000225 L mg C^{-1} min^{-1}, which is 138.7% faster than the slowest reaction rate (Table 1.18/Figure 1.13). BNZ1 and BNZ2 both have large reactivity spikes in their ^{3}NOM* depth profile. However, this reactivity spike is at different sections and ages in the core with a 0.0038414 ± 0.000225 L mg C^{-1} min^{-1} rate at a transient/permafrost segment with an age of 6,270 years old (BNZ1.4). The secondary spike was found in an active layer segment

only dated to be 4,580 years old (BNZ2.3) and had a rate of 0.00266 ± 0.000207 L mg C^{-1} min^{-1}. Aside from the large spike in reactivity in the transient layer of BNZ1, the rest of the cores rates are slower than BNZ2 with an average of 0.00160 ± 0.00112 L mg C^{-1} min^{-1} while BNZ2 average minus the spike in the active layer segment was 0.00197 ± 0.000393 L mg C^{-1} min^{-1} (Table 1.18/Figure 1.13). BNZ2 also had more stability in rates compared to BNZ1. From observing the PENOM's propensity for ^{3}NOM* production in the presence of sunlight there is a strong variability not only with depth of the NOM but also between each core. This variability is a key indicator that permafrost is not heterogeneous with respect to the production of ^{3}NOM* between watersheds and even between cores that are a matter of meters away from each other.

Similarly, compared to the rates observed in the media leached NOM, the literature reports a range of ^{3}NOM* production rates from 0.00125 L mg C^{-1} min^{-1} to 0.00225 L mg C^{-1} min^{-1} for a river located on the North Slope of Alaska as well as a river located in Georgia had an increased range from 0.0024 to 0.00425 (Cawley et al. 2013). There were no isolated permafrost NOM that exceed the maximum rate compared to the samples analyzed by Cawley et al. (2013) with the highest rate observed in BNZ1.4 at 0.00384 ± 0.000225 L mg C^{-1} min^{-1}. However, lower rates were observed in select isolated NOM, the majority of which were from active layer isolated NOM of BNZ1.1, BNZ1.2, and CPC2.2. These active layer segments all had rates less than 0.00100 L mg C^{-1} min^{-1} and thus, it can be concluded these active layer segments were less reactive to ^{3}NOM* and the functional group composition was not as conducive to the ROS production of ^{3}NOM*.

Observing the rates of ^{3}NOM* in regards to age found that within the same watershed the active layer aged at 1400 – 1460 years old rates of the CPC1.4 and CPC2.4 is 22.4% different from each other (Table 1.19). When observing the ^{3}NOM* rates of older samples, the rates were

less comparable between adjacent cores. The percent differences of these aged segments were as follows, 37.4% for 7,160 – 7,200 years old (BNZ1.6 and BNZ2.6), 30.1% for 6,630 – 6,880 years (BNZ1.5 and BNZ2.5), and 78% for 5,990 – 6,270 years (BNZ1.4 and BNZ2.4). The younger of the two segments tended to have higher rates of ^{3}NOM* production with the exception of 5,990 to 6,270 years where BNZ1 aged at 6,270 years old had a spike in ^{3}NOM* rate.

1.5. Conclusions:

This study showcases that collection and analysis of the surface waters associated with the permafrost location is important to determine the functional group composition of leached organic matter due to leachability of different metals, functional groups, and photoreactive organic matter is dependent upon the leaching media as observed with high salt, basic, and 18.2 MΩ water. Permafrost was determined to be heterogeneous for functional group composition and photoreactivity with carbon age and core location based off of two watershed sampling locations and duplicate cores taken 5 meters apart presenting different results. The isolated permafrost organic matter in these sub-Arctic boreal forest watersheds are photoreactive and in some cases more so than the reference material analyzed.

As for the soils metal concentrations this study observed that the majority of metal concentrations were enhanced with increased depth and carbon age, however these trends were only observed in BNZ watershed due to the broader radiocarbon age range compared to CPC. These metals had such low leachability that a percent leached was unable to be determined due to the error associated with instrumentation overshadowing the percentage. However, observations could be determined that BNZ and CPC leached metals differently and thus, the

complexation to metals on soils were not the same between watersheds. This difference was observed by seeing statistical linear regressions with leachate trace metal analysis of each watershed based on radiocarbon age. BNZ the majority of statistical trends for metals were steady and diminished with increasing age, while CPC majority were steady and enhanced with increasing age. The CPC core segments were younger in age overall and only found in the active layer and thus, hydrology could be a factor in metal transportation and leachability in that watershed.

Future studies should delve into how this heterogeneous organic matter with various leachability based on surface water composition impacts contaminant fate in the boreal forest sub-Arctic environment. As temperatures increase and permafrost thaws organic matter will be released along with the reactive oxygen species produced upon reaction with UV-rays and an influx of metals released into the surface waters, thus potentially altering the fate of contaminants in the environment.

1.6. Acknowledgements:

Funding for portions of this project was supplied by the Alaska Space Grant and National Institutes for Water Resources Graduate Student-Lead Proposal through the Water & Environmental Research Center at UAF and the U.S. Department of Interior – Geological Survey (USGS). A sincere thank you to Jamie Hollingsworth for the assistance of permafrost core sampling and access to the Long-Term Ecological Research Facilities of Bonanza Creek Experimental Forest and Caribou Poker Creek Experimental Watershed. Further thanks to the support or numerous students and collaborators for instrumentation assistance; Karen Spaleta,

Ken Severin, Nathan Graham, Kelly McCarthy, Ruth Osborne (Noratuk), Sara Ewers, Audrey Mutschlecner, Rachel Voight, and Tamara Harms.

1.7. References:

Abouleish, M. Y. Z. and Wells, M. J. M.: Trihalomethane formation potential of aquatic and terrestrial fulvic and humic acids: Examining correlation between specific trihalomethane formation potential and specific ultraviolet absorbance, Environ. Chem., 9, 450–461, doi:10.1071/EN12041, 2012.

Aiken, G. R., McKnight, D. M., Thorn, K. A. and Thurman, E. M.: Isolation of hydrophilic organic acids from water using nonionic macroporous resins, Org. Geochem., 18(4), 567–573, doi:10.1016/0146-6380(92)90119-I, 1992.

Barker, A. J., Douglas, T. A., Jacobson, A. D., McClelland, J. W., Ilgen, A. G., Khosh, M. S., Lehn, G. O. and Trainor, T. P.: Late season mobilization of trace metals in two small Alaskan arctic watersheds as a proxy for landscape scale permafrost active layer dynamics, Chem. Geol., 381, 180–193, doi:10.1016/j.chemgeo.2014.05.012, 2014.

Beckett, R., Jue, Z. and Giddings, J. C.: Determination of Molecular Weight Distributions of Fulvic and Humic Acids Using Flow Field-Flow Fractionation, Environ. Sci. Technol., 21(3), 289–295, doi:10.1021/es00157a010, 1987.

Belshe, E. F., Schuur, E. A. G., Bolker, B. M. and Bracho, R.: Incorporating spatial heterogeneity created by permafrost thaw into a landscape carbon estimate, J. Geophys. Res. Biogeosciences, 117, G01026, doi:10.1029/2011JG001836, 2012.

Blough, N. V. and Zepp, R. G.: Reactive Oxygen Species in Natural Waters, in Active Oxygen in Chemistry, edited by C. S. Foote, J. S. Valentine, A. Greenberg, and J. F. Liebman, pp. 280–333, Chapman & Hall, London., 1995.

Bodhipaksha, L. C., Sharpless, C. M., Chin, Y. P., Sander, M., Langston, W. K. and Mackay, A. A.: Triplet photochemistry of effluent and natural organic matter in whole water and isolates from effluent-receiving rivers, Environ. Sci. Technol., 49, 3453–3463, doi:10.1021/es505081w, 2015.

Bracho, R., Natali, S., Pegoraro, E., Crummer, K. G., Schädel, C., Celis, G., Hale, L., Wu, L., Yin, H., Tiedje, J. M., Konstantinidis, K. T., Luo, Y., Zhou, J. and Schuur, E. A. G.: Temperature sensitivity of organic matter decomposition of permafrost-region soils during laboratory incubations, Soil Biol. Biochem., 97, 1–14, doi:10.1016/j.soilbio.2016.02.008, 2016.

Brown, M.: Transmission spectroscopy examinations of natural waters, Estuar. Coast. Mar. Sci., 5, 309–317, doi:10.1016/0302-3524(77)90058-5, 1977.

Cao, J., Tao, S. and Li, B. G.: Leaching kinetics of water soluble organic carbon (WSOC) from upland soil, Chemosphere, 39(11), 1771–1780, doi:10.1016/S0045-6535(99)00071-5, 1999.

Cao, X., Aiken, G. R., Butler, K. D., Huntington, T. G., Balch, W. M., Mao, J. and Schmidt-Rohr, K.: Evidence for major input of riverine organic matter into the ocean, Org. Geochem., 116, 62–76, doi:10.1016/j.orggeochem.2017.11.001, 2018.

Cawley, K. M., Hakala, J. A. and Chin, Y. P.: Evaluating the triplet state photoreactivity of dissolved organic matter isolated by chromatography and ultrafiltration using an alkylphenol probe molecule, Limnol. Oceanogr. Methods, 7, 391–398, doi:10.4319/lom.2009.7.391, 2009.

Cawley, K. M., McKnight, D. M., Miller, P., Cory, R. M., Fimmen, R. L., Guerard, J. J., Dieser, M., Jaros, C., Chin, Y. P. and Foreman, C.: Characterization of fulvic acid fractions of dissolved organic matter during ice-out in a hyper-eutrophic, coastal pond in Antarctica, Environ. Res. Lett., 8, doi:10.1088/1748-9326/8/4/045015, 2013.

Chalbot, M. C. G., Chitranshi, P., Gamboa da Costa, G., Pollock, E. and Kavouras, I. G.: Characterization of water-soluble organic matter in urban aerosol by 1H-NMR spectroscopy, Atmos. Environ., 128, 235–245, doi:10.1016/j.atmosenv.2015.12.067, 2016.

Chantigny, M. H., Curtin, D., Beare, M. H. and Greenfield, L. G.: Influence of temperature on water-extractable organic matter and ammonium production in mineral soils, Soil Sci. Soc. Am. J., 74, 517–524, doi:10.2136/sssaj2008.0347, 2010.

Chen, H., Yang, Z., Chu, R. K., Tolic, N., Liang, L., Graham, D. E., Wullschleger, S. D. and Gu, B.: Molecular Insights into Arctic Soil Organic Matter Degradation under Warming, Environ. Sci. Technol., 52(8), 4555–4564, doi:10.1021/acs.est.7b05469, 2018.

Chen, Y., Senesi, N. and Schnitzer, M.: Information Provided on Humic Substances by E4/E6 Ratios, Soil Sci. Soc. Am. J., 41, 352–358, doi:10.2136/sssaj1977.03615995004100020037x, 1977.

Chin, Y. P., Alken, G. and O'Loughlin, E.: Molecular Weight, Polydispersity, and Spectroscopic Properties of Aquatic Humic Substances, Environ. Sci. Technol., 28(11), 1853–1858, doi:10.1021/es00060a015, 1994.

Chin, Y. P., Miller, P. L., Zeng, L., Cawley, K. M. and Weavers, L. K.: Photosensitized degradation of bisphenol A by dissolved organic matter, Environ. Sci. Technol., 38(22), 5888–5894, doi:10.1021/es0496569, 2004.

Choi, J. H., Kim, Y. G., Lee, Y. K., Pack, S. P., Jung, J. Y. and Jang, K. S.: Chemical characterization of dissolved organic matter in moist acidic tussock tundra soil using ultra-high resolution 15T FT-ICR mass spectrometry, Biotechnol. Bioprocess Eng., 22, 637–646, doi:10.1007/s12257-017-0121-4, 2017.

Christensen, T. H.: Cadmium soil sorprtion at low concentrations: I. Effect of time, cadium load, pH, and calcium, Water. Air. Soil Pollut., 21, 105–114, 1984.

Cieslewicz, J. and Gonet, S. S.: Properties of humic acids as biomarkers of lake catchment management, Aquat. Sci., 66, 178–184, doi:10.1007/s00027-004-0702-0, 2004.

Claret, F., Schäfer, T., Bauer, A. and Buckau, G.: Generation of humic and fulvic acid from Callovo-Oxfordian clay under high alkaline conditions, Sci. Total Environ., 317, 189–200, doi:10.1016/S0048-9697(03)00337-1, 2003.

Clark Ehlers, G. A., Forrester, S. T., Scherr, K. E., Loibner, A. P. and Janik, L. J.: Influence of the nature of soil organic matter on the sorption behaviour of pentadecane as determined by PLS analysis of mid-infrared DRIFT and solid-state 13C NMR spectra, Environ. Pollut., 158, 285–291, doi:10.1016/j.envpol.2009.07.003, 2010.

Cory, R. M., Miller, M. P., McKnight, D. M., Guerard, J. J. and Miller, P. L.: Effect of instrument-specific response on the analysis of fulvic acid fluorescence spectra, Limnol. Oceanogr. Methods, 8, 67–78, doi:10.4319/lom.2010.8.0067, 2010.

Cory, R. M., Ward, C. P., Crump, B. C. and Kling, G. W.: Sunlight controls water column processing of carbon in arctic frech waters, Science (80-.)., 345(6199), 925–928, doi:10.1126/science.1253119, 2014.

Dittmar, T., Koch, B., Hertkorn, N. and Kattner, G.: A simple and efficient method for the solid-phase extraction of dissolved organic matter (SPE-DOM) from seawater, Limnol. Oceanogr. Methods, 6, 230–235, doi:10.4319/lom.2008.6.230, 2008.

Duarte, R. M. B. O., Santos, E. B. H. and Duarte, A. C.: Spectroscopic characteristics of ultrafiltration fractions of fulvic and humic acids isolated from an eucalyptus bleached Kraft pulp mill effluent, Water Res., 37, 4073–4080, doi:10.1016/S0043-1354(03)00411-1, 2003.

Echevarria, G., Sheppard, M. I. and Morel, J. L.: Effect of pH on the sorption of uranium in soils, J. Environ. Radioact., 53, 257–264, doi:10.1016/S0265-931X(00)00116-8, 2001.

Fram, M. S., Fujii, R., Weishaar, J. L., Bergamaschi, B. a and Aiken, G. R.: How DOC Composition May Explain the Poor Correlation Between Specific Trihalomethane Formation Potential and Specific UV Absorbance, in US Geological Survey Toxics Substances Hydrology Program — Proceedings of the Technical Meeting, pp. 423–430, 1999.

Gabor, R. S., Burns, M. A., Lee, R. H., Elg, J. B., Kemper, C. J., Barnard, H. R. and McKnight, D. M.: Influence of leaching solution and catchment location on the fluorescence of water-soluble organic matter, Environ. Sci. Technol., 49, 4425–4432, doi:10.1021/es504881t, 2015.

Gao, Y., Yan, M. and Korshin, G. V.: Effects of ionic strength on the chromophores of dissolved organic matter, Environ. Sci. Technol., 49, 5905–5912, doi:10.1021/acs.est.5b00601, 2015.

Genc, A. and Ulupinar, E.: Transport of Lead (Pb2+) Ions Through Silty-Clayey Soils Under Acidic Conditions, Transp. Porous Media, 84, 699–709, doi:10.1007/s11242-010-9535-6, 2010.

Gligorovski, S., Strekowski, R., Barbati, S. and Vione, D.: Environmental Implications of Hydroxyl Radicals (•OH), Chem. Rev., 115, 13051–13092, doi:10.1021/cr500310b, 2015.

Grewer, D. M., Lafrenière, M. J., Lamoureux, S. F. and Simpson, M. J.: Redistribution of soil organic matter by permafrost disturbance in the Canadian High Arctic, Biogeochemistry, 128, 397–415, doi:10.1007/s10533-016-0215-7, 2016.

Guerard, J. J.: The Characterization of Dissolved Organic Matter and its Influence on the Photochemical Fate of Antibiotics used in Aquaculture, The Ohio State University., 2009.

Guerard, J. J. and Chin, Y. P.: Photodegradation of ormetoprim in aquaculture and stream-derived dissolved organic matter, J. Agric. Food Chem., 60, 9801–9806, doi:10.1021/jf302564d, 2012.

Guerard, J. J., Chin, Y. P., Mash, H. and Hadad, C. M.: Photochemical fate of sulfadimethoxine in aquaculture waters, Environ. Sci. Technol., 43(22), 8587–8592, doi:10.1021/es9020537, 2009.

Han, R., Lv, J., Luo, L., Wen, B. and Zhang, S.: Molecular-scale investigation of soil fulvic acid and water-extractable organic matter by high-resolution mass spectrometry and 1 H NMR spectroscopy, Environ. Chem., 16, 92–100, doi:10.1071/EN18124, 2019.

Hansen, A. M., Kraus, T. E. C., Pellerin, B. A., Fleck, J. A., Downing, B. D. and Bergamaschi, B. A.: Optical properties of dissolved organic matter (DOM): Effects of biological and photolytic degradation, Limnol. Oceanogr., 61, 1015–1032, doi:10.1002/lno.10270, 2016.

Helms, J. R., Stubbins, A., Ritchie, J. D., Minor, E. C., Kieber, D. J. and Mopper, K.: Absorption spectral slopes and slope ratios as indicators of molecular weight, source, and photobleaching of chromophoric dissolved organic matter, Limonology Oceanogr., 53(3), 955–969, 2008.

Herndon, E. M., Kinsman-Costello, L., Duroe, K. A., Mills, J., Kane, E. S., Sebestyen, S. D., Thompson, A. A. and Wullschleger, S. D.: Iron (Oxyhydr)Oxides Serve as Phosphate Traps in Tundra and Boreal Peat Soils, J. Geophys. Res. Biogeosciences, 124, 227–246, doi:10.1029/2018JG004776, 2019.

Hertkorn, N., Permin, A., Perminova, I., Kovalevskii, D., Yudov, M., Petrosyan, V. and Kettrup, A.: Comparative analysis of partial structures of a peat humic and fulvic acid using one- and two-dimensional nuclear magnetic resonance spectroscopy, in Journal of Environmental Quality, vol. 31, pp. 375–387., 2002.

Heslop, J. K., Chandra, S., Sobzcak, W. V., Davydov, S. P., Davydova, A. I., Spektor, V. V. and Walter Anthony, K. M.: Variable respiration rates of incubated permafrost soil extracts from the Kolyma River lowlands, north-east Siberia, Polar Res., 37(1), doi:10.1080/17518369.2017.1305157, 2017.

Heslop, J. K., Winkel, M., Walter Anthony, K. M., Spencer, R. G. M., Podgorski, D. C., Zito, P., Kholodov, A., Zhang, M. and Liebner, S.: Increasing organic carbon biolability with depth in yedoma permafrost: ramifications for future climate change, J. Geophys. Res. Biogeosciences, 124, 1–18, doi:10.1029/2018jg004712, 2019.

Hicks Pries, C. E., Schuur, E. A. G., Natali, S. M. and Crummer, K. G.: Old soil carbon losses increase with ecosystem respiration in experimentally thawed tundra, Nat. Clim. Chang., 6, 214–218, doi:10.1038/nclimate2830, 2016.

Holden, S. R., Berhe, A. A. and Treseder, K. K.: Decreases in soil moisture and organic matter quality suppress microbial decomposition following a boreal forest fire, Soil Biol. Biochem., 87, 1–9, doi:10.1016/j.soilbio.2015.04.005, 2015.

Huguet, A., Vacher, L., Relexans, S., Saubusse, S., Froidefond, J. M. and Parlanti, E.: Properties of fluorescent dissolved organic matter in the Gironde Estuary, Org. Geochem., 40, 706–719, doi:10.1016/j.orggeochem.2009.03.002, 2009.

Hur, J., Williams, M. A. and Schlautman, M. A.: Evaluating spectroscopic and chromatographic techniques to resolve dissolved organic matter via end member mixing analysis, Chemosphere, 63, 387–402, doi:10.1016/j.chemosphere.2005.08.069, 2006.

Ikeya, K. and Watanabe, A.: Direct expression of an index for the degree of humification of humic acids using organic carbon concentration, Soil Sci. Plant Nutr., 49(1), 47–53, doi:10.1080/00380768.2003.10409978, 2003.

Imai, A., Fukushima, T., Matsushige, K., Kim, Y. H. and Choi, K.: Characterization of dissolved organic matter in effluents from wastewater treatment plants, Water Res., 36, 859–870, doi:10.1016/S0043-1354(01)00283-4, 2002.

Jaffé, R., Boyer, J. N., Lu, X., Maie, N., Yang, C., Scully, N. M. and Mock, S.: Source characterization of dissolved organic matter in a subtropical mangrove-dominated estuary by fluorescence analysis, Mar. Chem., 84, 195–210, doi:10.1016/j.marchem.2003.08.001, 2004.

Jeppu, G. P. and Clement, T. P.: A modified Langmuir-Freundlich isotherm model for simulating pH-dependent adsorption effects, J. Contam. Hydrol., 129–130, 46–53, doi:10.1016/j.jconhyd.2011.12.001, 2012.

Johnson, R. L. and Schmidt-Rohr, K.: Quantitative solid-state 13 C NMR with signal enhancement by multiple cross polarization, J. Magn. Reson., 239, 44–49, doi:10.1016/j.jmr.2013.11.009, 2014.

Kaiser, E., Simpson, A. J., Dria, K. J., Sulzberger, B. and Hatcher, P. G.: Solid-state and multidimensional solution-state NMR of solid phase extracted and ultrafiltered riverine dissolved organic matter, Environ. Sci. Technol., 37(13), 2929–2935, doi:10.1021/es020174b, 2003.

Kim, H. C. and Yu, M. J.: Characterization of aquatic humic substances to DBPs formation in advanced treatment processes for conventionally treated water, J. Hazard. Mater., 143, 486–493, doi:10.1016/j.jhazmat.2006.09.063, 2007.

Kim, S., Kaplan, L. A. and Hatcher, P. G.: Biodegradable dissolved organic matter in a temperate and a tropical stream determined from ultra-high resolution mass spectrometry, Limnol. Oceanogr., 51(2), 1054–1063, doi:10.4319/lo.2006.51.2.1054, 2006.

Kimbrough, D. E., Cohen, Y., Winer, A. M., Creelman, L. and Mabuni, C.: A critical assessment of chromium in the environment, Crit. Rev. Environ. Sci. Technol., 29(1), 1–46, doi:10.1080/10643389991259164, 1999.

Kiss, K., Szalai, Z. Z., Jakab, G., Madarász, B., Zboray, N. N. N., Madarasz, B. and Zboray, N. N. N.: Characterization of Soil Organic Substances by UV-Vis Spectrophotometry in Some Soils of Hungary, in Soil Carbon, edited by A. . Hartemink and K. McSweeney, pp. 127–136, Springer., 2014.

Kitis, M., Karanfil, T., Wigton, A. and Kilduff, J. E.: Probing reactivity of dissolved organic matter for disinfection by-product formation using XAD-8 resin adsorption and ultrafiltration fractionation, Water Res., 36, 3834–3848, doi:10.1016/S0043-1354(02)00094-5, 2002.

Kitis, M., Karanfil, T. and Kilduff, J. E.: The reactivity of dissolved organic matter for disinfection by-product formation, Turkish J. Eng. Environ. Sci., 28, 167–179, doi:10.3906/sag-1207-67, 2004.

Korshin, G., Chow, C. W. K., Fabris, R. and Drikas, M.: Absorbance spectroscopy-based examination of effects of coagulation on the reactivity of fractions of natural organic matter with varying apparent molecular weights, Water Res., 43, 1541–1548, doi:10.1016/j.watres.2008.12.041, 2009.

Korshin, G. V., Benjamin, M. M. and Li, C.-W.: Use of differential spectroscopy to evaluate the structure and reactivity of humics, Water Sci. Technol., 40(9), 9–16 [online] Available from: https://iwaponline.com/wst/article-pdf/40/9/9/36923/9.pdf (Accessed 16 April 2020), 1999.

Ter Laak, T. L., Gebbink, W. A. and Tolls, J.: The effect of pH and ionic strength on the sorption of sulfachloropyridazine, tylosin, and oxytetracycline to soil, Environ. Toxicol. Chem., 25(4), 904–911, doi:10.1897/05-232R.1, 2006.

Lam, B. and Simpson, A. J.: Direct 1H NMR spectroscopy of dissolved organic matter in natural waters, Analyst, 133, 263–269, doi:10.1039/B713457F, 2008.

Lamhonwah, D., Lafrenière, M. J., Lamoureux, S. F. and Wolfe, B. B.: Evaluating the hydrological and hydrochemical responses of a High Arctic catchment during an exceptionally warm summer, Hydrol. Process., 31, 2296–2313, doi:10.1002/hyp.11191, 2017.

Lang, K., Wagnerová, D. M., Klementová, Š. and Kubát, P.: Humic substances - Excited states, quenching by metal ions, and photosensitized degradation of chlorophenols, Collect. Czechoslov. Chem. Commun., 62, 1159–1168, doi:10.1135/cccc19971159, 1997.

Lertpaitoonpan, W., Ong, S. K. and Moorman, T. B.: Effect of organic carbon and pH on soil sorption of sulfamethazine, Chemosphere, 76, 558–564, doi:10.1016/j.chemosphere.2009.02.066, 2009.

Li, A., Hu, J., Li, W., Zhang, W. and Wang, X.: Polarity based fractionation of fulvic acids, Chemosphere, 77, 1419–1426, doi:10.1016/j.chemosphere.2009.09.002, 2009.

Li, P. and Hur, J.: Utilization of UV-Vis spectroscopy and related data analyses for dissolved organic matter (DOM) studies: A review, Crit. Rev. Environ. Sci. Technol., 47(3), 131–154, doi:10.1080/10643389.2017.1309186, 2017.

Li, Y., Harir, M., Uhl, J., Kanawati, B., Lucio, M., Smirnov, K. S., Koch, B. P., Schmitt-Kopplin, P. and Hertkorn, N.: How representative are dissolved organic matter (DOM) extracts? A comprehensive study of sorbent selectivity for DOM isolation, Water Res., 116, 316–323, doi:10.1016/j.watres.2017.03.038, 2017.

Luster, J., Lloyd, T., Sposito, G. and Fry, I. V.: Multi-wavelength molecular fluorescence spectrometry for quantitative characterization of copper(II) and aluminum(III) complexation by dissolved organic matter, Environ. Sci. Technol., 30(5), 1565–1574, doi:10.1021/es950542u, 1996.

Ma, H., Allen, H. E. and Yin, Y.: Characterization of isolated fractions of dissolved organic matter from natural waters and a wastewater effluent, Water Res., 35(4), 985–996, doi:10.1016/S0043-1354(00)00350-X, 2001.

Maizel, A. C., Li, J. and Remucal, C. K.: Relationships between Dissolved Organic Matter Composition and Photochemistry in Lakes of Diverse Trophic Status, Environ. Sci. Technol., 51, 9624–9632, doi:10.1021/acs.est.7b01270, 2017.

Mao, J., Chen, N. and Cao, X.: Characterization of humic substances by advanced solid state NMR spectroscopy: Demonstration of a systematic approach, Org. Geochem., 42, 891–902, doi:10.1016/j.orggeochem.2011.03.023, 2011.

Mao, J., Kong, X., Schmidt-Rohr, K., Pignatello, J. J. and Perdue, E. M.: Advanced solid-state NMR characterization of marine dissolved organic matter isolated using the coupled reverse osmosis/electrodialysis method, Environ. Sci. Technol., 46, 5806–5814, doi:10.1021/es300521e, 2012.

McKnight, D. M., Boyer, E. W., Westerhoff, P. K., Doran, P. T., Kulbe, T. and Andersen, D. T.: Spectrofluorometric characterization of dissolved organic matter for indication of precursor organic material and aromaticity, Limnol. Oceanogr., 46(1), 38–48, doi:10.4319/lo.2001.46.1.0038, 2001.

McNamara, J. P., Kane, D. L. and Hinzman, L. D.: Hydrograph separations in an Arctic watershed using mixing model and graphical techniques, Water Resour. Res., 33(7), 1707–1719, doi:10.1029/97WR01033, 1997.

Miller, P. L. and Chin, Y. P.: Photoinduced degradation of carbaryl in a wetland surface water, J. Agric. Food Chem., 50(23), 6758–6765, doi:10.1021/jf025545m, 2002.

Mobed, J. J., Hemmingsen, S. L., Autry, J. L. and Mcgown, L. B.: Fluorescence characterization of IHSS humic substances: Total luminescence spectra with absorbance correction, Environ. Sci. Technol., 30(10), 3061–3065, doi:10.1021/es960132l, 1996.

Mueller, C. W., Rethemeyer, J., Kao-Kniffin, J., Löppmann, S., Hinkel, K. M. and Bockheim, J. G.: Large amounts of labile organic carbon in permafrost soils of northern Alaska, Glob. Chang. Biol., 21, 2804–2817, doi:10.1111/gcb.12876, 2015.

Müller, M. B., Fritz, W., Lankes, U. and Frimmel, F. H.: Ultrafiltration of Nonionic Surfactants and Dissolved Organic Matter, Environ. Sci. Technol., 38(4), 1124–1132, doi:10.1021/es0300416, 2004.

Mutschlecner, A. E., Guerard, J. J., Jones, J. B. and Harms, T. K.: Phosphorus Enhances Uptake of Dissolved Organic Matter in Boreal Streams, Ecosystems, 21, 675–688, doi:10.1007/s10021-017-0177-1, 2018a.

Mutschlecner, A. E., Guerard, J. J., Jones, J. B. and Harms, T. K.: Regional and intra-annual stability of dissolved organic matter composition and biolability in high-latitude Alaskan rivers, Limnol. Oceanogr., 63, 1605–1621, doi:10.1002/lno.10795, 2018b.

Naidu, R., Bolan, N. S., Kookana, R. S. and Tiller, K. G.: Ionic-strength and pH effects on the sorption of cadium and the surface charge of soils, Eur. J. Soil Sci., 45, 419–429, 1994.

Ohno, T.: Fluorescence inner-filtering correction for determining the humification index of dissolved organic matter, Environ. Sci. Technol., 36(4), 742–746, doi:10.1021/es0155276, 2002.

Page, S. E., Arnold, W. A. and McNeill, K.: Assessing the contribution of free hydroxyl radical in organic matter-sensitized photohydroxylation reactions, Environ. Sci. Technol., 45, 2818–2825, doi:10.1021/es2000694, 2011.

Painter, S. L., Moulton, J. D. and Wilson, C. J.: Modeling Challenges for predicting hydrologic response to degrading permafrost, Hydrogeol. J., 21, 221–224, doi:10.1007/s10040-012-0917-4, 2013.

Pardo, M. T., Guadalix, M. E. and Garcia-Gonzalez, M. T.: Effect of pH and background electrolyte on P sorption by variable charge soils, Geoderma, 54, 275–282, doi:10.1016/0016-7061(92)90109-K, 1992.

Parlanti, E., Wörz, K., Geoffroy, L. and Lamotte, M.: Dissolved organic matter fluorescence spectroscopy as a tool to estimate biological activity in a coastal zone submitted to anthropogenic inputs, Org. Geochem., 31, 1765–1781, doi:10.1016/S0146-6380(00)00124-8, 2000.

Pedersen, J. A., Simpson, M. A., Bockheim, J. G. and Kumar, K.: Characterization of soil organic carbon in drained thaw-lake basins of Arctic Alaska using NMR and FTIR photoacoustic spectroscopy, Org. Geochem., 42, 947–954, doi:10.1016/j.orggeochem.2011.04.003, 2011.

Pegoraro, E., Mauritz, M., Bracho, R., Ebert, C., Dijkstra, P., Hungate, B. A., Konstantinidis, K. T., Luo, Y., Schädel, C., Tiedje, J. M., Zhou, J. and Schuur, E. A. G.: Glucose addition increases the magnitude and decreases the age of soil respired carbon in a long-term permafrost incubation study, Soil Biol. Biochem., 129, 201–211, doi:10.1016/j.soilbio.2018.10.009, 2019.

Pengerud, A., Dignac, M. F., Certini, G., Strand, L. T., Forte, C. and Rasse, D. P.: Soil organic matter molecular composition and state of decomposition in three locations of the European Arctic, Biogeochemistry, 135, 277–292, doi:10.1007/s10533-017-0373-2, 2017.

Perminova, I. V., Dubinenkov, I. V., Kononikhin, A. S., Konstantinov, A. I., Zherebker, A. Y., Andzhushev, M. A., Lebedev, V. A., Bulygina, E., Holmes, R. M., Kostyukevich, Y. I., Popov, I. A. and Nikolaev, E. N.: Molecular Mapping of Sorbent Selectivities with Respect to Isolation of Arctic Dissolved Organic Matter as Measured by Fourier Transform Mass Spectrometry, Environ. Sci. Technol., 48, 7461–7468, doi:10.1021/es5015423, 2014.

Pernet-Coudrier, B., Varrault, G., Saad, M., Croue, J. P., Dignac, M. F. and Mouchel, J. M.: Characterisation of dissolved organic matter in Parisian urban aquatic systems: Predominance of hydrophilic and proteinaceous structures, Biogeochemistry, 106, 89–106, doi:10.1007/s10533-010-9480-z, 2011.

Petrone, K. C., Jones, J. B., Hinzman, L. D. and Boone, R. D.: Seasonal export of carbon, nitrogen, and major solutes from Alaskan catchments with discontinuous permafrost, J. Geophys. Res. Biogeosciences, 111, 1–13, doi:10.1029/2005JG000055, 2006.

Peuravuori, J. and Pihlaja, K.: Molecular size distribution and spectroscopic properties of aquatic humic substances, Anal. Chim. Acta, 337, 133–149, doi:10.1016/S0003-2670(96)00412-6, 1997.

Plaza, C., Pegoraro, E., Bracho, R., Celis, G., Crummer, K. G., Hutchings, J. A., Hicks Pries, C. E., Mauritz, M., Natali, S. M., Salmon, V. G., Schädel, C., Webb, E. E. and Schuur, E. A. G. G.: Direct observation of permafrost degradation and rapid soil carbon loss in tundra, Nat. Geosci., 12, 627–631, doi:10.1038/s41561-019-0387-6, 2019.

Pokrovsky, O. S., Bueno, M., Manasypov, R. M., Shirokova, L. S., Karlsson, J. and Amouroux, D.: Dissolved Organic Matter Controls Seasonal and Spatial Selenium Concentration Variability in Thaw Lakes across a Permafrost Gradient, Environ. Sci. Technol., 52, 10254–10262, doi:10.1021/acs.est.8b00918, 2018.

Polyakov, V., Orlova, K. and Abakumov, E.: Soils of the Lena River Delta, Yakutia, Russia: Diversity, Characteristics and Humic Acids Molecular Composition, Polarforschung, 88(2), 135–150, doi:10.2312/polarforschung.88.2.135, 2018.

Poulin, B. A., Ryan, J. N. and Aiken, G. R.: Effects of iron on optical properties of dissolved organic matter, Environ. Sci. Technol., 48, 10098–10106, doi:10.1021/es502670r, 2014.

Qualls, R. G. and Haines, B. L.: Biodegradability of dissolved organic matter in forest throughfall, soil solution, and stream water, Soil Sci. Soc. Am. J., 56, 578–586, doi:10.2136/sssaj1992.03615995005600020038x, 1992.

Raudina, T. V., Loiko, S. V., Lim, A., Manasypov, R. M., Shirokova, L. S., Istigechev, G. I., Kuzmina, D. M., Kulizhsky, S. P., Vorobyev, S. N. and Pokrovsky, O. S.: Permafrost thaw and climate warming may decrease the CO2, carbon, and metal concentration in peat soil waters of the Western Siberia Lowland, Sci. Total Environ., 634, 1004–1023, doi:10.1016/j.scitotenv.2018.04.059, 2018.

Raven, K. P., Jain, A. and Loeppert, R. H.: Arsenite and arsenate adsorption on ferrihydrite: Kinetics, equilibrium, and adsorption envelopes, Environ. Sci. Technol., 32(3), 344–349, doi:10.1021/es970421p, 1998.

Rember, R. D. and Trefry, J. H.: Increased concentrations of dissolved trace metals and organic carbon during snowmelt in rivers of the alaskan arctic, Geochim. Cosmochim. Acta, 68(3), 477–489, doi:10.1016/S0016-7037(03)00458-7, 2004.

Rodríguez, F. J., Schlenger, P. and García-Valverde, M.: A comprehensive structural evaluation of humic substances using several fluorescence techniques before and after ozonation. Part I: Structural characterization of humic substances, Sci. Total Environ., 476–477, 718–730, doi:10.1016/j.scitotenv.2013.11.150, 2014.

Rodríguez, F. J., Schlenger, P. and García-Valverde, M.: Monitoring changes in the structure and properties of humic substances following ozonation using UV-Vis, FTIR and 1H NMR techniques, Sci. Total Environ., 541, 623–637, doi:10.1016/j.scitotenv.2015.09.127, 2016.

Romanovsky, V. E., Gruber, S., Jin, H., Marchenko, S. S., Smith, S. L., Trombotto, D. and Walter, K. M.: Frozen Ground, in Global Outlook for Ice & Snow, pp. 411–419, Elsevier B.V., 2011.

Rosario-Ortiz, F. L. and Canonica, S.: Probe compounds to assess the photochemical activity of dissolved organic matter, Environ. Sci. Technol., 50, 12532–12547, doi:10.1021/acs.est.6b02776, 2016.

Sanderman, J., Farrell, M., Macreadie, P. I., Hayes, M., McGowan, J. and Baldock, J.: Is demineralization with dilute hydrofluoric acid a viable method for isolating mineral stabilized soil organic matter?, Geoderma, 304, 4–11, doi:10.1016/j.geoderma.2017.03.002, 2017.

Santos, L., Pinto, A., Filipe, O., Cunha, Â., Santos, E. B. H. and Almeida, A.: Insights on the optical properties of estuarine DOM - Hydrological and biological influences, edited by C.-L. Lee, PLoS One, 11(5), e0154519, doi:10.1371/journal.pone.0154519, 2016.

Schädel, C., Koven, C. D., Lawrence, D. M., Celis, G., Garnello, A. J., Hutchings, J., Mauritz, M., Natali, S. M., Pegoraro, E., Rodenhizer, H., Salmon, V. G., Taylor, M. A., Webb, E. E., Wieder, W. R. and Schuur, E. A. G.: Divergent patterns of experimental and model-derived permafrost ecosystem carbon dynamics in response to Arctic warming, Environ. Res. Lett., 13, 105002, doi:10.1088/1748-9326/aae0ff, 2018.

Schuur, E. A. G., McGuire, A. D., Schädel, C., Grosse, G., Harden, J. W., Hayes, D. J., Hugelius, G., Koven, C. D., Kuhry, P., Lawrence, D. M., Natali, S. M., Olefeldt, D., Romanovsky, V. E., Schaefer, K., Turetsky, M. R., Treat, C. C. and Vonk, J. E.: Climate change and the permafrost carbon feedback, Nature, 520, 171–179, doi:10.1038/nature14338, 2015.

Seifert, A. G., Roth, V. N., Dittmar, T., Gleixner, G., Breuer, L., Houska, T. and Marxsen, J.: Comparing molecular composition of dissolved organic matter in soil and stream water: Influence of land use and chemical characteristics, Sci. Total Environ., 571, 142–152, doi:10.1016/j.scitotenv.2016.07.033, 2016.

Shur, Y., Hinkel, K. M. and Nelson, F. E.: The transient layer: Implications for geocryology and climate-change science, Permafr. Periglac. Process., 16, 5–17, doi:10.1002/ppp.518, 2005.

Spencer, R. G. M., Bolton, L. and Baker, A.: Freeze/thaw and pH effects on freshwater dissolved organic matter fluorescence and absorbance properties from a number of UK locations, Water Res., 41, 2941–2950, doi:10.1016/j.watres.2007.04.012, 2007.

Świetlik, J. and Sikorska, E.: Characterization of natural organic matter fractions by high pressure size-exclusion chromatography, specific UV absorbance and total luminescence spectroscopy, Polish J. Environ. Stud., 15(1), 145–153, 2006.

Taş, N., Prestat, E., McFarland, J. W., Wickland, K. P., Knight, R., Berhe, A. A., Jorgenson, T., Waldrop, M. P. and Jansson, J. K.: Impact of fire on active layer and permafrost microbial communities and metagenomes in an upland Alaskan boreal forest, ISME J., 8, 1904–1919, doi:10.1038/ismej.2014.36, 2014.

Throckmorton, H. M., Newman, B. D., Heikoop, J. M., Perkins, G. B., Feng, X., Graham, D. E., O'Malley, D., Vesselinov, V. V., Young, J., Wullschleger, S. D. and Wilson, C. J.: Active layer hydrology in an arctic tundra ecosystem: quantifying water sources and cycling using water stable isotopes, Hydrol. Process., 30, 4972–4986, doi:10.1002/hyp.10883, 2016.

Uyguner, C. S. and Bekbolet, M.: Evaluation of humic acid photocatalytic degradation by UV-vis and fluorescence spectroscopy, Catal. Today, 101, 267–274, doi:10.1016/j.cattod.2005.03.011, 2005.

Uyguner, C. S., Hellriegel, C., Otto, W. and Larive, C. K.: Characterization of humic substances: Implications for trihalomethane formation, Anal. Bioanal. Chem., 378, 1579–1586, doi:10.1007/s00216-003-2451-7, 2004.

Vonk, J. E., Mann, P. J., Dowdy, K. L., Davydova, A., Davydov, S. P., Zimov, N., Spencer, R. G. M., Bulygina, E. B., Eglinton, T. I. and Holmes, R. M.: Dissolved organic carbon loss from Yedoma permafrost amplified by ice wedge thaw, Environ. Res. Lett., 8, doi:10.1088/1748-9326/8/3/035023, 2013.

Waldrop, M. P., Wickland, K. P., White, R., Berhe, A. A., Harden, J. W. and Romanovsky, V. E.: Molecular investigations into a globally important carbon pool: Permafrost-protected carbon in Alaskan soils, Glob. Chang. Biol., doi:10.1111/j.1365-2486.2009.02141.x, 2010.

Walter Anthony, K., Daanen, R., Anthony, P., Schneider Von Deimling, T., Ping, C. L., Chanton, J. P. and Grosse, G.: Methane emissions proportional to permafrost carbon thawed in Arctic lakes since the 1950s, Nat. Geosci., 9, 679–682, doi:10.1038/ngeo2795, 2016.

Wan, D., Sharma, V. K., Liu, L., Zuo, Y. and Chen, Y.: Mechanistic Insight into the Effect of Metal Ions on Photogeneration of Reactive Species from Dissolved Organic Matter, Environ. Sci. Technol., 53, 5778–5786, doi:10.1021/acs.est.9b00538, 2019.

Wang, L., Wu, F., Zhang, R., Li, W. and Liao, H.: Characterization of dissolved organic matter fractions from Lake Hongfeng, Southwestern China Plateau, J. Environ. Sci., 21, 581–588, doi:10.1016/S1001-0742(08)62311-6, 2009.

Ward, C. P. and Cory, R. M.: Chemical composition of dissolved organic matter draining permafrost soils, Geochim. Cosmochim. Acta, 167, 63–79, doi:10.1016/j.gca.2015.07.001, 2015.

Ward, C. P. and Cory, R. M.: Complete and Partial Photo-oxidation of Dissolved Organic Matter Draining Permafrost Soils, Environ. Sci. Technol., 50, 3545–3553, doi:10.1021/acs.est.5b05354, 2016.

Weishaar, J. L., Aiken, G. R., Bergamaschi, B. A., Fram, M. S., Fujii, R. and Mopper, K.: Evaluation of specific ultraviolet absorbance as an indicator of the chemical composition and reactivity of dissolved organic carbon, Environ. Sci. Technol., 37, 4702–4708, doi:10.1021/es030360x, 2003.

Westerhoff, P., Aiken, G., Amy, G. and Debroux, J.: Relationships between the structure of natural organic matter and its reactivity towards molecular ozone and hydroxyl radicals, Water Res., 33(10), 2265–2276, doi:10.1016/S0043-1354(98)00447-3, 1999.

Wickland, K. P., Aiken, G. R., Striegl, R. G., Waldrop, M. P., Koch, J. C. and Jorgenson, M. T.: Dissolved organic carbon and nitrogen release from boreal Holocene permafrost and seasonally frozen soils of Alaska, Environ. Res. Lett., 13, 065011, doi:10.1088/1748-9326/aac4ad, 2018.

Wilson, H. F. and Xenopoulos, M. A.: Effects of agricultural land use on the composition of fluvial dissolved organic matter, Nat. Geosci., 2, 37–41, doi:10.1038/ngeo391, 2009.

Wong, H., Mok, K. M. and Fan, X. J.: Natural organic matter and formation of trihalomethanes in two water treatment processes, Desalination, 210, 44–51, doi:10.1016/j.desal.2006.05.031, 2007.

Woo, M. K.: Permafrost hydrology, Springer-Verlag Berlin Heidelberg., 2012.

Xi, J., He, M. and Lin, C.: Adsorption of antimony(V) on kaolinite as a function of pH, ionic strength and humic acid, Environ. Earth Sci., 60, 715–722, doi:10.1007/s12665-009-0209-z, 2010.

You, S. J., Yin, Y. and Allen, H. E.: Partitioning of organic matter in soils: Effects of pH and water/soil ratio, Sci. Total Environ., 227, 155–160, doi:10.1016/S0048-9697(99)00024-8, 1999.

Zhang, Z., Kane, D. L. and Hinzman, L. D.: Development and application of a spatially-distributed arctic hydrological and thermal process model (ARHYTHM), Hydrol. Process., 14, 1017–1044, doi:10.1002/(SICI)1099-1085(20000430)14:6<1017::AID-HYP982>3.0.CO;2-G, 2000.

Zherebker, A., Podgorski, D. C., Kholodov, V. A., Orlov, A. A., Yaroslavtseva, N. V., Kharybin, O., Kholodov, A., Spector, V., Spencer, R. G. M., Nikolaev, E. and Perminova, I. V.: The Molecular Composition of Humic Substances Isolated From Yedoma Permafrost and Alas Cores in the Eastern Siberian Arctic as Measured by Ultrahigh Resolution Mass Spectrometry, J. Geophys. Res. Biogeosciences, 124, doi:10.1029/2018jg004743, 2019.

Zhou, Z., Hua, B., Cao, X., Yang, J., Olk, D. C., Deng, B., Liu, F., Li, R. and Mao, J.: Chemical composition of dissolved organic matter from various sources as characterized by solid-state NMR, Aquat. Sci., 77, 595–607, doi:10.1007/s00027-015-0405-8, 2015.

Zsolnay, Á.: Dissolved organic matter: Artefacts, definitions, and functions, Geoderma, 113, 187–209, doi:10.1016/S0016-7061(02)00361-0, 2003.

1.8. Figures:

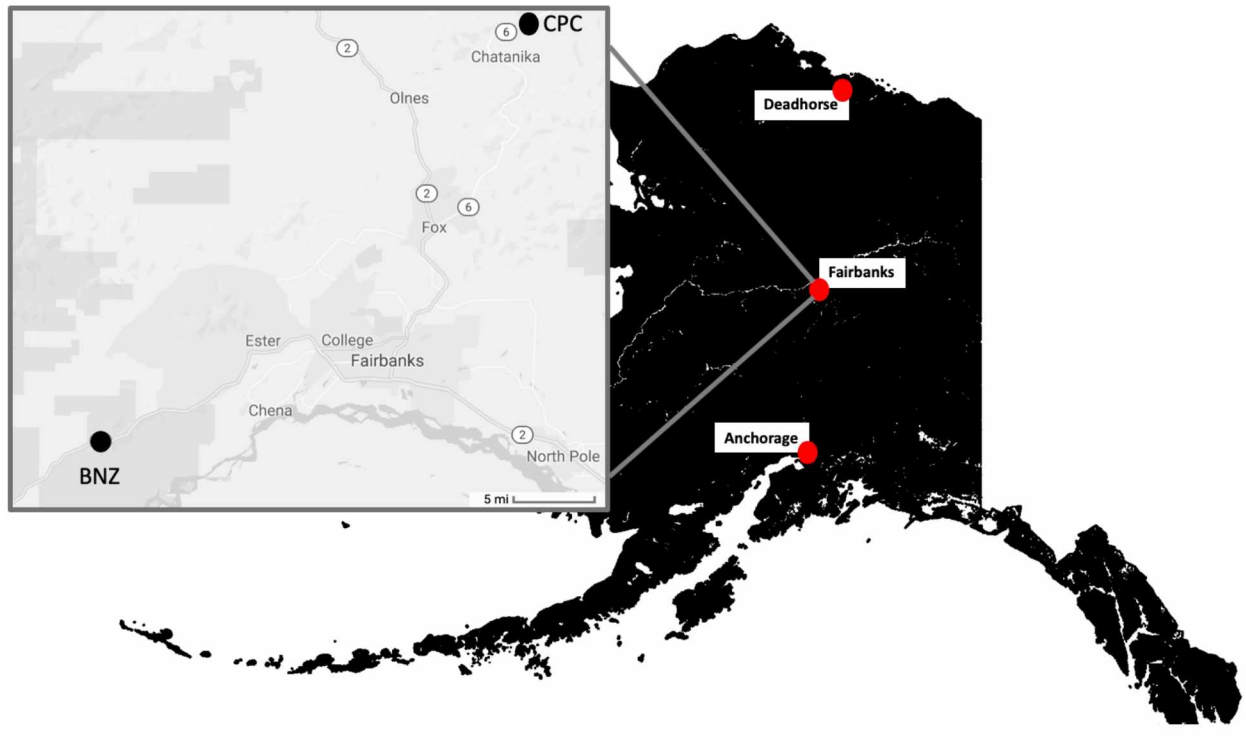

Figure 1.1: Sampling Site for Permafrost Cores

Map of sampling locations in Fairbanks, Alaska.

Figure 1.2: Permafrost Core from BNZ Site

Partial soil core from BNZ, which was wrapped in plastic wrap and placed on an aluminum foil wrapped acrylonitrile butadiene styrene (ABS) pipe sawed in half for transport and storage.

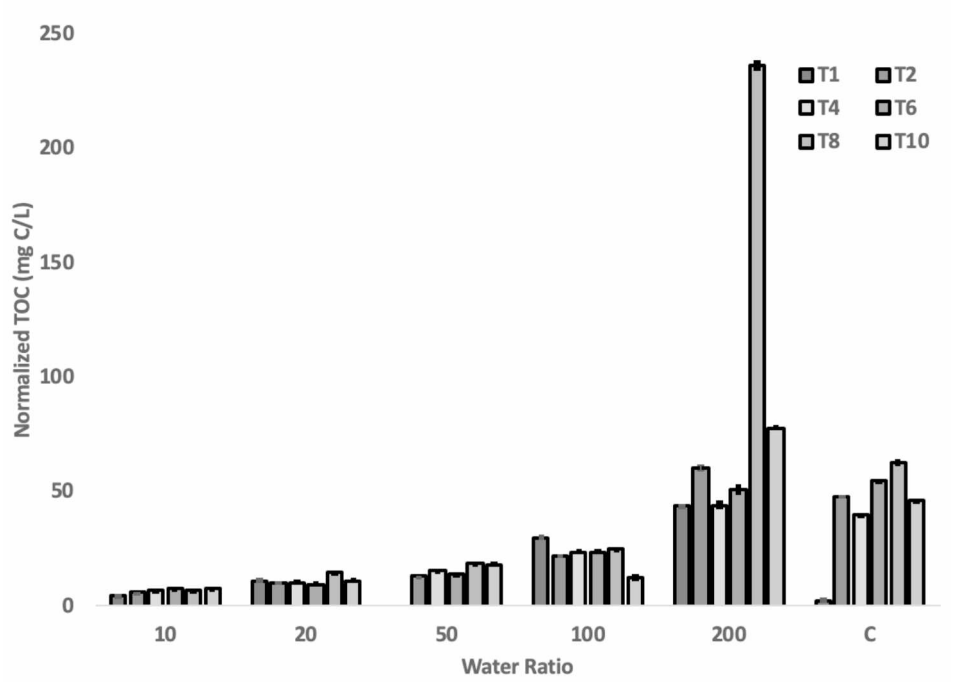

Figure 1.3: Carbon Concentration for Various Soil:Water

Total Organic Carbon in mg C L^{-1} for each ratio of soil to oH10 water; 1:10, 1:20, 1:50, 1:100, and 1:200, along with a control of 10 MΩ water at 1:200. Leachate was collected every other day with the exception of day one and day two. All values were corrected for dilution with 1:200 being a dilution factor of 1 and 1:10 being a dilution factor of 0.05.

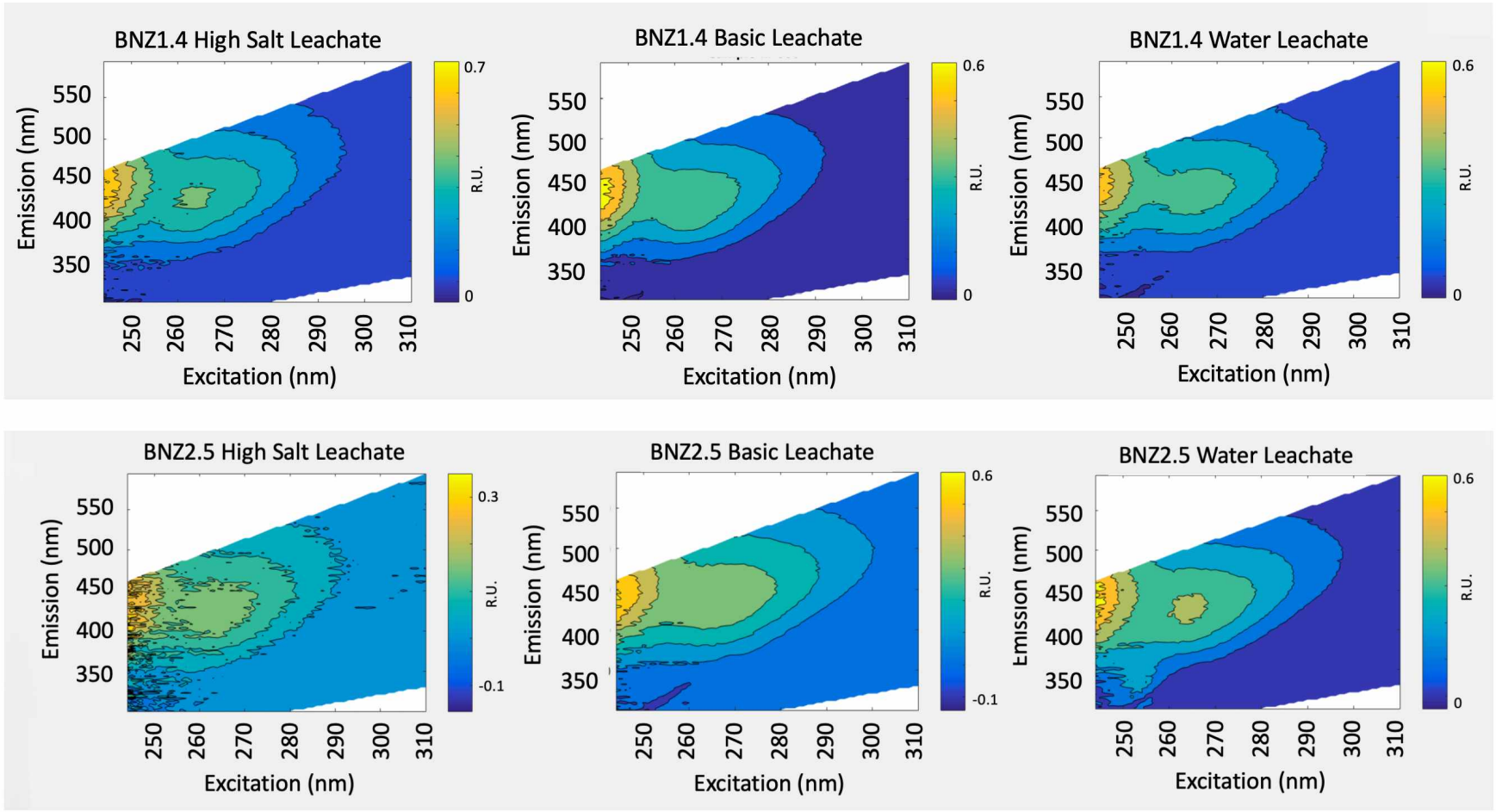

Figure 1.4: Media Leachate Fluorescence EEMs

Excitation – Emission Matrices (EEMs) collected on media leachate, showcasing that different leachate media.

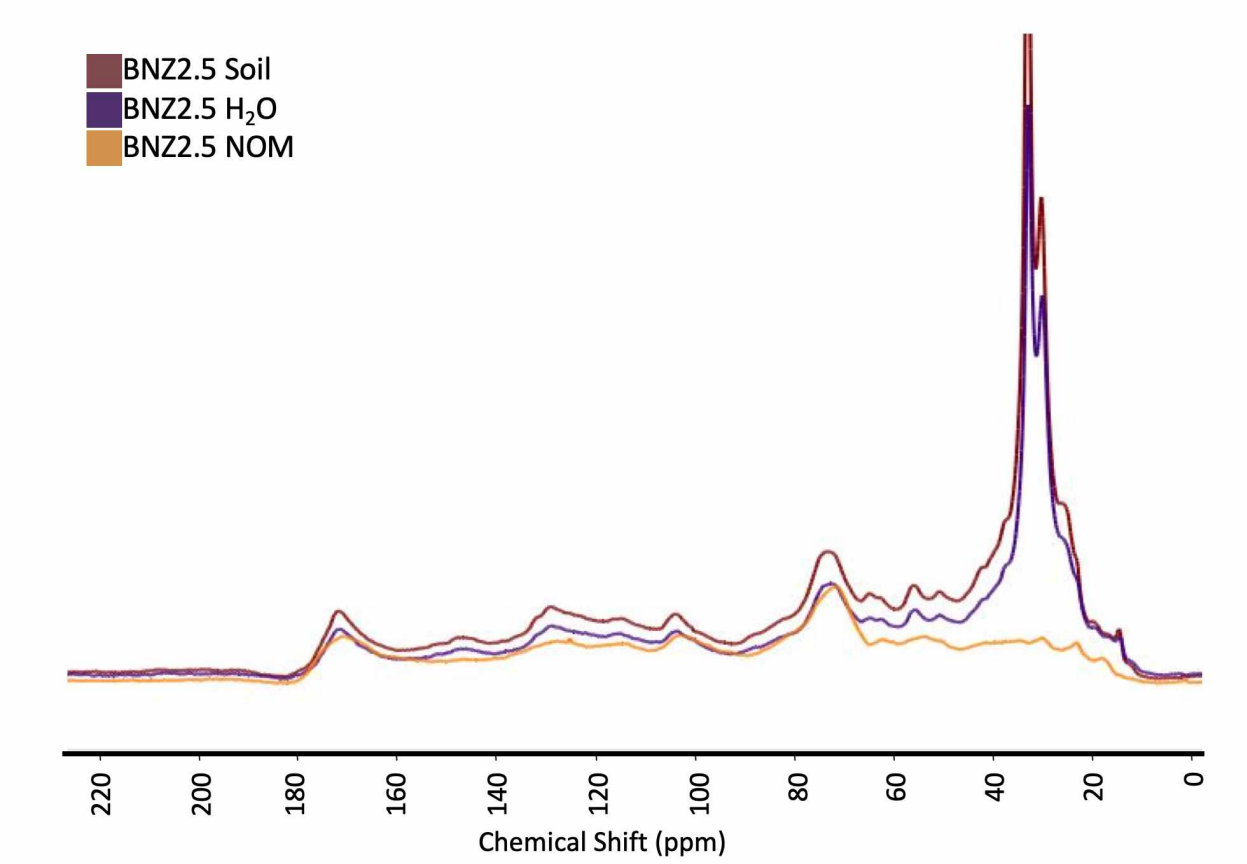

Figure 1.5: Soil Comparison to Leached Soil and NOM ^{13}C NMR Spectra

^{13}C Multi-CP MAS NMR spectra from before leaching (BNZ2.5 Soil), after leaching (BNZ2.5 H_2O), and NOM Isolated material (BNZ2.5 NOM) run on a 600 MHz Bruker NMR. ^{13}C spectra was processed by MestreNova Suite.

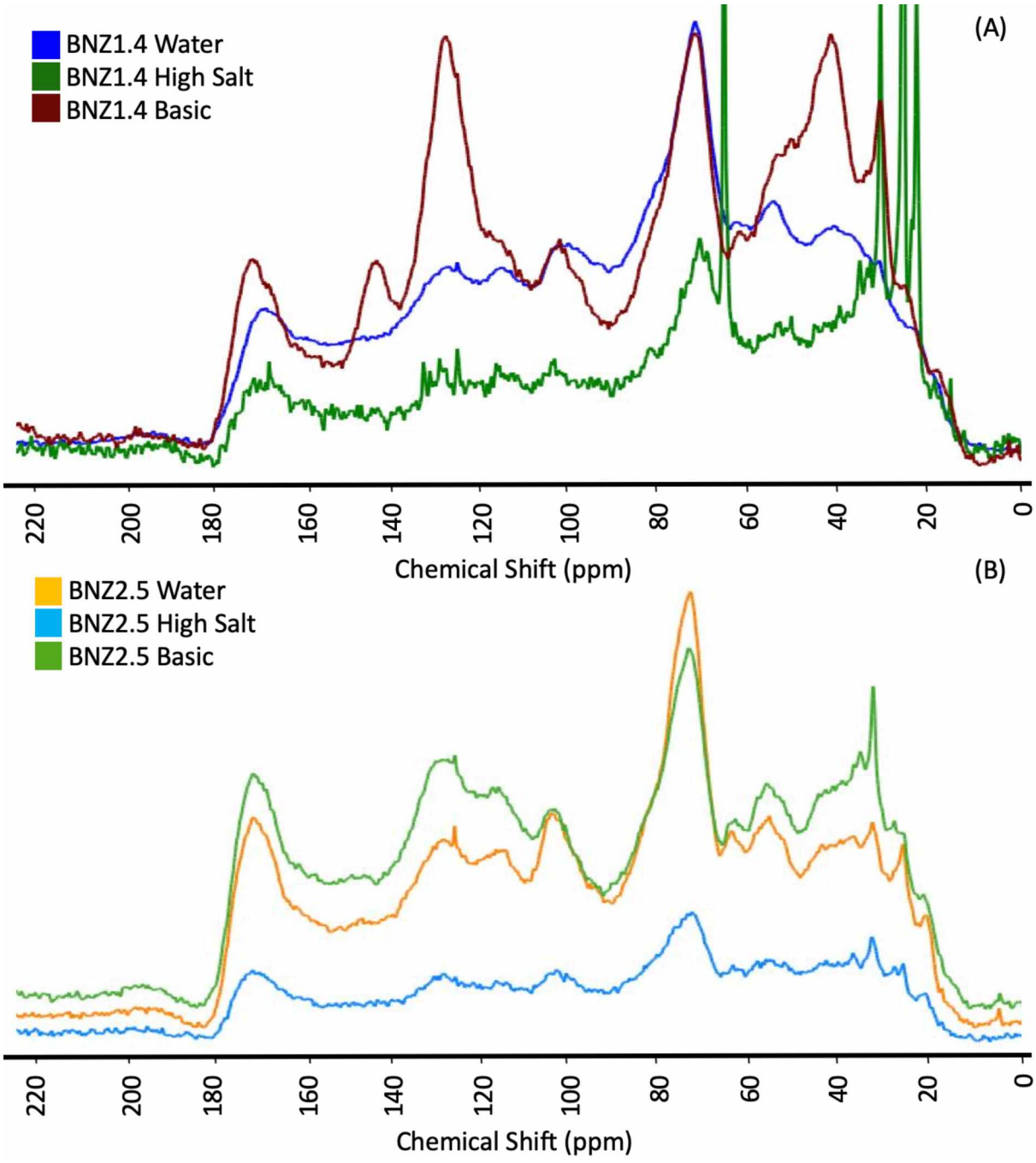

Figure 1.6: Media Leached NOM ^{13}C NMR Spectra

^{13}C Multi-CP MAS NMR spectra of isolated NOM from all three leaching media experiments run on a 600 MHz Bruker NMR. ^{13}C spectra was processed by MestreNova Suite.

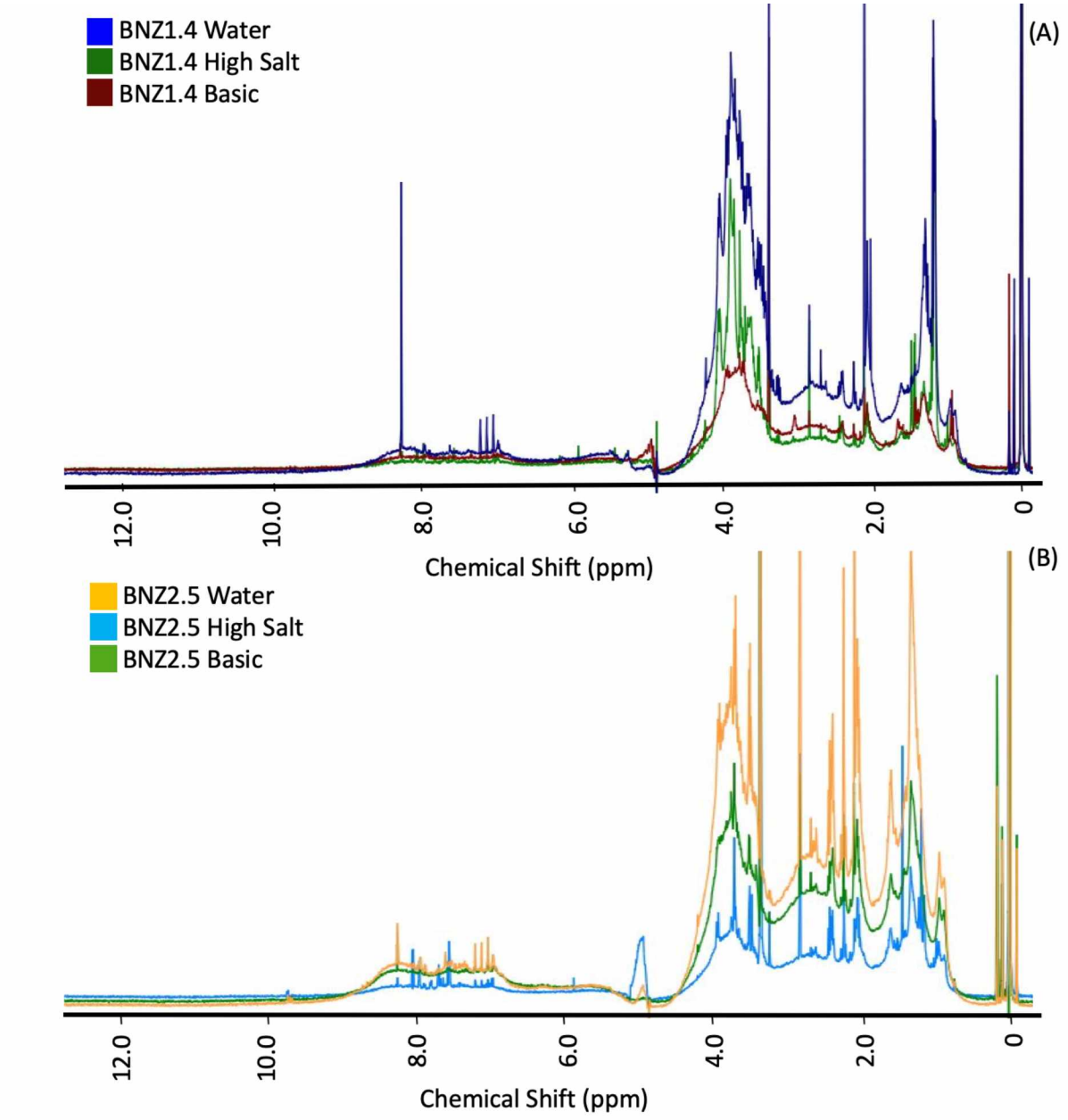

Figure 1.7: Media Leached NOM ^{1}H NMR Spectra

^{1}H NMR of 1mg NOM reconstituted in H_2O with a D_2O/TSP insert run on a 600 MHz Bruker NMR with SPR-WATERGATE water suppression technique. (A) BNZ1.4 isolated NOM from water, K_2SO_4, and pH 10 conditions. (B) BNZ2.5 isolated NOM from water, K_2SO_4, and pH 10 conditions. ^{1}H spectra were processed by MestreNova Suite.

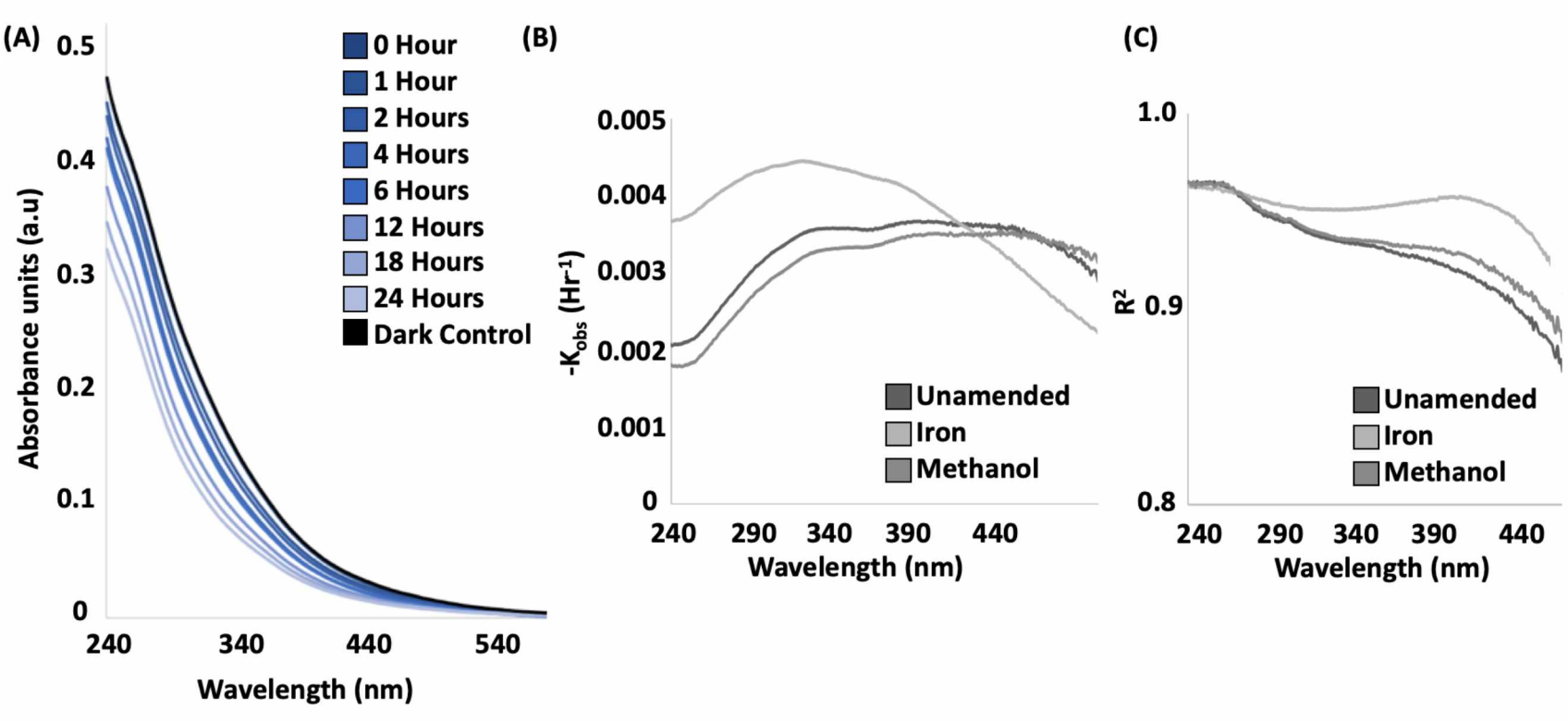

Figure 1.8: Absorbance Decay UV-Vis Graph

BNZ1.4 H_2O NOM reconstituted into a 10 mg C L^{-1} water solution an irradiated with UV light over a 24-hour span of time with different amendments to probe for •OH reactivity. (A) Absorbance decay over time in solar simulator, (B) rate of decay per wavelength for unamended, iron, and methanol amended samples, and (C) R^2 for the rate of decay values closer to 1 indicate a pseudo 1st order reaction.

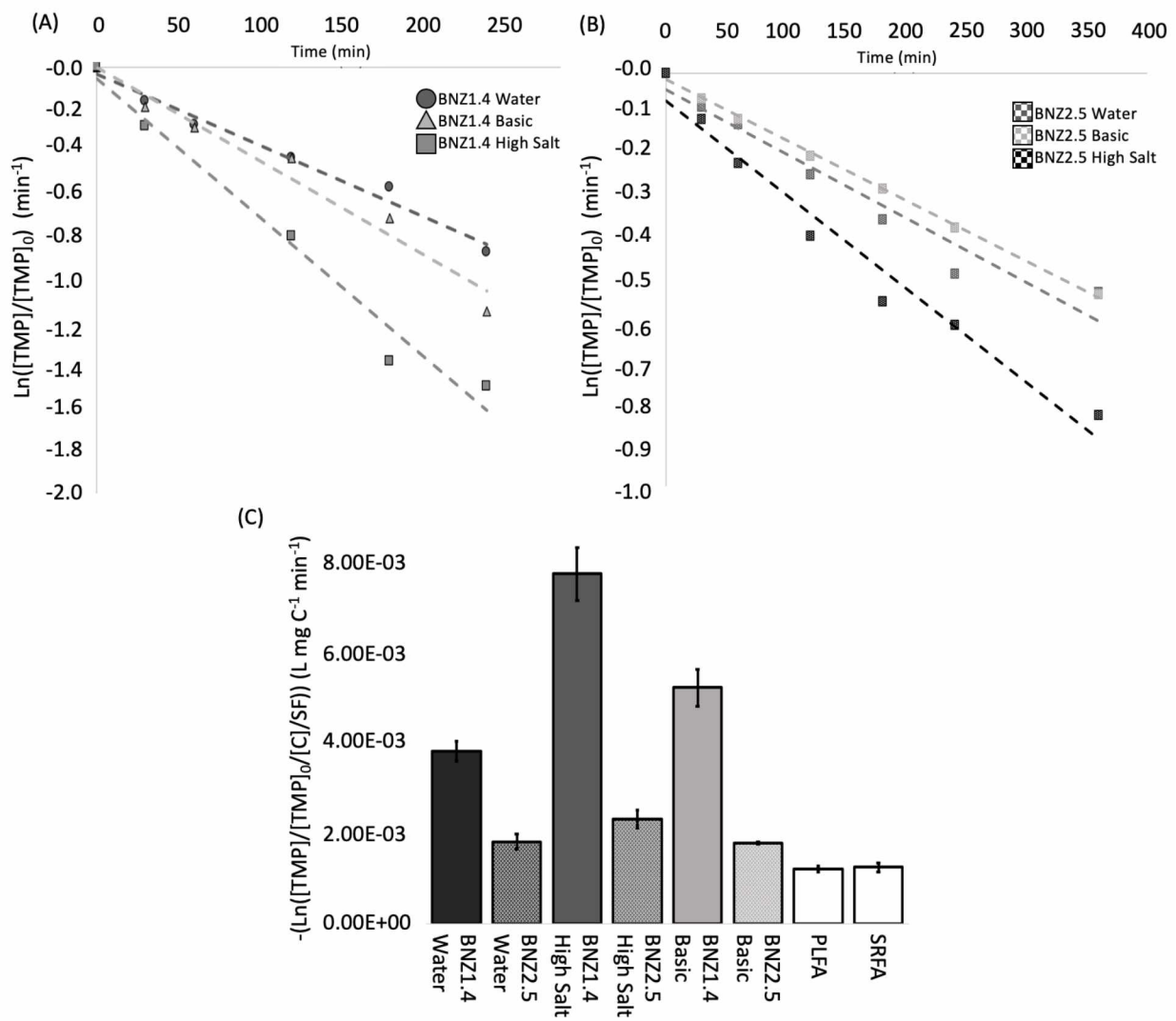

Figure 1.9: Media Leached NOM TMP Rate of Decay and ^{3}NOM* Rate of Production

(A) TMP loss represented from a decrease in fluorescence signal at λ_{ex} = 230 nm and λ_{em} = 305 nm for BNZ1.4 isolated NOM from various media (B) TMP loss represented from a decrease in fluorescence signal at λ_{ex} = 230 nm and λ_{em} = 305 nm for BNZ2.5 isolated NOM from various media. The concentration of TMP is determined through the use of a calibration curve ranging from 0.01uM to 30uM. Decay was normalized to carbon content of NOM solution. Each trendline represents the rate of TMP with the slope. (C) Bar graph shows absolute rate of TMP decay (^{3}NOM* production) screening factor normalized and associated error within the slope.

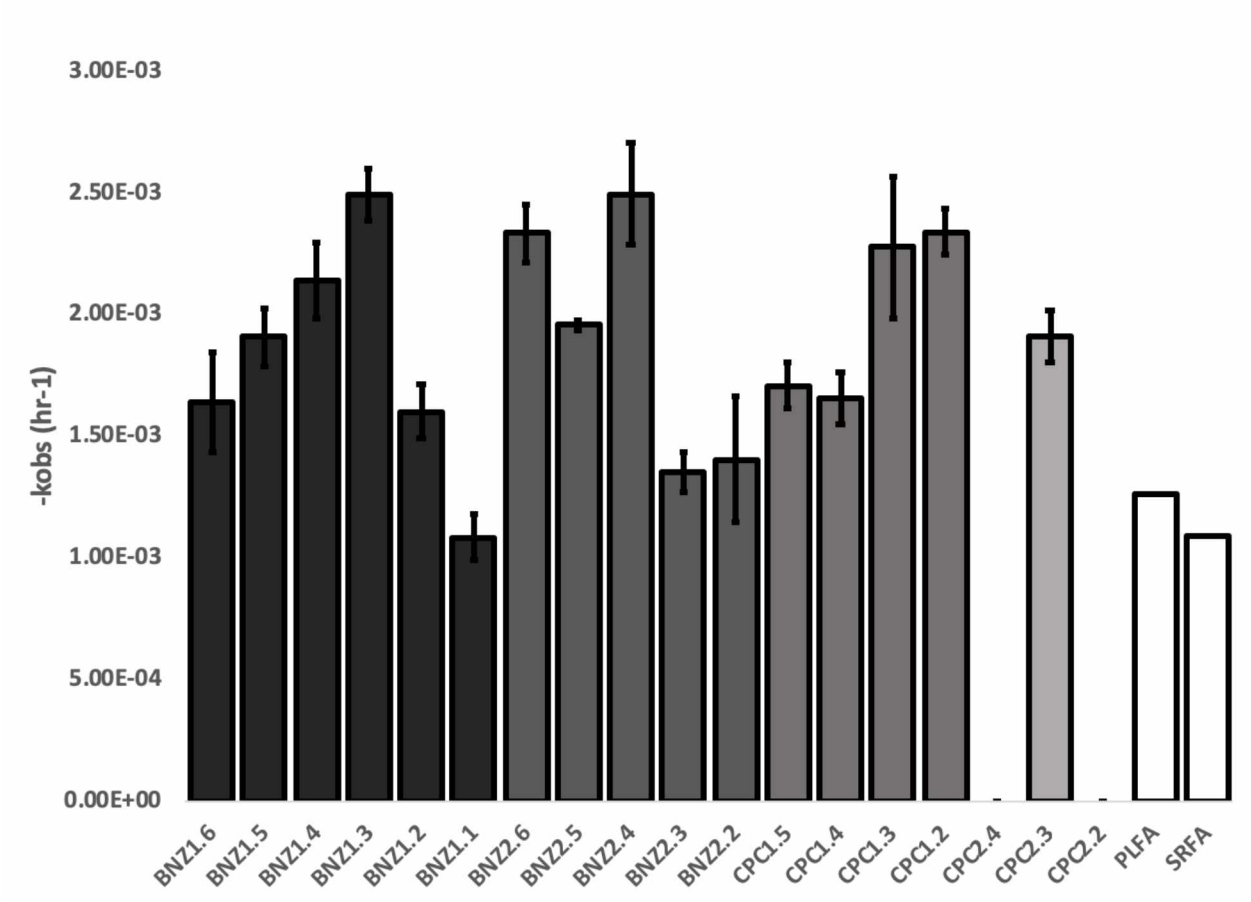

Figure 1.10: Unamended Photolysis Absorbance Decay Rate Graph

Rate of absorbance photolytic decay from unamended 10 mg C L^{-1} NOM solutions after being irradiated in an ATLAS Suntest for 24 hours. Error bars are the standard deviation between the duplicates run simultaneously. Rates were normalized to carbon content and screening ability of the NOM solution. CPC2.4 and CPC2.2 NOM isolates were unable to be reconstituted to appropriate concentrations.

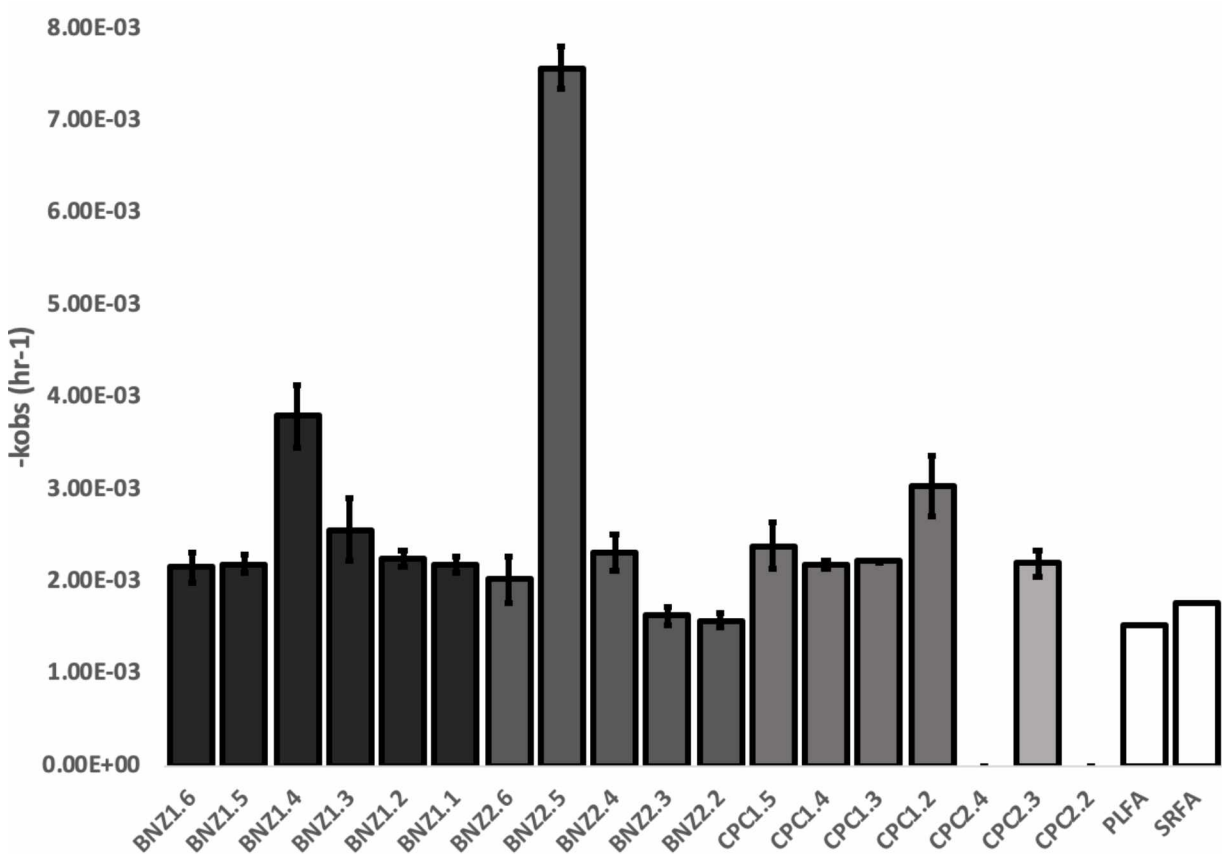

Figure 1.11: •OH Quenching Photolysis Absorbance Decay Rate Graph

Rate of absorbance photolytic decay from $FeCl_3$ amended 10 mg C L^{-1} NOM solutions after being irradiated in an ATLAS Suntest for 24 hours. Error bars are the standard deviation between the duplicates run simultaneously. Rates were normalized to carbon content and screening ability of the NOM solution. CPC2.4 and CPC2.2 NOM isolates were unable to be reconstituted to appropriate concentrations.

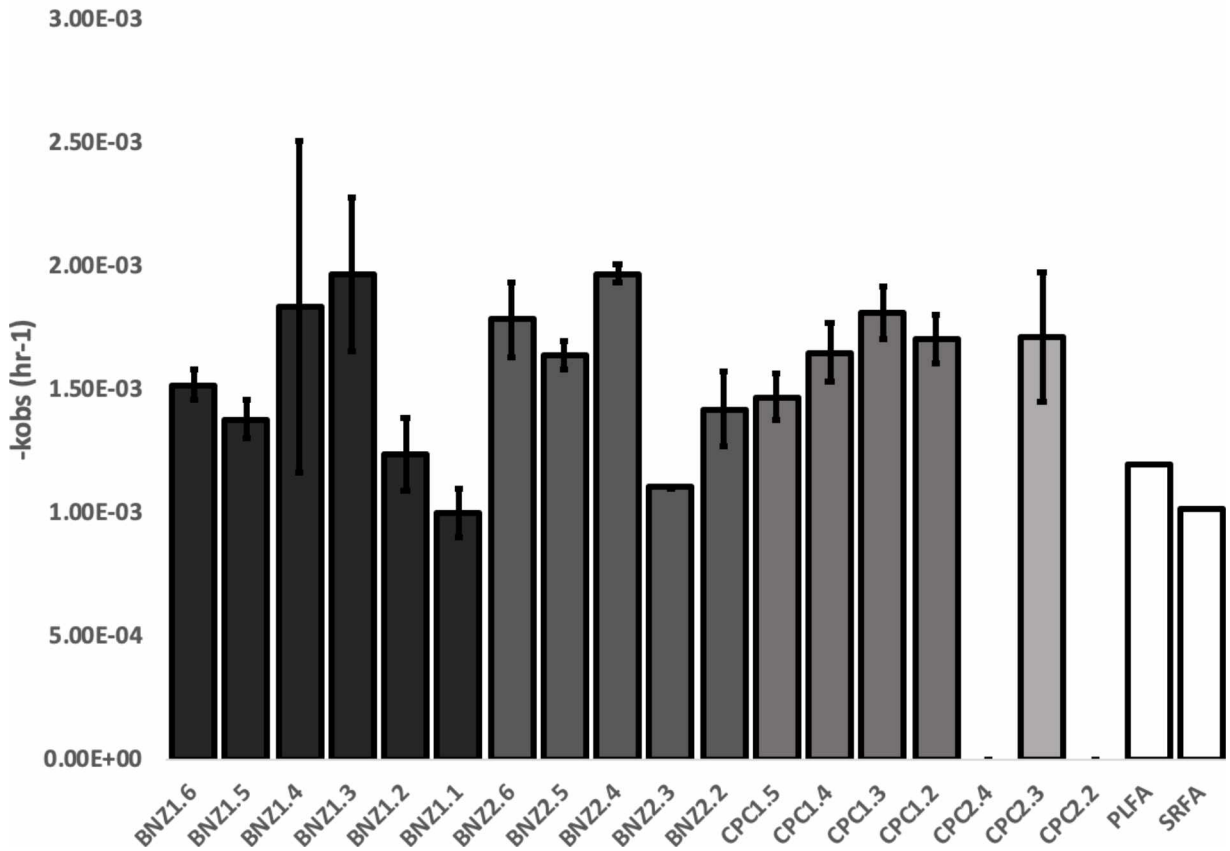

Figure 1.12: •OH Promotion Photolysis Absorbance Decay Rate Graph

Rate of absorbance photolytic decay from Methanol amended 10 mg C L^{-1} NOM solutions after being irradiated in an ATLAS Suntest for 24 hours. Error bars are the standard deviation between the duplicates run simultaneously. Rates were normalized to carbon content and screening ability of the NOM solution. CPC2.4 and CPC2.2 NOM isolates were unable to be reconstituted to appropriate concentrations.

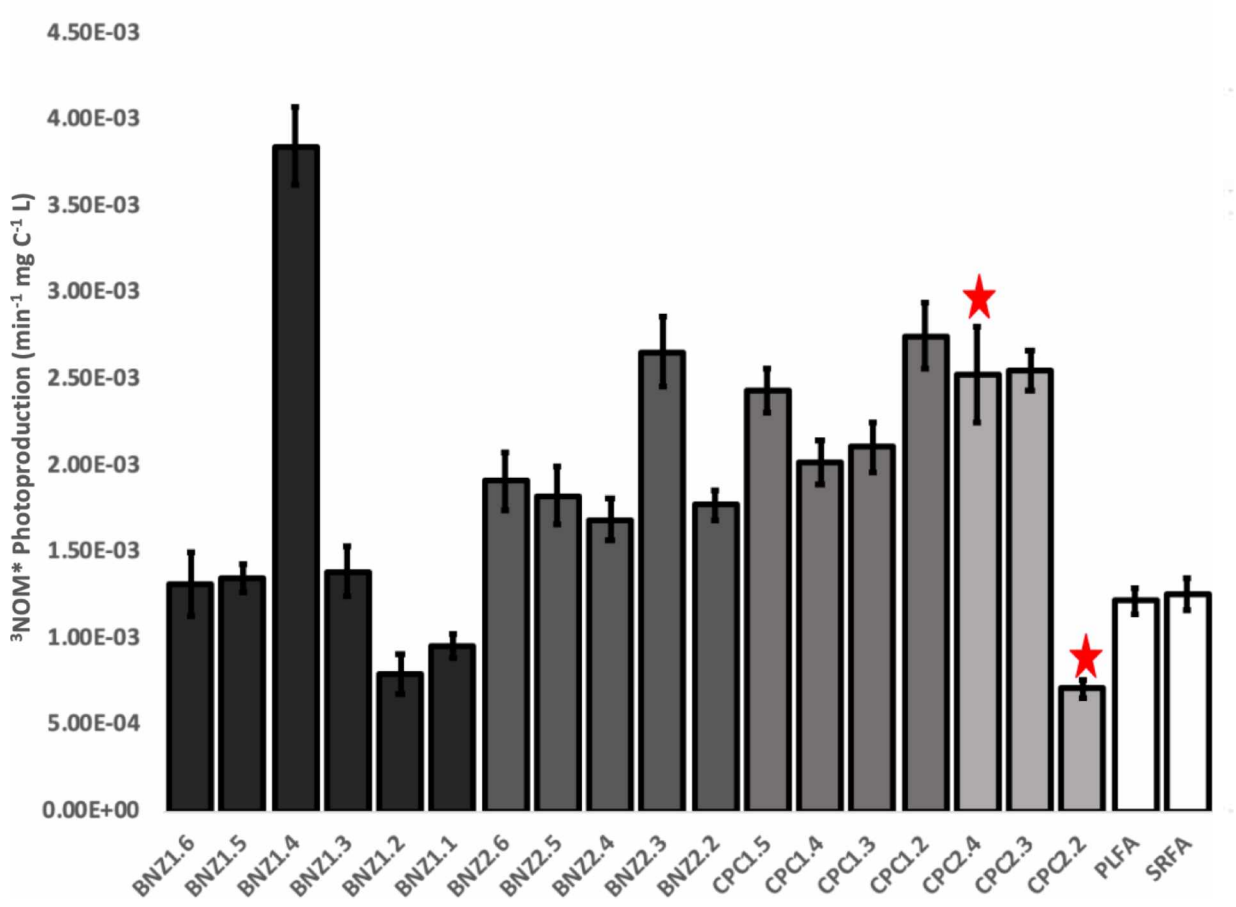

Figure 1.13: ^{3}NOM* Production Rate Graph

Absolute value of TMP decay as an indicator for 3NOM* production over time. Rates were normalized to carbon content and screening ability of the NOM solution run during unamended photolysis. Starred sampled were not corrected for screen factor, average screening factor was determined to be 0.881.

1.9. Tables:

Table 1.1: Optical Indices Informational Table for UV-Vis

Compiled optical indices equations and correlations utilized to interpret UV-Vis spectrum of leachate composition, along with references.

UV Absorbance Index	Abbrev-iation	Equation	Correlated with	Reference
Specific UV absorbance	$SUVA_{254}$	$\frac{Abs_{254nm}}{[Carbon]}$	Positive to molecular weight, positively to aromaticity, negatively to aliphatics	(Abouleish and Wells, 2012; Chin et al., 1994; Fram et al., 1999; Hansen et al., 2016; Imai et al., 2002; Kim and Yu, 2007; Kim et al., 2006; Kitis et al., 2002, 2004; Korshin et al., 1999, 2009; Müller et al., 2004; Pernet-Coudrier et al., 2011; Peuravuori and Pihlaja, 1997; Rodriguez et al., 2016; Świetlik and Sikorska, 2006; Uyguner and Bekbolet, 2005; Weishaar et al., 2003; Wong et al., 2007)
Specific UV absorbance	$SUVA_{280}$	$\frac{Abs_{280nm}}{[Carbon]}$	Positive to molecular weight, positively to aromaticity, negatively to aliphatics	(Chin et al., 1994; Hansen et al., 2016; Peuravuori and Pihlaja, 1997; Rodriguez et al., 2016; Uyguner and Bekbolet, 2005; Wang et al., 2009)
Spectral Slope Ratio	S_R	$\frac{Slope(LN(Abs_{275-295nm}))\ (nm^{-1})}{Slope(LN(Abs_{350-400nm}))\ (nm^{-1})}$	Negatively to molecular weight, increases with irradiation,	(Hansen et al., 2016; Helms et al., 2008; Li and Hur, 2017; Rodriguez et al., 2016)
Absorbance Ratio	E2:E3	$\frac{Abs_{250nm}}{Abs_{365nm}}$	Negatively to molecular weight	(Brown, 1977; Duarte et al., 2003; Guo and Chorover, 2003; Helms et al., 2008; Li et al., 2009; Peuravuori and Pihlaja, 1997; Rodriguez et al., 2016; Santos et al., 2016; Wang et al., 2009)
Absorbance Ratio	E2:E4	$\frac{Abs_{254nm}}{Abs_{436nm}}$	Positively correlated with soil humic acid of high lignin type compounds,	(Battin, 1998; Blough and Zepp, 1995; Cieslewicz and Gonet, 2004; Hur et al., 2006; Jaffé et al., 2004; Li and Hur, 2017; Rodríguez et al., 2016)
Absorbance Ratio	E2:E6	$\frac{Abs_{280nm}}{Abs_{665nm}}$	Positively correlated with soil humic acid of high lignin type compounds, degree of humification	(Chen et al., 1977; Cieslewicz and Gonet, 2004; Li and Hur, 2017; Rodríguez et al., 2016)
Absorbance Ratio	E4:E6	$\frac{Abs_{465nm}}{Abs_{665nm}}$	Negatively to molecular weight, positively to sediment humic acids, negatively with humification	(Brown, 1977; Chen et al., 1977; Chin et al., 1994; Claret et al., 2005; Kiss et al., 2014; Ma et al., 2001; Peuravuori and Pihlaja, 1997; Rodriguez et al., 2016; Stevenson, 1994; Uyguner et al., 2004; You et al., 1999)

Table 1.2: Optical Indices Informational Table for Fluorescence

Optical indices equations for correlations for interpretation of fluorescence excitation – emission matrices, along with references.

Fluorescence Index	Abbrev-iation	Equation	Correlated with	Reference
Fluorescence Index	FI	$\frac{Em_{470nm}@Ex_{370nm}}{Em_{520nm}@Ex_{370nm}}$	Source determination of microbial and terrestrial input.	(Cory et al., 2010b; Hansen et al., 2016; Kim et al., 2006; McKnight et al., 2001; Rodríguez et al., 2014, 2016)
Humification Index	HIX	$\frac{Area(Em_{435-480nm})@Ex_{254nm}}{Area(Em_{300-354nm}+Em_{435-480nm})@Ex_{254nm}}$	Indication of humification extent	(Gabor et al., 2015; Hansen et al., 2016; Ohno, 2002)
Freshness Index	α:β	$\frac{Em_{380nm}@Ex_{310nm}}{MAX(Em_{410-435nm})@Ex_{310nm}}$	How recently NOM was produced through recent degradation.	(Hansen et al., 2016; Parlanti et al., 2000; Wilson and Xenopoulos, 2009)
Biological Index	BIX	$\frac{Em_{380nm}@Ex_{310nm}}{Em_{430nm}@Ex_{310nm}}$	How recently NOM was produced through recent degradation.	(Hansen et al., 2016; Huguet et al., 2009)

Table 1.3: General Soil Characterization

General soil characterization including radiocarbon dating, depth, and soil layer type. Carbon to Nitrogen ratio was determined by Elemental Analyzer and the percent leachable carbon was determined through the comparison of soil carbon concentration and leachate carbon concentration (Equation 4). Determination of pH followed EPA method 9045D. Depths that have "N/A" were due to the core structure failure during freeze drying.

Sample Name	Radio Carbon Date	Radio Carbon Date Error	Moisture Percentage	Depth (cm)	Layer Type	C:N	C:N STD	Percent Leachable Carbon	Leachable Carbon Error	pH	pH Error
BNZ1.6	7200	40	52%	120	P	10.46	0.23	3%	1%	5.87	0.01
BNZ1.5	6880	30	46%	N/A	P	11.23	0.62	9%	2%	5.60	0.01
BNZ1.4	6270	30	48%	60	P/T	19.71	0.11	1%	1%	5.50	0.01
BNZ1.3	N/A	N/A	39%	N/A	T	22.67	0.03	0%	2%	5.38	0.04
BNZ1.2	N/A	N/A	29%	N/A	A	9.27	0.63	53%	2%	N/A	N/A
BNZ1.1	2520	25	52%	N/A	A	9.46	1.36	86%	1%	5.22	N/A
Average						**13.80**	**0.50**	**25%**	**1%**	**5.51**	**0.02**
STD						**5.84**	**0.49**	**36%**	**1%**	**0.24**	**0.02**
BNZ2.6	7160	35	75%	120	P	17.24	0.00	3%	1%	5.40	0.04
BNZ2.5	6630	30	65%	60	P/T	22.47	0.16	2%	1%	N/A	N/A
BNZ2.4	5990	30	N/A	N/A	T	23.73	0.10	1%	1%	5.40	0.01
BNZ2.3	4580	20	N/A	N/A	A	15.71	0.37	3%	2%	5.11	N/A
BNZ2.2	1550	15	N/A	N/A	A	13.79	0.33	16%	1%	4.88	0.02
Average						**18.59**	**0.19**	**5%**	**1%**	**5.20**	**0.02**
STD						**4.32**	**0.16**	**6%**	**0%**	**0.25**	**0.02**
CPC1.5	1590	20	58%	76	T	33.38	0.13	0%	2%	5.67	0.01
CPC1.4	1460	15	57%	66	A	24.51	0.24	1%	1%	5.54	0.02
CPC1.3	1330	20	52%	43	A	18.98	0.00	0%	4%	5.45	0.03
CPC1.2	75	15	48%	22	A	24.50	0.34	1%	1%	5.59	0.11
Average						**25.34**	**0.18**	**1%**	**2%**	**5.56**	**0.04**
STD						**5.96**	**0.15**	**0%**	**2%**	**0.09**	**0.04**
CPC2.4	1400	15	51%	90	T	44.41	0.97	0%	1%	5.36	N/A
CPC2.3	N/A	N/A	54%	59	A	21.63	0.17	1%	3%	5.29	0.04
CPC2.2	865	15	45%	29	A	24.31	0.17	1%	6%	5.02	0.01
Average						**30.12**	**0.44**	**1%**	**3%**	**5.22**	**0.02**
STD						**12.46**	**0.46**	**0%**	**2%**	**0.18**	**0.02**

Table 1.4: Soil XRF Metals

XRF results for the metal concentrations in soil samples. BDL indicates the metal concentrations were below detection limits.

	Al ppm Sh.Carb	+/- ppm Sh.Carb	Ca ppm Sh.Carb	+/- ppm Sh.Carb	K ppm Sh.Carb	+/- ppm Sh.Carb	Mg ppm Sh.Carb	+/- ppm Sh.Carb	Na ppm Sh.Carb	+/- ppm Sh.Carb	P ppm Sh.Carb	+/- ppm Sh.Carb	Si ppm Sh.Carb	+/- ppm Sh.Carb	Ti ppm Sh.Carb	+/- ppm Sh.Carb	Mn ppm Sh.Carb	+/- ppm Sh.Carb	Ba ppm Sh.Carb	+/- ppm Sh.Carb	S ppm Sh.Carb	+/- ppm Sh.Carb	Ti ppm ProTrace	+/- ppm ProTrace	V ppm ProTrace	+/- ppm ProTrace
BNZ1.6	4425.6	1.6	845.2	0.7	1107.1	266.3	856.3	90.9	642.3	129.2	48.9	11.8	16359.0	3.6	299.6	54.2	21.4	6.1	47.1	0.2	24.1	3.2	304.3	0.2	8.1	0.1
BNZ1.5	3786.6	1.4	850.8	0.6	1111.6	265.2	574.2	90.5	528.3	128.7	48.4	11.8	14120.5	3.2	303.6	53.9	17.8	6.0	50.1	0.2	219.2	3.2	267.6	0.2	6.0	0.1
BNZ1.4	4984.2	1.8	1040.2	0.8	1389.3	331.8	766.8	113.2	698.4	161.0	60.3	14.7	18153.5	4.1	400.8	67.5	22.1	7.5	63.2	0.2	172.3	4.0	359.1	0.3	8.1	0.1
BNZ1.3	4059.6	1.5	832.9	0.6	1157.3	266.3	572.0	90.9	575.8	129.2	50.4	11.8	14818.6	3.3	326.7	54.2	16.9	6.1	53.0	0.2	158.7	3.2	278.0	0.2	6.2	0.1
BNZ1.2	1812.5	1.0	1361.8	0.8	659.0	265.1	186.7	90.5	335.6	128.6	81.9	11.8	6530.8	2.1	200.2	53.9	10.9	6.0	45.0	0.2	441.4	3.2	97.7	0.1	2.7	0.0
BNZ1.1	715.3	0.6	1898.2	0.8	276.3	221.8	121.0	75.7	229.4	107.6	58.6	9.8	2898.5	1.3	73.5	45.1	52.4	5.0	29.2	0.1	200.0	2.7	40.2	0.1	1.3	0.0
Average	3297.3	1.3	1138.2	0.7	950.1	269.4	512.8	92.0	501.6	130.7	58.1	12.0	12146.8	2.9	267.4	54.8	23.6	6.1	47.9	0.2	202.6	3.3	224.5	0.2	5.4	0.1
STD	1661.9	0.5	424.0	0.1	406.3	35.2	299.9	12.0	182.5	17.1	12.7	1.6	6032.1	1.0	114.7	7.2	14.7	0.8	11.2	0.0	135.7	0.4	125.9	0.1	2.8	0.0
BNZ2.6	3282.9	1.3	893.0	0.7	1060.7	266.7	384.6	91.0	437.2	129.4	48.7	11.8	11970.6	3.0	301.2	54.3	15.4	6.1	53.4	0.2	423.6	3.3	212.8	0.2	5.2	0.1
BNZ2.5	N/A	N/A	N/A	N/A	N/A	N/A	N/A	N/A	N/A	N/A	N/A	N/A	N/A	N/A	N/A	N/A	N/A	N/A	N/A	N/A	N/A	N/A	N/A	N/A	N/A	N/A
BNZ2.4	3753.7	1.4	830.1	0.6	1112.4	264.9	507.0	90.4	509.2	128.5	49.2	11.8	13318.2	3.1	306.8	53.9	16.3	6.0	54.6	0.2	223.0	3.2	246.0	0.2	5.8	0.1
BNZ2.3	3467.4	1.4	877.2	0.6	1076.7	264.8	457.3	90.4	461.4	128.5	53.5	11.8	11550.2	2.9	301.1	53.9	14.7	6.0	55.3	0.2	252.8	3.2	218.0	0.2	5.7	0.1
BNZ2.2	2740.4	1.2	1006.0	0.7	918.4	265.0	310.6	90.4	430.5	128.6	65.4	11.8	9652.0	2.6	272.1	53.9	12.2	6.0	52.0	0.2	308.5	3.2	158.6	0.1	4.2	0.0
BNZ2.1	773.2	0.6	1401.2	0.7	310.2	197.1	113.8	67.3	202.6	95.7	61.7	8.8	3318.1	1.3	89.1	40.1	19.5	4.5	25.7	0.1	217.0	2.4	45.3	0.1	1.3	0.0
Average	2803.5	1.2	1001.5	0.7	895.7	251.7	354.7	85.9	408.2	122.1	55.7	11.2	9961.8	2.6	254.1	51.2	15.6	5.7	48.2	0.2	285.0	3.1	176.1	0.1	4.4	0.0
STD	1193.7	0.4	232.6	0.0	335.5	30.5	153.8	10.4	119.0	14.8	7.5	1.4	3938.9	0.7	93.2	6.2	2.7	0.7	12.7	0.0	85.5	0.4	79.7	0.1	1.8	0.0
CPC1.5	3041.8	1.1	588.0	0.5	683.5	197.2	551.6	67.3	375.1	95.7	43.2	8.8	10915.4	2.5	245.4	40.1	56.1	4.5	34.8	0.1	32.0	2.4	231.5	0.2	6.7	0.1
CPC1.4	3838.5	1.5	828.6	0.6	870.9	265.5	665.1	90.6	537.1	128.8	58.2	11.8	14901.0	3.4	329.5	54.0	47.7	6.0	47.0	0.2	55.5	3.2	303.4	0.2	8.0	0.1
CPC1.3	3835.5	1.5	798.4	0.6	843.6	265.4	689.3	90.6	563.9	128.8	53.3	11.8	15621.7	3.4	331.7	54.0	36.3	6.0	42.4	0.2	39.7	3.2	322.6	0.2	8.4	0.1
CPC1.2	3802.8	1.5	864.1	0.6	863.2	265.5	697.7	90.6	517.9	128.9	56.9	11.8	14323.1	3.3	342.0	54.0	57.0	6.0	44.7	0.2	59.0	3.2	301.5	0.2	8.0	0.1
Average	3629.7	1.4	769.8	0.6	815.3	248.4	650.9	84.8	498.5	120.5	52.9	11.0	13940.3	3.2	312.2	50.5	49.3	5.6	42.2	0.2	46.6	3.0	289.7	0.2	7.8	0.1
STD	392.2	0.2	124.1	0.1	88.6	34.1	67.7	11.7	84.4	16.6	6.8	1.5	2085.4	0.4	44.9	6.9	9.6	0.8	5.3	0.0	12.8	0.4	40.0	0.0	0.8	0.0
CPC2.4	4161.8	1.5	722.6	0.6	953.2	266.4	722.0	90.9	552.5	129.3	53.8	11.8	15640.0	3.5	339.3	54.2	32.8	6.1	46.8	0.2	32.8	3.2	319.9	0.2	9.1	0.1
CPC2.3	3699.3	1.4	834.7	0.6	859.8	265.4	649.9	90.6	511.4	128.8	55.2	11.8	14017.3	3.3	321.1	54.0	43.4	6.0	45.9	0.2	74.7	3.2	292.0	0.2	8.4	0.1
CPC2.2	3680.2	1.4	760.6	0.6	828.8	265.7	669.7	90.7	518.5	128.9	56.4	11.8	14372.6	3.3	334.9	54.0	34.4	6.0	42.8	0.2	76.5	3.2	301.6	0.2	7.9	0.1
Average	3847.1	1.5	772.6	0.6	880.6	265.8	680.5	90.7	527.5	129.0	55.1	11.8	14676.6	3.3	331.8	54.1	36.9	6.0	45.2	0.2	61.3	3.2	304.5	0.2	8.5	0.1
STD	272.7	0.1	57.0	0.0	64.8	0.5	37.2	0.2	22.0	0.3	1.3	0.0	853.0	0.1	9.5	0.1	5.7	0.0	2.1	0.0	24.7	0.0	14.2	0.0	0.6	0.0

	Cr ppm ProTrace	+/- ppm ProTrace	Fe ppm ProTrace	+/- ppm ProTrace	Co ppm ProTrace	+/- ppm ProTrace	Ni ppm ProTrace	+/- ppm ProTrace	Cu ppm ProTrace	+/- ppm ProTrace	Zn ppm ProTrace	+/- ppm ProTrace	As ppm ProTrace	+/- ppm ProTrace	Se ppm ProTrace	+/- ppm ProTrace	Br ppm ProTrace	+/- ppm ProTrace	Sr ppm ProTrace	+/- ppm ProTrace	Mo ppm ProTrace	+/- ppm ProTrace	Pb ppm ProTrace	+/- ppm ProTrace
BNZ1.6	16.5	0.1	2191.5	1.0	0.5	0.1	2.1	0.3	1.1	0.2	5.1	0.0	0.5	2.2	0.3	0.2	0.2	0.1	13.3	0.0	0.1	0.1	1.0	0.0
BNZ1.5	7.4	0.1	1473.8	0.8	0.5	0.1	1.7	0.3	1.4	0.2	3.7	0.0	BDL	2.2	0.2	0.2	0.4	0.1	11.6	0.0	BDL	0.1	1.0	0.0
BNZ1.4	9.5	0.1	1972.9	1.0	0.7	0.2	2.1	0.4	1.5	0.2	4.8	0.0	BDL	2.7	0.3	0.2	0.3	0.2	14.9	0.0	0.0	0.1	1.1	0.0
BNZ1.3	6.1	0.1	1447.4	0.8	0.5	0.1	1.6	0.3	1.4	0.2	3.6	0.0	BDL	2.2	0.2	0.2	0.3	0.1	11.4	0.0	0.0	0.1	0.9	0.0
BNZ1.2	2.4	0.0	657.0	0.4	0.3	0.1	1.2	0.3	1.5	0.2	1.0	0.0	BDL	2.2	0.1	0.2	0.8	0.1	6.3	0.0	BDL	0.1	0.5	0.0
BNZ1.1	1.4	0.0	1024.7	0.4	0.5	0.1	1.0	0.3	0.7	0.1	2.0	0.0	2.0	1.8	BDL	0.1	0.5	0.1	5.1	0.0	BDL	0.0	0.5	0.0
Average	7.2	0.1	1461.2	0.7	0.5	0.1	1.6	0.3	1.3	0.2	3.4	0.0	1.2	2.2	0.2	0.2	0.4	0.1	10.4	0.0	0.1	0.1	0.8	0.0
STD	5.5	0.0	571.5	0.3	0.1	0.0	0.5	0.0	0.3	0.0	1.6	0.0	1.1	0.3	0.1	0.0	0.2	0.0	3.9	0.0	0.0	0.0	0.3	0.0
BNZ2.6	4.9	0.1	1061.2	0.6	0.5	0.1	1.4	0.3	1.5	0.2	2.4	0.0	BDL	2.2	0.2	0.2	0.4	0.1	9.2	0.0	BDL	0.1	0.9	0.0
BNZ2.5	N/A	N/A	N/A	N/A	N/A	N/A	N/A	N/A	N/A	N/A	N/A	N/A	N/A	N/A	N/A	N/A	N/A	N/A	N/A	N/A	N/A	N/A	N/A	N/A
BNZ2.4	5.5	0.1	1293.4	0.7	0.5	0.1	1.5	0.3	1.3	0.2	3.2	0.0	BDL	2.2	0.2	0.2	0.3	0.1	10.4	0.0	BDL	0.1	0.9	0.0
BNZ2.3	5.4	0.1	1185.8	0.7	0.5	0.1	1.6	0.3	1.7	0.2	3.1	0.0	BDL	2.2	0.2	0.2	0.4	0.1	9.5	0.0	BDL	0.1	1.0	0.0
BNZ2.2	3.8	0.0	879.1	0.5	0.4	0.1	1.4	0.3	1.6	0.2	2.0	0.0	BDL	2.2	0.1	0.2	0.5	0.1	7.4	0.0	BDL	0.1	0.8	0.0
BNZ2.1	1.1	0.0	506.6	0.3	0.3	0.1	0.8	0.2	0.7	0.1	1.0	0.0	BDL	1.6	BDL	0.1	0.4	0.1	4.4	0.0	BDL	0.0	1.5	0.0
Average	4.1	0.0	985.2	0.6	0.4	0.1	1.4	0.3	1.4	0.1	2.3	0.0		2.1	0.2	0.2	0.4	0.1	8.2	0.0		0.1	1.0	0.0
STD	1.8	0.0	308.8	0.2	0.1	0.0	0.3	0.0	0.4	0.0	0.9	0.0		0.2	0.0	0.0	0.1	0.0	2.4	0.0		0.0	0.3	0.0
CPC1.5	7.6	0.1	2143.6	0.8	0.9	0.1	1.9	0.2	2.0	0.1	4.5	0.0	0.5	1.6	0.2	0.1	0.2	0.1	7.7	0.0	0.1	0.0	0.7	0.0
CPC1.4	7.9	0.1	2406.7	1.0	1.1	0.1	2.3	0.3	2.2	0.2	5.2	0.0	0.8	2.2	0.3	0.2	0.3	0.1	10.6	0.0	0.1	0.1	0.9	0.0
CPC1.3	6.4	0.1	2417.7	1.0	1.0	0.1	2.2	0.3	2.2	0.2	4.8	0.0	BDL	2.2	0.3	0.2	0.2	0.1	10.2	0.0	0.1	0.1	0.8	0.0
CPC1.2	6.6	0.1	2577.3	1.0	1.1	0.1	2.2	0.3	1.9	0.2	5.3	0.0	0.9	2.2	0.3	0.2	0.4	0.1	8.9	0.0	0.0	0.1	0.9	0.0
Average	7.1	0.1	2386.3	1.0	1.0	0.1	2.1	0.3	2.1	0.1	5.0	0.0	0.7	2.0	0.3	0.2	0.3	0.1	9.3	0.0	0.1	0.0	0.8	0.0
STD	0.7	0.0	179.6	0.1	0.1	0.0	0.2	0.0	0.1	0.0	0.4	0.0	0.2	0.3	0.0	0.0	0.1	0.0	1.3	0.0	0.0	0.0	0.1	0.0
CPC2.4	6.9	0.1	3009.3	1.1	0.9	0.1	2.2	0.3	2.0	0.2	5.3	0.0	1.4	2.2	0.3	0.2	0.3	0.1	9.9	0.0	0.0	0.1	0.9	0.0
CPC2.3	7.1	0.1	2581.5	1.0	0.9	0.1	2.3	0.3	2.1	0.2	4.8	0.0	0.6	2.2	0.3	0.2	0.2	0.1	9.9	0.0	0.0	0.1	0.8	0.0
CPC2.2	6.4	0.1	2444.4	1.0	0.8	0.1	2.1	0.3	2.2	0.2	4.7	0.0	BDL	2.2	BDL	0.2	0.1	0.1	9.4	0.0	BDL	0.1	0.8	0.0
Average	6.8	0.1	2678.4	1.1	0.9	0.1	2.2	0.3	2.1	0.2	4.9	0.0	1.0	2.2	0.3	0.2	0.2	0.1	9.7	0.0	0.0	0.1	0.8	0.0
STD	0.3	0.0	294.7	0.1	0.1	0.0	0.1	0.0	0.1	0.0	0.3	0.0	0.6	0.0	0.0	0.0	0.1	0.0	0.3	0.0	0.0	0.0	0.1	0.0

Table 1.5: Soil NMR Percentages

Soil NMR binning percentages for ^{13}C CP-MAS NMR analysis of HF washed soil to removed paramagnetic metals. Percentage determined based on area underneath the curve in specified chemical shifts; 0 – 45 ppm alkyl-C, 45 – 60 ppm methoxyl, 60 – 90 ppm carbohydrates, 90 – 120 ppm proton substituted aromatics, 120 – 140 ppm carbon substituted aromatics, 140 – 160 ppm oxygen substituted aromatics, 160 – 190 ppm carboxyl/aliphatic amides, 190 – 220 ppm aldehydes and ketones (Mao et al. 2012; Zhou et al. 2015; Kaiser et al. 2003). 90 – 160 ppm is classified as total aromatics.

Soil Sample	190-220 ppm	190-160 ppm	160-140 ppm	140-120 ppm	120-90 ppm	Sum 160-90 ppm	90-60 ppm	60-45 ppm	45-0 ppm
BNZ1.6	2%	8%	6%	10%	14%	31%	19%	11%	30%
BNZ1.4	5%	9%	6%	8%	10%	25%	15%	8%	40%
BNZ1.3	1%	6%	5%	8%	10%	23%	17%	8%	45%
BNZ1.2	1%	6%	5%	8%	14%	27%	24%	11%	30%
BNZ1.1	5%	10%	6%	8%	13%	28%	23%	8%	26%
Average	**3%**	**8%**	**6%**	**9%**	**12%**	**27%**	**20%**	**9%**	**34%**
STD	**2%**	**2%**	**1%**	**1%**	**2%**	**3%**	**4%**	**2%**	**8%**

Table 1.6: Optical Indices for Media Leachates

Optical indices of media leachate samples determined from UV-Vis spectrum and Fluorescence EEMs on a Horiba Fluorimeter in a 1 cm diameter quartz cuvette. Standard deviation is denoted as (±) in this table. Values are based on calculations found in Table 1.1 and 1.2. TOC = Total organic carbon concentration. TDN = Total dissolved nitrogen concentration.

Sample	TOC	TOC +/-	TDN	TDN +/-	Percent Carbon in NOM	NOM pH	ABS_{254}	ABS_{280}	$SR_{275/350}$	$SUVA_{254}$ (L mg C^{-1} m^{-1})	$SUVA_{280}$ (L mg C^{-1} m^{-1})	E4:E6	BIX	FI	Freshness	HIX
BNZ1.4 H_2O	4.534	0.040	0.222	0.009	32%	4.210	0.167	0.124	0.884	3.680	2.735	4.793	0.444	1.304	0.431	0.922
BNZ2.5 H_2O	7.127	0.087	0.506	0.017	50%	4.240	0.237	0.175	0.889	3.319	2.458	10.254	0.445	1.268	0.427	0.922
Average	**5.830**	**0.063**	**0.364**	**0.013**	**41%**	**4.225**	**0.202**	**0.150**	**0.886**	**3.500**	**2.597**	**7.523**	**0.444**	**1.286**	**0.429**	**0.922**
STD	**1.833**	**0.033**	**0.201**	**0.006**	**13%**	**0.021**	**0.049**	**0.036**	**0.003**	**0.255**	**0.196**	**3.861**	**0.001**	**0.026**	**0.003**	**0.000**
BNZ1.4 K_2SO_4	4.998	0.126	0.306	0.016	8%	4.110	0.120	0.084	0.879	2.395	1.688	7.663	0.709	1.275	0.607	0.868
BNZ2.5 K_2SO_4	1.714	0.034	0.061	0.008	15%	4.230	0.173	0.122	0.882	10.086	7.141	7.805	0.568	1.466	0.555	0.903
Average	**3.356**	**0.080**	**0.184**	**0.012**	**11%**	**4.170**	**0.146**	**0.103**	**0.881**	**6.240**	**4.415**	**7.734**	**0.639**	**1.370**	**0.581**	**0.885**
STD	**2.323**	**0.065**	**0.174**	**0.005**	**5%**	**0.085**	**0.038**	**0.027**	**0.002**	**5.438**	**3.855**	**0.101**	**0.100**	**0.135**	**0.037**	**0.025**
BNZ1.4 pH10	8.467	0.056	0.460	0.015	19%	2.890	0.426	0.337	0.883	5.034	3.976	10.977	0.398	1.119	0.373	0.969
BNZ2.5 pH10	4.415	0.055	0.218	0.031	18%	4.340	0.693	0.550	0.899	15.700	12.463	10.694	0.368	1.077	0.348	0.948
Average	**6.441**	**0.055**	**0.339**	**0.023**	**18%**	**3.615**	**0.560**	**0.443**	**0.891**	**10.367**	**8.219**	**10.836**	**0.383**	**1.098**	**0.361**	**0.958**
STD	**2.866**	**0.001**	**0.171**	**0.012**	**1%**	**1.025**	**0.189**	**0.151**	**0.011**	**7.541**	**6.001**	**0.200**	**0.022**	**0.030**	**0.017**	**0.015**
PLFA	N/A	N/A	N/A	N/A	67%	4.050	0.286	0.229	1.035	2.148	1.718	6.089	0.776	1.549	0.756	0.793
SRFA	N/A	N/A	N/A	N/A	56%	4.230	0.423	0.327	0.812	4.164	3.216	8.188	0.427	1.314	0.408	0.868

Table 1.7: Optical Indices for Reconstituted NOM

UV-Vis and Fluorescence optical indices for reconstituted NOM at a 10 mg C L^{-1} concentration. All samples were pH adjusted to circumneutral. Standard deviation is denoted as (±) in this table. Values are based on calculations found in Table 1.1 and 1.2. TOC = Total organic carbon concentration. TDN = Total dissolved nitrogen concentration.

Sample	TOC	TOC +/-	TDN	TDN +/-	ABS_{254}	ABS_{280}	S_R	$SUVA_{254}$ (L mg C^{-1} m^{-1})	$SUVA_{280}$ (L mg C^{-1} m^{-1})	E4:E6	BIX	FI	Freshness	HIX
BNZ1.6	10.164	0.033	0.507	0.015	0.494	0.377	0.800	4.856	3.710	14.634	0.398	1.208	0.380	0.945
BNZ1.5	9.381	0.225	0.493	0.021	0.493	0.374	0.808	5.253	3.987	29.672	0.406	1.193	0.390	0.980
BNZ1.4	8.392	0.192	0.403	0.025	0.411	0.311	0.818	4.903	3.706	17.371	0.415	1.319	0.392	0.961
BNZ1.3	7.341	0.144	0.294	0.019	0.433	0.327	0.803	5.895	4.455	23.890	N/A	N/A	N/A	N/A
BNZ1.2	9.829	0.081	0.474	0.019	0.330	0.257	0.709	3.359	2.610	25.211	0.381	1.175	0.367	0.930
BNZ1.1	9.569	0.173	0.370	0.017	0.269	0.219	0.643	2.806	2.285	19.861	0.383	1.305	0.378	0.870
Average	9.113	0.141	0.424	0.019	0.405	0.311	0.764	4.512	3.459	21.773	0.397	1.240	0.382	0.937
STD	1.054	0.072	0.083	0.004	0.090	0.063	0.071	1.181	0.836	5.526	0.015	0.067	0.010	0.042
BNZ2.6	9.098	0.051	0.431	0.013	0.405	0.311	0.794	4.455	3.418	32.576	0.419	1.201	0.404	0.961
BNZ2.5	10.028	0.169	0.556	0.007	0.426	0.328	0.849	4.250	3.266	14.672	0.400	1.165	0.383	0.964
BNZ2.4	8.439	0.061	0.393	0.016	0.388	0.298	0.823	4.601	3.533	14.045	0.404	1.159	0.385	0.946
BNZ2.3	8.715	0.069	0.446	0.007	0.391	0.299	0.785	4.482	3.434	18.823	0.412	1.161	0.395	0.961
BNZ2.2	9.644	0.108	0.491	0.022	0.371	0.288	0.742	3.842	2.989	16.634	0.410	1.191	0.391	0.951
Average	9.185	0.092	0.463	0.013	0.396	0.305	0.798	4.326	3.328	19.350	0.409	1.175	0.392	0.957
STD	0.653	0.048	0.062	0.007	0.021	0.015	0.040	0.299	0.212	7.626	0.007	0.019	0.008	0.008
CPC1.5	9.924	0.115	0.569	0.012	0.298	0.218	0.820	3.004	2.195	12.936	0.417	1.320	0.410	0.949
CPC1.4	9.660	0.106	0.513	0.010	0.332	0.248	0.746	3.434	2.572	20.173	0.423	1.267	0.414	0.929
CPC1.3	9.107	0.094	0.379	0.013	0.344	0.256	0.780	3.781	2.813	12.916	0.416	1.244	0.404	0.951
CPC1.2	9.650	0.136	0.542	0.014	0.345	0.259	0.777	3.576	2.685	12.828	0.359	1.260	0.343	0.949
Average	9.585	0.113	0.501	0.012	0.330	0.245	0.781	3.449	2.567	14.713	0.404	1.273	0.393	0.944
STD	0.343	0.018	0.085	0.002	0.022	0.019	0.030	0.329	0.266	3.640	0.030	0.033	0.033	0.011
PLFA	13.303	0.036	N/A	N/A	0.410	0.306	0.700	3.082	2.299	12.807	0.780	0.422	0.529	1.514
SRFA	10.160	0.040	N/A	N/A	0.271	0.206	0.798	2.668	2.024	5.486	0.427	0.380	0.616	1.343

Table 1.8: Media Leachate Trace Metal Concentrations

Media leachate samples were obtained prior to NOM isolation and filtered to 0.45 μm filters and acidified to 2% HNO_3 and analyzed by ICP-MS. Samples with the denoted with --- we not run for that metal. BDL = below detection limits and N/A are associated lack of error associated with BDL samples. **denoted samples are sample concentrations observed above the calibration curve.

	Na ppb	Na +/-	Mg ppb	Mg +/-	Al ppb	Al +/-	K ppb	K +/-	Ca ppb	Ca +/-	Ti ppb	Ti +/-	V ppb	V +/-	Cr ppb	Cr +/-	Mn ppb	Mn +/-	Fe ppb	Fe +/-	Co ppb	Co +/-
BNZ2.5 H_2O	BDL	N/A	246.4	12.9	137.9	0.2	618.6	27.5	BDL	N/A	3.9	0.1	11.9	0.2	0.4	0.0	3.5	0.0	188.6	1.4	0.1	0.0
BNZ2.5 K_2SO_4	1009.3	19.3	1347.0	14.4	861.5**	7.8	--	--	--	--	6.1	0.2	4.5	0.1	3.4	0.0	65.1	0.4	425.3	1.8	3.2	0.0
BNZ2.5 pH10	7597.9	20.6	40.7	1.9	937.6**	11.3	417.3	35.2	BDL	N/A	14.1	0.1	29.7	0.5	1.1	0.0	1.2	0.0	224.9	2.6	0.1	0.0
Average	4303.6	19.9	544.7	9.7	137.9	6.4	517.9	31.4			8.0	0.1	15.3	0.2	1.6	0.0	23.2	0.2	279.6	1.9	1.1	0.0
STD	4658.8	0.9	702.4	6.8		5.7	142.3	5.5			5.4	0.1	13.0	0.2	1.5	0.0	36.2	0.2	127.5	0.6	1.8	0.0
BNZ1.4 H_2O	86.9	27.2	197.1	6.0	70.2	0.1	BDL	N/A	210.4	4.0	1.4	0.1	5.7	0.0	0.1	0.0	0.8	0.0	46.0	0.9	0.1	0.0
BNZ1.4 K_2SO_4	---	---	---	---	775.4**	11.8	--	--	--	--	1.8	1.8	2.2	0.1	1.3	0.0	26.2	0.4	--	--	2.2	0.0
BNZ1.4 pH10	---	---	---	---	562.5	5.0	--	--	--	--	BDL	0.2	BDL	0.1	BDL	0.0	50.2	0.0	--	--	2.9	0.0
Average	86.9	27.2	197.1	6.0	316.3	5.6			210.4	4.0	1.6	0.7	3.9	0.1	0.7	0.0	25.8	0.2	46.0	0.9	1.7	0.0
STD					348.1	5.9					0.3	1.0	2.5	0.0	0.8	0.0	24.7	0.3			1.5	0.0
	Ni ppb	**Ni +/-**	**Cu ppb**	**Cu +/-**	**Zn ppb**	**Zn +/-**	**As ppb**	**As +/-**	**Se ppb**	**Se +/-**	**Sr ppb**	**Sr +/-**	**Mo ppb**	**Mo +/-**	**Sb ppb**	**Sb +/-**	**Ba ppb**	**Ba +/-**	**Pb ppb**	**Pb +/-**	**Bi ppb**	**Bi +/-**
BNZ2.5 H_2O	0.2	0.0	1.2	0.0	BDL	N/A	2.7	0.1	0.4	0.1	4.2	0.0	0.1	0.0	0.3	0.0	2.9	0.0	0.2	0.0	0.3	0.0
BNZ2.5 K_2SO_4	6.8	0.2	0.7	0.2	21.69	0.71	2.7	0.2	11.3	1.4	82.4	0.3	26.4	1.1	0.5	0.0	226.8**	1.2	0.5	0.0	0.3	0.0
BNZ2.5 pH10	0.6	0.0	3.0	0.1	BDL	N/A	3.9	0.1	0.2	0.0	0.8	0.0	0.2	0.0	0.4	0.0	2.9	0.0	0.3	0.0	0.3	0.0
Average	2.5	0.1	1.6	0.1	21.7	0.7	3.1	0.1	4.0	0.5	29.1	0.1	8.9	0.4	0.4	0.0	2.9	0.4	0.3	0.0	0.3	0.0
STD	3.7	0.1	1.2	0.1			0.7	0.1	6.4	0.8	46.1	0.2	15.2	0.6	0.1	0.0	0.1	0.7	0.1	0.0	0.0	0.0
BNZ1.4 H_2O	BDL	N/A	1.0	0.0	BDL	N/A	2.2	0.0	0.1	0.0	3.7	0.0	0.0	0.0	0.2	0.0	0.5	0.0	BDL	N/A	BDL	N/A
BNZ1.4 K_2SO_4	3.1	0.1	0.5	0.0	22.9	0.3	2.7	0.1	6.7	0.2	51.7	0.3	10.8	0.5	0.2	0.0	94.6	0.2	BDL	N/A	BDL	N/A
BNZ1.4 pH10	BDL	N/A	3.1	0.0	BDL	N/A	BDL	N/A	BDL	N/A	55.2	0.0	3.7	0.0	0.1	0.0	27.5	0.0	BDL	N/A	BDL	N/A
Average	3.1	0.1	1.5	0.0	22.9	0.3	2.4	0.1	3.4	0.1	36.9	0.1	4.9	0.2	0.2	0.0	40.9	0.1				
STD			1.3	0.0			0.3	0.0	4.7	0.1	28.8	0.2	5.5	0.3	0.0	0.0	48.5	0.1				

Table 1.9: Media Leached Soil ^{13}C NMR Percentages

Unleached soil compared to leached soil NMR differences in binning percentages were formulated from solid state ^{13}C CP-MAS NMR analysis. Percentage determined based on area underneath the curve in specified chemical shifts; 0 – 45 ppm alkyl-C, 45 – 60 ppm methoxyl, 60 – 90 ppm carbohydrates, 90 – 120 ppm proton substituted aromatics, 120 – 140 ppm carbon substituted aromatics, 140 – 160 ppm oxygen substituted aromatics, 160 – 190 ppm carboxyl/aliphatic amides, 190 – 220 ppm aldehydes and ketones (Mao et al. 2012; Zhou et al. 2015; Kaiser et al. 2003). 90 – 160 ppm is classified as total aromatics.

Sample	190-220 ppm	190-160 ppm	160-140 ppm	140-120 ppm	120-90 ppm	Sum 160-90 ppm	90-60 ppm	60-45 ppm	45-0 ppm
BNZ1.4 Soil	0.83%	5.83%	4.06%	7.55%	8.33%	19.93%	15.24%	7.97%	50.20%
BNZ1.4 H_2O NOM	0.97%	6.89%	7.33%	10.74%	18.38%	36.45%	27.93%	11.25%	16.50%
Difference	**-0.14%**	**-1.06%**	**-3.27%**	**-3.19%**	**-10.05%**	**-16.52%**	**-12.69%**	**-3.28%**	**33.70%**
BNZ1.4 Soil	0.83%	5.83%	4.06%	7.55%	8.33%	19.93%	15.24%	7.97%	50.20%
BNZ1.4 K_2SO_4 NOM	1.76%	7.03%	5.12%	7.85%	12.77%	25.73%	24.01%	9.55%	31.92%
Difference	**-0.93%**	**-1.19%**	**-1.06%**	**-0.30%**	**-4.44%**	**-5.80%**	**-8.77%**	**-1.58%**	**18.28%**
BNZ1.4 Soil	0.83%	5.83%	4.06%	7.55%	8.33%	19.93%	15.24%	7.97%	50.20%
BNZ1.4 pH10 NOM	0.92%	6.98%	6.54%	15.23%	14.93%	36.70%	21.13%	11.85%	22.42%
Difference	**-0.09%**	**-1.15%**	**-2.48%**	**-7.68%**	**-6.61%**	**-16.77%**	**-5.89%**	**-3.88%**	**27.78%**
BNZ2.5 Soil	0.95%	5.32%	4.61%	7.92%	10.63%	23.16%	16.86%	8.61%	45.11%
BNZ2.5 H_2O NOM	1.49%	9.97%	7.27%	11.11%	17.54%	35.91%	25.83%	9.52%	17.28%
Difference	**-0.54%**	**-4.65%**	**-2.66%**	**-3.19%**	**-6.91%**	**-12.75%**	**-8.97%**	**-0.91%**	**27.82%**
BNZ2.5 Soil	0.95%	5.32%	4.61%	7.92%	10.63%	23.16%	16.86%	8.61%	45.11%
BNZ2.5 K_2SO_4 NOM	1.62%	9.16%	6.87%	10.19%	16.26%	33.33%	24.67%	10.76%	20.47%
Difference	**-0.67%**	**-3.84%**	**-2.26%**	**-2.28%**	**-5.63%**	**-10.17%**	**-7.81%**	**-2.15%**	**24.64%**
BNZ2.5 Soil	0.95%	5.32%	4.61%	7.92%	10.63%	23.16%	16.86%	8.61%	45.11%
BNZ2.5 pH10 NOM	1.26%	10.37%	8.27%	13.43%	17.05%	38.76%	21.20%	9.47%	18.95%
Difference	**-0.31%**	**-5.05%**	**-3.66%**	**-5.52%**	**-6.42%**	**-15.60%**	**-4.35%**	**-0.86%**	**26.16%**

Table 1.10: Media Isolated NOM ^{13}C NMR Percentages

PPL isolated NOM NMR binning percentages for solid state ^{13}C CP-MAS NMR analysis. Percentage determined based on area underneath the curve in specified chemical shifts; 0 – 45 ppm alkyl-C, 45 – 60 ppm methoxyl, 60 – 90 ppm carbohydrates, 90 – 120 ppm proton substituted aromatics, 120 – 140 ppm carbon substituted aromatics, 140 – 160 ppm oxygen substituted aromatics, 160 – 190 ppm carboxyl/aliphatic amides, 190 – 220 ppm aldehydes and ketones (Mao et al. 2012; Zhou et al. 2015; Kaiser et al. 2003). 90 – 160 ppm is classified as total aromatics.

Sample	190-220 ppm	190-160 ppm	160-140 ppm	140-120 ppm	120-90 ppm	Sum 160-90 ppm	90-60 ppm	60-45 ppm	45-0 ppm
BNZ1.4 Soil	0.83%	5.83%	4.06%	7.55%	8.33%	19.93%	15.24%	7.97%	50.20%
BNZ2.5 Soil	0.95%	5.32%	4.61%	7.92%	10.63%	23.16%	16.86%	8.61%	45.11%
Average	**0.89%**	**5.58%**	**4.33%**	**7.73%**	**9.48%**	**21.54%**	**16.05%**	**8.29%**	**47.66%**
STD	**0.08%**	**0.36%**	**0.39%**	**0.26%**	**1.63%**	**2.28%**	**1.14%**	**0.45%**	**3.60%**
BNZ1.4 H_2O NOM	0.97%	6.89%	7.33%	10.74%	18.38%	36.45%	27.93%	11.25%	16.50%
BNZ2.5 H_2O NOM	1.49%	9.97%	7.27%	11.11%	17.54%	35.91%	25.83%	9.52%	17.28%
Average	**1.23%**	**8.43%**	**7.30%**	**10.92%**	**17.96%**	**36.18%**	**26.88%**	**10.38%**	**16.89%**
STD	**0.37%**	**2.18%**	**0.05%**	**0.26%**	**0.59%**	**0.38%**	**1.49%**	**1.22%**	**0.55%**
BNZ1.4 K_2SO_4 NOM	1.76%	7.03%	5.12%	7.85%	12.77%	25.73%	24.01%	9.55%	31.92%
BNZ2.5 K_2SO_4 NOM	1.62%	9.16%	6.87%	10.19%	16.26%	33.33%	24.67%	10.76%	20.47%
Average	**1.69%**	**8.09%**	**5.99%**	**9.02%**	**14.52%**	**29.53%**	**24.34%**	**10.15%**	**26.20%**
STD	**0.10%**	**1.51%**	**1.24%**	**1.66%**	**2.47%**	**5.37%**	**0.47%**	**0.86%**	**8.10%**
BNZ1.4 pH10 NOM	0.92%	6.98%	6.54%	15.23%	14.93%	36.70%	21.13%	11.85%	22.42%
BNZ2.5 pH10 NOM	1.26%	10.37%	8.27%	13.43%	17.05%	38.76%	21.20%	9.47%	18.95%
Average	**1.09%**	**8.67%**	**7.40%**	**14.33%**	**15.99%**	**37.73%**	**21.17%**	**10.66%**	**20.68%**
STD	**0.24%**	**2.40%**	**1.23%**	**1.27%**	**1.50%**	**1.46%**	**0.05%**	**1.69%**	**2.46%**
SRFA	2.03%	9.63%	6.71%	9.67%	15.90%	32.27%	20.40%	11.56%	24.11%
PLFA	0.44%	8.25%	5.26%	8.21%	9.58%	23.05%	16.83%	14.65%	36.79%

Table 1.11: Media Isolated NOM ^{1}H NMR Percentages

1 mg of PPL isolated NOM reconstituted in 18 MΩ H_2O with a TSP/D_2O insert was run on a 600 MHz Bruker ^{1}H NMR with NMR SPR-WATERGATE water suppression technique. Percentages were obtained from the comparison of the area underneath of the spectra with specified chemical shifts; 0.6 – 1.6 ppm material derived from linear terpenoids (MDLT), 1.6 – 3.2 ppm carboxyl rich alicyclic molecules (CRAM), 3.2 – 4.5 ppm carbohydrates, and 6.5 – 8.4 ppm aromatics (Lam & Simpson, 2008).

	8.4-6.5 ppm	4.5-3.2 ppm	3.2-1.6 ppm	1.6-0.6 ppm
BNZ1.4 H_2O	8.37%	47.46%	26.69%	17.48%
BNZ2.5 H_2O	10.21%	32.57%	35.50%	21.73%
Average	9.29%	40.02%	31.09%	19.60%
STD	**1.30%**	**10.53%**	**6.23%**	**3.00%**
BNZ1.4 K_2SO_4	6.62%	50.83%	22.24%	20.32%
BNZ2.5 K_2SO_4	9.42%	40.27%	29.72%	20.59%
Average	8.02%	45.55%	25.98%	20.45%
STD	**1.98%**	**7.47%**	**5.29%**	**0.19%**
BNZ1.4 pH10	11.57%	40.07%	31.80%	16.55%
BNZ2.5 pH10	12.09%	31.18%	36.54%	20.19%
Average	11.83%	35.62%	34.17%	18.37%
STD	**0.37%**	**6.29%**	**3.35%**	**2.57%**

Table 1.12: Media isolated NOM Photolysis Rates with Rate Differences

Reconstituted of 10 mg C L^{-1} NOM in 18 MΩ H_2O and pH adjusted to circumneutral with the addition of chemical probes for photolysis experiments. Screening factors are included and determined from equation 2 and the •OH photolysis rates of decay (ROD) were determined based off of equation 1. The difference in unamended sample with amended sample is included with unamended versus iron (P-I) and unamended versus methanol (P-M). The absolute value of TMP ROD is the rate of production for ^{3}NOM* through equation 3.

	Plain	Methanol	Iron	Plain		Methanol		Iron		Plain -		Plain -		^{3}NOM*		
Sample Name	SF	SF	SF	Rate 254 nm	+/-	Rate 254 nm	+/-	Rate 254 nm	+/-	Iron	+/-	Methanol	+/-	Rate	+/-	R^2
BNZ1.4	8.63E-01	8.60E-01	8.48E-01	2.14E-03	1.56E-04	1.84E-03	6.73E-04	3.79E-03	3.39E-04	-1.65E-03	3.73E-04	3.05E-04	6.91E-04	3.84E-03	2.25E-04	9.82E-01
BNZ1.4 K_2SO_4	8.35E-01	9.60E-01	9.37E-01	6.87E-03	1.24E-03	5.41E-03	7.31E-05	1.21E-02	7.99E-04	-5.23E-03	1.47E-03	1.46E-03	1.24E-03	7.77E-03	5.91E-04	9.76E-01
BNZ1.4 pH10	8.35E-01	8.29E-01	9.63E-01	2.77E-03	1.13E-04	1.91E-03	2.50E-04	4.71E-03	2.97E-03	-1.94E-03	2.97E-03	8.64E-04	2.75E-04	5.25E-03	4.07E-04	9.67E-01
BNZ2.5	8.56E-01	8.58E-01	8.29E-01	1.95E-03	1.78E-05	1.64E-03	5.68E-05	7.57E-03	2.30E-04	-5.62E-03	2.31E-04	3.16E-04	5.96E-05	1.82E-03	1.65E-04	9.47E-01
BNZ2.5 K_2SO_4	9.76E-01	9.76E-01	9.43E-01	6.67E-03	2.04E-04	4.50E-03	5.42E-04	1.08E-02	1.52E-03	-4.15E-03	1.53E-03	2.17E-03	5.79E-04	2.33E-03	1.90E-04	9.66E-01
BNZ2.5 pH10	8.19E-01	8.18E-01	7.95E-01	1.97E-03	1.56E-04	1.40E-03	5.01E-05	5.56E-03	3.06E-04	-3.59E-03	3.44E-04	5.72E-04	1.64E-04	1.79E-03	3.21E-05	9.98E-01
PLFA	9.07E-01	9.07E-01	8.79E-01	1.26E-03	N/A	1.20E-03	N/A	1.53E-03	N/A	-2.75E-04	N/A	5.71E-05	N/A	1.21E-03	7.31E-05	9.84E-01
SRFA	8.70E-01	8.66E-01	8.46E-01	1.09E-03	N/A	1.02E-03	N/A	1.77E-03	N/A	-6.84E-04	N/A	6.52E-05	N/A	1.25E-03	9.13E-05	9.93E-01

Table 1.13: Optical Indices for Water Leachates

Optical indices of water leachate samples determined from UV-Vis spectrum and Fluorescence EEMs on a Horiba Fluorimeter in a 1 cm diameter quartz cuvette. Values are based on calculations found in Table 1.1 and 1.2.

Sample	TOC	TOC +/-	TDN	TDN +/-	Leachate pH	Percent Carbon in NOM	NOM pH	ABS_{254}	ABS_{280}	$SR_{275/350}$	$SUVA_{254}$ (L mg C^{-1} m^{-1})	$SUVA_{280}$ (L mg C^{-1} m^{-1})	E4:E6	BIX	FI	Freshness	HIX
BNZ1.6	4.982	0.031	0.224	0.010	6.800	72%	3.460	0.204	0.153	0.846	4.093	3.069	9.601	0.411	1.286	0.397	1.014
BNZ1.5	5.185	0.102	0.321	0.021	5.850	64%	4.050	0.213	0.161	0.803	4.116	3.099	12.333	0.432	1.308	0.416	0.973
BNZ1.4	4.534	0.040	0.222	0.009	N/A	32%	4.210	0.167	0.124	0.884	3.680	2.735	4.793	0.444	1.304	0.431	0.922
BNZ1.3	5.333	0.098	0.274	0.004	5.730	63%	4.040	0.184	0.137	0.825	3.451	2.573	15.507	0.403	1.302	0.383	1.009
BNZ1.2	19.762	0.426	1.281	0.034	6.010	96%	4.120	0.467	0.361	0.786	2.364	1.826	9.266	0.453	1.304	0.428	0.934
BNZ1.1	30.541	0.398	1.363	0.008	5.990	69%	4.070	0.480	0.377	0.728	1.570	1.233	7.430	0.409	1.411	0.397	0.852
Average	**11.723**	**0.183**	**0.614**	**0.014**	**6.076**	**66%**	**3.992**	**0.286**	**0.219**	**0.812**	**3.212**	**2.423**	**9.822**	**0.425**	**1.319**	**0.409**	**0.950**
STD	**10.949**	**0.180**	**0.550**	**0.012**	**0.420**	**20%**	**0.268**	**0.146**	**0.117**	**0.054**	**1.028**	**0.744**	**3.741**	**0.020**	**0.046**	**0.019**	**0.061**
BNZ2.6	7.198	0.090	0.479	0.033	6.570	45%	4.410	0.270	0.205	0.818	3.757	2.849	11.480	0.454	1.317	0.442	0.971
BNZ2.5	7.127	0.087	0.506	0.017	5.920	50%	4.240	0.237	0.175	0.889	3.319	2.458	10.254	0.445	1.268	0.427	0.922
BNZ2.4	6.105	0.072	0.363	0.018	6.380	49%	4.440	0.214	0.160	0.853	3.506	2.624	31.098	0.454	1.275	0.438	0.940
BNZ2.3	9.098	0.159	0.501	0.023	6.130	43%	4.400	0.296	0.223	0.829	3.251	2.449	8.942	0.450	1.326	0.427	0.968
BNZ2.2	14.174	0.193	0.732	0.012	5.800	45%	4.520	0.385	0.296	0.776	2.719	2.087	9.653	0.446	1.351	0.426	0.976
Average	**8.740**	**0.120**	**0.516**	**0.021**	**6.160**	**46%**	**4.402**	**0.280**	**0.212**	**0.833**	**3.310**	**2.493**	**14.285**	**0.450**	**1.307**	**0.432**	**0.955**
STD	**3.224**	**0.053**	**0.134**	**0.008**	**0.318**	**3%**	**0.102**	**0.066**	**0.053**	**0.042**	**0.384**	**0.279**	**9.444**	**0.004**	**0.035**	**0.007**	**0.024**
CPC1.5	5.988	0.131	0.553	0.023	6.900	57%	4.190	0.147	0.102	0.852	2.461	1.709	22.291	0.476	1.419	0.474	0.919
CPC1.4	5.324	0.028	0.444	0.011	6.630	52%	4.150	0.139	0.102	0.800	2.604	1.908	8.555	0.487	1.420	0.464	0.902
CPC1.3	3.459	0.130	0.165	0.029	5.800	51%	4.190	0.098	0.069	0.816	2.828	2.003	2.802	0.473	1.369	0.467	0.912
CPC1.2	3.709	0.020	0.160	0.010	6.000	48%	4.440	0.102	0.072	0.846	2.752	1.929	13.236	0.458	1.387	0.436	0.908
Average	**4.620**	**0.077**	**0.331**	**0.018**	**6.333**	**52%**	**4.243**	**0.121**	**0.086**	**0.829**	**2.661**	**1.887**	**11.721**	**0.473**	**1.399**	**0.460**	**0.910**
STD	**1.231**	**0.062**	**0.199**	**0.010**	**0.518**	**4%**	**0.133**	**0.025**	**0.018**	**0.025**	**0.163**	**0.126**	**8.238**	**0.012**	**0.025**	**0.017**	**0.007**
CPC2.4	4.376	0.047	0.219	0.008	6.100	38%	N/A	0.134	0.097	0.782	3.067	2.227	8.315	0.461	1.384	0.440	0.947
CPC2.3	11.170	0.337	-0.035	0.011	N/A	33%	4.360	0.139	0.103	0.931	1.244	0.919	2.618	0.494	1.453	0.482	0.931
CPC2.2	4.632	0.266	0.175	0.012	N/A	4%	N/A	0.112	0.084	0.737	2.427	1.822	4.065	0.466	1.376	0.456	0.916
Average	**6.726**	**0.217**	**0.120**	**0.011**	**N/A**	**62%**	**N/A**	**0.129**	**0.095**	**0.817**	**2.246**	**3.627**	**4.999**	**0.474**	**1.404**	**0.459**	**0.931**
STD	**3.851**	**0.152**	**0.136**	**0.002**	**N/A**	**81%**	**N/A**	**0.014**	**0.009**	**0.102**	**0.925**	**1.750**	**2.961**	**0.018**	**0.042**	**0.021**	**0.016**
PLFA	N/A	N/A	N/A	N/A	N/A	67%	4.050	0.286	0.229	1.035	2.148	1.718	6.089	0.776	1.549	0.756	0.793
SRFA	N/A	N/A	N/A	N/A	N/A	56%	4.230	0.423	0.327	0.812	4.164	3.216	8.188	0.427	1.314	0.408	0.868

Table 1.14: Trace Metal Concentrations for Water Leachates

Water leachate samples were obtained prior to NOM isolation and filtered to 0.45 μm filters and acidified to 2% HNO_3 and analyzed by ICP-MS. Samples with the denoted with --- we not run for that metal. BDL = below detection limits and N/A are associated lack of error associated with BDL samples. *denotes samples NIST or SLRS did not pass during run time.

	Na	Na	Mg	Mg	Al	Al	K	K	Ca	Ca	Ti	Ti	V	V	Cr	Cr	Mn	Mn	Fe	Fe	Co	Co
	ppb	+/-	ppb	+/-	ppb	+/-	ppb	+/-	ppb	+/-	ppb	+/-	ppb	+/-	ppb	+/-	ppb	+/-	ppb	+/-	ppb	+/-
BNZ1.6	6188.1	106.6	330.0	8.5	62.7	0.3	675.4	36.5	BDL	N/A	2.7	0.1	5.6	0.1	0.6	0.0	3.9	0.0	52.6	0.8	0.1	0.0
BNZ1.5	6189.1	37.4	399.2	5.8	59.4	0.4	624.9	74.5	525.9	111.0	2.1	0.0	7.6	0.0	0.4	0.0	3.7	0.0	30.0	0.1	0.1	0.0
BNZ1.4	86.9	27.2	197.1	6.0	70.2	0.1	BDL	N/A	210.4	4.0	1.4	0.1	5.7	0.0	0.1	0.0	0.8	0.0	46.0	0.9	0.1	0.0
BNZ1.3	6316.2	54.2	282.2	11.0	73.4	0.2	632.0	22.6	BDL	N/A	2.5	0.0	8.2	0.0	0.2	0.0	0.3	0.0	35.0	0.7	0.1	0.0
BNZ1.2	6306.6	82.3	612.2	16.5	184.4	1.3	646.9	32.1	264.6	50.4	4.5	0.1	12.6	0.1	0.2	0.0	2.2	0.0	105.8	1.8	0.2	0.0
BNZ1.1	6180.3	46.4	775.9	8.3	65.4	0.3	1120.6	33.4	2100.6	132.0	1.9	0.0	1.9	0.0	0.1	0.0	90.8	0.3	261.2	3.2	1.0	0.0
Average	5211.2	59.0	432.7	9.3	85.9	0.4	739.9	39.8	775.4	74.3	2.5	0.0	6.9	0.0	0.3	0.0	16.9	0.1	88.4	1.3	0.3	0.0
STD	2511.1	29.9	219.0	4.0	48.5	0.4	213.6	20.1	894.2	58.3	1.1	0.0	3.5	0.0	0.2	0.0	36.2	0.1	88.9	1.1	0.4	0.0
BNZ2.6	BDL	N/A	335.1	8.6	87.1	1.0	189.5	20.9	BDL	N/A	3.9	0.1	19.1	0.1	0.4	0.0	5.8	0.1	66.1	1.5	0.1	0.0
BNZ2.5	BDL	N/A	246.4	12.9	137.9	0.2	618.6	27.5	BDL	N/A	3.9	0.1	11.9	0.2	0.4	0.0	3.5	0.0	188.6	1.4	0.1	0.0
BNZ2.4	5386.8	48.1	262.0	9.7	59.5	0.6	294.3	36.6	BDL	N/A	2.7	0.0	12.3	0.1	0.1	0.0	1.8	0.0	BDL	0.2	0.1	0.0
BNZ2.3	BDL	N/A	307.7	6.3	95.9	0.8	50.5	37.3	BDL	N/A	3.6	0.0	15.1	0.2	0.1	0.0	1.3	0.0	21.0	0.8	0.2	0.0
BNZ2.2	BDL	N/A	350.9	12.8	196.9	0.5	200.8	31.1	BDL	N/A	5.8	0.1	9.9	0.1	0.3	0.0	0.5	0.0	99.8	6.7	0.2	0.0
Average	5386.8	48.1	300.4	10.1	115.5	0.6	270.7	30.7			4.0	0.1	13.7	0.1	0.3	0.0	2.6	0.0	93.9	2.1	0.1	0.0
STD			45.3	2.8	53.5	0.3	213.0	6.8			1.1	0.0	3.6	0.1	0.1	0.0	2.1	0.0	70.9	2.6	0.0	0.0
CPC1.5	BDL	N/A	181.3	5.8	51.7	2.0	154.4	29.6	BDL	N/A	2.1	0.1	4.0	0.1	3.6	0.1	60.3	1.2	147.3	5.4	0.5	0.0
CPC1.4	BDL	N/A	111.3	2.0	49.1	0.4	152.5	24.8	BDL	N/A	1.1	0.1	5.0	0.1	0.3	0.0	105.9	1.4	141.0	2.0	0.6	0.0
CPC1.3	BDL	N/A	100.5	3.9	44.8	2.6	82.2	43.8	BDL	N/A	0.7	0.1	1.5	0.1	0.2	0.0	41.6	1.5	40.0	1.5	0.5	0.0
CPC1.2	BDL	N/A	95.2	1.7	49.3	0.2	BDL	N/A	BDL	N/A	0.6	0.1	0.2	0.0	0.1	0.0	29.1	0.4	31.3	1.4	0.3	0.0
Average			122.1	3.4	48.7	1.3	129.7	32.7			1.1	0.1	2.7	0.1	1.1	0.0	59.2	1.1	89.9	2.6	0.4	0.0
STD			40.1	1.9	2.9	1.2	41.1	9.9			0.7	0.0	2.2	0.0	1.7	0.0	33.7	0.5	62.8	1.9	0.1	0.0
CPC2.4	BDL	N/A	155.3	5.9	101.1	3.1	BDL	N/A	BDL	N/A	0.5	0.1	0.3	0.0	0.3	0.0	20.4	1.5	106.5	1.6	0.3	0.0
CPC2.3	BDL	N/A	BDL	N/A	62.7	0.2	BDL	N/A	BDL	N/A	1.0	0.0	3.5	0.0	0.7	0.0	47.3	0.2	131.1	6.9	0.3*	0.0
CPC2.2	BDL	N/A	BDL	N/A	50.9	0.0	BDL	N/A	BDL	N/A	0.6	0.0	0.5	0.0	BDL	N/A	24.2	0.1	96.8	6.2	0.2*	0.0
Average			155.3	5.9	71.6	1.1					0.7	0.0	1.4	0.0	0.5	0.0	30.6	0.6	111.5	4.9	0.3	0.0
STD					26.2	1.7					0.3	0.0	1.8	0.0	0.2	0.0	14.6	0.8	17.7	2.9	0.1	0.0
	Ni	**Ni**	**Cu**	**Cu**	**Zn**	**Zn**	**As**	**As**	**Se**	**Se**	**Sr**	**Sr**	**Mo**	**Mo**	**Sb**	**Sb**	**Ba**	**Ba**	**Pb**	**Pb**	**Bi**	**Bi**
	ppb	+/-	ppb	+/-	ppb	+/-	ppb	+/-	ppb	+/-	ppb	+/-	ppb	+/-	ppb	+/-	ppb	+/-	ppb	+/-	ppb	+/-
BNZ1.6	BDL	N/A	1.5	0.0	BDL	N/A	1.1	0.0	BDL	N/A	3.4	0.0	0.2	0.0	0.1	0.0	1.6*	0.0	BDL	N/A	0.0*	0.0
BNZ1.5	BDL	N/A	1.1	0.0	35.8	0.2	2.1	0.0	0.0	0.0	4.6	0.0	0.1	0.0	0.2	0.0	1.7*	0.0	BDL	N/A	0.1*	0.0
BNZ1.4	BDL	N/A	1.0	0.0	BDL	N/A	2.2	0.0	0.1	0.0	3.7	0.0	0.0	0.0	0.2	0.0	0.5	0.0	BDL	N/A	BDL	N/A
BNZ1.3	BDL	N/A	1.1	0.0	BDL	N/A	1.5	0.0	BDL	N/A	3.8	0.0	0.0	0.0	0.2	0.0	1.6	0.0	BDL	N/A	0.2	0.0
BNZ1.2	BDL	N/A	1.1	0.0	BDL	N/A	3.0	0.0	0.2	0.0	9.8	0.1	0.1	0.0	0.2	0.0	4.1	0.0	BDL	N/A	0.1	0.0
BNZ1.1	0.5	0.0	1.0	0.0	1.3	0.0	9.2	0.2	0.5	0.0	13.1	0.1	1.0	0.0	0.2	0.0	4.4	0.0	BDL	N/A	0.1	0.0
Average	0.5	0.0	1.2	0.0	18.6	0.1	3.2	0.0	0.2	0.0	6.4	0.0	0.3	0.0	0.2	0.0	2.3	0.0			0.1	0.0
STD			0.2	0.0	24.4	0.1	3.0	0.1	0.2	0.0	4.1	0.0	0.4	0.0	0.0	0.0	1.6	0.0			0.1	0.0
BNZ2.6	BDL	N/A	0.9	0.0	BDL	N/A	4.3	0.1	0.2	0.0	4.9	0.0	0.4	0.0	0.5	0.0	2.1	0.0	0.1	0.0	0.1	0.0
BNZ2.5	0.2	0.0	1.2	0.0	BDL	N/A	2.7	0.1	0.4	0.1	4.2	0.0	0.1	0.0	0.3	0.0	2.9	0.0	0.2	0.0	0.3	0.0
BNZ2.4	BDL	N/A	0.8	0.0	BDL	N/A	2.7	0.0	BDL	N/A	3.4	0.0	0.1	0.0	0.4	0.0	1.7*	0.0	BDL	N/A	0.14*	0.0
BNZ2.3	BDL	N/A	1.1	0.0	BDL	N/A	2.9	0.0	0.1	0.0	4.9	0.1	0.1	0.0	0.3	0.0	2.4*	0.1	BDL	N/A	0.06*	0.0
BNZ2.2	0.3	0.0	1.3	0.0	BDL	N/A	2.7	0.1	0.1	0.0	6.9	0.0	0.1	0.0	0.2	0.0	3.7	0.0	0.1	0.0	0.1	0.0
Average	0.3	0.0	1.0	0.0	BDL	N/A	3.1	0.1	0.2	0.0	4.9	0.0	0.1	0.0	0.3	0.0	2.6	0.0	0.1	0.0	0.2	0.0
STD	0.1	0.0	0.2	0.0			0.7	0.0	0.1	0.0	1.3	0.0	0.1	0.0	0.1	0.0	0.8	0.0	0.0	0.0	0.1	0.0
CPC1.5	2.0	0.1	1.8	0.0	BDL	N/A	3.4	0.1	0.3	0.0	6.3	0.1	0.5	0.0	0.1	0.0	3.8	0.1	0.1	0.0	0.1	0.0
CPC1.4	0.2	0.0	1.5	0.0	0.5	0.0	2.2	0.0	0.2	0.0	5.2	0.1	0.3	0.0	0.1	0.0	3.6	0.0	0.0	0.0	BDL	N/A
CPC1.3	0.0	0.1	1.6	0.1	0.8	0.1	0.5	0.0	0.4	0.0	3.0	0.1	0.1	0.0	0.0	0.0	2.1	0.1	0.1	0.0	0.1	0.0
CPC1.2	BDL	N/A	0.7	0.0	0.3	0.0	0.2	0.0	BDL	N/A	2.7	0.0	0.0	0.0	BDL	N/A	1.8	0.0	0.0	0.0	BDL	N/A
Average	0.7	0.0	1.4	0.0	0.6	0.1	1.6	0.0	0.3	0.0	4.3	0.1	0.2	0.0	0.1	0.0	2.8	0.1	0.1	0.0	0.1	0.0
STD	1.1	0.0	0.5	0.0	0.3	0.0	1.5	0.1	0.1	0.0	1.7	0.1	0.2	0.0	0.0	0.0	1.0	0.0	0.0	0.0	0.0	0.0
CPC2.4	0.4	0.0	1.7	0.0	8.1	0.2	0.5	0.0	BDL	N/A	3.4	0.1	0.1	0.0	0.0	0.0	2.7	0.1	0.1	0.0	0.1	0.0
CPC2.3	0.3*	0.0	BDL	N/A	BDL	N/A	3.8	0.1	0.2	0.0	4.8	0.0	0.5	0.0	0.2	0.0	3.8	0.0	0.0	0.0	BDL	N/A
CPC2.2	BDL	N/A	BDL	N/A	BDL	N/A	0.5	0.0	BDL	N/A	2.3	0.0	0.1	0.0	0.1	0.0	4.0	0.0	0.0	0.0	BDL	N/A
Average	0.3	0.0	1.7	0.0	8.1	0.2	1.6	0.1	0.2	0.0	3.5	0.0	0.2	0.0	0.1	0.0	3.5	0.0	0.0	0.0	0.1	0.0
STD	0.1	0.0					1.9	0.1			1.3	0.0	0.2	0.0	0.1	0.0	0.7	0.0	0.0	0.0		

Table 1.15: Water Isolated NOM ^{13}C NMR Percentages

PPL isolated NOM NMR binning percentages for solid state ^{13}C CP-MAS NMR analysis. Percentage determined based on area underneath the curve in specified chemical shifts; 0 – 45 ppm alkyl-C, 45 – 60 ppm methoxyl, 60 – 90 ppm carbohydrates, 90 – 120 ppm proton substituted aromatics, 120 – 140 ppm carbon substituted aromatics, 140 – 160 ppm oxygen substituted aromatics, 160 – 190 ppm carboxyl/aliphatic amides, 190 – 220 ppm aldehydes and ketones (Mao et al. 2012; Zhou et al. 2015; Kaiser et al. 2003). 90 – 160 ppm is classified as total aromatics.

Sample Name	190-220 ppm	190-160 ppm	160-140 ppm	140-120 ppm	120-90 ppm	Sum 160-90 ppm	90-60 ppm	60-45 ppm	45-0 ppm
BNZ1.6	0.32%	7.42%	7.07%	11.02%	19.92%	38.01%	28.02%	10.64%	15.60%
BNZ1.5	0.82%	9.24%	7.77%	11.25%	17.92%	36.94%	21.59%	10.15%	21.27%
BNZ1.4	0.97%	6.89%	7.33%	10.74%	18.38%	36.45%	27.93%	11.25%	16.50%
BNZ1.3	0.32%	9.83%	8.83%	13.02%	18.83%	40.68%	22.02%	9.97%	17.18%
BNZ1.2	1.80%	8.84%	6.62%	8.56%	17.27%	32.45%	33.29%	8.35%	15.26%
BNZ1.1	0.95%	6.33%	5.30%	6.69%	15.77%	27.76%	29.69%	10.08%	25.19%
Average	**0.86%**	**8.09%**	**7.15%**	**10.21%**	**18.02%**	**35.38%**	**27.09%**	**10.07%**	**18.50%**
STD	**0.55%**	**1.41%**	**1.18%**	**2.24%**	**1.42%**	**4.59%**	**4.53%**	**0.97%**	**3.92%**
BNZ2.6	1.98%	10.93%	8.23%	11.54%	16.98%	36.75%	23.45%	9.02%	17.88%
BNZ2.5	1.49%	9.97%	7.27%	11.11%	17.54%	35.91%	25.83%	9.52%	17.28%
BNZ2.4	0.95%	9.09%	7.11%	10.20%	18.02%	35.33%	25.85%	9.22%	19.55%
BNZ2.3	0.63%	8.95%	7.71%	10.92%	18.80%	37.44%	26.78%	9.38%	16.83%
BNZ2.2	1.93%	6.16%	4.88%	7.64%	17.77%	30.29%	35.14%	9.37%	17.10%
Average	**1.40%**	**9.02%**	**7.04%**	**10.28%**	**17.82%**	**35.15%**	**27.41%**	**9.30%**	**17.73%**
STD	**0.59%**	**1.78%**	**1.28%**	**1.55%**	**0.67%**	**2.83%**	**4.50%**	**0.19%**	**1.09%**
CPC1.5	2.36%	11.66%	6.84%	8.96%	17.85%	33.64%	29.75%	8.16%	14.42%
CPC1.4	2.06%	10.90%	6.97%	8.81%	18.64%	34.42%	29.82%	8.24%	14.56%
CPC1.3	1.64%	11.38%	7.22%	9.15%	18.25%	34.62%	28.83%	8.52%	15.01%
CPC1.2	1.61%	10.72%	7.04%	8.42%	18.94%	34.40%	30.32%	8.29%	14.66%
Average	**1.92%**	**11.16%**	**7.02%**	**8.83%**	**18.42%**	**34.27%**	**29.68%**	**8.30%**	**14.66%**
STD	**0.36%**	**0.43%**	**0.16%**	**0.31%**	**0.48%**	**0.43%**	**0.62%**	**0.15%**	**0.25%**
CPC2.4	1.41%	10.30%	7.14%	11.43%	16.82%	35.39%	25.99%	9.71%	17.20%
CPC2.3	0.18%	8.54%	6.52%	8.43%	17.55%	32.50%	34.23%	9.37%	15.18%
CPC2.2	2.19%	7.90%	7.04%	9.62%	17.49%	34.16%	20.38%	13.46%	21.90%
Average	**1.26%**	**8.91%**	**6.90%**	**9.83%**	**17.29%**	**34.01%**	**26.87%**	**10.85%**	**18.09%**
STD	**1.01%**	**1.24%**	**0.34%**	**1.51%**	**0.41%**	**1.45%**	**6.97%**	**2.27%**	**3.45%**
PLFA	0.44%	8.25%	5.26%	8.21%	9.58%	31.30%	16.83%	14.65%	36.79%
SRFA	2.03%	9.63%	6.71%	9.67%	15.90%	41.90%	20.40%	11.56%	24.11%

Table 1.16: Water Isolated NOM ^{1}H NMR Percentages

1 mg of PPL isolated NOM reconstituted in 18 MΩ H_2O with a TSP/D_2O insert was run on a 600 MHz Bruker ^{1}H NMR with NMR SPR-WATERGATE water suppression technique. Percentages were obtained from the comparison of the area underneath of the spectra with specified chemical shifts; 0.6 – 1.6 ppm material derived from linear terpenoids (MDLT), 1.6 – 3.2 ppm carboxyl rich alicyclic molecules (CRAM), 3.2 – 4.5 ppm carbohydrates, and 6.5 – 8.4 ppm aromatics (Lam & Simpson, 2008).

Sample Name	0.6-1.6 ppm	1.6-3.2 ppm	3.2-4.5 ppm	6.5-8.4 ppm
BNZ1.6	20.05%	30.68%	33.63%	15.64%
BNZ1.5	22.18%	37.65%	28.81%	11.36%
BNZ1.4	17.48%	26.69%	47.46%	8.37%
BNZ1.3	18.20%	38.90%	31.13%	11.77%
BNZ1.2	22.87%	27.36%	40.01%	9.76%
BNZ1.1	21.98%	24.22%	44.64%	9.16%
Average	**20.46%**	**30.92%**	**37.61%**	**11.01%**
STD	**2.24%**	**6.08%**	**7.58%**	**2.61%**
BNZ2.6	24.83%	36.05%	29.75%	9.37%
BNZ2.5	20.30%	31.18%	33.20%	15.32%
BNZ2.4	20.23%	32.36%	35.61%	11.80%
BNZ2.3	20.86%	27.97%	42.75%	8.42%
BNZ2.2	26.07%	25.53%	42.02%	6.37%
Average	**22.46%**	**30.62%**	**36.67%**	**10.25%**
STD	**2.78%**	**4.05%**	**5.63%**	**3.44%**
CPC1.5	17.49%	29.93%	44.04%	8.54%
CPC1.4	17.64%	28.73%	42.76%	10.86%
CPC1.3	18.02%	29.89%	43.56%	8.53%
CPC1.2	20.87%	31.41%	43.56%	4.15%
Average	**18.51%**	**29.99%**	**43.48%**	**8.02%**
STD	**1.59%**	**1.10%**	**0.53%**	**2.80%**
CPC2.4	18.79%	35.06%	36.37%	9.79%
CPC2.3	17.23%	30.00%	43.87%	8.89%
CPC2.2	11.07%	17.79%	56.26%	14.88%
Average	**15.70%**	**27.62%**	**45.50%**	**11.19%**
STD	**4.08%**	**8.88%**	**10.05%**	**3.23%**
PLFA	7.66%	16.68%	46.09%	29.57%
SRFA	10.28%	24.72%	43.85%	21.15%

Table 1.17: Iron Concentrations from Surface Water

Average surface water iron concentrations collected over a three-year seasonality study from surface waters in a near-by watershed. Iron concentrations were determined through ICP-MS analysis. +/- is the error determined through standard deviation from the average for the epilimnion (Epi.) and hypolimnion (Hypo.). Further, information and analysis of these samples can be found in Gagné, Section 3.3.2. and 3.4.3.

	Iron ppb	+/-
GSL Epi.	1255.7	1616.4
GSL Hypo.	3331.5	1696.0
OCT Epi.	5478.1	5737.8
OCT Hypo.	8011.5	5549.6
DNL Epi.	513.4	612.7
DNL Hypo.	739.6	589.6
GSBA	889.7	454.6
GSSC	1055.6	241.0
OCC	621.1	296.4

Table 1.18: Hydroxyl Radical Photolysis Rates of Absorbance Decay with Rate Differences

Reconstituted of 10 mg C L^{-1} NOM in 18 MΩ H_2O and pH adjusted to circumneutral with the addition of chemical probes for photolysis experiments. Screening factors are included and determined from equation 2 and the •OH photolysis rates of decay (ROD) were determined based off of equation 1. The difference in unamended sample with amended sample is included with unamended versus iron (P-I) and unamended versus methanol (P-M). ^{3}NOM* rates were determined through equation 3. N/A were samples not run due to lack of sample to reconstitute to 20 mg C L^{-1}. +/- is the error determined through standard deviation. *denoted photolysis rates were not screening factor.

	Plain	Methanol	Iron	Plain		Methanol		Iron		Plain -		Plain -		^{3}NOM*		
Sample Name	SF	SF	SF	Rate 254 nm	+/-	Rate 254 nm	+/-	Rate 254 nm	+/-	Iron	+/-	Methanol	+/-	Rate	+/-	R^2
BNZ1.6	8.38E-01	8.42E-01	8.14E-01	1.64E-03	2.02E-04	1.52E-03	6.17E-05	2.15E-03	1.65E-04	-5.15E-04	2.61E-04	1.17E-04	2.11E-04	1.31E-03	1.84E-04	8.99E-01
BNZ1.5	8.42E-01	8.43E-01	8.20E-01	1.90E-03	1.21E-04	1.38E-03	7.77E-05	2.19E-03	8.94E-05	-2.83E-04	1.50E-04	5.27E-04	1.44E-04	1.35E-03	8.35E-05	9.79E-01
BNZ1.4	8.63E-01	8.60E-01	8.48E-01	2.14E-03	1.56E-04	1.84E-03	6.73E-04	3.79E-03	3.39E-04	-1.65E-03	3.73E-04	3.05E-04	6.91E-04	3.84E-03	2.25E-04	9.82E-01
BNZ1.3	8.58E-01	8.44E-01	8.58E-01	2.49E-03	1.10E-04	1.97E-03	3.11E-04	2.56E-03	3.36E-04	-6.62E-05	3.54E-04	5.23E-04	3.30E-04	1.39E-03	1.44E-04	9.44E-01
BNZ1.2	8.87E-01	8.86E-01	8.60E-01	1.60E-03	1.12E-04	1.24E-03	1.48E-04	2.24E-03	8.67E-05	-6.38E-04	1.41E-04	3.60E-04	1.85E-04	7.90E-04	1.13E-04	9.07E-01
BNZ1.1	9.05E-01	9.05E-01	8.78E-01	1.08E-03	9.09E-05	1.00E-03	9.47E-05	2.17E-03	8.66E-05	-1.09E-03	1.26E-04	8.25E-05	1.31E-04	9.51E-04	6.64E-05	9.77E-01
Average	**8.66E-01**	**8.63E-01**	**8.46E-01**	**1.81E-03**	**1.32E-04**	**1.49E-03**	**2.28E-04**	**2.52E-03**	**1.84E-04**	**-7.06E-04**	**2.34E-04**	**3.19E-04**	**2.82E-04**	**1.60E-03**	**1.36E-04**	
STD	**2.62E-02**	**2.64E-02**	**2.46E-02**	**4.87E-04**	**4.05E-05**	**3.65E-04**	**2.36E-04**	**6.42E-04**	**1.23E-04**	**5.76E-04**	**1.11E-04**	**1.92E-04**	**2.12E-04**	**1.12E-03**	**6.07E-05**	
BNZ2.6	8.64E-01	8.64E-01	8.38E-01	2.33E-03	1.16E-04	1.79E-03	1.51E-04	2.01E-03	2.61E-04	3.17E-04	2.86E-04	5.45E-04	1.90E-04	1.91E-03	1.68E-04	9.51E-01
BNZ2.5	8.56E-01	8.58E-01	8.29E-01	1.95E-03	1.78E-05	1.64E-03	5.68E-05	7.57E-03	2.30E-04	-5.62E-03	2.31E-04	3.16E-04	5.96E-05	1.82E-03	1.65E-04	9.47E-01
BNZ2.4	8.68E-01	8.69E-01	8.42E-01	2.49E-03	2.09E-04	1.97E-03	3.66E-05	2.30E-03	1.95E-04	1.89E-04	2.86E-04	5.22E-04	2.12E-04	1.69E-03	1.21E-04	9.67E-01
BNZ2.3	8.68E-01	8.64E-01	8.36E-01	1.35E-03	8.43E-05	1.11E-03	3.22E-06	1.62E-03	1.00E-04	-2.74E-04	1.31E-04	2.44E-04	8.44E-05	2.66E-03	2.07E-04	9.61E-01
BNZ2.2	8.72E-01	8.70E-01	8.46E-01	1.40E-03	2.60E-04	1.42E-03	1.50E-04	1.57E-03	7.30E-05	-1.73E-04	2.70E-04	-2.01E-05	3.01E-04	1.77E-03	8.61E-05	9.85E-01
Average	**8.66E-01**	**8.65E-01**	**8.38E-01**	**1.91E-03**	**1.37E-04**	**1.58E-03**	**7.96E-05**	**3.02E-03**	**1.72E-04**	**-1.11E-03**	**2.41E-04**	**3.21E-04**	**1.69E-04**	**1.97E-03**	**1.49E-04**	
STD	**6.34E-03**	**4.88E-03**	**6.43E-03**	**5.22E-04**	**9.72E-05**	**3.35E-04**	**6.76E-05**	**2.56E-03**	**8.20E-05**	**2.53E-03**	**6.53E-05**	**2.31E-04**	**9.84E-05**	**3.93E-04**	**4.65E-05**	
CPC1.5	9.05E-01	9.06E-01	8.84E-01	1.71E-03	9.58E-05	1.47E-03	9.45E-05	2.38E-03	2.50E-04	-6.73E-04	2.68E-04	2.37E-04	1.35E-04	2.43E-03	1.24E-04	9.84E-01
CPC1.4	8.94E-01	8.94E-01	8.65E-01	1.65E-03	1.03E-04	1.65E-03	1.19E-04	2.18E-03	4.08E-05	-5.26E-04	1.11E-04	3.99E-06	1.58E-04	2.01E-03	1.26E-04	9.81E-01
CPC1.3	8.89E-01	8.89E-01	8.65E-01	2.27E-03	2.93E-04	1.81E-03	1.07E-04	2.23E-03	3.12E-07	4.31E-05	2.93E-04	4.61E-04	3.12E-04	2.10E-03	1.47E-04	9.70E-01
CPC1.2	8.89E-01	8.90E-01	8.63E-01	2.34E-03	9.47E-05	1.71E-03	9.56E-05	3.03E-03	3.34E-04	-6.95E-04	3.48E-04	6.32E-04	1.35E-04	2.75E-03	1.94E-04	9.69E-01
Average	**8.94E-01**	**8.95E-01**	**8.69E-01**	**1.99E-03**	**1.47E-04**	**1.66E-03**	**1.04E-04**	**2.46E-03**	**1.56E-04**	**-4.63E-04**	**2.55E-04**	**3.34E-04**	**1.85E-04**	**2.32E-03**	**1.48E-04**	
STD	**7.68E-03**	**8.01E-03**	**9.92E-03**	**3.63E-04**	**9.76E-05**	**1.44E-04**	**1.17E-05**	**3.94E-04**	**1.61E-04**	**3.46E-04**	**1.02E-04**	**2.73E-04**	**8.56E-05**	**3.35E-04**	**3.28E-05**	
CPC2.4	N/A	N/A	N/A	N/A	N/A	N/A	N/A	N/A	N/A	N/A	N/A	N/A	N/A	2.52E-03*	2.76E-04	9.43E-01
CPC2.3	8.93E-01	9.00E-01	8.66E-01	1.91E-03	1.07E-04	1.72E-03	2.61E-04	2.20E-03	1.42E-04	-2.89E-04	1.78E-04	1.91E-04	2.82E-04	2.54E-03	1.16E-04	9.87E-01
CPC2.2	N/A	N/A	N/A	N/A	N/A	N/A	N/A	N/A	N/A	N/A	N/A	N/A	N/A	7.05E-04*	4.82E-05	9.77E-01
Average	**N/A**	**N/A**	**N/A**	**N/A**	**N/A**	**N/A**	**N/A**	**N/A**	**N/A**	**N/A**	**N/A**	**N/A**	**N/A**	**1.92E-03**	**1.47E-04**	
STD	**N/A**	**N/A**	**N/A**	**N/A**	**N/A**	**N/A**	**N/A**	**N/A**	**N/A**	**N/A**	**N/A**	**N/A**	**N/A**	**1.28E-03**	**1.17E-04**	
PLFA	9.07E-01	9.07E-01	8.79E-01	1.26E-03	N/A	1.20E-03	N/A	1.53E-03	N/A	-2.75E-04	N/A	5.71E-05	N/A	1.21E-03	7.31E-05	9.84E-01
SRFA	8.70E-01	8.66E-01	8.46E-01	1.09E-03	N/A	1.02E-03	N/A	1.77E-03	N/A	-6.84E-04	N/A	6.52E-05	N/A	1.25E-03	9.13E-05	9.93E-01

Table 1.19: ^{3}NOM* Photolysis Rates Compared with Age

Percent difference of ^{3}NOM* photolysis rates were determined between cores in the same watershed at complimentary carbon ages determined by radiocarbon dating.

Year Range	Cores	% Difference Between Cores
1,400 - 1,460 Years	*CPC1.4 vs. CPC2.4*	22.4%
5,990 - 6,270 years	*BNZ1.4 vs BNZ2.4*	78.0%
6,630 - 6,880 years	*BNZ1.5 vs BNZ2.5*	30.1%
7,160 - 7,200 years	*BNZ1.6 vs BNZ2.6*	37.4%

1.10. Abbreviations:

•OH	Hydroxyl Radical
$^1O_2$	Singlet Oxygen
^{3}NOM*	Triplet State Natural Organic Matter
ABS	Absorbance using UV-Vis
β:α	Freshness Index (Equation in Table 1.2)
Basic Leachate	Leaching Media of pH10 with NaOH
BDL	Below Detection Limits
BIX	Biological Index (Equation in Table 1.2)
BNZ	Bonanza Creek (Soil sample Table 1.3)
C:N	Carbon Nitrogen Ratio
CPC	Caribou Poker Creek (Soil sample Table 1.3)
CRAM	Carboxylic Rich Alicyclic Molecules
DNL	Doughnut Lake
E2:E3	ABS250/ABS365 (Equation in Table 1.1)
E2:E4	ABS254/ABS436 (Equation in Table 1.1)
E2:E6	ABS280/ABS665 (Equation in Table 1.1)
E4:E6	ABS465/ABS665 (Equation in Table 1.1)
EEM	Excitation Emission Matrix
Epi.	Lake Epilimnion
FI	Fluorescence Index (Equation in Table 1.2)
FT-ICR-MS	Fourier Transform Ion Cyclotron Resonance Mass Spectrometry
GSB	Goldstream Blueberry Bog Soil
GSBA	Goldstream Stream at Ballaine Road
GSL	Goldstream Lake
GSSC	Goldstream Stream at Sheep Creek Road
High Salt Leachate	Leaching Media of 0.5 M K_2SO_4 Humification Index (Equation in Table
HIX	1.2)
Hypo.	Lake Hypolimion
ICP-MS	Inductively Coupled Plasma Mass Spectrometry
Iron Amended	Photolysis Samples with Iron Added
LTER	Long Term Ecological Research Facility
MDLT	Material Derived from Linear Terpenoids
Methanol Amended	Photolysis Samples with Methanol Added
Multi-CP-MAS	Multi – Cross Polarization Magic Angle Spinning (Section 1.3.7.)
N/A	Not applicable
NMR	Nuclear Magnetic Resonance
NOM	Natural Organic Matter
OCC	O'Connor Creek
OCT	Octopus Lake
P-I	Plain (unamended) Photolysis Rates minus Iron Amended Rates
P-M	Plain (unamended) Photolysis Rates minus Methanol Amended Rates
PENOM	Permafrost Extractable Natural Organic Matter
PLFA	Pony Lake Fulvic Acid
PPL	Isolation Polymer (Dittmar et al. 2008)

ProTrace	XRF Method
ROD	Rate of Decay
ROS	Reactive Oxygen Species
Sb.Carb	XRF Method
SF	Screening Factor (Equation 2)
SPR-W5-WATERGATE	NMR Method (Section 1.3.7.)
S_R	Spectral Ratio (Equation in Table 1.1)
SRFA	Suwannee Rive Fulvic Acid
STD	Standard Deviation (error) also denoted at +/-
$SUVA_{254}/SUVA_{280}$	Specific Ultraviolet Absorbance
TDN	Total Dissolved Nitrogen
TMP	2,4,6-Trimethylphenol
TOC	Total Organic Carbon
Unamended Photolysis	Photolysis Samples with no additions added
UV-Vis	Ultraviolet-visible spectrophotometry
Water Leachate	Leaching Media of 18 MΩ
XRF	X-Ray Fluorescence

Chapter 2 Permafrost Thaw Impacts on Natural Organic Matter Photoreactivity and Functional Group Composition in sub-Arctic Alaskan Thermokarst Lakes[2]

2.1. Abstract:

Organic matter has the potential to release into surface waters through leaching from soils and surface waters. Thermokarst lake formation is a common occurrence in discontinuous permafrost regions, through the rapid thaw and deposition of permafrost ice wedges subsiding the land into lake depressions that fill with water. Permafrost degradation has been observed to increase greenhouse gas emissions through the microbial degradation; however, photochemical reactivity is an important factor in the environment as it alters the functional group composition of natural organic matter providing implications on environmental changes to surface water pH, micronutrients, and metal cycling. Observing how permafrost soil leaching can influence the functional group composition and photoreactivity is important to assist future interpretations of chemical reactions and greenhouse gas emission models as old sequestered carbon integrates with modern carbon altering CO_2 and CH_4 production. This study observed various permafrost degraded thermokarst lakes, permafrost soil leachate, and ground water natural organic matter isolates to address the following. 1) Does permafrost degradation affect the functional group composition of thermokarst lake natural organic matter and 2) does permafrost degradation affect the photoreactivity of the surface water? These questions were addressed through the utilization of ^{13}C and ^{1}H nuclear magnetic resonance and photochemical experiments to observe the photoreactivity of radicals, hydroxyl radical, and triplet excited state natural organic matter isolated from permafrost leached material. Thermokarst lakes studied were within the same

[2] Gagné, K.R., Ewers, S.C., Murphy, C.J., Daanen, R., Walter Anthony, K., and Guerard, J.J. Permafrost Thaw Impacts on Natural Organic Matter Photoreactivity and Functional Group Composition in sub-Arctic Alaskan Thermokarst Lakes. Prepared for submission in Biogeosciences.

watershed and ecosystem showed differences in functional group composition and photoreactivity between each other and between seasons of winter and summer.

2.2. Introduction:

Yedoma permafrost is rich in organic carbon and ice (Heslop et al. 2019; Strauss et al. 2017; Zimov et al. 2006) and was formed in unglaciated regions during the last ice age when syngeneic sediment, peat, and ice accumulated (Heslop et al. 2019; Schirrmeister et al. 2011; Strauss et al. 2017). The high ice content causes yedoma permafrost to have an increased susceptibility to thaw and the formation of thermokarst lakes due to rapid talik (thaw bulb) formation and is geographically found in interior Alaska (Heslop et al. 2015, 2019; Kessler et al. 2012; Schneider Von Deimling et al. 2015). This thermokarst lake development causes a release of mobile water-soluble organic carbon and it is imperative to understand the functional group composition and reactivity in order to observe how permafrost organic carbon influences thermokarst lake water quality and biogeochemistry.

Inland waters have observed exportation of organic carbon during periods of permafrost degradation (Abbott et al. 2014; Heslop et al. 2017; Vonk et al. 2013). Previous studies have determined the residence time of water in permafrost soils before transport to surface waters is three to seven days (Vonk et al. 2013). Once in the surface waters, permafrost extractable natural organic matter (PENOM) begins to alter the microbial activity (Drake et al. 2015; Dutta et al. 2006; Heslop et al. 2015, 2019; Lipson et al. 2012, 2013; Mann et al. 2014; Plaza et al. 2019; Schuur et al. 2008; Spencer et al. 2015; Vonk et al. 2013; Waldrop et al. 2010; Yang et al. 2016), greenhouse gas emissions (Hodgkins et al. 2014; McCalley et al. 2014; Schuur et al. 2009, 2015; Tveit et al. 2015; Walter Anthony et al. 2016; Yang et al. 2016), and biogeochemistry (Barker et al. 2014; Frey and McClelland, 2009; Pokrovsky et al. 2018b, 2018a). There is a current lack of

understanding for the production of reactive oxygen species (ROS) in the presence of ultraviolet rays in permafrost influenced surface waters, as observed in the minimal literature sources, which all occurred in Arctic Alaskan streams and lakes; CO_2 release upon photomineralization (Cory et al. 2013, 2014), •OH (Grannas et al. 2006; Page et al. 2014), and ^{3}NOM* (Cawley et al. 2009). Determining the ROS production by PENOM prior to infiltration into the surface waters is important for implications upon the natural processes through negatively impacting biota (Cooke et al. 2003; Vehmaa et al. 2013; Wolf et al. 2018), attenuation of pollutants (Bodhipaksha et al. 2017; Xie et al. 2018), partially oxidizes NOM to affect molecular signature and alter abilities of the NOM (Cory et al. 2010b; Scully et al. 2003). ROS production is affected by the inorganic species present in the waters and thus provides insight on how inorganic compounds could be inhibiting the ability for reactivity in the waters (Vaughan and Blough, 1998; Wolf et al. 2018). Determining the photochemical reactivity of PENOM prior to its release in surface waters allows for an unaltered perception on how PENOM may alter surface water reactivity. Additionally, literature has limited studies that observe the functional group composition of permafrost underlain waters through the use of nuclear magnetic resonance to determine the functional group composition of NOM isolated will differ based on the filtration technique from an Alaskan Arctic lake (Grannas et al. 2006) and the observation of functional group composition for comparison between Arctic Alaska surface waters (Cory et al. 2007). The use of NMR functional group composition characterization is important as it provides a nondestructive method to observe carbon functional groups as well as allows for easy qualitative assessment of functional group comparison between samples.

This study utilized the isolation of sub-Arctic thermokarst lake water, ground water, and permafrost soil leachates to develop an increased understanding of functional group composition

through functional groups analysis via solid state and liquid state NMR, as well as photoreactivity production of reactive oxygen species, •OH and ^{3}NOM*.

2.3. Methods:

2.3.1. Sampling location:

The Goldstream valley watershed is a sub-Arctic residential watershed 30 km from Fairbanks, Alaska in the discontinuous permafrost zone (Figure 2.1). This study region has a mean annual temperature of -2.4°C and a mean annually precipitation of 274 mm (Fairbanks Int. Airport, 1981–2010, U.S. National Climatic Data Center (Arguez et al. 2010) and is covered by boreal forest vegetation. Boreal forest vegetation includes black spruce (Picae mariana), white spruce (Picea glauca), moss (hylocomium et al.), alder (Alnus viridis), and tussock cotton grass (Eriophorum vaginatum). The permafrost underlying the study lakes is classified as Pleistocene yedoma due to its high organic and ice content (Elder et al. 2019). Isolated natural organic matter was obtained from three lakes of varying permafrost degradation (GSL, DNL, and OCT), a high carbon content well (BSGW), active layer soils (GSP), and permafrost soil (FTP) obtained from the Cold Regions Research and Engineering Laboratory (CRREL) permafrost tunnel located adjacent to Goldstream valley watershed.

Epilimnion waters were collected into acid washed polypropylene carboys and directly transported to the laboratory in a cooler where they were processed for NOM isolation. Ground water was obtained from a high dissolved methane, high carbon content residential well at the western edge of the watershed. This water was sampled via an outdoor tap before filtration and softener systems in July 2016. Lake samples were collected from the epilimnion at the area of seasonal sampling during winter and summer for DNL and GSL, and summer only for OCT (Table 2.1). These specific locations were chosen as they represent various permafrost

degradation from closed to open thermokarst lakes. Additionally, these lakes were a part of a more extensive seasonality study that provides more in depth understanding of the geochemistry of the system.

Additional surface waters were collected during a three-year seasonality study (March 2016 to October 2018) from epilimnion and hypolimnion of GSL, DNL, and OCT lakes in an attempt to capture spring thaw, summer, fall freeze up, and winter water chemistry. This study utilizes the UV-Vis and fluorescence scans to determine seasonality variability, however further trace metal analysis information can be found in (Gagné, Section 3.4.). Samples were collected, placed in a cooler, and immediately (<5 hours) analyzed in the laboratory.

Active layer samples were obtained using a SIPRE corer during March 2018. Immediately after collection, cores were wrapped in plastic and placed in a -80°C freezer in a So-Low Ultra-Low Upright Freezer U85-22 (Environmental Equipment: Cincinnati, OH) upon return to the laboratory. Soil cores were then freeze dried on a FreeZone Plus 12 Liter Cascade Console Freeze Dry System (Labconco; Kansas City, MO) followed by storage in acid washed plastic bags in the dark until analysis was conducted. Depth of the cores were no more than 60 cm deep, however actual depth was unable to be determined as the active layer did not fully freeze and patches of supra-permafrost waters were discovered while coring. Permafrost core samples obtained from the CRREL tunnel utilized a round key hole saw attached to a power drill at 20 m from the tunnel opening, 54 m, and 81 m. These depths represented 19,000 years, 27,000 years, and 33,000 years respectively (MacKelprang et al. 2017).

Once soils were freeze-dried and leached in 18.2 MΩ water following Gagné et al. (Section 1.3.3 and 1.3.4.) leaching protocol. Leachate and surface waters were then filtered with GWV high capacity groundwater sampling capsules to 0.45 um (PALL, Port Washington, New

York). Following filtering, aliquots of the samples were removed for analysis for trace metal concentrations, total organic carbon, total nitrogen, anion concentration, UV-Vis and fluorescence scans. These aliquots were utilized in a separate additional seasonality study (Gagné, Chapter 3). The remaining 20 – 40 L of water were then acidified to pH 2 with concentrated hydrochloric acid, and pumped at an 18 mL min^{-1} flow rate onto Bond-Elut PPL solid phase extraction cartridges (Agilent; Santa Clara, CA), extracted with methanol (Dittmar et al. 2008), and freeze-dried to obtain a shelf stable solid material for further analysis.

2.3.2. Photolysis Experiments:

Photolysis experiments to determine rate of absorbance decay caused by radical quenching and promotion, unamended rate of absorbance decay, and the rate of ^{3}NOM* production. All rates and experiments are explained in detail in Gagné, Section 1.3.5 and 1.3.6.

2.3.3. NMR Experiments:

^{1}H and ^{13}C NMR experiments are previously explained in detail in Gagné, Section 1.3.7.

2.3.4. Optical Methods:

Fluorescence and UV-Vis are previously explained in detail in Gagné, Section 1.3.6. A detailed table of optical indices is also included as Table 1.1 and Table 1.2.

2.3.5. Statistical Approach:

Optical indices were determined statistically different or the same using a T-test in Prism8 for macOS Version 8.1.2. (GraphPad; San Diego, CA) with a p-value <0.05 for

epilimnion versus hypolimnion and summer versus winter. Thermokarst lakes optical indices were determined to be statistically different or not based on permafrost degradation through ANOVA in Prism8 for macOS Version 8.1.2. with a p-value <0.05 indicating statistical differences between the thermokarst lakes. Outliers were removed in seasonality sample analysis using Prism8 for macOS Version 8.1.2. removing outliers test ROUT with a Q = 1% prior to statistical analysis, averages retained the outliers. All linear regressions with respect to radiocarbon age for functional group composition, optical indices, and photoreactivty were conducted using Prism8 for macOS Version 8.1.2. linear regression statistical approach.

2.4. Results and Discussion:

2.4.1. Functional Group Composition:

2.4.1.1. General NMR Results:

In general, the surface and ground waters had a relative carbon functional group composition with aliphatics (0 – 45 ppm) representing the largest percentage of the ^{13}C NMR spectrum at a range of 23.47 – 32.66% (Table 2.2/Figure 2.2). The second most abundant carbon functional group is characterized as the overall aromatic groups (90 – 160 ppm), which represent -22.42 – 29.10% of the ^{13}C NMR spectra. While aliphatics and aromatics represented approximately 50% of the entire ^{13}C NMR spectra, carbohydrates (60 – 90 ppm) also represented a large proportion of the isolated NOM functional groups ranging from 14.80 – 21.22% of the spectra. Meanwhile, the average of the active layer was mostly comprised of carbohydrates at 32.23 ± 3.75% and aromatics at 29.58 ± 5.29% (Table 2.2/Figure 2.3). Aliphatics only represented 20.48 ± 3.70%, however this lowered percentage is possibly due to the leachability of aliphatics being minimal from active layer and permafrost layer soils (Gagné, Section

1.4.2.2.). The rest of the ^{13}C NMR spectrum from active layer indicated less then 10% for all other functional groups. Active layer NOM had a different functional group composition compared to permafrost soil NOM. Deeper permafrost soils had increased aromatic content with a range from 25.14 – 38.08% for the total aromatic representation in the NMR spectrum. Aliphatics represented another quarter of the isolated PENOM ranging from 24.09 – 30.13% of the ^{13}C NMR spectrum. Carbohydrates were the third largest portion of the NMR spectrum with a range of 14.57 – 21.83%. The rest of the NMR spectrum functional groups on average integrated to less than 15% of the spectrum for each binning region.

Proton functional group analysis on isolate water NOM that possess carboxyl rich alicyclic molecules (CRAMs 1.6 – 3.2 ppm) represented the largest percentage ^{1}H NMR spectra of the NOM with a range of 40.50 – 44.70% (Table 2.3/Figure 2.2). Followed by material derived from linear terpenoids (MDLT 0.6 – 1.6 ppm) which represented 25.27 – 29.80% of the ^{1}H NMR spectrum. Similar to the ^{13}C NMR spectrum carbohydrates represented around 20% of the NOM material with a range of 19.93 – 27.87% and an average of 23.60% (Table 2.3). However, this carbohydrate percentage may be underestimated due to the water suppression technique utilized suppressing upwards of 30% of the signal in the carbohydrate region of the ^{1}H NMR spectrum (Lam & Simpson 2008). Contrary to ^{13}C aromatic content, ^{1}H aromatics represented the smallest amount of the ^{1}H NMR with a range of 4.14 – 7.69% (Table 2.3). This contradiction could be due to the aromatics having more substitution and less hydrogen groups attached to the aromatic ring. However, similar to the ^{13}C NMR spectrum for the active layer there was an increase in aromatic content to an average of 11.17 ± 0.43% and carbohydrate content with an average of 39.80 ± 0.14%. Active layer CRAMs represented 28.17 ± 0.70% and MDLT followed with 20.86 ± 0.99% (Table 2.3). Meanwhile, aromatic content of the permafrost

again increased in comparison to active layer and waters with the ^{1}H NMR showcasing that 10.02 – 32.13% of the proton functional groups in PENOM is aromatic in nature (Table 2.3/Figure 2.3). Carbohydrates were also increased in PENOM samples to a range of 25.13 – 34.25%. However, CRAMs were the second most common functional group in the proton spectrum with a range spanning 33.48 – 36.92% and MDLT representing less then carbohydrates at a range of 20.65 – 27.93% (Table 2.3/Figure 2.3). The differences in aromatic groups was showcased in both carbon and proton functional group analysis with increased aromatic content found in the permafrost compared to active layer and waters. Similarly, carbohydrate content was highest in active layer in both carbon and proton functional group analysis.

2.4.1.2. Reference Material compared to Literature:

The reference NOM utilized in this study are surface water samples isolated from a lake and a river making the reference material more similar in nature to the waters in this study compared to the soil NOM. However, the isolation for PLFA and SRFA utilize different non-polar resin than surface waters, which were isolated via non-polar PPL cartridges. Li et al. (2017) determined that NOM extracts isolated from non-polar resin like PPL cartridges were grouped together through the principal component analysis of TOC, NMR, and Fourier-transform ion cyclotron resonance mass spectrometry (FT-ICR-MS) (Li et al. 2017). The binning ranges of reference materials analyzed using CP-MAS ^{13}C NMR vary between studies and thus, herein only observational comparisons can be made between literature and this study (Cawley et al. 2013; Chin et al. 2004; Fimmen et al. 2007; Guerard, 2009; Westerhoff et al. 1999). As this study utilized a multi-CP-MAS experiment allowing for a more uniformly sensitive spectrum over the functional groups, a more robust and quantifiable ^{13}C NMR spectra was achieved

(Johnson and Schmidt-Rohr, 2014). Additionally, some studies excluded 90 – 120 ppm binning range (Chin et al. 2004; Guerard, 2009). Aliphatic functional group analysis using ^{13}C NMR was higher in PLFA compared to SRFA (Chin et al. 2004; Guerard, 2009). Meanwhile, the majority of the spectra with the exception of aliphatics were higher in SRFA compared to PLFA (Guerard, 2009). This overall comparison of binning percentages between reference NOM ^{13}C NMR provides evidence that the carbon functional groups in this study were similar to literature (Table 2.2). Contrary to Chin et al. (2004) carbonyl carbons (190 – 220 ppm) were observed to have a lower percentage value for PLFA when compared to SRFA; however, the observed percentage was similar to another study conducted by Cawley et al. (2013) who observed a 0.3% while, this study observed 0.4% for PLFA carbonyl content.

Literature values for isolate NOM ^{1}H NMR spectrum are much more limited in comparison to ^{13}C NMR spectrum and variability in the spectrum is increased due to the use of different solvents for resuspension, for example; D_2O (Li et al. 2017; Rodríguez et al. 2016), DMSO (Han et al. 2019), and NaOD (Hertkorn et al. 2013), while this study resuspended the isolated NOM using H_2O. Additionally, care must be made comparing relative integrations as the binning may be slightly skewed between different studies similarly with ^{13}C NMR due to where solvent influenced the spectrum differently. SRFA was characterized with D_2O resuspension (Rodríguez et al. 2016), while PLFA ^{1}H NMR was not found in literature. The studies discussed in the section are ones where relative integrations are published. There are others who ran NOM samples but without publishing the percentages (Lam and Simpson, 2008). The relative integration chemical shift bins observed for SRFA and a Nordic lake fulvic acid (NAFA) reference material that compare most similarly with this study observed that SRFA had 42.3% MDLT and NAFA had 38.9% MDLT (Rodríguez et al. 2016). This percentage is much larger

than what was observed in this study however, the samples were resuspended in D_2O and used a different NMR method both of which could alter the functional group percentages, as well as the SRHA and NAFA could be from different batch numbers (Rodríguez et al. 2016). Thus, the most important observation was that SRFA had a higher percentage of MDLT to NAFA, which was observed throughout the different binning regions.

2.4.1.3. Waters compared to Literature:

When comparing ^{13}C NMR percentages to literature the binning values can vary slightly based on the authors' discretion on functional group ranges. However, aliphatics (0 – 60 ppm) were consistently the largest percentage. This study observed aliphatics 0 – 45 ppm and 45 – 60 ppm summation for isolated NOM from surface waters in the thermokarst lakes to range from 36.76% to 42.35%. A sample obtained from an Arctic lake (Toolik Lake) isolated using C-18 saw an aliphatic percentage of 45.8% very similar to the results observed in the sub-Arctic thermokarst lakes (Grannas et al. 2006). Similarly, Minnesota lakes also observed a high aliphatic carbon percentage, however these authors did not integrate 60 – 110 ppm so the exact percentages cannot be compared (Westerhoff et al. 1999). Furthermore, aromatic content of the surface waters in this study ranged from 12.05% to 15.72%, which is comparable to literature values for Toolik lake at 13.6% (Grannas et al. 2006).

Groundwater isolation is difficult due to the low carbon content of ground water, however, a few ground water isolations were found in studies from Minnesota and Bangladesh (Mladenov et al. 2015; Westerhoff et al. 1999). Groundwater in literature was isolated using XAD-8 resin from 6 sampling locations in Bangladesh, where groundwater was determined to be heterogeneous based on wide spread ranges for functional group binning percentages. Sub-Arctic

ground water had a total of 45.98% aliphatic composition while, Bangladesh aliphatic composition ranged from 45.3% to 63.2% (Mladenov et al. 2015) and Minnesota had a composition of 61% aliphatics when only observing four bins, thus this percentage is higher than had the authors done 6 ranges as this study and Bangladesh samples (Westerhoff et al. 1999). This study observed 90 – 120 ppm as proton substituted aromatics to include a secondary peak in the spectrum for a total percentage of 9.44% while, Mladenov et al. (2015) interpreted the region from 90 – 110 ppm as acetal functional groups had a much lower overall percentage for the ground waters sampled with a maximum value of 3.34%. This discrepancy in functional group distribution was also observed in the aromatic region of 110 – 165 ppm where sub-Arctic ground water came out to 17.06%, while Bangladesh ranged from 14.1% to 25.8% with an average of 22.8% (Mladenov et al. 2015). Sub-Arctic groundwater has some similarities with other areas but overall had a different functional group composition and although isolating groundwater is difficult due to low carbon concentration it is important to isolate groundwater in the sampling area to ensure adequate representation of ground water influence on surface waters.

No current literature was found for NOM isolated from waters that included relative interpretations of functional group binning for ^{1}H utilizing the same or relatively similar ^{1}H NMR techniques. Thus, ^{1}H NMR spectra of surface waters were not compared to literature values in this study.

2.4.1.4. Soils compared to Literature:

Active layer and permafrost soils have been determined to have heterogeneity both within a watershed and between watersheds (Gagné, Section 1.4.1.3. and Section 1.4.3.2.). Due to this heterogeneity, it is no surprise that the active layers NOM collected within the same area have

varying functional group composition and direct comparison to other watershed samples should be used with caution. Thus, the following comparison is not on direct percentage values but through overall observations with different permafrost extracted NOM in literature. In general, aliphatic, aromatic, and carbohydrate functional groups comprised the majority of the NMR spectra (73 – 84%), observed in both this current study and literature (Gagné, Section 1.4.3.2). Similarly, carboxyl/aliphatic amides and aliphatic methoxyl ^{13}C NMR spectrum functional group percentages were variable depending on sample and represented 6% to 13% of the NMR spectra (Table 2.4) (Gagné, Section 1.4.3.2.2). Ketone functional group composition was always the smallest fraction of the ^{13}C NMR spectra for all soil NOM analyzed in this study and literature (Gagné, Section 1.4.3.2.2).

Hertkorn et al. (2002) observed peat soil humic acid and fulvic acid isolate via a NaOD resuspension for ^{1}H NMR analysis with the following binning ranges; 0.5 – 1.95 ppm, 1.95 – 3.1 ppm, 3.1 – 4.6 ppm, 4.7 – 6.0 ppm, and 6.0 – 10.0 ppm due to not requiring the suppression of water. MDLT content from peat soil humic acid isolation was very similar to the MDLT of active layers and permafrost soils in the sub-Arctic at 24.9% (Hertkorn et al. 2002). Aromatic ^{1}H content was also most similar to the HA fraction at 15.6%, however the HA peat soil had a highest percentage possibly due to the increased chemical shift range (Hertkorn et al. 2002). Active layer and permafrost layers in sub-Arctic watershed averaged 10.58%. Observing similar MDLT and aromatic relative integrations as humic acid fraction from peat soil values indicates that the isolate obtained from NOM leaching of soils in this study were more humic acid in nature. Overall, with the limited samples available for comparison of ^{1}H NMR the spectrum obtained from the NOM isolates in the studies sub-Arctic watershed are comparable to literature

and provide additional samples for future comparisons, with the exception of surface water samples due to no literature values found.

2.4.1.5. Isolated Samples compared to Reference Material:

In order to determine if the isolated NOM in this study site were more terrestrial or microbial like in their functional group composition, the reference material NMR spectra binning percentages had the sample NMR spectra binning percentages subtracted from it to determine the difference in relative integration for a chemical shift region (Equation 1). From this analysis the sum of relative integration difference for PLFA and SRFA we compared with a smaller total percentage indicating a closer similarity to the reference material, ie. BSP had a 7.78% total with SRFA comparison and a 27.93% total with PLFA comparison (Table 2.4). Based off this analysis BSP is more terrestrial like, as this thermokarst lake NOM has more similar NMR results with SRFA. This terrestrial source material seems to be consistent with all samples including soil leachates, with the exception of the ground water and DNL Summer. For the ground water, SRFA was 25.14% different and PLFA was decreased to 14.97% different, indicating the ground water had increased similarity in functional group composition to PLFA or microbial derived NOM making it less terrestrial in source material (Table 2.4). With the highest difference in aliphatic, carbohydrate, and aromatic chemical shift ranges, doubling relative integration differences in BSGW compared to SRFA. Additionally, DNL Summer also saw a decrease in terrestrial sourced material as DNL Summer observed a lower relative integration difference with PLFA at 19.42% compared to SRFA at 20.81% (Table 2.4). The two percent totals are closer than groundwater indicating DNL Summer has an increased terrestrial signal compared to BSGW but a decreased terrestrial signal compared to GSL and OCT, potentially

caused from ground water influx into DNL, as DNL is open to ground water influence. The largest difference between PLFA and the samples collected was determined to be in the 0 – 45 ppm aliphatic range where the average difference was 11.53 ± 3.82%, while the rest of the NMR spectra had an average of less than 6% difference between PLFA and the sample of choice. SRFA on the other hand all binning ranges had an average less than 5%, again showcasing the similarity the isolated NOMs had with terrestrial inputs.

$$|\text{Spectrum \#1 \%} - \text{Spectrum \#2 \%}| = \text{Difference in relative integration}$$

Equation 1: Determination of NMR spectrum differences for seasonality variability between lake NOM samples.

Although the soil functional group composition is variable between and within watersheds, the majority of the functional group bins relative integrations were similar compared to the reference NOM ^{13}C NMR spectra. Aliphatics and aliphatic methoxyl groups were found to be less in the active layer in comparison to the reference NOMs. This decrease in aliphatic functional groups was expected, as aliphatics have been observed to not leach heavily from the soils (Gagné, Section 1.4.2.2). Additionally, carbohydrates were observed to be in a higher abundance in active layer. While, aromatic total and carboxyl/aliphatic amides were more variable within the active layer from each core compared to the reference NOM. Permafrost soil NOM has a different functional group composition than active layer NOM and thus, has a different comparison trend with reference material NOM. Permafrost NOM aliphatic composition was greater than active layer NOM and the percentage was between PLFA and SRFA aliphatic, while aliphatic methoxyl groups were more variable with FTP2 being between and FTP1 and FTP3 being less than reference NOM similarly to active layer samples. Similarly,

a decreased functional group composition of aliphatic methoxyl groups is due to aliphatics being retained on the soil matrix (Gagné, Section 1.4.2.2). Increased variability occurred throughout the rest of the NMR spectra 60 – 220 ppm within the permafrost samples, as the radiocarbon dates span 14,000 years supporting that permafrost is heterogeneous (Gagné, Section 1.4.3.2.). Overall, when compared to the reference materials, all soil leachates were most similar to the terrestrial reference material of SRFA with relative integration difference in spectrum percentages ranging from 5.78 – 28.96%, while PLFA differences ranged from 26.57 – 52.13% (Table 2.4). This similarity to terrestrial derived reference material makes sense as the soil is a terrestrial source.

Surface water proton functional group composition was compared to reference material to determine if the samples were less terrestrially sourced (PLFA) or terrestrially sourced (SRFA) just as was completed for ^{13}C NMR data (Equation 1) (Table 2.5). Unlike ^{13}C NMR results the waters more similar to microbial composition were OCT Summer and DNL Winter, while ground water and DNL Summer were more terrestrial like in the proton functional groups. Meanwhile, the soils from active layer and permafrost soils were consistently more similar to terrestrial sourced reference material proton functional group characterization just as the soils were with carbon functional group characterization (Table 2.4/Table 2.5)

2.4.1.6. Waters compared to Soils:

The varying degrees of permafrost degradation underneath these thermokarst lakes allows for the interaction of permafrost and active layer soils. Due to this interaction it is important to compare the functional group composition of the soils in this study with the waters to determine how soils may be influencing the functional groups of the water NOM (Table 2.6). The

following comparisons have been completed using permafrost soils at the edge of the watershed. While permafrost is heterogeneous the use of the current permafrost was required due to deep active layers and inability to collect permafrost samples within the vicinity of the surface waters. Additionally, the use of the CRREL permafrost tunnel allowed for unaltered permafrost to be isolated, while collection of permafrost from the center of the residential watershed may have previously thawed due to building construction in the area. Overall, all of the waters were most similar to FTP2 followed by FTP3. This similarity is also consistent with groundwater water and thus, surface water comparison to groundwater was also conducted to determine which isolate is controlling the functional group composition of the surface waters, which determined the surface waters were all greater than 31% different from the ground water (Table 2.6). This larger difference with groundwater indicates that the majority of water NOM is probably most influenced from soil leaching into the thermokarst lake. OCT Summer was most similar to FTP2 with a 7.26% difference, however the range for the waters compared to FTP2 was 7.25 – 22.66% relative integration difference, with the greatest difference in groundwater (Table 2.6). The surface waters were most dissimilar to FTP1 at greater than 50% difference between samples and FTP3. Meanwhile, the groundwater was most dissimilar to both active layer samples at 52.69% (GSP2) and 54.08% (GSP1) (Table 2.6). This discrepancy between active layer and ground water is most likely caused by the ground water not being in contact with the active layer as the aquifer is most likely within the permafrost layers or through permafrost at 72.5 meters deep.

The comparison of soil NOM isolates and water NOM isolate produced similar results with the hydrogen functional group characterization as was observed in carbon functional group characterization (Table 2.7). The waters were most similar in overall binning percentages to FTP2 followed by FTP3. However, unlike the carbon NMR results FTP1 was third in rank for

similarities instead of last. Carbon NMR allows for an increase in chemical shift compared to proton NMR, allowing for the observation of more functional groups to be distinguished.

2.4.1.7. Winter versus Summer Functional Group Distribution:

When observing seasonality differences in GSL and DNL through the observation of the difference in relative integration for a chemical shift region (equation 1), ^{13}C functional groups had a decrease in functional group composition variability during the wintertime with a 6.38% total difference compared to summertime that had a 13.66% difference in the spectrum (Table 2.8). The major seasonality difference was observed in the aliphatic and aromatic ranges. As aliphatics in summertime observed a 5.06% difference but winter only had a 1.47% difference between the open and closed lakes. Meanwhile, aromatics observed a difference of 6.23% in the summer and 1.01% in wintertime. Overall, winter had less than 2% difference for each binning region with a difference as low as 0.11% for carbohydrates. This decrease in variability during wintertime could be due to the lack of lateral flow through active layers, as samples were isolated in January when the majority of the active layer is frozen. Soil temperatures collected from 0 cm to 90 cm observed an average of -2.3°C to 0.82°C from January 2016 to January 2018 (Liljedahl, 2019). Lateral flow rates in summertime were not collected during this study and future studies of these lakes should include data of this type.

Unlike carbon functional group characterization proton functional group characterization saw a decrease in seasonal variability for summer time observing only a 7.18% difference between GSL and DNL lake NMR spectra with all functional group ranges having < 2.5% (Table 2.9). Meanwhile, winter proton group differences observed a total of 13% with the majority coming from a difference in carbohydrate composition of 6.69% difference between the two

spectra, which was not observed with the carbon functional group analysis. Hydrogen NMR results indicate that winter had an increased variability between the two taliks that was contradictive to ^{13}C NMR analysis. This illustrates the importance for conducting both ^{13}C NMR and ^{1}H NMR analysis as you may get varying results due to the sensitivity for observing differences in functional group functional group composition (Figure 2.4).

2.4.2. Optical Indices:

2.4.2.1. Overall Lake Whole Water Samples for Three Years:

Samples isolated in this study were a part of a larger three-year seasonality study where between 12 and 18 individual samples were taken from various months throughout the year including during ice coverage (Gagné, Chapter 3). Samples were taken from the epilimnion and hypolimnion for GSL, OCT, and DNL thermokarst lakes. The majority of these samples between top and bottom were not statistically different based of a two-tailed T-Test for optical indices. (Table 2.10). This lack of difference is caused by the shallow nature of the thermokarst lakes and thus, only the epilimnion of these thermokarst lakes will be discussed. S_R was observed to be statistically different through an ANOVA between all thermokarst lake tops including BSP. BSP values were obtained from a smaller subset of samples with only seven samples collected and analyzed during the last two years of the three-year study. The highest value observed in DNL with an average of 0.964 ± 0.076, while the lowest S_R value was observed in OCT with an average of 0.799 ± 0.026 (Table 2.11). Since S_R is negatively correlated with molecular weight based off of this value OCT has the highest molecular weight for the NOM observed in the waters, while DNL has the lowest molecular weight. Due to the variability of iron within each water system the corrected $SUVA_{254}$ following Poulin et al. (2014) was utilized for interpretation

of these values (Poulin et al. 2014). $SUVA_{254}$ values correlate positively with molecular weight but are most commonly used to obtain interpretations on functional group analysis without the use of other instrumentation methods such as NMR and FT-ICR-MS. Aromaticity has been observed to have a positive correlation with $SUVA_{254}$ values, while aliphatic functional groups correlate negatively. The highest $SUVA_{254}$ value was observed in OCT at an average of 2.429 ± 1.125 L mg C^{-1} m^{-1}, which agrees with molecular weight correlations observed with S_R, OCT has the highest molecular weight based off of optical indices. The lowest $SUVA_{254}$ value was observed in GSL with an average of 0.996 ± 0.256 L mg C^{-1} m^{-1} followed closely by DNL with an average value of 1.061 ± 0.238 L mg C^{-1} m^{-1}. Although, GSL, DNL, and BSP were very close in their average values statistically all thermokarst lake samples $SUVA_{254}$ were statistically different. E2:E3 is a ratio of absorbance values from each UV-Vis spectrum and has been observed to correlate with molecular weight, and thus not surprisingly OCT had the lowest value at 4.100 ± 0.415. This low value correlates with a high molecular weight of the NOM found within the OCT surface waters over a three-year study. GSL and DNL have values similar to each other at 8.553 ± 1.133 and 8.190 ± 1.241, these large standard deviations indicate that E2:E3 is more variable than the other optical indices. This variability may be the cause of E2:E3 indicating that GSL NOM has a lower molecular weight than DNL while other optical indices correlated with DNL having the lowest molecular weight. However, E2:E3 was observed in this study to allow for further comparisons to literature values of other water systems. E2:E3 was also statistically different in all of the thermokarst lakes.

FI values between all lake tops and BSP were found to be significantly different through an ANOVA (Table 2.10). GSL and BSP had similar high FI values at 1.626 ± 0.049 and 1.607 ± 0.024 (Table 2.11). These two values were observed to be not statistically different through a t-

test. However, when BSP was ignored for thermokarst lake top comparison the three thermokarst lakes were still observed to be statistically different and thus, the two closed thermokarst lakes source material were comparable to each other and were less terrestrial sourced. DNL and OCT values were more terrestrially sourced material at 1.563 ± 0.087 and 1.543 ± 0.105 (Table 2.11), these two lakes were not statistically different. The statistical difference observed with the ANOVA was between the closed thermokarst lakes and the partially open thermokarst lakes with GSL and DNL and GSL and OCT.

HIX optical index values were not statistically different between samples throughout the three-year seasonal study. Due to this lack of statistical difference conclusions cannot be interpreted on how permafrost degradation may influence the degree of degradation of plant material. The range of HIX values were observed from GSL at 0.932 ± 0.014 to OCT at 0.958 ± 0.033 (Table 2.11). Although thermokarst lakes were not significantly different to determine the degree of humification, increased HIX values correlates with an increase in humification of the NOM (Table 2.10). All HIX values from this sub-Arctic boreal watershed were much greater than the reference materials PLFA (0.793) and SRFA (0.868), indicative of the waters have an increased degree of degradation from plant remains outside of the microbial – terrestrial NOM source spectrum (Table 2.11).

$\beta:\alpha$ and BIX while have different values provide similar correlation in degradation and behave similarly with DNL having the highest value and OCT having the lowest value. Both indices are statistically different between all thermokarst lake types (Table 2.10). Unlike FI both $\beta:\alpha$ and BIX show a statistical difference between GSL and BSP, as well as between DNL and OCT. DNL had the highest $\beta:\alpha$ value at 0.709 ± 0.15 and OCT had the lowest at 0.576 ± 0.052 (Table 2.11). The larger $\beta:\alpha$ and BIX values correlate to increased degradation in the

thermokarst lake through microbial activity and thus, DNL and GSL which were not statistically different from each other were the two thermokarst lakes with the most recently degraded NOM. This microbial degradation can be observed through the increased production of CH_4 production through the observation of methane bubbles and open ice in the wintertime due to high methane seepage (Walter Anthony et al. 2018).

2.4.2.2. Isolate Date Specific Whole Water Samples:

UV-Vis optical indices developed by previous studies are utilized to observe correlations on general NOM characterization (Table 1.1 & Table 1.2). Reference materials of PLFA and SRFA have values of 1.035 and 0.812 respectively for S_R (Table 2.12). All of the surface waters and permafrost leachates values for S_R fell between the values described by the reference materials. For example, GSL had an average S_R of 0.842 ± 0.025, OCT was 0.867 for summer, DNL was 0.953 ± 0.085, and BSP was 0.928. Differences greater than 0.1 shows a difference in optical indices for organic material (McKnight et al. 2001). DNL S_R average indicates the organic matter is different from the other water samples. This larger value indicates that DNL is less terrestrial sourced, as indicated by having a value closer to PLFA. Due to the large S_R value obtained DNL NOM may have a lower molecular weight to the other samples based on the negative correlation associated with S_R. The active layer leachate presented with a lower S_R value compared to the waters at 0.590 ± 3.16E-5, while the permafrost leachates were similar to the waters at 0.943 (FTP1), 0.888 (FTP2), and 0.913 (FTP3) (Table 2.10). This lower active layer S_R could be influencing GSL, OCT, and BSP through lateral surface flow through the active layer during summer, along with influence from plant material that had low S_R of 0.6 for Alder, 0.6 for Poplar, and 0.3 for Spruce (Mutschlecner et al. 2018a), causing these thermokarst

lakes to have a lower and similar S_R in comparison to DNL. These three thermokarst lakes presented values between the two reference materials indicating NOM sourced from both microbial and terrestrial sources, which had an intermediate molecular weight. Groundwater influence had an S_R value of 0.927, which does not have a 0.1 difference between any of the surface waters and thus, cannot be determined to affect the S_R values from ground water influence onto the surface waters. The values for S_R are higher than what was found in literature on interior Alaska stream waters, which had an average of 0.809 ± 0.042 (Mutschlecner et al. 2018b). This indicates that the thermokarst lakes have lower molecular weight NOM when compared to the stream waters.

$SUVA_{280}$ values are also reported in Table 2.12, but only $SUVA_{254}$ values will be discussed here. The $SUVA_{254}$ correction was deemed necessary as some samples had values greater than 5.0, which indicates iron absorbance interference in the UV-Vis spectrum (Mladenov et al. 2015; Weishaar et al. 2003). $SUVA_{254}$ values for the thermokarst lake waters only were corrected for high iron concentrations using a correction factor determined following Poulin et al. (2014) oxic study using iron titration of NOM isolated from a fen in the vicinity of the watershed utilized in this study (Table 2.13). Iron increases the absorbance values of the UV-Vis spectrum (Poulin et al. 2014). Following the iron titration for the nearby fen confirmed iron addition increases the value of $SUVA_{254}$ with increased Fe concentration.

$$\mathrm{SUVA_{Corrected}} = \frac{\mathrm{SUVA} * (0.075[\mathrm{Fe\ III}] + 0.809)}{2.303}$$

Equation 2: Correction equation for $SUVA_{254/280}$ was determined with an R^2 of 0.975 for Fe concentrations upwards of 5 ppm.

$SUVA_{254}$ for soil NOM reconstituted values were not corrected as the correction factors were sample type specific and could only be utilized for lake waters. $SUVA_{254}$ values for all water NOM and soil NOM were outside the reference material range from PLFA and SRFA at 2.148 L mg C^{-1} m^{-1} and 4.164 L mg C^{-1} m^{-1} respectively, with the exception of FTP3 (Table 2.12). GSL had an average of 1.538 ± 0.598 L mg C^{-1} m^{-1}, OCT had the highest value of 2.487 L mg C^{-1} m^{-1}, DNL had an average of 1.171 ± 0.297 L mg C^{-1} m^{-1}, and BSP had a value of 1.039 L mg C^{-1} m^{-1}. There was no $SUVA_{254}$ value obtained for the ground water sample during isolation however, previously sampled wells had an average $SUVA_{254}$ value for well waters was 1.735 ± 1.313 L mg C^{-1} m^{-1} over a 3-month span, with outliers removed the average for ground water decreased to 1.172 ± 0.493 L mg C^{-1} m^{-1} (Gagné, Chapter 3). Active layer leachate SUVA value was 1.868 L mg C^{-1} m^{-1}, higher than GSL and DNL thermokarst lakes. Permafrost leachate were similar to active layer leachate values at 1.978 L mg C^{-1} m^{-1} (FTP1), 1.718 L mg C^{-1} m^{-1} (FTP2), and 2.279 L mg C^{-1} m^{-1} (FTP3) (Table 2.12). These $SUVA_{254}$ values correlate with the interpretation that the permafrost and active layer were more aromatic, less aliphatic, and have a higher molecular weight in comparison to surface waters. These $SUVA_{254}$ observations are inconsistent with the NMR aromatic percentage. This could be due to $SUVA_{254}$ only taking into consideration the optically active aromatic content and thus, both NMR and UV-Vis optical indices should be considered jointly for the overall characterization of NOM. The increase in aliphatic content observed by the $SUVA_{254}$ values in the surface waters would be coming from an ecosystem input as these boreal forest, sub-Arctic soils do not readily leach out aliphatic content (Gagné, Section 1.4.2.2). Previous work conducted on permafrost underlain surface waters in the form of streams was conducted by Mutschlecner et al. (2018b) in interior sub-Arctic and Arctic Alaska observed an average $SUVA_{254}$ values of 3.463 ± 0.278 L mg C^{-1} m^{-1}. This is much higher

than the observed average for sub-Arctic thermokarst lakes in this watershed, which was 1.491 ± 0.608 L mg C^{-1} m^{-1}, with a maximum value of 2.487 L mg C^{-1} m^{-1} in the transitional thermokarst lake summer sample (Table 2.12). Mutschlescner et al. (2018b) did not correct the $SUVA_{254}$ values for the iron interference, which could be causing an increase in absorbance value and thus, increasing the $SUVA_{254}$ values. Iron values were not disclosed by Mutschlecner et al. (2018b) however, a sample was taken from a common stream source at Caribou Poker Creek LTER (CPC) site for trace metal analysis. CPC had an iron concentration of 100.8 μg L^{-1} determined in this study with a $SUVA_{254}$ value of 3.38 L mg C^{-1} m^{-1} determined by Mutschlecner et al. (2018b). Thus, it is possible for iron to be inflating these literature values.

E2:E3 is the absorbance ratio between 250 nm and 365 nm that correlates negatively with molecular weight. The thermokarst lakes reconstituted NOM in the study site had higher E2:E3 ratios compared to the literature values of PLFA and SRFA who had ratios of 4.843 and 4.979 respectively (Table 2.12). Although this comparison is between whole water observations for the surface waters and NOM isolation for the reference materials, when observing the NOM isolates the ratios were still greater than the reference material, suggesting a lower molecular weight than the reference isolates. On average, GSL had a E2:E3 ratio of 8.227 ± 0.462, OCT ratio was 5.867, DNL averaged to 9.106 ± 1.001 and BSP had a value of 8.115. The ground water whole water had the lowest E2:E3 at 6.547 an indication that groundwater had a larger molecular weight compared to the surface waters. Additionally, the soil leachate from active layer had an average E2:E3 less than reference material at 4.67 ± 0.020. However, permafrost leachate from the sampling location for this study came out to have a higher E2:E3 ratio than active layer at 5.238 (FTP1), 6.261 (FTP2), 6.178 (FTP3). Permafrost leachate E2:E3 correlates to smaller molecular weight which, could be infiltrating the surface water thermokarst lakes increasing the

E2:E3 as permafrost leachate functional group composition is dependent on location and samples were not collected of permafrost beneath the thermokarst lakes (Gagné, Section 1.4.3.1). The comparison of E2:E3 values between samples and other published values is isolated to specific sample types; soils (Kiss et al. 2014), additional reference material (Rodríguez et al. 2016; Wan et al. 2019) and waste water effluent (Wan et al. 2019). Overlapping reference material occurred with SRFA which had a E2:E3 value of 4.979 in this study and a value of 4.697 in literature (Rodríguez et al. 2016). The value observed in this study was only slightly larger and thus, if it were an instrument and method discrepancy causing the increased values for the thermokarst lake surface waters they would not be 4 units higher. These increased values were considered to be true and correct for the surface waters observed as well as consistent as observed by a seasonality study of surface waters in this study site location. Soils leachates observed in literature came from Hungary and had E2:E3 values ranging from 3.19 to 4.52 (Kiss et al. 2014). These soil values were observed to be similar but less than the active layer leachates. This discrepancy in soil values could be due to the two sampling locations having variations in soil type and ecosystem and thus, Hungary samples may have a higher NOM molecular weight in their soil leachates.

Fluorescence indices equations and correlations are found in Table 1.2. FI microbial sourced value was obtained from PLFA with a value of 1.549, while the terrestrial sourced reference material had a value of 1.314 (Table 2.12). Similar observations for PLFA and SRFA have been repeated in other studies; PLFA FI at 1.453 and SRFA at 1.300 (Guerard et al. 2009). The discrepancy in PLFA could be due to the different instruments used to obtain the fluorescence scans as discussed in a previous section (Cory et al. 2010a). NOM samples isolated by XAD-resin had FI ranging from 1.7 to 2.0 for microbially derived NOM; while terrestrial

derived FI values were < 1.40 (Cory et al. 2010a). When observing thermokarst lake values for FI it was observed GSL had an average value of 1.659 ± 0.057, OCT had a value of 1.535, DNL had an average value of 1.540 ± 0.034, and BSP had a value of 1.634 (Table 2.12). These surface waters were similar to PLFA or higher than PLFA FI value indicating less of a terrestrial sourced material in the surface water composition with BSP having a high lowest terrestrial signature. These carbon rich lakes are highly susceptible to microbial degradation, which is increasing the export of CH_4 and CO_2 into the atmosphere (Elder et al. 2019; Walter Anthony et al. 2016, 2018). This area of high microbial degradation has the potential to influence the NOM source material to have an influx of microbial derived NOM. Ground water has a high FI value as well at 1.664 while soil leachates had values less than all the water samples with active layer averaging 1.329 ± 0.011 and permafrost leachate having values of 1.506 (FTP1) and 1.530 (FTP2) (Table 2.12). These lower values are consistent with terrestrial organic matter sourcing and both values are between the reference material values. Above PLFA, FI values also occurred in interior Alaska stream water samples which ranged from 1.260 to 1.590 and had an average of 1.520 ± 0.039 (Mutschlecner et al. 2018b). The highest FI value came from the most northern stream that was underlain by permafrost (Mutschlecner et al. 2018b) similarly with the two closed thermokarst lakes having the highest FI values. Ground water FI values have been observed in literature to have various FI based off of age with values ranging from 1.460 to 1.570 over ground waters aged <5 years through >30 years (Mladenov et al. 2015), providing insight that ground water is less terrestrial in source based off an FI greater than PLFA. Active layer leachates have been obtained from other study sites near to this watershed by Wickland et al. (2018) who observed FI's between PLFA and SRFA at 1.300 to 1.450 for the upper 100 cm of soil similar to the active layer values in this study.

HIX values are indicative of humification or the degree of degradation from plant remains with a large HIX correlated with increased humification (Gabor et al. 2015; Hansen et al. 2016; Ohno, 2002). HIX values for surface waters isolated in this study observed a HIX value of 0.945 ± 0.097 for a GSL average, 0.920 for OCT, 0.956 ± 0.097 for a DNL average, and 0.952 for BSP (Table 2.12). Ground water HIX value was low in comparison to the surface waters with the exception of OCT at 0.924. Meanwhile, active layer leachate had the lowest HIX average at 0.892 ± 0.013 and permafrost leachates had higher HIX values in comparison to active layer at 0.946 (FTP1) and 0.927 (FTP2). All HIX values in this study were greater than the reference materials PLFA (0.793) and SRFA (0.868) indicative of the waters and leachates having an increased degree of degradation from plant remains. HIX values for arctic stream waters in interior Alaska averaged 0.900 ± 0.051 (Mutschlecner et al. 2018b) along with soil leachates from interior Alaska had HIX values ranging from 0.760 to 0.890 (Wickland et al. 2018). These values showcase a higher degree of humification in boreal forest and tundra ecosystems compared to PLFA and SRFA reference material.

$\beta:\alpha$ and BIX values follow similar trends with each other, with $\beta:\alpha$ having decreased values compared to BIX. However, when plotted against each other, the $R^2 = 0.999$, showcasing a linear relationship. All of samples $\beta:\alpha$ values with the exception of active layer leachate fell between the reference material of PLFA and SRFA, which had values of 0.756 and 0.408 respectively (Table 2.12). Average $\beta:\alpha$ values for GSL surface waters was 0.700 ± 0.0173, OCT was 0.582, DNL had an average of 0.674 ± 0.023, and BSP had a value of 0.680. Meanwhile, ground water $\beta:\alpha$ was 0.676. Active layer leachates averaged a low $\beta:\alpha$ value of 0.391 ± 0.007, while permafrost leachate had $\beta:\alpha$ values of 0.569 (FTP1) and 0.573 (FTP2). Limited sources of $\beta:\alpha$ values exist in the literature currently. Interior Alaska stream water was observed to have an

average of 0.530 ± 0.026 (Mutschlecner et al. 2018b) and a California soil leachate observed a similar $\beta:\alpha$ value at 0.540 (Hansen et al. 2016). These high $\beta:\alpha$ values observed in the surface waters are indicative of having a higher proportion of fresh NOM, which correlates with these boreal forest thermokarst lakes having increased microbial activity through the production of CH_4 and CO_2 through microbial degradation of NOM in the waters, especially during growth of the thermokarst lakes through further permafrost degradation (Elder et al. 2019; Walter Anthony et al. 2016, 2018).

2.4.2.3. Seasonal Optical Indices:

When observing winter and summer optical indices for GSL and DNL differences of greater than 0.1 shows a difference in organic material source (McKnight et al. 2001). GSL and DNL saw these differences in E2:E3 and $SUVA_{254}$. DNL additionally saw a difference of >0.1 for S_R. However, when comparing all whole waters over three years GSL and DNL hypolimnion observed seasonal differences for S_R, while E2:E3 and $SUVA_{254}$ did not observe a statistical difference in season over three years (Table 2.14). DNL and GSL had decreased S_R values in wintertime from 1.013 to 0.927 for DNL and 0.860 to 0.824 for GSL (Table 2.12), which correlates with increased molecular weight. However, S_R also increases with increase in sun irradiation and thus, the summertime S_R could be artificially increased due to increased sun exposure in sub-Arctic summers.

Both thermokarst lakes had a decrease in $SUVA_{254}$ and $SUVA_{280}$ values which correlates positively with aromaticity and thus, wintertime saw a decrease in aromatic content in the organic matter most likely due to the cut off from later surface water flow through the active layer and aromatic rich ground vegetation. However, samples were not taken of this lateral

surface water flow into the thermokarst lakes so a comparison cannot be conducted. Plant leachates observed from sub-Arctic Alaska by Mutschlecner et al. (2018a) saw that plant leachates had low $SUVA_{254}$ values of 0.6 mg C^{-1} m^{-1} for alder, 0.6 mg C^{-1} m^{-1} for poplar, and 1.8 mg C^{-1} m^{-1} for spruce (Mutschlecner et al. 2018a). DNL Winter had a very low $SUVA_{254}$ value of 0.961 mg C^{-1} m^{-1} (Table 2.12), this low value is below the literature range for samples, as observed in literature, which has seen a range from 1.3 to 5.1 L mg C^{-1} m^{-1} (Cawley et al. 2013; Guerard and Chin, 2012; Hansen et al. 2016; Mutschlecner et al. 2018b; Westerhoff et al. 1999). GSL Winter and BSP (collected in winter) all fell short of the literature range with values of 1.115 L mg C^{-1} m^{-1} and 1.039 L mg C^{-1} m^{-1} respectively (Table 2.12). These low values were all consistently taken under the ice, while literature samples were all during ice free times. Additionally, these low values could be due to lateral flow from plant material or literature having higher values due to not being corrected for iron. This low $SUVA_{254}$ is correlated with low aromaticity and in wintertime the organic matter samples did have decreased hydrogen aromatic content as observed with ^{1}H NMR analysis.

All of GSL had a negative difference between summer and winter values for the ratios of absorbance at different wavelengths, while DNL had a positive difference. E2:E3 correlates negatively with molecular weight, therefore the molecular weight of the organic matter decreased in wintertime. Alternatively, DNL had the opposite effect on UV-Vis indices between seasons indicating that wintertime in the open thermokarst lake had an increase in organic matter molecular weight. This decrease in E2:E3 indicates an increase in molecular weight could be infiltrating into the closed thermokarst lake from the ground water which, has lower value of 6.547.

Fluorescence optical indices showcased a different story in that GSL BIX, FI, β:α, and HIX values were not different between summer and winter, while DNL HIX was increased in winter based off of the notion that values >0.1 show differences in material (Table 2.12) (McKnight et al. 2001). However, when utilizing t-test statistics on whole water analysis over a three-year period only select sample locations had seasonal statistical differences in fluorescent indices. FI saw an increase in winter values in GSL epilimnion only correlating with an increase in microbial sourced NOM in winter (Table 2.14). While HIX was observed to have increased values in OCT epilimnion, which correlates to an increased extent of humification from summer into winter. OCT also observed seasonal differences with an increase in winter values for the hypolimnion in β:α and BIX, providing a correlation with an increase in the production of NOM through recent degradation of source material. These fluorescence optical indices provide an overall correlation with various factors that indicate the functional group composition of NOM. Optical indices were determined to not explain seasonality differences in organic matter composition and surface water chemistry accurately. Further, seasonality observations occurred utilizing trace metal analysis in the same watershed over a three-year study by Gagné, Section 3.4.

2.4.3. Radical Photolysis:

2.4.3.1. Unamended Waters:

Absorbance rates of decayed were determined to be pseudo-1st order of the UV-Vis spectrum and were calculated utilizing Equation 1 with R^2 values greater than 0.8, which represented the rate absorbance decay brought on by photobleaching (Figure 2.5). For simplicity the rates observed and compared between sampled were for 254 nm wavelength. First and

foremost, the three main thermokarst lakes rates for unamended photolysis for GSL and DNL of 0.00140 ± 0.00027 L mg^{-1} C^{-1} hr^{-1} and 0.00148 ± 0.00024 L mg^{-1} C^{-1} hr^{-1} respectively in wintertime (Table 2.15). While, the summer rates were lower at 0.00115 ± 0.000004 L mg^{-1} C^{-1} hr^{-1} and 0.00125 ± 0.00001 L mg^{-1} C^{-1} hr^{-1} for GSL and DNL. OCT had a summer rate of 0.00193 ± 0.00029 L mg^{-1} C^{-1} hr^{-1}. Meanwhile, unamended photolysis samples had the highest rate from the ground water sample with a rate of 0.00216 ± 0.00051 L mg^{-1} C^{-1} hr^{-1}. Reference materials of SRFA and PLFA saw photobleaching rates of rate of 0.00109 L mg^{1} C^{-1} hr^{-1} for SRFA 0.00126 L mg^{-1} C^{-1} hr^{-1} for PLFA.

$$\text{Photobleaching Rate} = \frac{-\text{Slope}(\text{LN}(\text{Avg}_{\text{Abs}_{T(x)}})}{[\text{Carbon}]} \text{x} \frac{1}{\text{SF}}$$

Equation 3: Determination for photobleaching rate through UV-Vis analysis of samples with various amendments. Units are represented in hr^{-1} mg C^{-1} L.
SF represents screen factor (Equation 4).

$$\text{SF} = \frac{1 - 10^{-\alpha_\lambda l}}{2.303 \alpha_\lambda l}$$

Equation 4: Screening factor equation to determine light screening ability of sample, utilizes time zero for values.

2.4.3.2. Comparison to Reference Materials:

During the comparison of waters to reference material unamended photolysis rate of decay only GSL and DNL photobleached at rates that fell within the range of PLFA and SRFA, all other samples had faster rates of photobleaching than reference material (Figure 2.5). When it came to waters GSL and DNL Summer were the only two samples that fell between PLFA and SRFA unamended photolysis rates. GSL Summer was the most similar water NOM photobleaching to SRFA at a percent difference of 5.79% (Table 2.16). Meanwhile, DNL

Summer had a slower decay rate than PLFA but was most similar of all of the water NOMs to PLFA with a percent difference of only 0.13%. All other waters had faster rates of unamended absorbance decay with GSL Winter being closest to the reference material and BSGW had the fastest rate, furthest away from PLFA and SRFA rates of decay. Overall, all of the waters with the exception of GSL Summer were closest in comparison to PLFA reference material indicating a potential for less terrestrial influence however, due to not being between terrestrial and microbial reference material rates it is difficult to say whether its most similar to microbial derived NOM.

Photobleaching rates permafrost NOM isolates were overall faster than SRFA and PLFA reference material. However, active layer isolates photobleached more slowly than PLFA (Figure 2.5). When the absolute value of SRFA and PLFA percent differences to FTP isolates were averaged together FTP1 was most dissimilar to reference material at 44.16%, while FTP2 were most similar to reference materials at 7.92% (Table 2.16). Active layers both observed slower rates than PLFA but faster rates compared to SRFA, when averaged together the discrepancy to reference materials were consistent between GSP1 and GSP2 at 7.3%.

2.4.3.3. Water Rates versus Soil Rates:

The observation of water NOM photolysis rates compared to active layer and permafrost NOM is important for understanding how the underlying permafrost may be affecting the rates of photolysis. In general, active layer photobleaching rates were slower than water absorbance decay rates for unamended photolysis, with the exception of GSL Summer compared to GSP2 (Figure 2.5). GSL Summer was most similar to the unamended photobleaching rates of active layer soil NOM, with an average percent difference of 1.44% (Table 2.16). Both summer

isolations from GSL and DNL had slower rates of photobleaching decay compared to FTP1, FTP2, and FTP3. Meanwhile, GSL and DNL Winter rates only observed slower rates compared to FTP1 and FTP3. For most lake isolates (OCT Summer, GSL Winter, DNL Winter, and BSP) photobleaching most resembled photobleaching rates of permafrost NOM. While, GSL Summer and DNL Summer photobleaching rates most resembled active layer photobleaching rates. This change in resemblance for summer GSL and DNL could be due to the increased surface water hydrology through active layer soils in the summer. Similarly, this same scenario was observed between DNL Summer and Winter, as winter for GSL, DNL, and BSP most closely resembled permafrost compared to active layer as the active layer was frozen during the time of water collection. Meanwhile, OCT Summer most closely resembled the rates of permafrost this could be influenced by a lack of surface hydrology or that permafrost is actively thawing more readily underneath due to the transitional nature of the thermokarst lake. Without further studies to determine the flux of surface water flows into the thermokarst lake this is only the beginning of a hypothesis.

2.4.3.4. Ground Water Comparison to Soils and Waters:

BSGW most similarly compares to permafrost for all absorbance decay photolysis experiments based on percent differences between absorbance decay rates for all experiment amendments (Table 2.16). Thus, surface waters were compared to groundwater absorbance decay to observe how groundwater may affect the photolysis of thermokarst lake surface waters. Overall, BSGW had the highest rates for all photolysis •OH experiments. For unamended photolysis experiments BSP and OCT Summer were most similar to BSGW rates. However, BSP has no groundwater connection and the high reactivity of the NOM is likely caused by how

young the small thermokarst lake is in recent thaw. GSL Summer was furthest from BSPGW at 61.22%, because GSL Summer was the least reactive to absorbance decay in the presence of sunlight overall. Based off of percent differences it appears that GSL Summer is most influenced by active layer leaching and permafrost and has no groundwater influence as expected for a closed thermokarst lake.

2.4.3.5. •OH Amended Photobleaching:

•OH promotion by the addition of Fe observes an increase in absorbance decay rates compared to unamended photobleaching rates, depending on the extent of Fe association to NOM and its impact on the efficiency to utilize the photo-Fenton reaction (Table 2.17/Equation 5). Due to the high iron waters of this watershed radical promotion may be skewed due to iron already complexed to the NOM molecules as Fe concentrations of a 100 mg C L^{-1} sample of NOM observed 4.68 ± 1.71 μg L^{-1} for PLFA, 4.31 ± 0.82 μg L^{-1} for SRFA, and 79.52 ± 1.09 μg L^{-1} for GSL Summer (Milke, 2018). Observing differences in unamended and amended photolysis allows for an interpretation of how radicals, such as •OH, play a role in the photolysis of NOM samples. The difference of unamended and •OH promoted showcases which samples have enhanced •OH production with the addition of Fe increasing the photo-Fenton reaction of the sample. A positive difference indicates that iron addition slows the photobleaching rate of the NOM and thus, does not promote •OH production. While, a large negative value indicates that •OH promotes the rate of photobleaching and the NOM has the potential to be influenced by •OH promotion through the addition of Fe into the system (Equation 6). However, if the error of the difference exceeds the difference the rate of unamended and amended are not statistically different from each other and •OH does not get promoted during photolysis. Active layer (GSP1)

was the only sample that did not observe a change in rate when Fe was added to the sample, thus •OH is not significantly promoted in the sample (Table 2.17/Figure 2.7). Meanwhile, OCT Summer observed a decrease in photobleaching rate in the presence of Fe addition. The positive difference indicates that OCT Summer NOM does not have the •OH promoting ability similar to the other samples. All other samples had a negative difference in rates, with that largest difference occurring during wintertime with over 100% difference between the unamended and Fe amended photobleaching rates. GSL Winter had a difference of -0.00514 L mg^{-1} C^{-1} hr^{-1}, which was a difference of 130% from the unamended photobleaching rate. Following GSL Winter difference in photobleaching rates was BSP with a rate difference of -0.00521 L mg^{-1} C^{-1} hr^{-1} at a 122% difference. DNL Winter still showcased a large difference of 100% with a rate difference of -0.00294 L mg^{-1} C^{-1} hr^{-1}. This large difference in photolysis rates was similar in that winter samples also had the highest overall rates for unamended photobleaching making winter more reactive to photolysis. GSL Summer observed a change in rate of -0.00207 L mg^{-1} C^{-1} hr^{-1}, which was very similar to ground waters change in rate of -0.00227 L mg^{-1} C^{-1} hr^{-1}. DNL Summer and soil NOM had much smaller change in photobleaching rates by an order of magnitude, differences in rates ranged from -0.000123 L mg^{-1} C^{-1} hr^{-1} (DNL Summer) to -0.000607 L mg^{-1} C^{-1} hr^{-1} (FTP2). Overall, the difference is rates were higher than reference material for winter samples, while the majority of the other NOM samples with decreased rate differences fell between the microbial and terrestrial reference material. Winter NOM samples had higher rates of photobleaching brought on by the photo-Fenton reaction.

$$Fe\ (II) + H_2O_2 \rightarrow Fe\ (III) + OH^- + \bullet OH$$

Equation 5: Photo-Fenton reaction that occurs in the presence of sunlight in freshwaters (Southworth and Voelker, 2003; Zepp et al. 1992)

$$k_{unamended} - k_{amended} = \text{Rate difference}$$

Equation 6: Rate difference between unamended and amended to determine how radicals are affecting the photo bleachability of NOM samples.

Alternatively, quenching radical production through the addition of methanol allows for the observation of which NOM samples naturally produce radicals in the presence of sunlight and to what extent. The larger the positive value when observing unamended rate difference from methanol amended rates have the most natural radical production occurred. However, if there is no statistical difference between unamended and methanol amended samples will produce an error greater than the rate difference. In the case of no statistical difference observed in GSL Winter, groundwater, and FTP2, radical quenching observed no difference in photobleaching rate and thus, natural radical production is minimal or not occurring in these specific samples and study (Table 2.17/Figure 2.8). Unlike in the •OH promotion rate differences there was not one season that observed higher difference. The largest rate difference was in OCT Summer at 0.000752 L mg^{-1} C^{-1} hr^{-1}, which was a 48% rate difference. The natural production of radicals is highest in OCT Summer compared to the other samples. Aside from the samples that showed no natural production DNL Summer had the lowest rate of natural radical production due to the difference in rate being an order of magnitude lower than all other samples analyzed at 0.0000747 L mg^{-1} C^{-1} hr^{-1} or a 9% rate difference. Overall, all NOM samples had a larger rate difference than the two reference materials of PLFA (0.0000652 L mg^{-1} C^{-1} hr^{-1}) and SRFA (0.0000571 L mg^{-1} C^{-1} hr^{-1}). The range of rate differences and thus, natural radical production from the samples was variable depending on the type as the soil was not consistently lower or higher than the water samples. Since the highest and lowest rate difference was found within the

water samples, the active layers and permafrost layers rate differences fell within the bounds of water natural radical production.

2.4.3.6. •OH rates with Age Trends:

Permafrost leachate isolated NOM photobleaching rates did not have a linear regression with ^{14}C age. The youngest PENOM analyzed had the highest rate of photobleaching with a rate of 0.00183 ± 0.00029 L mg^{-1} C^{-1} hr^{-1}, followed by the oldest sample with a rate of 0.00168 ± 0.00006 L mg^{-1} C^{-1} hr^{-1}, and the slowest rate was with the middle aged PENOM with a rate of 0.00126 ± 0.00010 L mg^{-1} C^{-1} hr^{-1} (Table 2.15). This trend of rates followed through for observing the difference in unamended rates with •OH promotion rates. The largest difference in rates was observed with the youngest PENOM sample, indicating that the youngest isolated PENOM material was most influenced by Fe addition for the formation of •OH. While, the middle sample was the least influenced by Fe addition. However, the youngest PENOM had the most natural radical production in the presence of UV-rays based on the large difference between unamended and methanol amended photobleaching rates, meanwhile the middle permafrost sample was determined to have no natural radical production. The PENOM is a representation of ancient, 19,000 to 33,000-year-old, carbon which were source by an old terrestrial and microbial degradation.

2.4.4. Triplet Excited State Photolysis:

$^{3}NOM^{*}$ photoproduction is probed by the degradation of TMP in photolysis experimentation. $^{3}NOM^{*}$ photoproduction rates were determined using equation 7 based on TMP concentrations over an elapsed period of time. Unlike •OH photolysis, the highest rate of

TMP degradation was observed with the summer NOM isolates, suggesting triplet photoproduction activity was strongest in the summertime. OCT Summer had the highest rate at 0.00215 min^{-1} mg C^{-1} L, followed by GSL and DNL Summer isolates with rates of 0.00198 ±0.00011 min^{-1} mg C^{-1} L and 0.00175 ± 0.00012 min^{-1} mg C^{-1} L (Table 2.18/Figure 2.9). DNL Winter on the other hand had the slowest rate for ^{3}NOM* photoreactivity at 0.0145 ± 0.0030 min^{-1} mg C^{-1} L while, GSL Winter had a rate of 0.00184 ± 0.00019 min^{-1} mg C^{-1} L. Ground water had a rate similar to DNL Summer at 0.00177 ± 0.00030 min^{-1} mg C^{-1} L and BSP had a rate similar to GSL Summer at 0.00199 ± 0.00043 min^{-1} mg C^{-1} L.

$$^3\text{NOM}^*\text{production rate} = -\left(\frac{\text{LN}\left(\left[\text{TMP}\right]_x / \left[\text{TMP}\right]_0\right)}{[\text{Carbon}]} \text{x} \frac{1}{\text{SF}}\right)$$

Equation 7: Determination of ^{3}NOM production rate, which starts out at the rate of TMP loss. Units are in min^{-1} mg C^{-1} L. SF stands for screening factor determined by equation 3.

^{3}NOM* photoreactivity in soil isolated PENOM varied on both ends of the spectrum depending on whether the sample was classified as active layer or permafrost. Active layer averaged out to have the slowest rate of ^{3}NOM* photoproduction at a rate of 0.00081 ± 0.00004 min^{-1} mg C^{-1} L (Table 2.18). Meanwhile, the youngest permafrost sample had the highest rate of ^{3}NOM* photoproduction at a rate of 0.00236 ± 0.00021 min^{-1} mg C^{-1} L, followed by the medium aged permafrost layer at 0.00153 ± 0.00027 min^{-1} mg C^{-1} L and the oldest permafrost at a rate of 0.00144 ± 0.00031 min^{-1} mg C^{-1} L. Reference material of SRFA and PLFA had the following rate for ^{3}NOM* photoproduction of 0.00109 ± 0.0009 min^{-1} mg C^{-1} L and 0.00110 ± 0.00007 min^{-1} mg C^{-1} L (Gagné, Section 1.4.3.3.2)

2.4.4.1. ^{3}NOM* Soil Rates compared to Reference Materials:

Overall, the rate of ^{3}NOM* for active layer isolated NOM was slower than reference materials at a difference for GSP1 at 26.75% slower than PLFA and 25.87% slower than SRFA. Meanwhile, GSP2 was 33.92% slower than PLFA and 33.05% slower than SRFA (Table 2.19). Due to the similar difference an average was obtained between the differences between PLFA and SRFA for the rest of the samples. Permafrost cores had a faster rate of ^{3}NOM* compared to reference materials, however the difference in rate varied with depth. The youngest permafrost soil core was the fastest rate compared to reference material with a 73.10% faster rate followed by FTP2 and FTP3 at 32.75% and 26.85% respectively.

2.4.4.2. ^{3}NOM* Soil Rates Compared to Water Rates:

Similarly, to the permafrost NOM samples all of the water sample ^{3}NOM* rates were higher than the reference material. This increase in rates could be caused by an influence in permafrost NOM leaching into the surface waters as the difference between rates in the water and in permafrost NOM are much lower than differences between active layer and reference material with a maximum different of 39.87% (Table 2.19). However, when it came to comparison with reference material DNL Winter had the lowest percentage at 27.58% and the maximum difference was observed in OCT Summer at 64.98%. Waters were equally different from active layer ^{3}NOM* rates as the difference in rates ranged from 56.31% – 90.47%. Alternatively, the rates of waters were all slower than the rate of FTP1 and faster than FTP2 and FTP3. The most similar ^{3}NOM* rate of production was observed between DNL Winter and FTP3 at 0.74%, DNL Winter was also slower than FTP2 rate of ^{3}NOM*.

2.4.4.3. ^{3}NOM* Groundwater Rates to All Samples:

Groundwater rates of ^{3}NOM* when compared to surface waters and soils had the highest variability as some rates were faster while others were slower. Active layer had the largest difference at 70.89% and 77.22%, while permafrost and surface waters were more similar (Table 2.19). Permafrost highest percent difference was having a 28.80% increased rate of ^{3}NOM* compared to ground water. The comparison to surface waters saw DNL both summer and winter having a decreased rate compared to BSGW. DNL Summer was closest to BSGW rate with a percent difference of 0.78% and DNL Winter was the furthest from BSGW rate at 19.82%. Overall, the decreased percent difference between waters and permafrost NOM indicates that permafrost NOM is likely influencing the ^{3}NOM* rates, as well as groundwater due to the even closer rate differences between the surface water and groundwater.

2.4.4.4. ^{3}NOM* compared to Literature:

The rate of ^{3}NOM* is difficult to compare to literature as previous studies converted apparent quantum yield from a rate; however, these studies used a single wavelength Hg lamp and not a broad wavelength solar simulator like in this current study (Bodhipaksha et al. 2015; Maizel et al. 2017). This difference in wavelength results in inconsistent conversions from rate to apparent quantum yield. Thus, comparison of rates was limited to rates determined by Cawley et al. (2009) and Gagné (Section 1.4.3.3.2.). Cawley et al. (2009) utilized different isolation techniques to obtain NOM isolates from a North Slope river in Alaska, the rates ranged from 0.00125 to 0.00225 min^{-1} mg C^{-1} L. The range observed in North Slope Alaska also encompassed the rates obtained in this study on thermokarst lake NOM and ground water NOM, which ranged from 0.00145 to 0.00215 min^{-1} mg C^{-1} L (Table 2.18). The only samples that rates did not fall

within this range were both active layer samples that had slower rates than literature values from the North Slope, active layer samples had slower rates overall with rates lower than 0.00100 min^{-1} mg C^{-1} L (Gagné, Section 1.4.3.3.2.).

2.5. Conclusions:

Permafrost is actively thawing and leaching organic natural organic matter into surface waters which, influences the functional group composition and photoreactivity of surface waters underlain by permafrost. This study provided insight on the functional group composition of thermokarst lakes and soil leachates through ^{13}C and ^{1}H NMR analysis of functional groups and found that the aromatic composition was majority substituted based on ^{13}C aromatics dominating the spectrum, while ^{1}H NMR was minimal. Surface waters were most similar to the functional group composition of permafrost soil isolated NOM through comparison to ^{13}C and ^{1}H functional groups. This similarity indicates that permafrost organic matter is influencing the functional group composition of surface water natural organic matter. Additionally, differences between seasons for functional group analysis was observed as winter ^{13}C had decreased variability between the closed and opened thermokarst lake, with the largest variability in summer occurring from increase in aromatic carbon content.

Photoreactivity observed increased photobleaching in wintertime samples and these rates of photobleaching were higher than the rates observed in the reference material of SRFA and PLFA. This increased photobleaching introduces the idea that potentially obtaining a boreal forest, sub-Arctic reference material is important in order to compare to additional samples that may not mimic the traditionally thought terrestrial to microbial NOM spectrum. This increased rate of photobleaching was additionally observed in the production of $^{3}NOM^{*}$ as all rates of

sampled NOM were faster than the rate of ^{3}NOM* by PLFA and SRFA. When comparing photobleaching rates of surface waters to soil, the percentage difference was lowest between permafrost NOM and surface water NOM, indication that permafrost is influencing the rate of natural photolysis. When it came to utilizing the photo-Fenton reaction to produce •OH the largest production occurred in winter samples with over 100% increases in •OH influence, while natural radical production occurred most readily in the summertime. This natural radical production of permafrost natural organic matter has the potential to influence surface water natural radical production as the percent difference observed in thermokarst lakes in the summer was similar to the percent difference in permafrost soil NOM.

This study observed influences from permafrost into surface waters however, further research should be conducted to determine if these influences are location based. Additionally, observing permafrost influence on streams would be beneficial as streams continuous transport material to other areas. Furthermore, the observation of additional reactive oxygen species produced from photolysis would increase the understanding of permafrost thaw influences on photochemical reactivity on permafrost. The natural organic matter collected from thermokarst lake and permafrost should additionally undergo microbial incubations to observe how permafrost degradation influences the rate of CO_2 and CH_4 production. As temperatures increase the release of permafrost natural organic matter is inevitable and thus, obtaining a holistic understanding of the variability in functional group composition and photoreactivity will allow for a better understanding of how the rates of CO_2 and CH_4 production will be affected through permafrost thaw in the future allowing for better estimates by climate models.

2.6. Acknowledgements:

Funding for portions of this project was supplied by the Alaska Space Grant and National Institutes for Water Resources Graduate Student-Lead Proposal through the Water & Environmental Research Center and the U.S. Department of Interior – Geological Survey. Access to residential lakes were obtained through permits supplied by NSF Grant 1500931, Methane release from thermokarst lakes: Thresholds and feedbacks in the lakes to watershed hydrology-permafrost systems. A sincere thank you to PI's on the NSF project for allowing access and providing intellectual support; Anna Liljedahl, Daivd Barnes, Vladimir E Romanovsky, and Katey Walter Anthony. Thank you to Ronald Daanen and Alexander Kholodov for assistance in collecting and obtaining active layer samples and Tom Douglas at Cold Regions Research and Engineering Laboratory with the U.S.A. Army for access and sampling of the CRREL permafrost tunnel. Further thanks to the support or numerous students and collaborators for instrumentation assistance and sampling companionship; Bridget Eckhardt, Madison Ross, Nicole Ramos, Dallon Knight, Nina Ruckhaus, Ruth Osborne (Noratuk), Audrey Mutschlecner, Rachel Voight, Ragen Davey, and Tamara Harms.

2.7. References:

Abbott, B. W., Larouche, J. R., Jones, J. B., Bowden, W. B. and Balser, A. W.: Elevated dissolved organic carbon biodegradability from thawing and collapsing permafrost, J. Geophys. Res. Biogeosciences, 119(10), 2049–2063, doi:10.1002/2014JG002678, 2014.

Anthony Arguez, Imke Durre, Scott Applequist, Mike Squires, Russell Vose, Xungang Yin, and Rocky Bilotta (2010). NOAA's U.S. Climate Normals (1981-2010). [Fairbanks Int. Airport]. NOAA National Centers for Environmental Information. DOI:10.7289/V5PN93JP [November 2019].

Barker, A. J., Douglas, T. A., Jacobson, A. D., McClelland, J. W., Ilgen, A. G., Khosh, M. S., Lehn, G. O. and Trainor, T. P.: Late season mobilization of trace metals in two small Alaskan arctic watersheds as a proxy for landscape scale permafrost active layer dynamics, Chem. Geol., 381, 180–193, doi:10.1016/j.chemgeo.2014.05.012, 2014.

Bodhipaksha, L. C., Sharpless, C. M., Chin, Y. P., Sander, M., Langston, W. K. and Mackay, A. A.: Triplet photochemistry of effluent and natural organic matter in whole water and isolates from effluent-receiving rivers, Environ. Sci. Technol., 49, 3453–3463, doi:10.1021/es505081w, 2015.

Bodhipaksha, L. C., Sharpless, C. M., Chin, Y. P. and MacKay, A. A.: Role of effluent organic matter in the photochemical degradation of compounds of wastewater origin, Water Res., 110, 170–179, doi:10.1016/j.watres.2016.12.016, 2017.

Cawley, K. M., Hakala, J. A. and Chin, Y. P.: Evaluating the triplet state photoreactivity of dissolved organic matter isolated by chromatography and ultrafiltration using an alkylphenol probe molecule, Limnol. Oceanogr. Methods, 7, 391–398, doi:10.4319/lom.2009.7.391, 2009.

Cawley, K. M., McKnight, D. M., Miller, P., Cory, R. M., Fimmen, R. L., Guerard, J. J., Dieser, M., Jaros, C., Chin, Y. P. and Foreman, C.: Characterization of fulvic acid fractions of dissolved organic matter during ice-out in a hyper-eutrophic, coastal pond in Antarctica, Environ. Res. Lett., 8, doi:10.1088/1748-9326/8/4/045015, 2013.

Chin, Y. P., Miller, P. L., Zeng, L., Cawley, K. M. and Weavers, L. K.: Photosensitized degradation of bisphenol A by dissolved organic matter, Environ. Sci. Technol., 38(22), 5888–5894, doi:10.1021/es0496569, 2004.

Cooke, M. S., Evans, M. D., Dizdaroglu, M. and Lunec, J.: Oxidative DNA damage: Mechanisms, mutation, and disease, FASEB J., 17(10), 1195–1214, doi:10.1096/fj.02-0752rev, 2003.

Cory, R. M., Mcknight, D. M., Chin, Y. P., Miller, P. and Jaros, C. L.: Chemical characteristics of fulvic acids from Arctic surface waters: Microbial contributions and photochemical transformations, J. Geophys. Res., 112, G04S51, doi:10.1029/2006JG000343, 2007.

Cory, R. M., Miller, M. P., McKnight, D. M., Guerard, J. J. and Miller, P. L.: Effect of instrument-specific response on the analysis of fulvic acid fluorescence spectra, Limnol. Oceanogr. Methods, 8, 67–78, doi:10.4319/lom.2010.8.0067, 2010a.

Cory, R. M., McNeill, K., Cotner, J. P., Amado, A., Purcell, J. M. and Marshall, A. G.: Singlet Oxygen in the Coupled Photochemical and Biochemical Oxidation of Dissolved Organic Matter, Environ. Sci. Technol., 44(10), 3683–3689, doi:10.1021/es902989y, 2010b.

Cory, R. M., Crump, B. C., Dobkowski, J. A. and Kling, G. W.: Surface exposure to sunlight stimulates CO 2 release from permafrost soil carbon in the Arctic, PNAS, 110(9), 3429–3434, doi:10.1073/pnas.1214104110, 2013.

Cory, R. M., Ward, C. P., Crump, B. C., Kling, G. W., Ward, C. P. and Kling, G. W.: Sunlight controls water column processing of carbon in arctic fresh waters, Science (80-.)., 345, 925–928, doi:10.1126/science.1253119, 2014.

Dittmar, T., Koch, B., Hertkorn, N. and Kattner, G.: A simple and efficient method for the solid-phase extraction of dissolved organic matter (SPE-DOM) from seawater, Limnol. Oceanogr. Methods, 6, 230–235, doi:10.4319/lom.2008.6.230, 2008.

Drake, T. W., Wickland, K. P., Spencer, R. G. M., McKnight, D. M. and Striegl, R. G.: Ancient low-molecular-weight organic acids in permafrost fuel rapid carbon dioxide production upon thaw, Proc. Natl. Acad. Sci. U. S. A., 112(45), 13946–13951, doi:10.1073/pnas.1511705112, 2015.

Dutta, K., Schuur, E. A. G., Neff, J. C. and Zimov, S. A.: Potential carbon release from permafrost soils of Northeastern Siberia, Glob. Chang. Biol., 12, 2336–2351, doi:10.1111/j.1365-2486.2006.01259.x, 2006.

Elder, C. D., Schweiger, M., Lam, B., Crook, E. D., Xu, X., Walker, J., Walter Anthony, K. M. and Czimczik, C. I.: Seasonal Sources of Whole-Lake CH 4 and CO 2 Emissions From Interior Alaskan Thermokarst Lakes, J. Geophys. Res. Biogeosciences, 124(5), 1209–1229, doi:10.1029/2018JG004735, 2019.

Emond, A. M., R. P. Daanen, G. R. C. Graham, K. W. Anthony, A. K. Liljedahl, B. J. Minsley, D. L. Barnes, and V. E. Romanovsky. 2018. Airborne electromagnetic and magnetic survey, Goldstream Creek watershed, interior Alaska.

Fimmen, R. L., Cory, R. M., Chin, Y. P., Trouts, T. D. and McKnight, D. M.: Probing the oxidation-reduction properties of terrestrially and microbially derived dissolved organic matter, Geochim. Cosmochim. Acta, 71, 3003–3015, doi:10.1016/j.gca.2007.04.009, 2007.

Frey, K. E. and McClelland, J. W.: Impacts of permafrost degradation on arctic river biogeochemistry, Hydrol. Process., 23(1), 169–182, doi:10.1002/hyp.7196, 2009.

Gabor, R. S., Burns, M. A., Lee, R. H., Elg, J. B., Kemper, C. J., Barnard, H. R. and McKnight, D. M.: Influence of leaching solution and catchment location on the fluorescence of water-soluble organic matter, Environ. Sci. Technol., 49, 4425–4432, doi:10.1021/es504881t, 2015.

Grannas, A. M., Martin, C. B., Chin, Y. P. and Platz, M.: Hydroxyl radical production from irradiated Arctic dissolved organic matter, Biogeochemistry, 78(1), 51–66, doi:10.1007/s10533-005-2342-4, 2006.

Guerard, J. J.: The Characterization of Dissolved Organic Matter and its Influence on the Photochemical Fate of Antibiotics used in Aquaculture, The Ohio State University., 2009.

Guerard, J. J. and Chin, Y. P.: Photodegradation of ormetoprim in aquaculture and stream-derived dissolved organic matter, J. Agric. Food Chem., 60, 9801–9806, doi:10.1021/jf302564d, 2012.

Guerard, J. J., Miller, P. L., Trouts, T. D. and Chin, Y. P.: The role of fulvic acid composition in the photosensitized degradation of aquatic contaminants, Aquat. Sci., 71, 160–169, doi:10.1007/s00027-009-9192-4, 2009.

Han, R., Lv, J., Luo, L., Wen, B. and Zhang, S.: Molecular-scale investigation of soil fulvic acid and water-extractable organic matter by high-resolution mass spectrometry and 1 H NMR spectroscopy, Environ. Chem., 16, 92–100, doi:10.1071/EN18124, 2019.

Hansen, A. M., Kraus, T. E. C., Pellerin, B. A., Fleck, J. A., Downing, B. D. and Bergamaschi, B. A.: Optical properties of dissolved organic matter (DOM): Effects of biological and photolytic degradation, Limnol. Oceanogr., 61, 1015–1032, doi:10.1002/lno.10270, 2016.

Hertkorn, N., Permin, A., Perminova, I., Kovalevskii, D., Yudov, M., Petrosyan, V. and Kettrup, A.: Comparative analysis of partial structures of a peat humic and fulvic acid using one- and two-dimensional nuclear magnetic resonance spectroscopy, in Journal of Environmental Quality, vol. 31, pp. 375–387., 2002.

Hertkorn, N., Harir, M., Koch, B. P., Michalke, B. and Schmitt-kopplin, P.: High field NMR Spectroscopy and FTICR Mass Spectrometry: Powerful Discovery Tools for the Molecular Level Characterization of Marine Dissolved Organic Matter, Biogeosciences, 10, 1583–1624, doi:10.5194/bg-10-1583-2013, 2013.

Heslop, J. K., Walter Anthony, K. M., Sepulveda-Jauregui, A., Martinez-Cruz, K., Bondurant, A., Grosse, G. and Jones, M. C.: Thermokarst lake methanogenesis along a complete talik profile, Biogeosciences, 12, 4317–4331, doi:10.5194/bg-12-4317-2015, 2015.

Heslop, J. K., Chandra, S., Sobzcak, W. V., Davydov, S. P., Davydova, A. I., Spektor, V. V. and Walter Anthony, K. M.: Variable respiration rates of incubated permafrost soil extracts from the Kolyma River lowlands, north-east Siberia, Polar Res., 37(1), doi:10.1080/17518369.2017.1305157, 2017.

Heslop, J. K., Winkel, M., Walter Anthony, K. M., Spencer, R. G. M., Podgorski, D. C., Zito, P., Kholodov, A., Zhang, M. and Liebner, S.: Increasing organic carbon biolability with depth in yedoma permafrost: ramifications for future climate change, J. Geophys. Res. Biogeosciences, 124, 1–18, doi:10.1029/2018jg004712, 2019.

Hodgkins, S. B., Tfaily, M. M., McCalley, C. K., Logan, T. A., Crill, P. M., Saleska, S. R., Rich, V. I. and Chanton, J. P.: Changes in peat chemistry associated with permafrost thaw increase greenhouse gas production, Proc. Natl. Acad. Sci., 111(16), 5819–5824, doi:10.1073/pnas.1314641111, 2014.

Johnson, R. L. and Schmidt-Rohr, K.: Quantitative solid-state 13 C NMR with signal enhancement by multiple cross polarization, J. Magn. Reson., 239, 44–49, doi:10.1016/j.jmr.2013.11.009, 2014.

Kaiser, E., Simpson, A. J., Dria, K. J., Sulzberger, B. and Hatcher, P. G.: Solid-State and Multidimensional Solution-State NMR of Solid Phase Extracted and Ultrafiltered Riverine Dissolved Organic Matter, Environ. Sci. Technol., 37(13), 2929–2935, doi:10.1021/es020174b, 2003.

Kessler, M. A., Plug, L. J. and Walter Anthony, K. M.: Simulating the decadal- to millennial-scale dynamics of morphology and sequestered carbon mobilization of two thermokarst lakes in NW Alaska, J. Geophys. Res. Biogeosciences, 117, G00M06, doi:10.1029/2011JG001796, 2012.

Kiss, K., Szalai, Z., Jakab, G., Madarász, B. and Zboray, N.: Characterization of Soil Organic Substances by UV-Vis Spectrophotometry in Some Soils of Hungary, in Soil Carbon, pp. 127–136, Springer International Publishing., 2014.

Lam, B. and Simpson, A. J.: Direct 1H NMR spectroscopy of dissolved organic matter in natural waters, Analyst, 133, 263–269, doi:10.1039/B713457F, 2008.

Li, Y., Harir, M., Uhl, J., Kanawati, B., Lucio, M., Smirnov, K. S., Koch, B. P., Schmitt-Kopplin, P. and Hertkorn, N.: How representative are dissolved organic matter (DOM) extracts? A comprehensive study of sorbent selectivity for DOM isolation, Water Res., 116, 316–323, doi:10.1016/j.watres.2017.03.038, 2017.

Liljedahl, A. (2019). Climate data from the Goldstream Creek Watershed study of Methane Release from Thermokarst Lakes. University of Alaska Fairbanks, Water and Environmental Research Center. URL: http://ine.uaf.edu/werc/werc-projects/goldstream/ Fairbanks, Alaska, variously paged. [11/3/19].

Lipson, D. A., Zona, D., Raab, T. K., Bozzolo, F., Mauritz, M. and Oechel, W. C.: Water-table height and microtopography control biogeochemical cycling in an Arctic coastal tundra ecosystem, Biogeosciences, 9, 577–591, doi:10.5194/bg-9-577-2012, 2012.

Lipson, D. A., Raab, T. K., Goria, D. and Zlamal, J.: The contribution of Fe(III) and humic acid reduction to ecosystem respiration in drained thaw lake basins of the Arctic Coastal Plain, Global Biogeochem. Cycles, 27, 399–409, doi:10.1002/gbc.20038, 2013.

Mackelprang, R., Burkert, A., Haw, M., Mahendrarajah, T., Conaway, C. H., Douglas, T. A. and Waldrop, M. P.: Microbial survival strategies in ancient permafrost: Insights from metagenomics, ISME J., 11, 2305–2318, doi:10.1038/ismej.2017.93, 2017.

Maizel, A. C., Li, J. and Remucal, C. K.: Relationships between Dissolved Organic Matter Composition and Photochemistry in Lakes of Diverse Trophic Status, Environ. Sci. Technol., 51, 9624–9632, doi:10.1021/acs.est.7b01270, 2017.

Mann, P. J., Sobczak, W. V., LaRue, M. M., Bulygina, E., Davydova, A., Vonk, J. E., Schade, J., Davydov, S., Zimov, N., Holmes, R. M. and Spencer, R. G. M.: Evidence for key enzymatic controls on metabolism of Arctic river organic matter, Glob. Chang. Biol., 20(4), 1089–1100, doi:10.1111/gcb.12416, 2014.

Mao, J., N. Chen, and X. Cao. 2011. Characterization of humic substances by advanced solid state NMR spectroscopy: Demonstration of a systematic approach. Org. Geochem. **42**: 891–902. doi:10.1016/j.orggeochem.2011.03.023

McCalley, C. K., Woodcroft, B. J., Hodgkins, S. B., Wehr, R. A., Kim, E.-H., Mondav, R., Crill, P. M., Chanton, J. P., Rich, V. I., Tyson, G. W. and Saleska, S. R.: Methane dynamics regulated by microbial community response to permafrost thaw, Nature, 514, 478–481, doi:10.1038/nature13798, 2014.

McKnight, D. M., Boyer, E. W., Westerhoff, P. K., Doran, P. T., Kulbe, T. and Andersen, D. T.: Spectrofluorometric characterization of dissolved organic matter for indication of precursor organic material and aromaticity, Limnol. Oceanogr., 46(1), 38–48, doi:10.4319/lo.2001.46.1.0038, 2001.

Milke, K. P.: Metal(loid) liberation from Alaskan coal combustion products as a function of time in various aqueous media, University of Alaska Fairbanks., 2018.

Mladenov, N., Zheng, Y., Simone, B., Bilinski, T. M., McKnight, D. M., Nemergut, D., Radloff, K. A., Rahman, M. M. and Ahmed, K. M.: Dissolved Organic Matter Quality in a Shallow Aquifer of Bangladesh: Implications for Arsenic Mobility, Environ. Sci. Technol., 49, 10815–10824, doi:10.1021/acs.est.5b01962, 2015.

Mutschlecner, A. E., Guerard, J. J., Jones, J. B. and Harms, T. K.: Phosphorus Enhances Uptake of Dissolved Organic Matter in Boreal Streams, Ecosystems, 21, 675–688, doi:10.1007/s10021-017-0177-1, 2018a.

Mutschlecner, A. E., Guerard, J. J., Jones, J. B. and Harms, T. K.: Regional and intra-annual stability of dissolved organic matter composition and biolability in high-latitude Alaskan rivers, Limnol. Oceanogr., 63, 1605–1621, doi:10.1002/lno.10795, 2018b.

Ohno, T.: Fluorescence inner-filtering correction for determining the humification index of dissolved organic matter, Environ. Sci. Technol., 36(4), 742–746, doi:10.1021/es0155276, 2002.

Page, S. E., Logan, J. R., Cory, R. M. and McNeill, K.: Evidence for dissolved organic matter as the primary source and sink of photochemically produced hydroxyl radical in arctic surface waters, Environ. Sci. Process. Impacts, 16, 807–822, doi:10.1039/c3em00596h, 2014.

Plaza, C., Pegoraro, E., Bracho, R., Celis, G., Crummer, K. G., Hutchings, J. A., Hicks Pries, C. E., Mauritz, M., Natali, S. M., Salmon, V. G., Schädel, C., Webb, E. E. and Schuur, E. A. G. G.: Direct observation of permafrost degradation and rapid soil carbon loss in tundra, Nat. Geosci., 12, 627–631, doi:10.1038/s41561-019-0387-6, 2019.

Pokrovsky, O. S., Bueno, M., Manasypov, R. M., Shirokova, L. S., Karlsson, J. and Amouroux, D.: Dissolved Organic Matter Controls Seasonal and Spatial Selenium Concentration Variability in Thaw Lakes across a Permafrost Gradient, Environ. Sci. Technol., 52, 10254–10262, doi:10.1021/acs.est.8b00918, 2018a.

Pokrovsky, O. S., Karlsson, J. and Giesler, R.: Freeze-thaw cycles of Arctic thaw ponds remove colloidal metals and generate low-molecular-weight organic matter, Biogeochemistry, 137, 321–336, doi:10.1007/s10533-018-0421-6, 2018b.

Poulin, B. A., Ryan, J. N. and Aiken, G. R.: Effects of iron on optical properties of dissolved organic matter, Environ. Sci. Technol., 48, 10098–10106, doi:10.1021/es502670r, 2014.

Rodríguez, F. J., Schlenger, P. and García-Valverde, M.: Monitoring changes in the structure and properties of humic substances following ozonation using UV-Vis, FTIR and 1H NMR techniques, Sci. Total Environ., 541, 623–637, doi:10.1016/j.scitotenv.2015.09.127, 2016.

Schirrmeister, L., Grosse, G., Wetterich, S., Overduin, P. P., Strauss, J., Schuur, E. A. G. and Hubberten, H. W.: Fossil organic matter characteristics in permafrost deposits of the northeast Siberian Arctic, J. Geophys. Res. Biogeosciences, 116, G00M02, doi:10.1029/2011JG001647, 2011.

Schneider Von Deimling, T., Grosse, G., Strauss, J., Schirrmeister, L., Morgenstern, A., Schaphoff, S., Meinshausen, M. and Boike, J.: Observation-based modelling of permafrost carbon fluxes with accounting for deep carbon deposits and thermokarst activity, Biogeosciences, 12, 3469–3488, doi:10.5194/bg-12-3469-2015, 2015.

Schuur, E. A. G., Bockheim, J., Canadell, J. G., Euskirchen, E., Field, C. B., Goryachkin, S. V., Hagemann, S., Kuhry, P., Lafleur, P. M., Lee, H., Mazhitova, G., Nelson, F. E., Rinke, A., Romanovsky, V. E., Shiklomanov, N., Tarnocai, C., Venevsky, S., Vogel, J. G. and Zimov, S. A.: Vulnerability of Permafrost Carbon to Climate Change: Implications for the Global Carbon Cycle, Bioscience, 58(8), 701–714, doi:10.1641/b580807, 2008.

Schuur, E. A. G., Vogel, J. G., Crummer, K. G., Lee, H., Sickman, J. O. and Osterkamp, T. E.: The effect of permafrost thaw on old carbon release and net carbon exchange from tundra, Nature, 459, 556–559, doi:10.1038/nature08031, 2009.

Schuur, E. A. G., McGuire, A. D., Schädel, C., Grosse, G., Harden, J. W., Hayes, D. J., Hugelius, G., Koven, C. D., Kuhry, P., Lawrence, D. M., Natali, S. M., Olefeldt, D., Romanovsky, V. E., Schaefer, K., Turetsky, M. R., Treat, C. C. and Vonk, J. E.: Climate change and the permafrost carbon feedback, Nature, 520, 171–179, doi:10.1038/nature14338, 2015.

Scully, N. M., Cooper, W. J. and Tranvik, L. J.: Photochemical effects on microbial activity in natural waters: The interaction of reactive oxygen species and dissolved organic matter, FEMS Microbiol. Ecol., 46, 353–357, doi:10.1016/S0168-6496(03)00198-3, 2003.

Southworth, B. A. and Voelker, B. M.: Hydroxyl radical production via the photo-fenton reaction in the presence of fulvic acid, Environ. Sci. Technol., 37(6), 1130–1136, doi:10.1021/es020757l, 2003.

Spencer, R. G. M., Mann, P. J., Dittmar, T., Eglinton, T. I., McIntyre, C., Holmes, R. M., Zimov, N. and Stubbins, A.: Detecting the signature of permafrost thaw in Arctic rivers, Geophys. Res. Lett., 42, 2830–2835, doi:10.1002/2015GL063498.Received, 2015.

Strauss, J., Schirrmeister, L., Grosse, G., Fortier, D., Hugelius, G., Knoblauch, C., Romanovsky, V., Schädel, C., Schneider von Deimling, T., Schuur, E. A. G., Shmelev, D., Ulrich, M. and Veremeeva, A.: Deep Yedoma permafrost: A synthesis of depositional characteristics and carbon vulnerability, Earth-Science Rev., 172, 75–86, doi:10.1016/j.earscirev.2017.07.007, 2017.

Tveit, A. T., Urich, T., Frenzel, P. and Svenning, M. M.: Metabolic and trophic interactions modulate methane production by Arctic peat microbiota in response to warming, Proc. Natl. Acad. Sci. U. S. A., 112(19), E2507–E2516, doi:10.1073/pnas.1420797112, 2015.

Vaughan, P. P. and Blough, N. V.: Photochemical formation of hydroxyl radical by constituents of natural waters, Environ. Sci. Technol., 32, 2947–2953, doi:10.1021/es9710417, 1998.

Vehmaa, A., Hogfors, H., Gorokhova, E., Brutemark, A., Holmborn, T. and Engström-Öst, J.: Projected marine climate change: Effects on copepod oxidative status and reproduction, Ecol. Evol., 3(13), 4548–4557, doi:10.1002/ece3.839, 2013.

Vonk, J. E., Mann, P. J., Dowdy, K. L., Davydova, A., Davydov, S. P., Zimov, N., Spencer, R. G. M., Bulygina, E. B., Eglinton, T. I. and Holmes, R. M.: Dissolved organic carbon loss from Yedoma permafrost amplified by ice wedge thaw, Environ. Res. Lett., 8, doi:10.1088/1748-9326/8/3/035023, 2013.

Waldrop, M. P., Wickland, K. P., White III, R., Berhe, A. A., Harden, J. W., Romanovsky, V. E., Molecular investigations into a globally important carbon pool: permafrost-protected carbon in Alask an soils, Glob. Chang. Biol., 16, 2543–2554, doi:10.1111/j.1365-2486.2009.02141.x, 2010.

Walter Anthony, K., Daanen, R., Anthony, P., Schneider Von Deimling, T., Ping, C. L., Chanton, J. P. and Grosse, G.: Methane emissions proportional to permafrost carbon thawed in Arctic lakes since the 1950s, Nat. Geosci., 9, 679–682, doi:10.1038/ngeo2795, 2016.

Walter Anthony, K., Schneider von Deimling, T., Nitze, I., Frolking, S., Emond, A., Daanen, R., Anthony, P., Lindgren, P., Jones, B. and Grosse, G.: 21St-Century Modeled Permafrost Carbon Emissions Accelerated By Abrupt Thaw Beneath Lakes, Nat. Commun., 9(1), doi:10.1038/s41467-018-05738-9, 2018.

Wan, D., Sharma, V. K., Liu, L., Zuo, Y. and Chen, Y.: Mechanistic Insight into the Effect of Metal Ions on Photogeneration of Reactive Species from Dissolved Organic Matter, Environ. Sci. Technol., 53, 5778–5786, doi:10.1021/acs.est.9b00538, 2019.

Weishaar, J. L., Aiken, G. R., Bergamaschi, B. A., Fram, M. S., Fujii, R. and Mopper, K.: Evaluation of specific ultraviolet absorbance as an indicator of the chemical composition and reactivity of dissolved organic carbon, Environ. Sci. Technol., 37, 4702–4708, doi:10.1021/es030360x, 2003.

Westerhoff, P., Aiken, G., Amy, G. and Debroux, J.: Relationships between the structure of natural organic matter and its reactivity towards molecular ozone and hydroxyl radicals, Water Res., 33(10), 2265–2276, doi:10.1016/S0043-1354(98)00447-3, 1999.

Wickland, K. P., Aiken, G. R., Striegl, R. G., Waldrop, M. P., Koch, J. C., Jorgenson, M. T., Aiken, G. R., Koch, J. C., Jorgenson, M. T., Striegl, R. G., Neff, J. C., Aiken, G. R., Striegl, R. G., Waldrop, M. P., Koch, J. C. and Jorgenson, M. T.: Dissolved organic carbon and nitrogen release from boreal Holocene permafrost and seasonally frozen soils of Alaska, Environ. Res. Lett., 13, 065011, doi:10.1088/1748-9326/aac4ad, 2018.

Wolf, R., Thrane, J. E., Hessen, D. O. and Andersen, T.: Modelling ROS formation in boreal lakes from interactions between dissolved organic matter and absorbed solar photon flux, Water Res., 132, 331–339, doi:10.1016/j.watres.2018.01.025, 2018.

Xie, X., Zhang, Z., Hu, Y. and Cheng, H.: A mechanistic kinetic model for singlet oxygen mediated self-sensitized photo-oxidation of organic pollutants in water, Chem. Eng. J., 334, 1242–1251, doi:10.1016/j.cej.2017.11.070, 2018.

Yang, Z., Wullschleger, S. D., Liang, L., Graham, D. E. and Gu, B.: Effects of warming on the degradation and production of low-molecular-weight labile organic carbon in an Arctic tundra soil, Soil Biol. Biochem., 95, 202–211, doi:10.1016/j.soilbio.2015.12.022, 2016.

Zepp, R. G., Faust, B. C., Jürg, H. and Holgné, J.: Hydroxyl Radical Formation in Aqueous Reactions (pH 3-8) of Iron(II) with Hydrogen Peroxide: The Photo-Fenton Reaction, Environ. Sci. Technol., 26, 313–319, doi:10.1021/es00026a011, 1992.

Zhou, Z., Hua, B., Cao, X., Yang, J., Olk, D. C., Deng, B., Liu, F., Li, R. and Mao, J.: Chemical composition of dissolved organic matter from various sources as characterized by solid-state NMR, Aquat. Sci., 77(4), 595–607, doi:10.1007/s00027-015-0405-8, 2015.

Zimov, S. A., Davydov, S. P., Zimova, G. M., Davydova, A. I., Schuur, E. A. G., Dutta, K. and Chapin, I. S.: Permafrost carbon: Stock and decomposability of a globally significant carbon pool, Geophys. Res. Lett., 33, L20502, doi:10.1029/2006GL027484, 2006.

2.8. Figures:

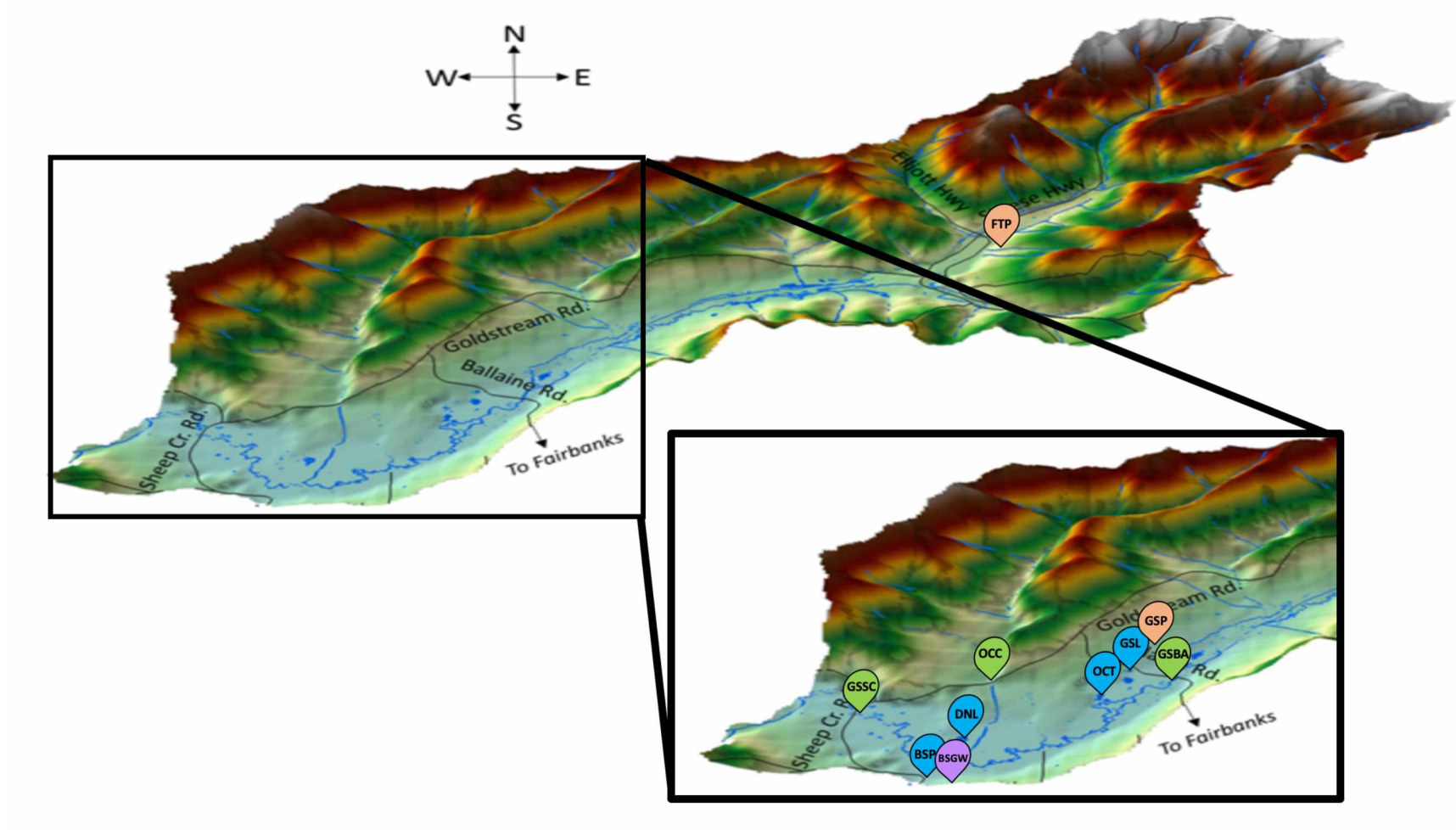

Figure 2.1: Sampling Site for all Waters Collected

Soil and water samples collected from a residential watershed during three-year seasonal sampling campaign; abbreviations found in Table 2.1. Blue = thermokarst lakes, green = streams, purple = groundwater, and peach = soils. Reference: Emond et al. 2018.

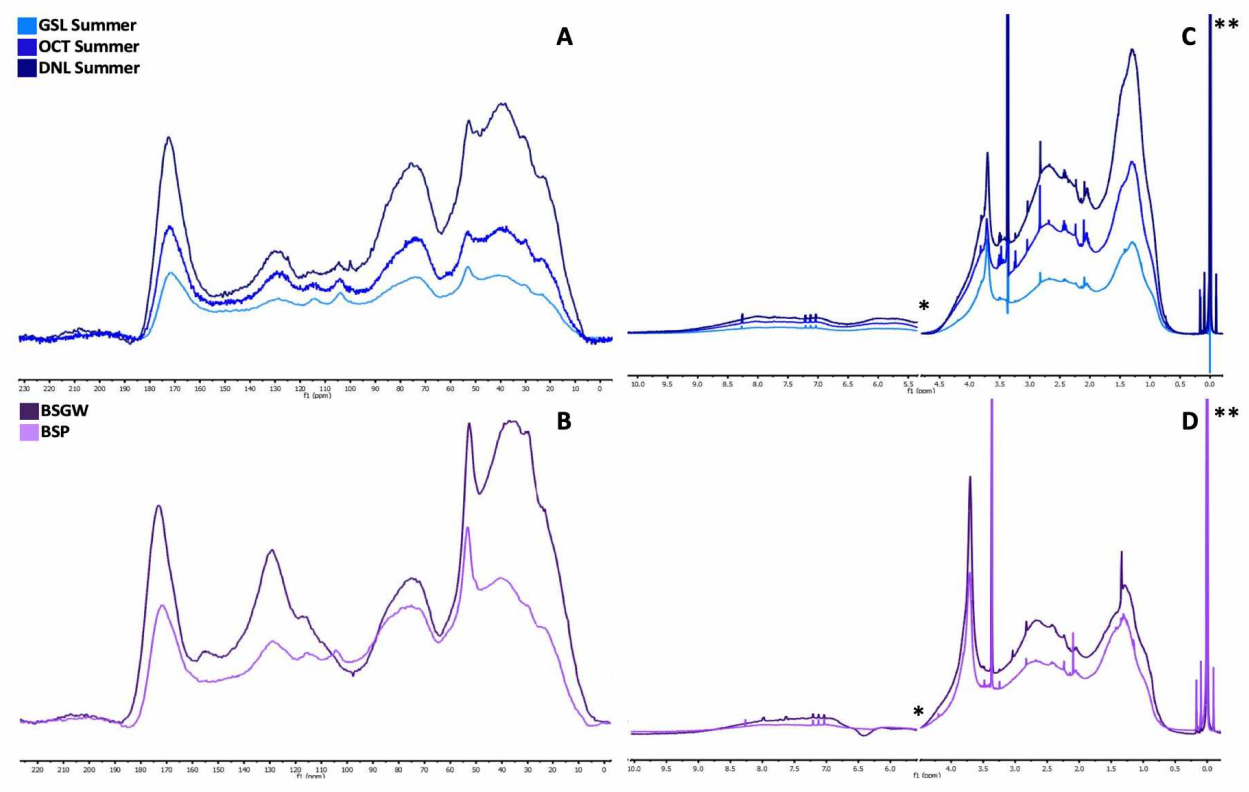

Figure 2.2: ^{13}C and ^{1}H NMR Spectra for Select Water NOM

(A,B) ^{13}C Multi-CP MAS NMR spectra of isolated NOM from Summer isolated NOM from thermokarst lakes (GSL, OCT, DNL), BSP, and BSGW (Table 2.1) all were run on a 600 MHz Bruker NMR for 32,000 scans. (C,D) ^{1}H NMR of 1mg NOM reconstituted in H_2O with a D_2O/TSP insert run on a 600 MHz Bruker NMR with SPR-W5-WATERGATE water suppression technique for 10,000 scans. (*) denotes portion of the NMR spectra removed due to residual water signal, range of spectra varies per sample based on residual water signal present. Area around water signal was excluded from binning percentages observed in Table 2.2. (**) 0 ppm signal associated with the TSP/D_2O insert. Both ^{13}C and ^{1}H spectra were processed by MestreNova Suite.

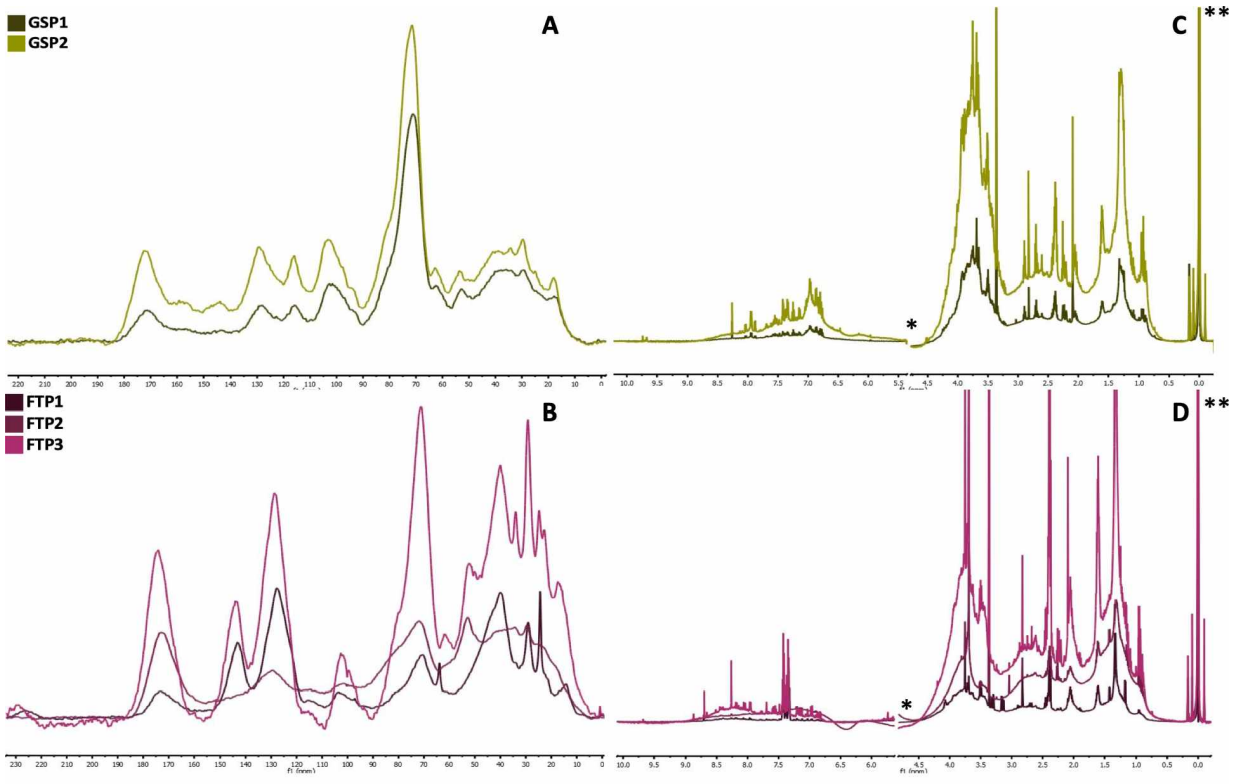

Figure 2.3: ^{13}C and ^{1}H NMR Spectra for Soil NOM

(A, B) ^{13}C Multi-CP MAS NMR spectra of isolated NOM from soil leachate for active layer samples (GSP1 and GSP2) and permafrost soils (FTP1, FTP2, FTP3) (Table 2.1) run on a 600 MHz Bruker NMR for 32,000 scans. (C, D) ^{1}H NMR of 1mg NOM reconstituted in H_2O with a D_2O/TSP insert run on a 600 MHz Bruker NMR with SPR-W5-WATERGATE water suppression technique for 10,000 scans. (*) denotes portion of the NMR spectra removed due to residual water signal, range of spectra varies per sample based on residual water signal present. Area around water signal was excluded from binning percentages observed in Table 2.2. (**) 0 ppm signal associated with the TSP/D_2O insert. Both ^{13}C and ^{1}H spectra were processed by MestreNova Suite.

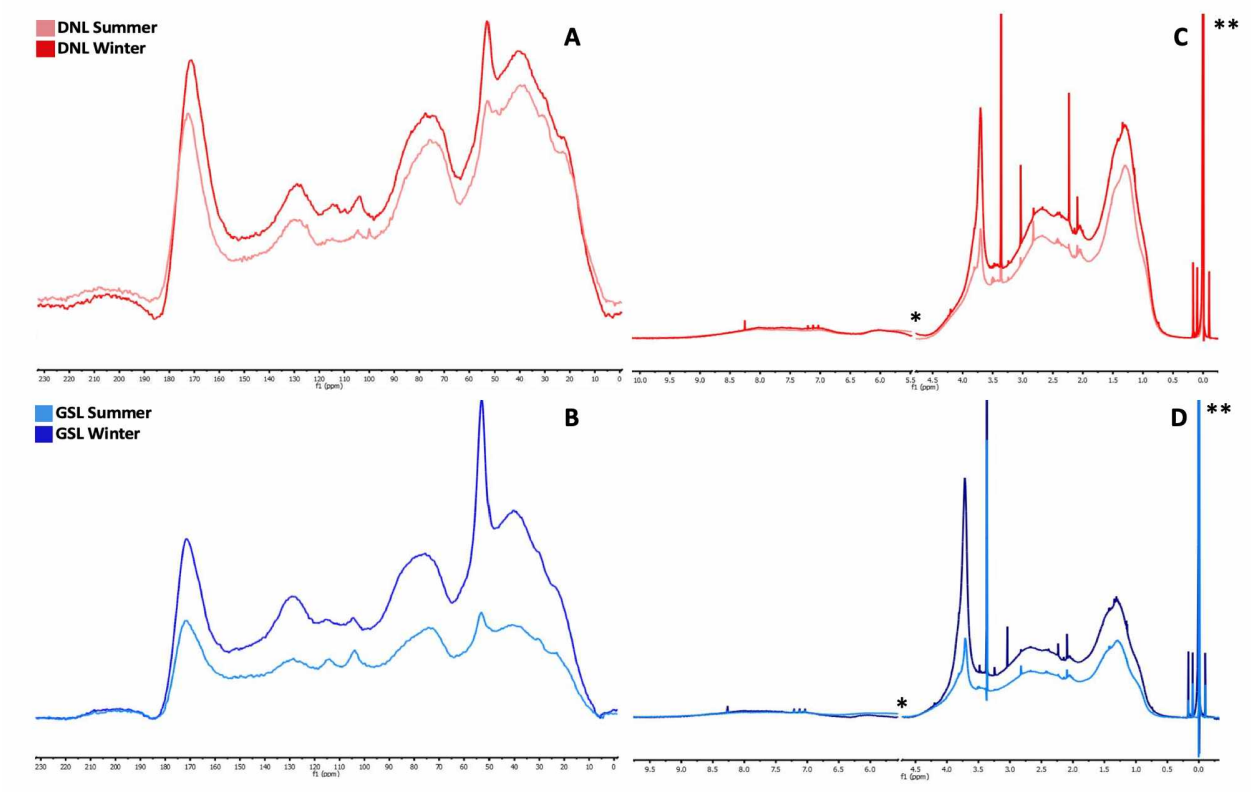

Figure 2.4: ^{13}C and ^{1}H NMR Spectra for Seasonality Variability

(A, B) ^{13}C Multi-CP MAS NMR spectra of isolated NOM from winter collected and summer collected thermokarst lake samples run on a 600 MHz Bruker NMR for 32,000 scans. (C, D) ^{1}H NMR of 1mg NOM reconstituted in H_2O with a D_2O/TSP insert run on a 600 MHz Bruker NMR with SPR-W5-WATERGATE water suppression technique for 10,000 scans. (*) denotes portion of the NMR spectra removed due to residual water signal, range of spectra varies per sample based on residual water signal present. Area around water signal was excluded from binning percentages observed in Table 2.2. (**) 0 ppm signal associated with the TSP/D_2O insert. Both ^{13}C and ^{1}H spectra were processed by MestreNova Suite.

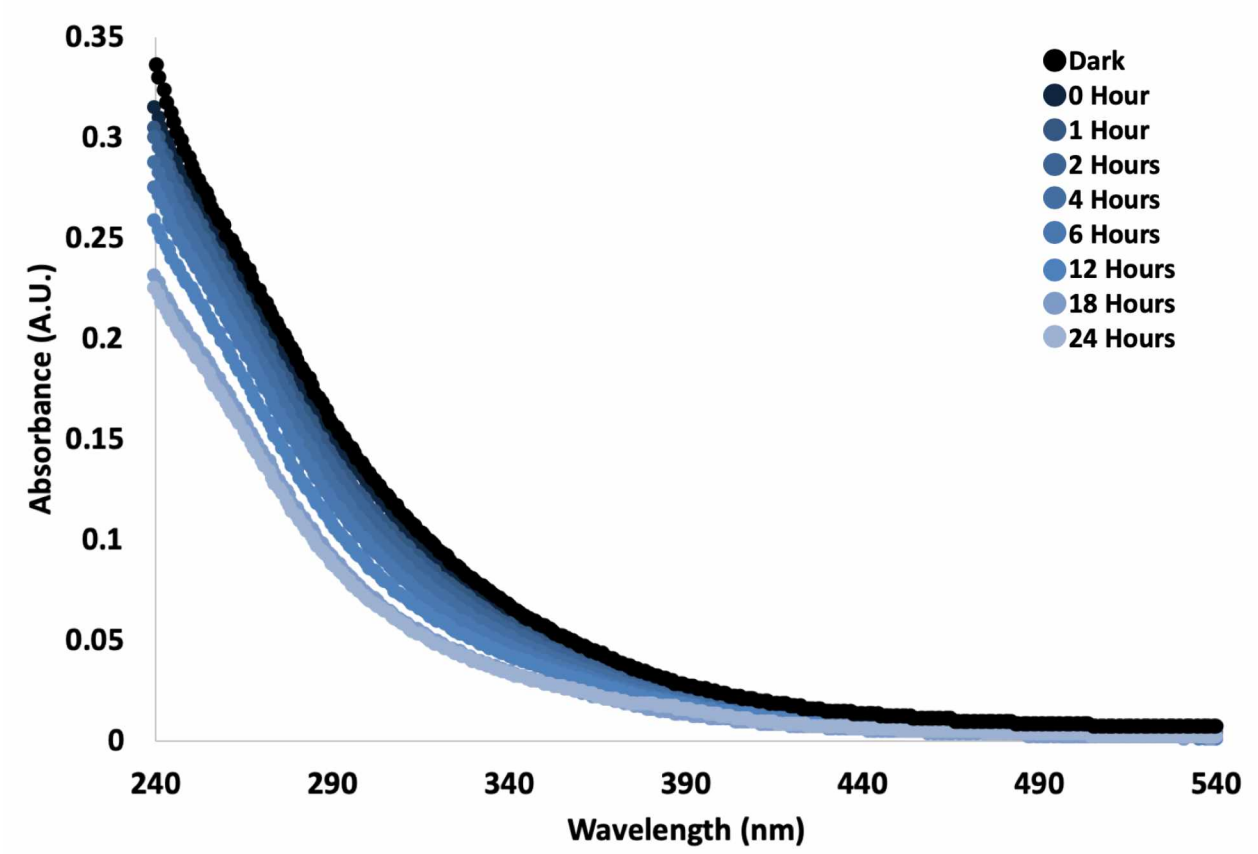

Figure 2.5: GSL Summer Unamended Absorbance Decay

Absorbance decay of Goldstream Lake (GSL) Summer PPL isolate reconstituted to 10 mg C L^{-1}, in water and irradiated in a solar simulator over a 24-hours.

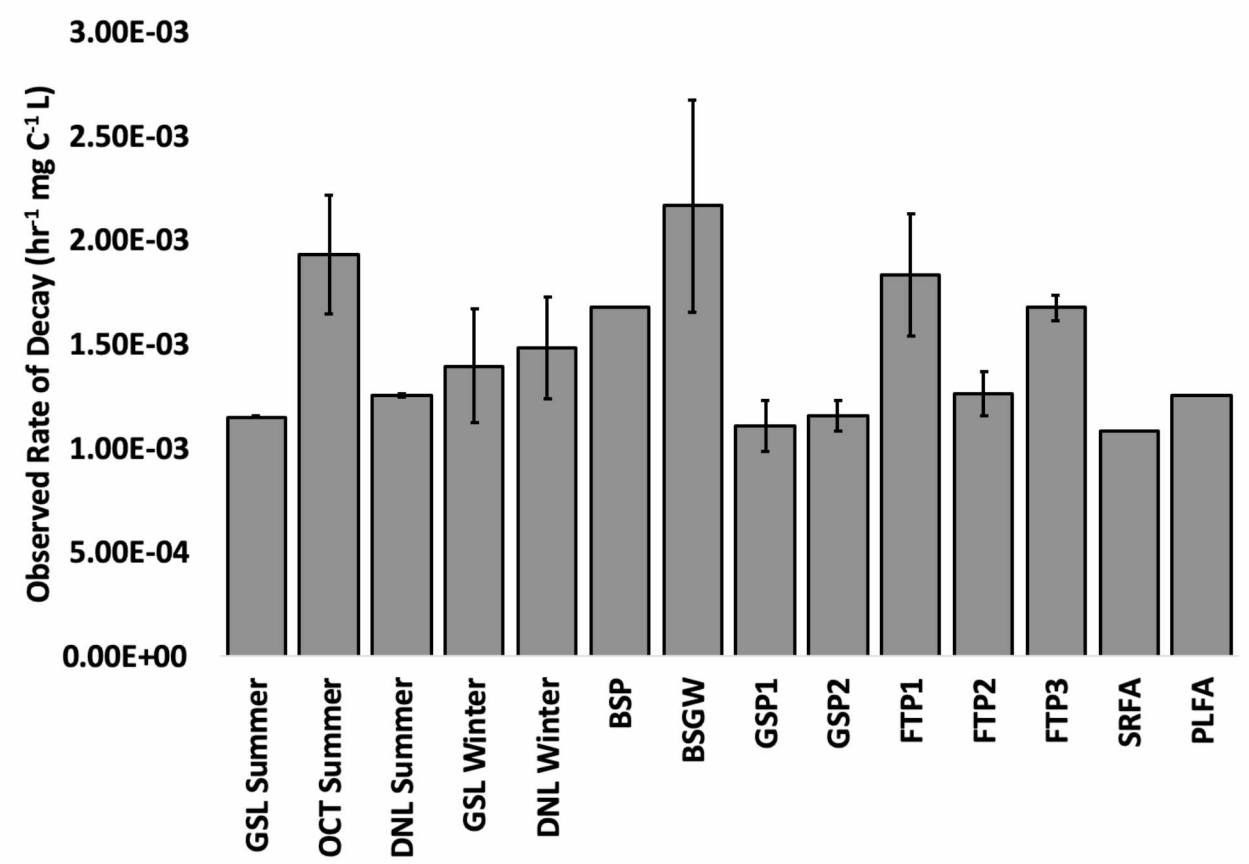

Figure 2.6: Unamended Photobleaching Rates

Rate of absorbance photolytic decay from unamended 10 mg C L^{-1} NOM solutions after being irradiated in an ATLAS Suntest for 24 hours. Error bars are the standard deviation between the duplicates run simultaneously. Samples without error bars were not run in duplicate so error could not be determined. Rates were normalized to carbon content and screening ability of the NOM solution. Abbreviated names found in Table 2.1, PLFA (Pony Lake Fulvic Acid – microbial sourced reference material), and SRFA (Suwannee River Humic Acid – terrestrial sourced reference material).

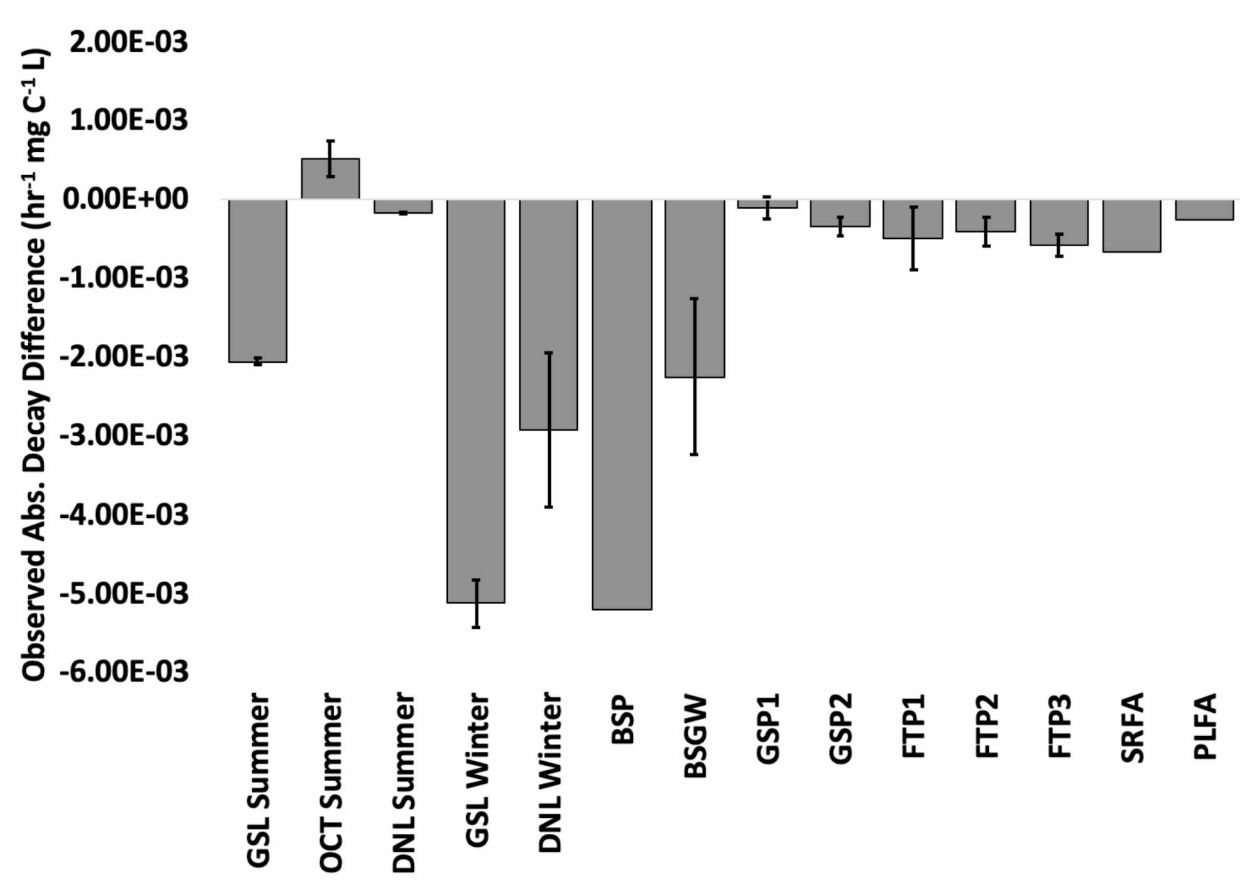

Figure 2.7: Difference Between Unamended and Iron Amended Photolysis Rates

The difference between unamended samples and iron amended samples after the rate of absorbance photolytic decay was determined through irradiating 10 mg C L^{-1} NOM solutions in an ATLAS Suntest for 24 hours. Error bars are the propagated error between photolytic decay rates. Samples without error bars were not run in duplicate so error could not be propagated. Positive difference indicates that unamended photolysis rate was higher than iron amended observed absorbance decay rate. Abbreviated names found in Table 2.1, PLFA (Pony Lake Fulvic Acid – microbial sourced reference material), and SRFA (Suwannee River Humic Acid – terrestrial sourced reference material).

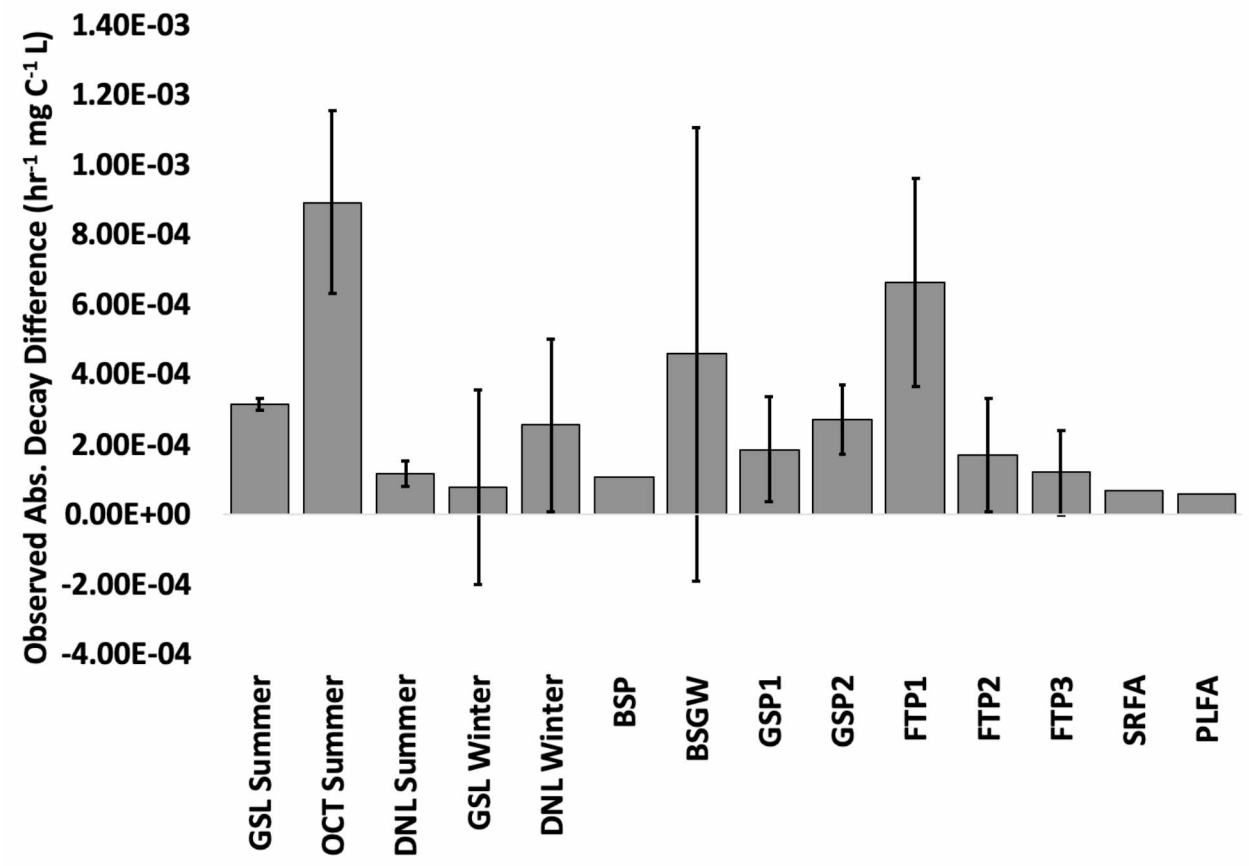

Figure 2.8: Difference Between Unamended and Methanol Amended Photolysis Rates

The difference between unamended samples and methanol amended samples after the rate of absorbance photolytic decay was determined through irradiating 10 mg C L^{-1} NOM solutions in an ATLAS Suntest for 24 hours. Error bars are the propagated error between photolytic decay rates. Samples without error bars were not run in duplicate so error could not be propagated. Positive difference indicates that unamended photolysis rate was higher than methanol amended observed absorbance decay rate. Abbreviated names found in Table 2.1, PLFA (Pony Lake Fulvic Acid – microbial sourced reference material), and SRFA (Suwannee River Humic Acid – terrestrial sourced reference material).

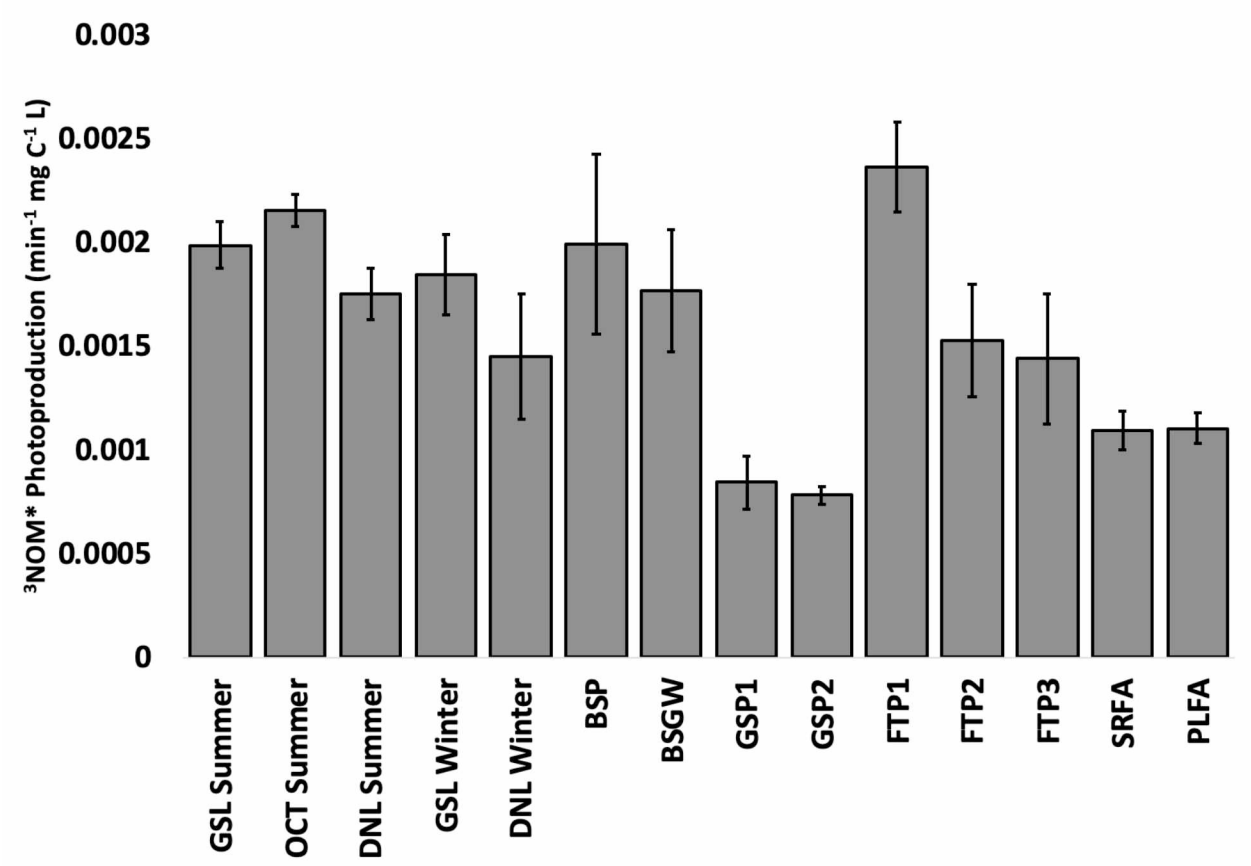

Figure 2.9: Rate of ^{3}NOM* Production

TMP loss represented from a decrease in fluorescence signal at λ_{ex} = 230 nm and λ_{em} = 305 nm for isolated NOM from various water and leachate samples. The concentration of TMP is determined through the use of a calibration curve ranging from 0.01uM to 30uM. The absolute value of the TMP loss rate is representative of ^{3}NOM* rate of production depicted on this bar graph. Abbreviated names found in Table 2.1, PLFA (Pony Lake Fulvic Acid – microbial sourced reference material), and SRFA (Suwannee River Humic Acid – terrestrial sourced reference material).

2.9. Tables:

Table 2.1: General Sampling Locations Information

General information about sampling soils and sampling waters collected for NOM isolation, including sampling time period and radiocarbon age. Values denoted with an asterisks (*) were obtained from Elder et al. 2019. Values denoted with a double-asterisks (**) were obtained from Mackelprang et al. 2017. BSGW has undisclosed location due to privacy reasons as it is a residential home.

Name	Condensed Name	Latitude (ºN)	Longitude (ºW)	Surface Area (m^2)	Max Depth (m)	Permafrost Degradation Classification	Estimated Age of Lake in Calendar Years	Radiocarbon Age of Soil Carbon	Sampling Dates	
Goldstream Lake	GSL	64.916	-147.847	10,000*	4.7*	Closed	>120*		Jan 2017	June 2017
Octopus Lake	OCT	64.907	-147.860	22,000	2	Transitional			Aug 2018	
Doughnut Lake	DNL	64.899	-147.908	34,000*	3.8*	Open	1,000*		Jan 2017	Aug 2018
Blacksheep Pond	BSP	64.888	-147.920	540	0.5	2nd Gen. Closed			Mar 2017	
Residential Well	BSGW	undisclosed	undisclosed	N/A	72.5				July 2016	
Goldstream Active Layer	GSP	64.920	-147.830		0.19-0.26				Apr 2018	
Fox Tunnel Permafrost	FTP1	64.951	-147.621		20			19,000**	Apr 2018	
	FTP2	64.951	-147.621		54			27,000**	Apr 2018	
	FTP3	64.951	-147.621		81			33,000**	Apr 2018	

Table 2.2: ^{13}C NMR Binning Percentages

^{13}C NMR binning percentages determined for isolated NOM using multi-CP-MAS ^{13}C NMR. 0 – 45 ppm alkyl-C, 45 – 60 ppm methoxyl, 60 – 90 ppm carbohydrates, 90 – 120 ppm proton substituted aromatics, 120 – 140 ppm carbon substituted aromatics, 140 – 160 ppm oxygen substituted aromatics, 160 – 190 ppm carboxyl/aliphatic amides, 190 – 220 ppm aldehydes and ketones (Mao et al. 2012; Zhou et al. 2015; Kaiser et al. 2003). 90 – 160 ppm is classified as total aromatics. Abbreviations for samples are denoted in Table 2.1.

Sample	190-220 ppm	160-190 ppm	140-160 ppm	120-140 ppm	90-120 ppm	Sum 90-160 ppm	60-90 ppm	45-60 ppm	0-45 ppm
GSL SUMMER	1.25%	12.12%	6.43%	8.56%	13.66%	28.65%	21.22%	13.02%	23.75%
OCT SUMMER	1.23%	12.86%	5.87%	9.04%	12.64%	27.56%	20.80%	12.33%	25.22%
DNL SUMMER	1.47%	13.14%	4.75%	7.30%	10.37%	22.42%	20.61%	13.55%	28.80%
GSL WINTER	2.26%	11.48%	6.31%	9.41%	12.48%	28.20%	19.71%	14.89%	23.47%
DNL WINTER	1.88%	13.20%	6.28%	8.65%	12.26%	27.19%	19.60%	13.19%	24.93%
BSP	1.99%	11.08%	6.22%	9.42%	13.46%	29.10%	20.36%	14.00%	23.47%
BSGW	0.82%	11.89%	5.87%	11.19%	9.44%	26.50%	14.80%	13.31%	32.66%
GSP1	1.94%	9.88%	6.48%	10.27%	16.57%	33.32%	29.58%	7.42%	17.86%
GSP2	1.24%	5.98%	3.93%	6.96%	14.96%	25.84%	34.88%	8.96%	23.10%
FTP1	1.34%	6.04%	9.11%	20.86%	8.11%	38.08%	14.57%	9.83%	30.13%
FTP2	1.45%	13.43%	5.29%	8.96%	10.90%	25.14%	21.83%	12.55%	25.60%
FTP3	2.13%	11.44%	7.44%	13.56%	9.74%	30.74%	21.38%	10.22%	24.09%
SRFA	2.03%	9.63%	6.71%	9.67%	15.90%	32.27%	20.40%	11.56%	24.11%
PLFA	0.44%	8.25%	5.26%	8.21%	9.58%	23.05%	16.83%	14.65%	36.79%

Table 2.3: ^{1}H NMR Binning Percentages

1 mg of PPL isolated NOM reconstituted in 18 MΩ H_2O with a TSP/D_2O insert was run on a 600 MHz Bruker ^{1}H NMR with NMR SPR-W5-WATERGATE water suppression technique. Percentages were obtained from the comparison of the area underneath of the spectra with specified chemical shifts; 0.6 – 1.6 ppm material derived from linear terpenoids (MDLT), 1.6 – 3.2 ppm carboxyl rich alicyclic molecules (CRAM), 3.2 – 4.5 ppm carbohydrates, and 6.5 – 8.4 ppm aromatics (Lam & Simpson, 2008). Abbreviations for samples are denoted in Table 2.1.

	6.5-8.4 ppm	3.2-4.5 ppm	1.6-3.2 ppm	0.6-1.6 ppm
GSL SUMMER	5.89%	22.21%	43.36%	28.54%
OCT SUMMER	5.58%	19.93%	44.70%	29.80%
DNL SUMMER	7.44%	24.24%	42.25%	26.06%
GSL WINTER	4.14%	27.87%	40.50%	27.49%
DNL WINTER	4.29%	21.18%	44.47%	29.76%
BSP	4.23%	25.16%	42.84%	27.76%
BSGW	7.69%	24.64%	42.41%	25.27%
GSP1	11.48%	39.71%	28.66%	20.15%
GSP2	10.87%	39.90%	27.67%	21.56%
FTP1	11.62%	34.25%	33.48%	20.65%
FTP2	10.02%	25.13%	36.92%	27.93%
FTP3	8.90%	32.13%	34.61%	24.35%
PLFA	6.92%	16.19%	46.61%	30.29%
SRFA	9.36%	24.81%	44.52%	21.31%
NAFA	15.40%	30.17%	37.21%	17.22%

Table 2.4: ^{13}C Chemical Shift Comparison to Reference Material

Isolated water and soil NOM ^{13}C NMR spectra were compared to PLFA and SRFA spectra utilizing equation 1 to determine similarities in carbon functional groups to microbial and terrestrial sourced reference materials, with total difference representing the summation of difference in relative integration. Abbreviations for samples are denoted in Table 2.1.

Sample	Comparison Sample	190-220 ppm	160-190 ppm	Sum 90-160 ppm	60-90 ppm	45-60 ppm	0-45 ppm	Total Difference
GSL SUMMER	PLFA	0.81%	3.87%	5.60%	4.39%	1.63%	13.04%	29.34%
OCT SUMMER	PLFA	0.79%	4.61%	4.51%	3.97%	2.32%	11.57%	27.77%
DNL SUMMER	PLFA	1.03%	4.89%	0.63%	3.78%	1.10%	7.99%	19.42%
GSL WINTER	PLFA	1.82%	3.23%	5.15%	2.88%	0.24%	13.32%	26.64%
DNL WINTER	PLFA	1.44%	4.95%	4.14%	2.77%	1.46%	11.86%	26.62%
BSP	PLFA	1.55%	2.83%	6.05%	3.53%	0.65%	13.32%	27.93%
BSGW	PLFA	0.38%	3.64%	3.45%	2.03%	1.34%	4.13%	14.97%
GSP1	PLFA	1.50%	1.63%	10.27%	12.75%	7.23%	18.93%	52.31%
GSP2	PLFA	0.80%	2.27%	2.79%	18.05%	5.69%	13.69%	43.29%
FTP1	PLFA	0.90%	2.21%	15.03%	2.26%	4.82%	6.66%	31.88%
FTP2	PLFA	1.01%	5.18%	2.09%	5.00%	2.10%	11.19%	26.57%
FTP3	PLFA	1.69%	3.19%	7.69%	4.55%	4.43%	12.70%	34.25%
GSL SUMMER	SRFA	0.78%	2.49%	3.62%	0.82%	1.46%	0.36%	9.53%
OCT SUMMER	SRFA	0.80%	3.23%	4.71%	0.40%	0.77%	1.11%	11.02%
DNL SUMMER	SRFA	0.56%	3.51%	9.85%	0.21%	1.99%	4.69%	20.81%
GSL WINTER	SRFA	0.23%	1.85%	4.07%	0.69%	3.33%	0.64%	10.81%
DNL WINTER	SRFA	0.15%	3.57%	5.08%	0.80%	1.63%	0.82%	12.05%
BSP	SRFA	0.04%	1.45%	3.17%	0.04%	2.44%	0.64%	7.78%
BSGW	SRFA	1.21%	2.26%	5.77%	5.60%	1.75%	8.55%	25.14%
GSP1	SRFA	0.09%	0.25%	1.05%	9.18%	4.14%	6.25%	20.96%
GSP2	SRFA	0.79%	3.65%	6.43%	14.48%	2.60%	1.01%	28.96%
FTP1	SRFA	0.69%	3.59%	5.81%	5.83%	1.73%	6.02%	23.67%
FTP2	SRFA	0.58%	3.80%	7.13%	1.43%	0.99%	1.49%	15.42%
FTP3	SRFA	0.10%	1.81%	1.53%	0.98%	1.34%	0.02%	5.78%

Table 2.5: ^{1}H NMR Chemical Shift Comparison to Reference Material

Isolated water and soil NOM ^{1}H NMR spectra were compared to PLFA and SRFA spectra utilizing equation 1 to determine similarities in proton functional groups to microbial and terrestrial sourced reference materials, with total difference representing the summation of difference in relative integration. Abbreviations for samples are denoted in Table 2.1.

Sample	Comparison Sample	6.5-8.4 ppm	3.2-4.5 ppm	1.6-3.2 ppm	0.6-1.6 ppm	Total Difference
GSL SUMMER	PLFA	1.03%	6.03%	3.24%	1.75%	12.05%
OCT SUMMER	PLFA	1.34%	3.74%	1.91%	0.49%	7.48%
DNL SUMMER	PLFA	0.53%	8.06%	4.36%	4.23%	17.17%
GSL WINTER	PLFA	2.78%	11.68%	6.11%	2.80%	23.37%
DNL WINTER	PLFA	2.62%	4.99%	2.14%	0.53%	10.28%
BSP	PLFA	2.68%	8.98%	3.77%	2.53%	17.95%
BSGW	PLFA	0.77%	8.45%	4.20%	5.02%	18.44%
GSP1	PLFA	4.56%	23.52%	17.95%	10.14%	56.16%
GSP2	PLFA	3.95%	23.71%	18.94%	8.73%	55.34%
FTP1	PLFA	4.70%	18.07%	13.13%	9.63%	45.53%
FTP2	PLFA	3.10%	8.94%	9.68%	2.36%	24.08%
FTP3	PLFA	1.98%	15.94%	11.99%	5.94%	35.86%
GSL SUMMER	SRFA	3.48%	2.60%	1.15%	7.23%	14.46%
OCT SUMMER	SRFA	3.78%	4.89%	0.18%	8.49%	17.34%
DNL SUMMER	SRFA	1.92%	0.57%	2.27%	4.75%	9.51%
GSL WINTER	SRFA	5.22%	3.06%	4.01%	6.18%	18.47%
DNL WINTER	SRFA	5.07%	3.63%	0.05%	8.45%	17.20%
BSP	SRFA	5.13%	0.35%	1.68%	6.45%	13.61%
BSGW	SRFA	1.67%	0.17%	2.11%	3.96%	7.92%
GSP1	SRFA	2.12%	14.89%	15.85%	1.16%	34.02%
GSP2	SRFA	1.51%	15.09%	16.85%	0.25%	33.70%
FTP1	SRFA	2.25%	9.44%	11.04%	0.65%	23.39%
FTP2	SRFA	0.65%	0.32%	7.59%	6.62%	15.19%
FTP3	SRFA	0.46%	7.32%	9.90%	3.04%	20.73%
GSL SUMMER	NAFA	9.52%	7.95%	6.16%	11.32%	34.94%
OCT SUMMER	NAFA	9.83%	10.24%	7.49%	12.58%	40.13%
DNL SUMMER	NAFA	7.96%	5.92%	5.04%	8.84%	27.77%
GSL WINTER	NAFA	11.26%	2.30%	3.30%	10.26%	27.12%
DNL WINTER	NAFA	11.11%	8.99%	7.26%	12.54%	39.90%
BSP	NAFA	11.17%	5.00%	5.64%	10.54%	32.35%
BSGW	NAFA	7.72%	5.53%	5.20%	8.05%	26.49%
GSP1	NAFA	3.93%	9.54%	8.54%	2.93%	24.94%
GSP2	NAFA	4.53%	9.73%	9.54%	4.34%	28.14%
FTP1	NAFA	3.79%	4.09%	3.73%	3.43%	15.04%
FTP2	NAFA	5.39%	5.04%	0.28%	10.71%	21.41%
FTP3	NAFA	6.50%	1.96%	2.59%	7.13%	18.19%

Table 2.6: ^{13}C NMR Chemical Shift Comparison of Water NOM to Soil NOM

Isolated water NOM ^{13}C NMR spectra were compared to active layer and permafrost layer NOM spectra utilizing equation 1 to determine similarities in carbon functional groups to observe potential influence from soil leaching into the waters from thaw, with total difference representing the summation of difference in relative integration. Abbreviations for samples are denoted in Table 2.1.

Sample	Comparison Sample	190-220 ppm	160-190 ppm	Sum 90-160 ppm	60-90 ppm	45-60 ppm	0-45 ppm	Total Difference
GSL SUMMER	GSP1	0.69%	2.25%	4.67%	8.36%	5.60%	5.88%	32.12%
OCT SUMMER	GSP1	0.71%	2.98%	5.76%	8.78%	4.91%	7.36%	36.27%
DNL SUMMER	GSP1	0.47%	3.27%	10.90%	8.97%	6.13%	10.94%	51.57%
GSL WINTER	GSP1	0.31%	1.61%	5.11%	9.88%	7.47%	5.60%	35.10%
DNL WINTER	GSP1	0.06%	3.33%	6.13%	9.98%	5.77%	7.07%	38.47%
BSP	GSP1	0.05%	1.20%	4.21%	9.22%	6.58%	5.61%	31.08%
BSGW	GSP1	1.12%	2.02%	6.81%	14.78%	5.89%	14.80%	54.08%
GSL SUMMER	GSP2	0.01%	6.15%	2.81%	13.66%	4.05%	0.65%	32.73%
OCT SUMMER	GSP2	0.01%	6.89%	1.71%	14.08%	3.37%	2.12%	34.53%
DNL SUMMER	GSP2	0.23%	7.17%	3.42%	14.26%	4.58%	5.70%	41.13%
GSL WINTER	GSP2	1.01%	5.51%	2.36%	15.17%	5.92%	0.37%	37.67%
DNL WINTER	GSP2	0.64%	7.23%	1.35%	15.28%	4.23%	1.84%	37.31%
BSP	GSP2	0.74%	5.10%	3.26%	14.52%	5.03%	0.37%	35.28%
BSGW	GSP2	0.42%	5.92%	0.66%	20.08%	4.35%	9.56%	52.69%
GSL SUMMER	FTP1	0.09%	6.08%	9.43%	6.64%	3.19%	6.39%	52.36%
OCT SUMMER	FTP1	0.11%	6.82%	10.53%	6.23%	2.51%	4.91%	50.70%
DNL SUMMER	FTP1	0.13%	7.10%	15.66%	6.04%	3.72%	1.33%	54.16%
GSL WINTER	FTP1	0.91%	5.44%	9.88%	5.13%	5.06%	6.67%	51.71%
DNL WINTER	FTP1	0.54%	7.16%	10.89%	5.03%	3.37%	5.20%	51.37%
BSP	FTP1	0.64%	5.04%	8.98%	5.79%	4.17%	6.67%	50.97%
BSGW	FTP1	0.52%	5.85%	11.58%	0.23%	3.49%	2.53%	38.44%
GSL SUMMER	FTP2	0.20%	1.31%	3.51%	0.61%	0.47%	1.86%	12.27%
OCT SUMMER	FTP2	0.22%	0.57%	2.42%	1.03%	0.22%	0.38%	7.26%
DNL SUMMER	FTP2	0.02%	0.29%	2.72%	1.21%	1.00%	3.20%	11.15%
GSL WINTER	FTP2	0.81%	1.95%	3.07%	2.12%	2.34%	2.14%	15.49%
DNL WINTER	FTP2	0.43%	0.23%	2.05%	2.23%	0.64%	0.67%	8.92%
BSP	FTP2	0.54%	2.35%	3.97%	1.46%	1.45%	2.14%	15.88%
BSGW	FTP2	0.63%	1.54%	1.37%	7.03%	0.76%	7.06%	22.66%
GSL SUMMER	FTP3	0.88%	0.68%	2.09%	0.16%	2.79%	0.34%	16.88%
OCT SUMMER	FTP3	0.90%	1.42%	3.18%	0.58%	2.11%	1.13%	18.31%
DNL SUMMER	FTP3	0.66%	1.70%	8.32%	0.76%	3.33%	4.71%	29.05%
GSL WINTER	FTP3	0.13%	0.04%	2.53%	1.67%	4.66%	0.62%	17.68%
DNL WINTER	FTP3	0.25%	1.76%	3.55%	1.78%	2.97%	0.84%	19.74%
BSP	FTP3	0.14%	0.37%	1.63%	1.02%	3.78%	0.62%	16.63%
BSGW	FTP3	1.30%	0.45%	4.24%	6.58%	3.09%	8.57%	28.47%
GSL SUMMER	BSGW	0.76%	8.57%	20.38%	4.82%	7.54%	25.59%	32.12%
OCT SUMMER	BSGW	0.08%	6.79%	23.24%	0.29%	8.28%	32.29%	36.27%
DNL SUMMER	BSGW	0.41%	5.98%	25.84%	5.27%	8.96%	23.10%	51.57%
GSL WINTER	BSGW	0.63%	1.54%	1.37%	7.03%	0.76%	7.06%	35.10%
DNL WINTER	BSGW	0.82%	11.89%	26.50%	14.80%	13.31%	32.66%	38.47%
BSP	BSGW	0.82%	11.89%	26.50%	14.80%	13.31%	32.66%	31.08%

Table 2.7: ^{1}H NMR Chemical Shift Comparison of Water NOM to Soil NOM

Isolated water NOM ^{1}H NMR spectra were compared to active layer and permafrost layer NOM spectra utilizing equation 1 to determine similarities in proton functional groups to observe potential influence on functional group composition from soil leaching, with total difference representing the summation of difference in relative integration. Abbreviations for samples are denoted in Table 2.1.

Sample	Comparison Sample	6.5-8.4 ppm	3.2-4.5 ppm	1.6-3.2 ppm	0.6-1.6 ppm	Total Difference
GSL SUMMER	GSP1	5.59%	17.49%	14.70%	8.38%	46.17%
OCT SUMMER	GSP1	5.90%	19.78%	16.04%	9.64%	51.36%
DNL SUMMER	GSP1	4.03%	15.46%	13.59%	5.91%	38.99%
GSL WINTER	GSP1	7.34%	11.84%	11.84%	7.33%	38.34%
DNL WINTER	GSP1	7.18%	18.53%	15.81%	9.61%	51.13%
BSP	GSP1	7.25%	14.54%	14.18%	7.61%	43.58%
BSGW	GSP1	3.79%	15.07%	13.74%	5.12%	37.72%
GSL SUMMER	GSP2	4.99%	17.69%	15.70%	6.98%	45.35%
OCT SUMMER	GSP2	5.29%	19.97%	17.03%	8.24%	50.53%
DNL SUMMER	GSP2	3.43%	15.66%	14.58%	4.50%	38.17%
GSL WINTER	GSP2	6.73%	12.03%	12.83%	5.92%	37.52%
DNL WINTER	GSP2	6.58%	18.72%	16.80%	8.20%	50.30%
BSP	GSP2	6.64%	14.74%	15.17%	6.20%	42.75%
BSGW	GSP2	3.18%	15.26%	14.74%	3.71%	36.89%
GSL SUMMER	FTP1	5.73%	12.04%	9.89%	7.88%	35.54%
OCT SUMMER	FTP1	6.04%	14.33%	11.22%	9.14%	40.73%
DNL SUMMER	FTP1	4.17%	10.01%	8.77%	5.41%	28.36%
GSL WINTER	FTP1	7.47%	6.38%	7.03%	6.83%	27.71%
DNL WINTER	FTP1	7.32%	13.08%	10.99%	9.11%	40.49%
BSP	FTP1	7.38%	9.09%	9.37%	7.11%	32.94%
BSGW	FTP1	3.93%	9.61%	8.93%	4.61%	27.09%
GSL SUMMER	FTP2	4.13%	2.92%	6.44%	0.61%	14.10%
OCT SUMMER	FTP2	4.44%	5.20%	7.77%	1.87%	19.28%
DNL SUMMER	FTP2	2.57%	0.88%	5.33%	1.87%	10.65%
GSL WINTER	FTP2	5.87%	2.74%	3.58%	0.45%	12.64%
DNL WINTER	FTP2	5.72%	3.95%	7.54%	1.83%	19.05%
BSP	FTP2	5.78%	0.03%	5.92%	0.17%	11.91%
BSGW	FTP2	2.33%	0.49%	5.48%	2.66%	10.96%
GSL SUMMER	FTP3	3.01%	9.92%	8.75%	4.18%	25.87%
OCT SUMMER	FTP3	3.32%	12.20%	10.08%	5.44%	31.05%
DNL SUMMER	FTP3	1.46%	7.88%	7.64%	1.71%	18.69%
GSL WINTER	FTP3	4.76%	4.26%	5.89%	3.13%	18.04%
DNL WINTER	FTP3	4.61%	10.95%	9.86%	5.41%	30.82%
BSP	FTP3	4.67%	6.97%	8.23%	3.41%	23.27%
BSGW	FTP3	1.21%	7.49%	7.79%	0.92%	17.41%

Table 2.8: ^{13}C Seasonality Variability

^{13}C NMR spectra seasonality variability determined via equation 1 for the comparison of Closed and Open thermokarst lakes during winter and summer. A decreased percentage indicates a decrease in variability in the carbon functional groups during the season. Differences were determined by the difference in relative integration found in equation 1, with total difference representing the summation of difference in relative integration. Abbreviations for samples are denoted in Table 2.1.

Sample	190-220 ppm	160-190 ppm	140-160 ppm	120-140 ppm	90-120 ppm	Sum 90-160 ppm	60-90 ppm	45-60 ppm	0-45 ppm	Total Difference
GSL SUMMER	1.25%	12.12%	6.43%	8.56%	13.66%	28.65%	21.22%	13.02%	23.75%	
DNL SUMMER	1.47%	13.14%	4.75%	7.30%	10.37%	22.42%	20.61%	13.55%	28.80%	
Difference Summer	0.22%	1.02%				6.23%	0.60%	0.53%	5.06%	13.66%
GSL WINTER	2.26%	11.48%	6.31%	9.41%	12.48%	28.20%	19.71%	14.89%	23.47%	
DNL WINTER	1.88%	13.20%	6.28%	8.65%	12.26%	27.19%	19.60%	13.19%	24.93%	
Difference Winter	0.38%	1.72%				1.01%	0.11%	1.69%	1.47%	6.38%

Table 2.9: ^{1}H Seasonality Variability

^{1}H NMR spectra seasonality variability determined via equation 1 for the comparison of Closed and Open thermokarst lakes during winter and summer. A decreased percentage indicates a decrease in variability in the carbon functional groups during the season. Abbreviations for samples are denoted in Table 2.1.

	6.5-8.4 ppm	3.2-4.5 ppm	1.6-3.2 ppm	0.6-1.6 ppm	Total Difference
GSL SUMMER	5.89%	22.21%	43.36%	28.54%	
DNL SUMMER	7.44%	24.24%	42.25%	26.06%	
Difference Summer	1.56%	2.03%	1.11%	2.48%	7.18%
GSL WINTER	4.14%	27.87%	40.50%	27.49%	
DNL WINTER	4.29%	21.18%	44.47%	29.76%	
Difference Winter	0.15%	6.69%	3.97%	2.28%	13.09%

Table 2.10: Statistical Results for Epilimnion versus Hypolimnion and ANOVA's between Thermokarst lake

T-Tests were utilized to determine if the epilimnion (top) and hypolimnion (bottom) were statistically different. A Welch's T-Test was completed when the variance between samples was determined to be statistically different and thus, required a Welch T-Test to be utilized are denoted with *** in the table. Additionally, ANOVA tests were completed on only the epilimnion, one with and without BSP. The darker the shading in the box (decreased p-value) the more statistically different the results. The sample amount is found within each box as (top sample number/bottom sample number). Sample abbreviations for samples are denoted in Table 2.1, data abbreviations are denoted in Table 1.1 and Table 1.2, epilimnion (epi.), and hypolimnion (hypo.).

Statistical Test	S_R	E2:E3	BIX	FI	Freshness	HIX	$SUVA_{254}$	$SUVA_{280}$
ANOVA Lakes Top (GSL,OCT,DNL,BSP)	53	52	53	50	53	53	31	47
ANOVA Lakes Top (GSL,OCT,DNL)	46	45	46	44	46	47	40	40
T-Test GSL Epi. Vs. Hypo.	16/18	16/17	16/18	16/17***	16/18***	16/18***	15/16	15/16***
T-Test OCT Epi. Vs. Hypo.	12/13	11/13	12/14	12/12	12/14	12/14	12/13	12/13
T-Test DNL Epi. Vs. Hypo.	13/15***	14/15	14/14	14/15	14/14	14/15	11/11	11/11
T-Test GSL Epi. Vs. Hypo.	18/7	17/7	18/7	17/6***	18/7	18/6***	16/7	16/7
						***Welch T-Test		
P-Value Legend	<0.0001	<0.0010	<0.0100	<0.0500		Number of samples located within cell		

Table 2.11: Optical Indices Averages over a Three-Year Span

Optical Indices determined by Table 1.1 and Table 1.2 for thermokarst lakes sampled and isolated for NOM. These averages span summer and winter from 2016 to 2018. Standard deviation is denoted as (±) in this table. Sample abbreviations for samples are denoted in Table 2.1, data abbreviations are denoted in Table 1.1 and Table 1.2. and epilimnion (epi.).

Sample	S_R	+/-	E2:E3	+/-	FI	+/-	HIX	+/-	Freshness	+/-	BIX	+/-	$SUVA_{254}$ (L mg C^{-1} m^{-1})	+/-	$SUVA_{280}$ (L mg C^{-1} m^{-1})	+/-
GSL Epi.	0.856	0.050	8.553	1.133	1.626	0.049	0.932	0.014	0.709	0.015	0.744	0.023	0.996	0.256	0.980	0.250
OCT Epi.	0.799	0.026	4.998	0.415	1.543	0.105	0.958	0.033	0.576	0.052	0.600	0.049	2.429	1.125	2.392	1.142
DNL Epi.	0.964	0.076	8.190	1.241	1.563	0.087	0.941	0.065	0.679	0.018	0.710	0.021	1.061	0.328	1.051	0.324
BSP	0.924	0.065	7.398	0.828	1.607	0.024	0.945	0.009	0.659	0.024	0.673	0.024	1.139	0.421	1.123	0.417

Table 2.12: Optical Indices for Individual Samples

Optical indices collected during the sampling day of NOM isolation, including soil leachate from active layer and permafrost layer. *SUVA values are iron corrected (Poulin et al. 2014). Standard deviation is denoted as (±) in this table. The absorbance at 254 nm and 280 nm were multiplied by dilution factor to obtain the corrected absorbance of greater than 1 A.U. Samples with N/A did not have values determined. Sample abbreviations for samples are denoted in Table 2.1 and data abbreviations are denoted in Table 1.1 and Table 1.2. TOC = Total organic carbon concentration. TDN = Total dissolved nitrogen concentration.

	pH	TOC (mg C L^{-1})	+/-	TDN (mg N L-1)	+/-	254 nm (A.U)	280 nm (A.U.)	S_R	E2:E3	BIX	FI	Freshness	HIX	$SUVA_{254}$ (L mg C^{-1} m^{-1})	$SUVA_{280}$ (L mg C^{-1} m^{-1})
GSL SUMMER	8.2	55.723	1.088	2.726	0.031	3.007	2.047	0.860	7.900	0.704	1.618	0.688	0.937	1.960*	1.924*
OCT SUMMER	8.46	36.257	0.647	0.155	0.003	2.289	1.655	0.867	5.867	0.600	1.535	0.582	0.920	2.487*	2.458*
DNL SUMMER	8.43	58.040	0.306	0.174	0.012	2.285	1.497	1.013	9.818	0.723	1.516	0.690	0.887	1.381*	1.375*
GSL WINTER	6.3	124.393	1.295	5.988	0.075	3.142	2.080	0.824	8.553	0.741	1.699	0.713	0.953	1.115*	1.101*
DNL WINTER	5.09	60.164	0.161	2.902	0.054	1.495	0.984	0.893	8.394	0.700	1.564	0.657	1.025	0.961*	0.960*
BSP	N/A	215.791	3.937	16.569	0.300	6.414	4.304	0.928	8.115	0.695	1.634	0.680	0.952	1.039*	1.020*
BSGW	6.93	N/A		N/A		0.342	0.243	0.927	6.547	0.687	1.664	0.676	0.924	N/A	N/A
GSP1	5.2	N/A		N/A		0.565	0.453	0.590	4.688	0.415	1.337	0.395	0.882	N/A	N/A
GSP2	5.15	26.080	0.802	-0.028	0.008	0.487	0.399	0.590	4.660	0.419	1.322	0.386	0.901	1.868	1.531
FTP1	8.05	2.927	0.177	0.492	0.011	0.058	0.042	0.943	5.238	0.583	1.506	0.569	0.946	1.978	1.431
FTP2	7.72	11.683	0.107	1.279	0.053	0.201	0.140	0.888	6.261	0.576	1.530	0.573	0.927	1.718	1.195
FTP3	8.3	23.650	0.300	1.868	0.042	0.539	0.372	0.913	6.178	N/A	N/A	N/A	N/A	2.279	1.571
PLFA	N/A	N/A	N/A	N/A	N/A	0.286	0.229	1.035	4.843	0.776	1.549	0.756	0.793	2.148	1.718
SRFA	N/A	N/A	N/A	N/A	N/A	0.423	0.327	0.812	4.979	0.427	1.314	0.408	0.868	4.164	3.216
GSL Average	7.250	90.058	1.192	4.357	0.053	3.075	2.063	0.842	8.227	0.723	1.659	0.700	0.945	1.538	1.513
+/-	1.344	48.557	0.146	2.306	0.031	0.095	0.023	0.025	0.462	0.026	0.057	0.017	0.011	0.598	0.582
DNL Average	6.760	59.102	0.233	1.538	0.033	1.890	1.241	0.953	9.106	0.711	1.540	0.674	0.956	1.171	1.168
+/-	2.362	1.502	0.103	1.929	0.030	0.558	0.363	0.085	1.007	0.016	0.034	0.023	0.097	0.296	0.293
GSP Average	5.175	26.080	0.802	-0.028	0.008	0.526	0.426	0.590	4.674	0.417	1.329	0.391	0.892	1.868	1.531
+/-	0.035	N/A	N/A	N/A	N/A	0.055	0.038	0.000	0.020	0.003	0.011	0.007	0.013	N/A	N/A

Table 2.13: Iron Concentration Utilized for $SUVA_{254}/SUVA_{280}$ Correction

Iron concentrations obtained from ICP-MS (Gagné, Section 3.4.3) utilized in determining to the correction factor for $SUVA_{254}/SUVA_{280}$ based on Poulin et al. (2014). Total Fe was assumed to be all Fe^{+3} due to not collected or analyzed in anoxic conditions. Correction Factor was determined by Equation 2. Abbreviations for samples are denoted in Table 2.1.

	Total Iron ppb	+/-
GSL SUMMER	502.8	2.0
OCT SUMMER	1470.2	32.5
DNL SUMMER	115.5	1.1
GSL WINTER	2964.6	16.7
DNL WINTER	1242.8	2.3
BSP	72.1	2.8
BSGW	430.0	3.9
GSP1	187.9	4.1
GSP2	112.0	2.4
FTP1	13.1	2.0
FTP2	347.7	2.5
FTP3	376.8	3.4

Table 2.14: Statistical Results Determining for Seasonality between Samples

T-Tests were utilized to determine if the epilimnion (top) and hypolimnion (bottom) summer and winter samples were statistically different. A Welch's T-Test was completed when the variance between samples was determined to be statistically different and thus, required a Welch T-Test to be utilized are denoted with *** in the table. The darker the shading in the box (decreased p-value) the more statistically different the results. The sample amount is found within each box as (summer sample number/winter sample number). Orange gradient indicates that the average was higher in summer, while the blue gradient indicates that the average was higher in the winter. Sample abbreviations for samples are denoted in Table 2.1, data abbreviations are denoted in Table 1.1 and Table 1.2, and epilimnion (epi.), and hypolimnion (hypo.).

Summer vs. Winter T-Test Sample	S_R	E2:E3	BIX	FI	Freshness	HIX	$SUVA_{254}$	$SUVA_{280}$
GSL Epi.	10/8	10/7***	10/8***	9/8	10/8	10/8	8/8***	8/8***
GSL Hypo.	8/8	8/8	8/8	8/8	8/8	8/8	7/8***	7/8***
OCT Epi.	9/4***	9/4	9/5	7/5***	9/5	9/5	9/4	9/4
OCT Hypo.	8/4	7/4***	8/4	8/4	8/4	8/4	8/4	8/4
DNL Epi.	8/7***	8/7***	7/7	8/7	7/7	8/7	6/5	6/5
DNL Hypo.	8/5***	8/6	8/6	8/6	8/6	8/6	6/5***	6/5***
Increased in Winter (P-Value Legend)	<0.0001	<0.0010	<0.0100	<0.0500		***Welch T-Test		
Increased in Summer (P-Value Legend)	<0.0001	<0.0010	<0.0100	<0.0500		Number of samples located within cell		

Table 2.15: NOM Photolysis Rate of Absorbance Decay

Reconstituted of 10 mg C L^{-1} NOM in 18 MΩ H_2O and pH adjusted to circumneutral with the addition of chemical probes for photolysis experiments. Screening factors (SF) are included and determined from equation 4 and the absorbance rate of decay at 254 nm were determined based off of equation 3 with the units of hr^{-1} mg C^{-1} L based on pseudo-first order rate kinetics. The error associated with these values are standard deviations and represented by ± in the table. Samples without errors were not run in duplicate and an error could not be determined. Abbreviations for samples are denoted in Table 2.1.

	Unamended		Iron		Methanol		Unamended		Iron		Methanol	
	SF	+/-	SF	+/-	SF	+/-	Rate 254nm	+/-	Rate 254nm	+/-	Rate 254nm	+/-
GSL Summer	9.24E-01	5.49E-04	9.08E-01	4.10E-04	9.24E-01	2.19E-04	1.15E-03	4.01E-06	3.22E-03	4.72E-05	8.36E-04	1.50E-05
OCT Summer	8.68E-01	1.13E-06	8.42E-01	1.28E-04	8.69E-01	1.62E-04	1.93E-03	2.86E-04	1.56E-03	4.94E-05	1.18E-03	1.40E-04
DNL Summer	8.98E-01	5.15E-05	8.76E-01	8.95E-05	8.99E-01	6.25E-05	1.25E-03	6.34E-06	1.44E-03	6.86E-07	1.14E-03	3.58E-05
GSL Winter	9.23E-01	6.01E-03	8.94E-01	7.35E-03	9.24E-01	5.89E-03	1.40E-03	2.75E-04	6.54E-03	1.36E-04	1.32E-03	5.13E-05
DNL Winter	8.74E-01	4.31E-02	8.88E-01	1.88E-02	9.16E-01	1.57E-02	1.48E-03	2.43E-04	4.42E-03	9.52E-04	1.23E-03	3.92E-05
BSP	9.35E-01		9.14E-01		9.35E-01		1.68E-03		6.89E-03		1.57E-03	
BSGW	8.71E-01	1.35E-02	8.57E-01	7.31E-03	8.83E-01	3.47E-03	2.16E-03	5.11E-04	4.43E-03	8.50E-04	1.71E-03	4.00E-04
GSP1	8.84E-01		8.58E-01		8.84E-01		1.11E-03	1.20E-04	1.23E-03	6.41E-05	9.25E-04	8.88E-05
GSP2	8.82E-01		8.54E-01		8.83E-01		1.16E-03	7.54E-05	1.51E-03	8.89E-05	8.87E-04	6.54E-05
FTP1	9.42E-01		9.16E-01		9.43E-01		1.83E-03	2.94E-04	2.44E-03	2.84E-04	1.27E-03	7.87E-05
FTP2	9.04E-01		8.80E-01		9.04E-01		1.26E-03	1.05E-04	1.68E-03	1.45E-04	1.10E-03	1.21E-04
FTP3	9.15E-01		9.02E-01		9.28E-01		1.68E-03	5.97E-05	2.27E-03	1.29E-04	1.56E-03	1.06E-04
SRFA	8.70E-01		8.46E-01		8.66E-01		1.09E-03		1.77E-03		1.02E-03	
PLFA	9.07E-01		8.79E-01		9.07E-01		1.26E-03		1.53E-03		1.20E-03	

Table 2.16: Percent Difference in Unamended Photobleaching Rates

The percent difference was determined from the rates of absorbance decay determined by equation 3 based on pseudo-first order rate kinetics found in Table 2.15 for unamended photolysis rates to compare to reference material, active layer, permafrost layer, and ground water photolysis rates in order to observe similarities associated with NOM in this watershed from potential influx through soil leaching and groundwater infiltration. Abbreviations for samples are denoted in Table 2.1.

Unamended	% Difference from PLFA	% Difference from SRFA	% Difference from GSP1	% Difference from GSP2	Average Active Layer	% Difference from FTP1	% Difference from FTP2	% Difference from FTP3	Average Permafrost Layers	% Difference BSGW
GSL Summer	-8.83%	5.79%	3.61%	-0.73%	**1.44%**	-45.66%	-9.45%	-37.19%	**30.77%**	-61.22%
OCT Summer	42.33%	56.06%	54.04%	50.00%	**52.02%**	5.33%	41.73%	14.16%	**20.41%**	-11.42%
DNL Summer	-0.13%	14.47%	12.30%	7.97%	**10.14%**	-37.33%	-0.75%	-28.73%	**22.27%**	-53.23%
GSL Winter	10.58%	25.08%	22.93%	18.64%	**20.79%**	-26.89%	9.96%	-18.16%	**18.33%**	-43.13%
DNL Winter	16.36%	30.77%	28.64%	24.38%	**26.51%**	-21.17%	15.74%	-12.39%	**16.43%**	-37.57%
BSP	28.72%	42.87%	40.78%	36.61%	**38.70%**	-8.72%	28.11%	0.12%	**6.50%**	-25.36%
BSGW	53.11%	66.42%	64.47%	60.56%	**62.52%**	16.73%	52.53%	25.48%	**31.58%**	0.00%
GSP1	-12.43%	2.18%		-4.34%	**4.34%**	-49.06%	-13.05%	-40.67%	**34%**	-64.47%
GSP2	-8.10%	6.52%	4.34%		**4.34%**	-44.97%	-8.72%	-36.49%	**30%**	-60.56%
FTP1	37.20%	51.11%	49.06%	44.97%	**47.01%**		36.60%	8.84%	**22.72%**	-16.73%
FTP2	0.62%	15.22%	13.05%	8.72%	**10.89%**	-36.60%		-27.99%	**32.29%**	-52.53%
FTP3	28.60%	42.75%	40.67%	36.49%	**38.58%**	-8.84%	27.99%		**12.28%**	-25.48%

Table 2.17: Difference in Absorbance Decay Rates

The difference in unamended sample with amended sample is included with unamended versus iron and unamended versus methanol determined from comparing photolysis rates within sample type NOM found in Table 2.15 using equation 6 units of hr^{-1} mg C^{-1} L. Additionally, the percent difference was determined through the use of the same photolysis rates. Error was propagated from the standard deviation of each rate used in determining the difference and denoted as ±. Abbreviations for samples are denoted in Table 2.1.

	Plain - Iron	+/-	% Difference	Plain - Methanol	+/-	% Difference
GSL Summer	-2.07E-03	4.74E-05	94.75%	3.13E-04	1.55E-05	31.56%
OCT Summer	3.73E-04	2.90E-04	21.37%	7.52E-04	3.18E-04	48.36%
DNL Summer	-1.83E-04	6.38E-06	13.60%	1.13E-04	3.64E-05	9.44%
GSL Winter	-5.14E-03	3.06E-04	129.63%	7.47E-05	2.79E-04	5.50%
DNL Winter	-2.94E-03	9.83E-04	99.75%	2.54E-04	2.47E-04	18.76%
BSP	-5.21E-03		121.69%	1.07E-04		6.57%
BSGW	-2.27E-03	9.92E-04	68.72%	4.58E-04	6.49E-04	23.64%
GSP1	-1.23E-04	1.36E-04	10.47%	1.84E-04	1.50E-04	18.07%
GSP2	-3.49E-04	1.17E-04	26.21%	2.71E-04	9.98E-05	26.48%
FTP1	-6.07E-04	4.08E-04	28.45%	5.63E-04	3.04E-04	36.34%
FTP2	-4.13E-04	1.79E-04	28.10%	1.68E-04	1.60E-04	14.25%
FTP3	-5.92E-04	1.42E-04	30.05%	1.19E-04	1.22E-04	7.34%
SRFA	-6.84E-04		47.92%	6.52E-05		6.20%
PLFA	-2.75E-04		19.73%	5.71E-05		4.65%

Table 2.18: ^{3}NOM* Photolysis Rates

Reconstituted of 10 mg C L^{-1} NOM in 18 MΩ H_2O and pH adjusted to circumneutral with the addition of TMP were run for 4-6 hours and the rate of TMP degradation was converted to the rate of ^{3}NOM* production with equation 7, with units of min^{-1} mg C^{-1} L. Error within this table is the standard deviation of duplicate photolysis runs and denoted as ±. R^2 was determined based on the best fit line for TMP degradation plots found in Figure 2.9. Abbreviations for samples are denoted in Table 2.1.

	^{3}NOM* Rate	+/-	R^2
GSL Summer	1.98E-03	1.10E-04	9.88E-01
OCT Summer	2.15E-03	8.01E-05	9.97E-01
DNL Summer	1.75E-03	1.24E-04	9.90E-01
GSL Winter	1.84E-03	1.91E-04	9.59E-01
DNL Winter	1.45E-03	3.02E-04	8.52E-01
BSP	1.99E-03	4.32E-04	8.41E-01
BSGW	1.77E-03	2.96E-04	8.99E-01
GSP1	8.41E-04	1.30E-04	8.93E-01
GSP2	7.82E-04	4.26E-05	9.88E-01
FTP1	2.36E-03	2.15E-04	9.60E-01
FTP2	1.53E-03	2.72E-04	8.63E-01
FTP3	1.44E-03	3.10E-04	8.11E-01
SRFA	1.09E-03	9.13E-05	9.66E-01
PLFA	1.10E-03	7.31E-05	9.78E-01

Table 2.19: Percent Differences in ^{3}NOM* Rates

The percent difference was determined from the rates of ^{3}NOM* production determined by equation 7 found in Table 2.18 for TMP photolysis rates to compare to reference material, active layer, permafrost layer, and ground water photolysis rates in order to observe similarities associated with NOM in this watershed from potential influx through soil leaching and groundwater infiltration. Abbreviations for samples are denoted in Table 2.1.

^{3}NOM*	% Difference from PLFA	% Difference from SRFA	% Difference from GSP1	% Difference from GSP2	Average Active Layer	% Difference from FTP1	% Difference from FTP2	% Difference from FTP3	Permafrost Layers	% Difference BSGW
GSL Summer	57.24%	58.06%	80.89%	86.94%	**83.92%**	-17.27%	26.13%	32.03%	**25.15%**	11.68%
OCT Summer	64.58%	65.38%	87.55%	93.39%	**90.47%**	-9.21%	34.04%	39.87%	**27.71%**	19.72%
DNL Summer	45.59%	46.44%	70.20%	76.56%	**73.38%**	-29.57%	13.79%	19.78%	**21.04%**	-0.78%
GSL Winter	50.44%	51.27%	74.67%	80.90%	**77.79%**	-24.52%	18.89%	24.85%	**22.76%**	4.36%
DNL Winter	27.14%	28.02%	52.93%	59.69%	**56.31%**	-47.94%	-5.29%	0.74%	**17.99%**	-19.82%
BSP	57.53%	58.36%	81.16%	87.20%	**84.18%**	-16.95%	26.45%	32.35%	**25.25%**	12.00%
BSGW	46.33%	47.18%	70.89%	77.22%	**74.06%**	-28.80%	14.57%	20.55%	**21.31%**	0.00%
GSP1	-26.75%	-25.87%		7.34%	**7.34%**	-94.85%	-57.81%	-52.24%	**68.30%**	-70.89%
GSP2	-33.92%	-33.05%	-7.34%		**7.34%**	-100.44%	-64.47%	-59.01%	**74.64%**	-77.22%
FTP1	72.71%	73.49%	94.85%	100.44%	**97.65%**		42.92%	48.63%	**45.78%**	28.80%
FTP2	32.31%	33.18%	57.81%	64.47%	**61.14%**	-42.92%		6.03%	**24.47%**	-14.57%
FTP3	26.41%	27.29%	52.24%	59.01%	**55.63%**	-48.63%	-6.03%		**27.33%**	-20.55%

2.10. Abbreviations:

•OH	Hydroxyl Radical
^{3}NOM*	Triplet State NOM
β:α	Freshness (Equation in Table 1.2)
BIX	Biological Index (Equation in Table 1.2)
BSP	Blacksheep Pond
CPC	Caribou Poker Creek
CRAM	Carboxyl Rich Alicyclic Molecules
CRREL	Cold Regions Research and Engineering Laboratory
DNL	Doughnut Lake
E2:E3	Absorbance Ratio (Equation in Table 1.1)
Epi.	Epilimnion
FI	Fluorescence Index (Equation in Table 1.2)
FT-ICR-MS	Fourier-Transform Ion Cyclotron Resonance Mass Spectrometry
FTP	Fox Tunnel Permafrost (Sample Details Table 2.1)
GSBA	Goldstream Stream at Ballaine Road
GSGW	Goldstream Groundwater
GSL	Goldstream Lake
GSP	Goldstream Active Layer
GSSC	Goldstream Stream at Sheep Creek Road
HIX	Humification Index (Equation in Table 1.2)
Hypo.	Hypolimnion
ICP-MS	Inductively Coupled Plasma Mass Spectrometry
Iron Amended	Photolysis Samples with Iron Added
LTER	Long Term Ecological Research Facility
MDLT	Material Derived from Linear Terpenoids
Methanol Amended	Photolysis Samples with Methanol Added
Multi-CP-MAS	Multi-Cross Polarization Magic Angle Spinning (Section 1.3.7.)
NAFA	Nordic Lake Fulvic Acid
NMR	Nuclear Magnetic Resonance
NOM	Natural Organic Matter
OCC	O'Connor Creek
OCT	Octopus Lake
PENOM	Permafrost Extractable Natural Organic Matter
Plain – Iron	Plain (unamended) photolysis rates minus Iron amended rates
Plain – Methanol	Plain (unamended) photolysis rates minus Methanol amended rates
PLFA	Pony Lake Fulvic Acid
PPL	Isolation Polymer (Dittmar et al. 2008)
ROS	Reactive Oxygen Species
SF	Screening Factor (Equation 4)
SPR-W5-WATERGATE	NMR Method (Section 1.3.7.)
S_R	Spectral Ratio (Equation in Table 1.1)
SRFA	Suwannee River Fulvic Acid
$SUVA_{254}/SUVA_{280}$	Specific Ultraviolet Absorbance

TDN	Total Dissolved Nitrogen
TMP	2,4,6-Trimethylphenol
TOC	Total Organic Carbon
Unamended	Photolysis Samples with no additions added
UV-Vis	Ultraviolet-visible spectrophotometry

Chapter 3: Seasonal Geochemistry in a sub-Arctic Watershed Underlain by Discontinuous Permafrost[3]

3.1. Abstract:

Rising temperatures in high latitudes put permafrost at an increased risk of thaw. Discontinuous permafrost in the sub-Arctic are the most susceptible soils to this abrupt thaw caused by the increase in atmospheric and soil temperatures. This abrupt thaw has the potential to form thermokarst lakes, which provide an environment for plants and animals. However, thermokarst formations have the potential to leach out metals from the soil into the surface waters thus, altering the biochemistry cycle within the thermokarst lake environment. It is important to obtain a better understanding of how permafrost thaw influences these geochemical cycles through the introduction or absorption potential of various metals as permafrost leaches out various metals. This study utilized previous data of determining the percentage of frozen material under three main thermokarst lakes within the same watershed to assess how geochemical cycling may differ between the thermokarst lakes. The watershed utilized allows for the same ecosystem, weather patterns, and organic matter sources to remain as consistent between the thermokarst lakes as possible so that the fluctuations of metals during the season may be tied to the freeze and thaw cycles of the permafrost. Samples collected during the winter season was observed in order to obtain an under the ice sample analysis when the thermokarst lakes are theoretically isolated from lateral surface water flows through the active layer. This case study brought to light that the collection and analysis of optical indices and metals allows for the potential for interpretation of how much permafrost underlays the thermokarst lake.

[3] Gagné, K.R., Eckhardt, B.E., Barnes, D., Liljedahl, A., Winkel, M., Harms, T., Daanen, R., Romanovsky, V.E., Guerard, J.J. Seasonal Geochemistry in a sub-Arctic Watershed Underlain by Discontinuous Permafrost. Prepared for submission in Biogeosciences.

Additionally, higher metal concentrations were observed in the 75 – 100% frozen soil underlain thermokarst lake. These high metal concentrations have the potential to be influenced by lateral surface water flow through active layer soils from the active layer not fully freezing. This case study bridges the gap between stream geochemistry and thermokarst lake geochemistry for observing influences from permafrost degradation and allowed the ability to observe seasonal variability in trace metals through a sub-Arctic winter season.

3.2. Introduction:

Interior Alaska in the sub-Arctic region is the home to boreal forests and yedoma permafrost. This yedoma permafrost has a high ice content and is rich with sequestered carbon containing 1307 Pg carbon, >25% of that is susceptible to release into waters (Strauss et al. 2017; Walter Anthony et al. 2014; Winkel et al. 2019). This carbon concentration is observed in two different categories of permafrost, surface permafrost (0 – 3 m) and deep permafrost (> 3 m), deep permafrost is 50 – 80% ice rich and thus, has less carbon (Schädel et al. 2015). However, unlike streams, thermokarst lakes can tap into both surface and deep permafrost as the permafrost degrades and the thermokarst lake deepens, which allows for an increased carbon pool to release into the thermokarst lake water. Temperatures are increasing drastically in this region, at 0.6°C per year, which is twice as fast as the global average (Heslop et al. 2017; Stocker et al. 2013) thus, increasing the susceptibility for this ice-rich permafrost to thaw. Additionally, increased air temperature has altered the weather to increase precipitation, and this increased precipitation increases rates of permafrost thaw (Grant et al. 2017; Iijima et al. 2014; Neumann et al. 2019). When ice-rich permafrost thaws the soil collapses and forms a thermokarst (Kokelj et al. 2013), and proceeds to fill with water that can lead to substantial export of trace elements

into the watershed (Larouche et al. 2015). The formation of thermokarst lakes is a mode of abrupt thaw and, once abrupt thaw occurs in an area, the increase in flowing water will cause an increase in localized thaw and erosion (Jorgenson et al. 2006). This abrupt thaw allows for the bottom of the hypolimnion to be lined with plant material that was once the surface of the land. Thermokarst lakes have been estimated to cover 1.3×10^6 km^2 (Olefeldt et al. 2016) and are likely to drastically modify the terrain morphology, hydrology and biogeochemical processes in the localized watershed and through climate change thermokarst lake production will likely increase (Chin et al. 2016; Frey and McClelland 2009; Kokelj et al. 2013; Thienpont et al. 2013). These drastic changes include the release of gases, micronutrients, and changing hydrological flow paths that were previously frozen allowing for more leaching of metals and organic matter into the surface waters.

Many studies have observed an increase in the release of greenhouse gases such as CH_4 and CO_2 into the atmosphere from thermokarst lakes (Elder et al. 2019; Walter Anthony et al. 2018; Winkel et al. 2019). Although there has been substantial research completed on greenhouse gas emissions from thermokarst lakes, there is a lack of research conducted on geochemical cycling and micronutrient cycling within these thermokarst lakes, which may help explain their increased greenhouse gas emissions. The majority of the geochemical metal cycling research has been conducted on streams and rivers in the Arctic; Alaska (Barker et al. 2014; Kling et al. 1992; Larouche et al. 2015; Rember and Trefry 2004), Russia (Bagard et al. 2011; Holmes et al. 2000; Savenko et al. 2019), sub-Arctic streams and rivers (Giesler et al. 2014), and thermokarst lakes (Pokrovsky et al. 2018a). Limited research has been conducted on thermokarst thaw ponds and is limited to Sweden Arctic location thus far (Pokrovsky et al. 2018b). However, all of these studies have one thing in common that is limiting the potential for a holistic

understanding of geochemical cycling influenced by permafrost thaw. There is a lack of under ice, winter sampling for both sub-Arctic and Arctic research sites, some studies estimate that interpolation of winter samples is underestimated due to the low discharge of streams in winter (Holmes et al. 2000; Maclean et al. 1999; Petrone et al. 2006). Thus, it is critical to observe under the ice geochemistry cycling as it has not been focused on before and winter estimates may be off. These studies have observed increases in solutes and carbon inputs from lateral flow through active layer soils, which further increased during increased depth of active layer and during large flushing events for Al, Ba, Fe, and Mn (Barker et al. 2014), Cu, Fe, Pb, and Ba (Rember and Trefry 2004), rare earth elements, Al, and Fe (Bagard et al. 2011), Se (Pokrovsky et al. 2018a), and Ba (Savenko et al. 2019). Additionally, carbon concentrations were observed to increase with events of high discharge in the Arctic and sub-Arctic surface waters (Bagard et al. 2011; Giesler et al. 2014; Rember and Trefry 2004). These studies believe it is the hydrological connections through active layers soils increasing the concentrations of solutes within the surface waters and the water chemistry is dependent upon the source of water (Bagard et al. 2011; Barker et al. 2014; Giesler et al. 2014; Kling et al. 1992; Larouche et al. 2015; Pokrovsky et al. 2018a; Rember and Trefry 2004).

The increased conditions of permafrost degradation allow for an increase in water-rock interaction and leaching of once frozen permafrost into surface water flow (Frey et al. 2007). Carbon and nitrogen are important micronutrients in surface waters, especially in a permafrost degrading as this carbon released is highly biodegradable and susceptible to photodegradation oxidation, to what extent is still up for debate by researchers and thus, more information is crucial for multiple ecosystems and locations (Cory et al. 2014; Drake et al. 2015; Schuur et al. 2015; Wickland et al. 2007). A particular interest for this study is carbon concentrations as

carbon concentrations have been observed in Arctic rivers to have the highest concentrations globally (Dittmar and Kattner 2003; Frey and McClelland 2009) as they draw from carbon-rich soils and surface waters such as thermokarst lakes. While, nitrogen release introduces an increase in nutrients for potential microbial activity (Keuper et al. 2012) and plant growth (Chapin et al. 2005; Keuper et al. 2012). Studies have observed that carbon concentrations are expected to decline as permafrost thaws in Alaska due to adsorption to mineral soils (Carey 2003; Frey and McClelland 2009; Maclean et al. 1999; Petrone et al. 2006, 2007; Striegl et al. 2005, 2007) after an initial increase from active permafrost thaw (Striegl et al. 2007; Toohey et al. 2016). These increased carbon concentrations are due to the shallow flow paths through organic rich active-layer soils (Frey and McClelland 2009). Additionally, carbon concentrations remain high in the watershed due to limited decomposition rates associated with waterlogged soils and anoxic conditions present in this watershed (Frey and McClelland 2009), as during summer the watershed is a wetland which does not dry to completion by the time winter arrives freezing the soils, limiting the decomposition rate. Carbon and nitrogen have the potential of two sources through leaching from the pore waters of the thermokarst lakes and through surface water flow through active layers and soils.

Modeling for surface water sources in this study utilized chloride as a tracer to determine between ground and surface sourced water, as chloride is a tracer for precipitation and weathering (Lockwood et al. 1995; McNamara et al. 1997). Metal concentrations were normalized to chloride concentrations as chloride is a tracer for estimating the relative concentration of surface water to baseflow water (Barker et al. 2014). Chloride is a free ion in the environment that has a decreased chance of moving through the soil and being significantly transformed in the process (Albek 1999; Barker et al. 2014; Lockwood et al. 1995). Additionally,

organic carbon has been observed in the complexation of metals especially with Fe and Al in Arctic and sub-Arctic surface waters (Pokrovsky et al. 2018b; Pokrovsky and Schott 2002; Stolpe et al. 2013; Weyhenmeyer et al. 2014). Trace metals bind to specific functional groups of the organic matter and can be transported or transformed by organic matter complexation. Complexation of metals to organic matter can occur based on the functional group composition of the organic matter causing increases in metal transportation throughout the watershed. Thus, metals were also normalized to carbon in this study to observe trends of metals being sourced by areas of organic carbon input, such as active layer and permafrost soil leaching.

This study collected samples from three thermokarst lakes year-round at defined intervals in order to observe geochemical cycling through the summer and winter during ice on conditions. The surface waters were chosen in this study due to being confined in the same watershed, providing the same water sources, and the previous knowledge of permafrost degradation underlaying each body of water (Emond et al. 2018). The knowledge of the extent of permafrost thaw allows for this study to be a case study to observe differences in the aquatic chemistry in these bodies of water. Observations between the variability between summer months (April to September) and winter months under ice conditions (October to March) in order to observe how micronutrients (eg. Cu, Co, Fe, Mn, Mo, Ni, V, Sr), carbon, nitrogen, and other metals are affected by seasonality changes in thermokarst lakes underlain by various amounts of permafrost were made. Select stream samples were taken during periods of ice-free water, however, the permafrost degradation of the stream locations was all the same so permafrost degradation was not a driving factor for the stream geochemistry.

3.3. Methods:

3.3.1 Sampling locations:

Goldstream Valley is a 258 km^2 (Emond et al. 2018) residential watershed located in sub-Arctic Fairbanks, Alaska underlain by discontinuous permafrost with a mean annual temperature of -2.4°C and a mean annual precipitation of 274 mm (Fairbanks Int. Airport, 1981–2010, U.S. National Climatic Data Center). The watershed is covered by boreal forest vegetation of black spruce (*Picae mariana*), white spruce (*Picea glauca),* moss (*hylocomium et al.)*, alder (*Alnus viridis*), and tussock cotton grass (*Eriophorum vaginatum*), with no previous glacier coverage. The hydrology of the watershed is fed by the Alaskan White Mountain Range and empties into the Minto Flats and Tanana River.

The thermokarst lakes and streams overlay Pleistocene yedoma permafrost, which is rich in organic carbon and ice (Elder et al. 2019). These water bodies are situated in a complex quaternary deposit formed by silt and gravel deposition (Elder et al. 2019; Muhs and Budahn 2006). Samples were collected from an assortment of surface waters and well waters from March 2016 to October 2018 in an attempt to capture spring thaw, summer, fall freeze up, and winter water chemistry (Table 3.1/Figure 2.1). Each thermokarst lake had samples taken from both the hypolimnion and epilimnion, with the exception of BSP due to shallow waters. Streams samples could not be obtained due to thick ice pack and artesian conditions may occur increasing the chances of flooding. As artesian conditions are commonly observed in watersheds underlain with ice-rich permafrost, as the permafrost forms an impenetrable barrier to downward flow (Callegary et al. 2013; Yoshikawa and Hinzman 2003), which can increase the pressure within the stream system. Additionally, accessibility restraints to residential property caused some sampling months to be missed for select locations.

Permafrost degradation was known based on an airborne electromagnetic (AEM) survey collected by R. Daanen and A. Emond from the Alaska Division of Geological & Geophysical Surveys (Emond et al. 2018). AEM collected resistivity data of the watershed and R. Daanen and A. Emond interpreted it with the assistance of well log data of the area. The watershed was first segregated into different geophysical regions; silt, gravel, fractured bedrock, and bedrock. These geophysical regions were observed below 2 km elevation as the dry, unfrozen material observed similar resistivities to frozen material and was only known to be in south facing slopes. Once separated into the geophysical regions resistivities were separated to determine a percentage of frozen material as 100%, 75%, 50%, 25%, and 0% (Table 3.1). The percentage was based off of the surface water location and was for deep cross sections under the waters, thus lateral flow may still be possible through shallow aquifers or surface water runoff. The characterization of the hydrology is complicated in discontinuous permafrost due to the potential of different flow paths (macropores, inter-hummock regions, and water tracks) (Carey and Woo 2000; O'Donnell and Jones 2006). The authors acknowledge that the streams meander through areas of various permafrost degradation percentages however, the percentage frozen was determined at the sampling location. All streams are for the majority underlain by permafrost with areas of talik formation.

At the time of collection a YSI hydrolab probe was utilized during sampling days where warmer temperatures allowed for probe usage and the following was obtain: pH, temperature, dissolved oxygen, and conductivity (Table 3.2). Samples were collected in 250 mL brown acid washed polyethylene bottles and placed in a cooler until transported to the laboratory. Hypolimnion thermokarst lake samples were collected using a Van Dorn water sampler sent to the bottom of the thermokarst lake and rinsed out with hypolimnion water before collection of

the sample for analysis. Upon return to the laboratory, samples were filtered through an 18.2 MΩ water rinsed 0.45 μm syringe filter allocated to the proper sample receptacle. Once filtered UV-Vis and fluorescence scans were obtained with the necessary dilution to ensure the absorbance did not exceed 1.0 A.U. at 254nm before fluorescence, this data was utilized in Gagné, Section 2.4.2. Total organic carbon samples were placed in glass vials and acidified using HCl for storage in the dark at 4°C. Samples for cation and anion analysis were placed into plastic bottles and placed into a -18°C freezer. Trace metal analysis samples were placed into a brown plastic bottle and were diluted to 2% HNO_3 solution. Size exclusion samples were diluted to a solution of 0.1 M NaCl buffered by 1 mM Na_2HPO_4 and 1 mM KH_2PO_4 in glass vials and placed in the dark at 4°C.

3.3.2. Instrumentation:

Total non-purgeable organic carbon and total dissolved nitrogen analysis were run on a Shimadzu TOC-L CPH (Shimadzu Scientific Instruments, LOQ = 0.1 mg C L^{-1}, LOQ = 0.05 mg N L^{-1}) using non-dispersive, infrared gas analysis following combustion organic carbon content of samples.

Ion chromatography anions was determined using two models of Thermo Fischer Dionex ion chromatography systems. A Dionex ICS 5100 equipped with an AG18 2mm diameter guard column and AS18 2mm diameter column and a Dionex ICS 2000 equipped with Metpac, AG22 fast 2mm diameter guard column, AS22 fast 2mm diameter column, with an eluent of 4.5mM Na carbonate + 1.4 mM Na bicarbonate with an isocratic method at 0.30 ml min^{-1}. Chloride and sulfate were the only anions quantitatively observed, due to high carbonate concentrations

obscuring the anion spectra. Carbonate is a known issue of Alaskan watersheds with variable permafrost extent (Frey and McClelland 2009; Keller et al. 2007).

Select fresh water samples were analyzed for size fraction analysis of the NOM fraction using a Postnova AF2000-FFF (Postnova Analytics, Landsberf, Germany) coupled to a UV-Vis diode array detector (UV-DAD; Shimadzu SPD-M20A) prior to ICP-MS analysis. Samples were simultaneously collected using a PostNova fraction collector in acid washed metal free 13 x 100 mm polystyrene test tubes. The FFF channel was equipped with a 500 μm spacer and a 300 Da nominal cut-off polyethersulfone (PES) membrane using 5mM ammonium acetate mobile phase, while the UV-DAD detector was set to a wavelength of 254 nm and 280 nm. Two separate injections were completed through injecting 400 μL of 0.45 μm filtered samples onto the FFF membrane in order to get adequate sample amounts for fractions. Fractions were then collected during the duration of time NOM was observed through the UV-DAD at a minute a piece for each tube, all tubes that were observed in collecting through the UV-DAD detector were compiled and acidified to a 2% HNO_3 solution and run via an Agilent 7500ce (Agilent Technologies, Santa Clara, CA) inductively coupled plasma-mass spectrometer (ICP-MS) followed EPA method 300.8 for the following trace metals; Li, Na, Mg, Al, K, Ca, Ti, V, Cr, Mn, Fe, Co, Ni, Cu, Zn, As, Se, St, Mo, Ag, Cd, Sb, Ba, Pb, Bi, Th, and U.

All instrumentation techniques utilized quality control samples and blank checks every 10 – 15 samples with an external calibration curves to obtain the most reliable data. ICP-MS analysis utilized an internal standard throughout the run using the following metals; Ge, Y, Sc, Rh, and Ir. Additionally, the ICP-MS ran reference standards (SLRS-5 and NIST 1640a) to ensure proper tuning of the instrument along with the quality control samples run throughout.

Determination of molecular size of the natural organic matter mimicked McAdams et al. (2017). Duplicate injections were made on an Agilent 1100 Series reverse-phase high pressure liquid chromatography (Agilent Technologies, Santa Clara, CA) equipped with a Waters Protein-Pak^{TM} 125Å, 7.8 x 300 mm column (Waters Corporation, Milford, MA). Mobile phase was 0.1 M NaCl purchased from Alfa Aesar (Massachusetts, USA), buffered by 1 mM Na_2HPO_4 from EMD Chemical Inc. (Georgia, USA) and 1 mM KH_2PO_4 purchased from Alfa Aesar (Massachusetts, USA). Calibration curve was obtained by running size exclusion chromatography standards purchased from PSS Polymer (Amherst, MA); 208 Da (BatchNo: pssp1b), 1,100 Da (BatchNo: pss130504-2), 3,610 Da (BatchNo: pss200504), 4,230 Da (BatchNo: pss21125-2), 6,520 Da (BatchNo: pss8124-3), 10,600 Da (BatchNo: pss17042), and 2,070,000 Da (BatchNo: pss310511). Additionally, acetone, PLFA, and SRFA were run in conjunction to natural samples as quality controls. All samples were pumped at a 1.0 mL^{-1} flow rate over 15 minutes.

3.3.3. Statistical Approach:

Three principal component analyses (PCA) were utilized to determine how samples varied and correlated with each other. PCA was run using JMP Pro 13 Version 13.2 (JMP; Cary, NC) after z-score normalization of sample data. A z-score normalizes samples to a standard bell curve and provides a number ranging from -3 to +3 based off of how close to the standard deviation the original value was (Equation 1). The use of a z-score ensures that the PCA was not skewed by large concentrations such as Fe and Na.

$$z = \frac{x - \mu}{\sigma}$$

Equation 1: Determination of a z-score (z) with the use of the sample value (x), average (μ), and standard deviation (σ).

Once the z-scores were determined for the sample values three PCAs were run utilizing various data analysis to determine how they may correlate with each other. These three PCAs are denoted as O, M, and OM observe different data analyses. The O PCA utilizes the optical indices along with molecular weight, carbon concentration, and nitrogen values (Table 3.3). The M PCA included trace metal, carbon, nitrogen, and chloride values, while OM PCA included all values from O and M. The use of PCA was to determine correlations between the following; water type, years, monthly seasonality, epilimnion and hypolimnion, permafrost degradation, and streams.

Statistics with the exception of PCA analysis was conducted using Prism8 for macOS Version 8.1.2. (GraphPad; San Diego, CA). Outliers from the three-year study for each sample was determined using the ROUTs outlier test with a threshold of 1% for the false discovery rate using a Gaussian distribution. The ROUTs outlier test was conducted on the concentration or ratio from each individual sampling location and season, for example GSL epilimnion winter and summer were treated separately for outliers. All unpaired t-tests were conducted using Prism8 for macOS Version 8.1.2. T-test determined if hypolimnion and epilimnion samples were statistically different with p-value <0.05. T-tests were conducted on the following data sets to compare specific samples to determine differences in epilimnion and hypolimnion as well as summer versus winter; ICP-MS metals; carbon, nitrogen, metals normalized with chloride, and metals normalized with carbon. Overall metal normalized to carbon and chloride t-test was conducted to determine differences between summer and winter. Additionally, a T-Test was conduct to determine variability in trace metal concentrations between sampling years. Further, ordinary one-way ANOVA tests were completed to compare the three major thermokarst lakes of DNL, OCT, and GSL and the three streams on the same data set treatments as discussed

above. ANOVA's were utilized to determine statistically significant differences using Prism8 for macOS Version 8.1.2. with a p-value < 0.05, between different levels of permafrost degradation. Simultaneously, all T-tests and ANOVAs were analyzed to determine whether the standard deviation variance between samples were different (p-value <0.05) and if a Welchs version of T-test or ANOVA was statistically necessary. Variance was determined by Brown-Forsythe test for ANOVA statistics. Those samples are marked with an asterisk in their respective tables.

3.4. Results:

Whole water samples were obtained in 2016, 2017, and 2018. These three years varied in temperature, rainfall, and snowfall. Both rainfall (Figure 3.1) and snowfall (Figure 3.2) increased within this three-year with 2016 having the least amount of rainfall and snowfall. The winter of 2015 – 2016 had warmer air temperatures (Figure 3.3), which also caused an increase in soil temperatures during the summer months (Figure 3.4).

3.4.1. Principal Component Analysis:

The eigenvectors associated with the principal components for the three PCA models described a varying amount of the sample set (Table 3.4). PCA O top four principal components represented 61.5% with principal components 1 through 12 being classified as significant through the Barlett test (Figure 3.5). PCA M had the largest portion of the sample set of which it described with the top four principal components representing 63.4% (Figure 3.6). While PCA OM only represented 51.1% with the first four principal components (Figure 3.7). Both M and OM principal components 1 through 22 were determined to be significant through the Barlett test.

Water type of stream water, thermokarst lake water, and well waters were separated through PCA correlations in the O PCA model (Figure 3.8). This was showcased by well waters separating completely from the surface waters and thermokarst lake and stream waters clustered nearby but had minimal overlapping. This lack of overlapping was most prominent in PCA O. Due to separation of water type, PCA analysis of epilimnion versus hypolimnion was conducted to observe if there was a change in water chemistry within the thermokarsts. All PCA models showcased that the epilimnion and hypolimnion were indistinguishable in all PCA models (Figure 3.9). Additionally, observation of stream correlation on all three PCA models found that OCC, GSBA, and GSSC all clustered together as streams, while they separated when compared to thermokarst lake waters (Figure 3.10).

The sampling campaign was conducted in 2016, 2017, and 2018. These years saw the most separation through PCA correlation from the analysis of PCA M (Figure 3.11). Ground water was included in the PCA analysis; however the well samples were removed after analysis to only depict surface waters on the yearly PCA, due in part by the observations made during water type results. The analysis of all three PCA model outputs provided no indication of seasonality as monthly samples all overlapped in the quadrants, along with summer and winter samples (Figure 3.12).

Permafrost degradation is a key component of this watershed case study and thus, PCA models were observed through comparing permafrost degradation. During this observation PCA M and OM were able to decipher and separate out each thermokarst lake with various levels of permafrost degradation into individual clusters of correlation (Figure 3.13). To verify this correlation BSP samples, a 100% closed thermokarst lake, was introduced and cluster with GSL, the main 75 – 100% closed thermokarst lake.

3.4.2. Overall Metal Composition:

Trace metal analysis conducted through the use of an Agilent 7500 CE ICP-MS collected metal concentrations for 27 metals over three years of sampling. These metals were broken up into groups based on concentration for an overall metal composition report: > 1000 ppb, 100 – 1000 ppb, 10 – 100 ppb, 1 – 10 ppb, and < 1 ppb. The averages of each sample location were obtained for summer and for winter and can be observed in more detail in Table 3.5 to Table 3.7. Thermokarst lakes and streams had different metals in the classification bins but the majority of the trace metals fell below 1 ppb in concentration. Sodium, Mg, K, Ca, and Fe had the largest concentrations of > 1000 ppb in most cases. While the majority of the metals fell below 1 ppb which included: Co, Cu, Se, Mo, Ag, Cd, Sb, Pb, Bi, and U.

Streams varied on whether the concentration of the metal was less than or greater than the thermokarst lake concentrations. The same concentrations ranges were observed in the stream averages (Table 3.8). Sodium, Mg, K, and Ca had the highest concentration in streams as well with > 1000 ppb over the three years. Meanwhile, Fe concentrations were decreased in the streams at an average of 100 – 1000 ppb alongside Mn and Sr. The majority of the trace metals in streams fell <10 ppb: Li, Ti, V, Ni, Cu, Cr, Zn, As, Se, Mo, Co, Ag, Cd, Sb, Pb, Bi, and U.

3.4.3. Major Metals Composition:

The major metal cation concentrations were classified as those that exceeded 1000 ppb in the surface water sample; Na, Mg, K, Ca, and Fe. Winter was determined to have statistically higher concentrations in select thermokarst lakes within the epilimnion and hypolimnion samples. The epilimnion and hypolimnion were found to be statistically different in major metal concentrations only for GSL (Table 3.9). When it came to seasonal variability all major metals

were observed to have statistically significant increase in concentrations in the majority of samples. Sodium was deemed to have no statistical increase in GSL hypolimnion, while Mg and Ca saw no statistical increase in GSL hypolimnion and OCT epilimnion. Potassium saw no statistical increases in GSL hypolimnion, OCT epilimnion, or DNL epilimnion, and Fe saw no statistical increases in GSL hypolimnion and all samples collected from OCT (Table 3.10).

The overall averages of the three thermokarst lakes observed Na, Mg, K, and Ca highest in GSL thermokarst lake epilimnion and hypolimnion and lowest in OCT epilimnion and hypolimnion, with the exception of Mg concentration in the hypolimnion was observed the lowest in DNL (Tables 3.5/Table 3.6). Meanwhile, Fe was observed the highest in OCT epilimnion and hypolimnion and lowest in DNL epilimnion and hypolimnion.

3.4.4. Statistical Results:

3.4.4.1. Trace Metal Analysis:

3.4.4.1.1 Inter-Annual Variability:

The following metals were shown to be statistically different between the three years through an ANOVA test with or without Welch correction: Ti, Cr, Se 78, Se 82, Ag, Cd, Sb, Bi and U (Table 3.11). With these metals further statistical analysis was conducted to determine which year or years were different from each other using a t-test between 2016 and 2017, 2017 and 2018, and 2016 and 2018. The year of 2016 was observed to be statistically different due to an increase in average concentration for Ag, while Cd and Bi had statistically lower average concentrations as results from the two T-tests 2016 v. 2017 and 2016 v. 2018 observed statistical differences. Meanwhile, Se 82 and Sb had an increased concentration in 2017 and Se 78 had an increased concentration while U had a decreased concentration different in 2018. However, Ti

and Cr only had one t-test that showed a statistical difference and thus, the year difference could not be determined.

3.4.4.1.2. Effect of Thermokarst Lake Stratification:

The depths of the thermokarst lakes have a maximum depth of 5 m with the ability to turnover in summer and winter. The comparison of metal concentrations was observed through t-test to determine if the epilimnion and hypolimnion were statistically different or the same. A p-value of < 0.05 determines the epilimnion and hypolimnion metal concentrations were different over the three-year span. A select few metals were statistically different between the epilimnion and hypolimnion and varied between thermokarst lake (Table 3.9). GSL epilimnion and hypolimnion were different in Na, Mg, K, Ca, Cr, Fe, Ni, Cu, Sr, and Ba. Meanwhile, DNL only varied with V and As concentrations and OCT only varied with Al and Co. There are no overlapping metals indicating no net cause for certain metals to be statistically different between the epilimnion and hypolimnion.

GSL and BSP are two closed thermokarst lakes with a permafrost degradation of 75 – 100% frozen. Due to this similarity GSL epilimnion and BSP were only statistically different with Fe concentration (Table 3.9).

3.4.4.1.3. Intra-Annual Variability:

During the observation of metal concentrations over time patterns can be discerned between summer and winter. The metals increase or decrease during certain months and seasons (Figure 3.14). Winter months were classified as months with ice coverage on the thermokarst lakes from October to March, streams ice over slower. Winter months also correlated with

average daily temperatures for sampling days to be below 0°C. Freeze-up and freshet were excluded from determining the seasonal difference due to the lack of samples obtained during those times would not allow for a statistical significance. A statistical difference between summer and winter months were determined using a t-test with a p-value of < 0.05. The epilimnion and hypolimnion of samples were kept separate to determine seasonality to ensure observing total concentrations hides seasonality variability do to turnover in the thermokarst lakes (Table 3.10). GSL hypolimnion appeared to be an exception to seasonality differences as the samples only had two metals in which showed statistical differences between summer and winter: V and Bi. Sodium was seasonally statistically different in all sampling locations with the exception of GSL hypolimnion. All other metals with seasonal variability had at least two sampling locations that were not statistically different. GSL hypolimnion and OCT epilimnion were not statistically different for the following metals; Mg, Ca, Cr, Mn, and Sr. While V was statistically different with all samples except DNL epilimnion and hypolimnion.

The following metals were observed to have seasonal variability within 50% of the thermokarst lake samples with varying samples; K, Ti, Fe, Co, As, and Ba (Table 3.10). Bismuth only saw seasonal variability with GSL epilimnion and hypolimnion, while U saw seasonal variability in GSL and DNL epilimnions. Nickel and Cu observed statistical difference in season for GSL epilimnion only, while Ag only observed statistical difference in DNL epilimnion. All but one metal showed an increase in concentration during summer when statistically different between the seasons. The increase was within the mean of the metal concentration, some extremes may overlap between seasons (Figure 3.14C/D). Copper was the only metal to have an increased concentration in summer, which was only statistically variable in GSL epilimnion (Figure 3.14B/D). Metals not observed to have a difference in concentration between seasons are

considered to be steady over the year. Lack of samples obtained in streams only allowed for the following statistical observations in streams; GSBA was the only stream with greater then 3 samples collected in winter time as GSBA remains ice free longer. All metal concentrations were consistent between summer and winter collects for location and metals in samples with an $n > 3$ (Table 3.12).

3.4.4.1.4. Effect of Permafrost Extent:

The determination of metal concentration variability between thermokarst lake based on permafrost degradation was observed using an ANOVA test between the thermokarst lakes epilimnion and hypolimnion. Data utilized in this statistical test was between overall metal concentrations and not based off of season and the outliers were previously removed during the statistical analysis of seasonal variability above. A large array of metal concentrations were determined to be statistically different between the thermokarst lakes in both epilimnion and hypolimnion; Na, Mg, K, Ca, Ti, V, Cr, Fe, Co, Ni, Cu, As, Sr, Mo, Sb, Ba, and U (Table 3.5/Table 3.6). Additionally, Mn was also statistically different within the hypolimnion of the thermokarst lakes (Table 3.5). The following metals were considered not statistically different in either the epilimnion or the hypolimnion: Zn, Ag, Cd, Pb, and Bi (Table 3.5/Table 3.6). Meanwhile, streams observed only statistical differences in six metals; Mg, K, Fe, Sr, Mo, and Ba (Table 3.8).

3.4.4.2. Chloride Analysis:

3.4.4.2.1. Correlation of Metals to Chloride Concentrations:

Observations of chloride concentrations with relation to other metal concentrations utilized Pearson correlations to observe statistically significant linear trends. There were correlations, r values nearing 1 and -1 for both Pearson correlation statistics. With the highest correlation observed with Li to Cl providing a strong negative linear correlation. Summer had the most correlations with chloride and various metals: Na, Mg, Ca, Cr, Ni, Se 78, Se 82, Sr, and Ba all had Spearman r-values greater than 0.5 (Figure 3.15). Again, summer samples had the highest correlation in comparison to winter. The correlation between metals when a strong correlation was observed the majority were positive relationships with the exception of Li (Figure 3.16). The strongest relationship observed was between Li and Ca at a Pearson value of 0.979907.

3.4.4.2.2. Metal to Chloride Ratio Intra-Annual Variability:

Normalizing to chloride decreased the number of total samples as some samples lacked quantifiable chloride or quantifiable metal concentrations, original sample numbers found in Table 3.10. Table 3.13 represents which samples had a statistical difference in seasonal concentrations of metal to chloride ratios as well as the sample number associated with the statistical observations. Care should be taken in interpreting any locations with less than or equal to 3 sample points (italicized in table). Normalizing to chloride limited the metals that showed seasonality trends, all of which were higher ratios in wintertime (Table 3.13). Thermokarst lake OCT lost the ability to determine seasonality as winter ratio samples decreased to three or less samples. Additionally, the standard deviation between summer and winter for most ratios were significantly different and thus, WELCH's t-tests were required to determine significant

difference between sample sets. The use of WELCH's t-test limited the number of ratios with significant seasonality differences in select surface water locations to Li, Mg, Al, Co, As, Mo, Cd, Sb, Pb, and U in GSL hypolimnion and Se for the GSL epilimnion. The epilimnion of OCT was the only surface water obtained from OCT that showed seasonal variability with metals specifically Pb. DNL saw seasonal variability in the epilimnion for Ca, Mn, Fe, Co, Sr, Ag, and Ba, while the hypolimnion observed seasonal variability in Mg, Ti, Mn, and Ba. Observing chloride ratios limited the metals that could be caused from the influence of permafrost thaw based off of the results from the ANOVA.

When streams and thermokarst lake water samples were observed together as an overall chloride normalized metal ratio values were observed to have increased in winter for Na, Cr, and Se 82 (Table 3.14). Meanwhile, summer had increased ratios with Li, Cu, Mo, Cd, Sb, and Pb. While observing the metal – chloride relationship graphs (Figure 3.17) there appeared to be tighter clustering within one season compared to another. In order to determine the variability and thus, the clustering within the seasons the standard deviations were determined for each metal – chloride relationship (Table 3.15). The majority of the metals analyzed in this study had a decrease in variability within winter sample collection for chloride normalized ratios. There was a decrease in variability observed in N, Li, Mg, Al, K, Ca, Ti, Na, Mn, Co, Ni, Cu, Zn, Sr, Mo, Ag, Cd, Sb, Ba, Pb, Bi, and U in winter.

3.4.4.2.3. Chloride Ratio Effect of Permafrost Extent:

An ANOVA statistical test revealed the epilimnion to have statistical differences with the following metals; Al, Ti, V, Fe, Co, and As (Table 3.16). OCT consistently had the highest metal – chloride ratio value while DNL and GSL shared equally the lowest ratio with DNL having the

lowest value for Al, V, and Co. The hypolimnion observed a different story for determining differences between thermokarst lakes based on permafrost degradation with Al, K, Ti, V, Cr, Mn, Fe, Co, Cu, As, Mo, and Ba chloride ratios being statistically different (Table 3.17). Again, OCT had the highest ratio for all metal – chloride. GSL and OCT were lowest depending upon the metal DNL had the lowest ratio for the following metals; Cr, Mn, Fe, Co, and Mo. Unlike with the epilimnion Al and V had the lowest ratio values in GSL instead of DNL. When it came to streams only Mo and Ba had statistical difference at the three stream locations, which is consistent with the fact that the stream locations were all underlain with similar permafrost degradation and all converge at GSSC location (Table 3.18). Overall, all metal – chloride ratios that were observed to have statistical difference among the surface water locations were also statistically different without the normalization process (Table 3.5/Table 3.6).

3.4.4.3. Nitrogen Analysis:

Seasonality for the overall nitrogen concentrations for winter and summer from all samples combined observed statistical difference with decreased variability (Table 3.19). Meanwhile, individual surface water locations observed that nitrogen concentrations remained steady year-round (Table 3.20).

3.4.4.4. Carbon Analysis:

Seasonality for the overall carbon concentrations for winter and summer from all samples combined observed statistical differences with an overall decrease in variability in winter (Table 3.19). An overall average of carbon and nitrogen concentration had decreased variability in summer. Meanwhile, individual surface water locations observed statistical differences only with

carbon concentrations in thermokarst lake epilimnion with increased concentrations in wintertime, while nitrogen concentrations remained steady year-round (Table 3.20). Additionally, carbon concentrations decreased in variability and increased in concentration during the winter. Carbon only had a statistical difference between epilimnion and hypolimnion concentrations for GSL (Table 3.21).

During the observation of how permafrost can influence the carbon and nitrogen concentrations of surface water ANOVAs were conducted on the epilimnion and hypolimnion. Carbon concentrations were statistical different between the thermokarst lake epilimnions and thermokarst lake hypolimnions. The highest concentration of carbon for both the epilimnion and hypolimnion was observed in GSL, while the lowest concentrations were observed in OCT (Table 3.22). Streams alternatively had no statistical differences in carbon concentrations, however there was a statistical difference in nitrogen concentrations (Table 3.23). Stream nitrogen was also statistically different, with a high concentration in OCC.

3.4.4.4.1. Correlation of Metals to Carbon Concentrations:

Linear correlations of metal – carbon relationship observed V, Fe, Zn, As, Cd, and Bi to not have any linear relationship during summer or winter (Table 3.24). When these linear regressions were observed using statistical analysis a p-value <0.05 indicated the slope of the graph was significantly different from zero, however, not all of these linear regressions had high R^2 values. Table 3.24 showcases all of the metals that showed trended significantly different from zero and R^2 values of greater than 0.8, between 0.5 and 0.8, and less than 0.5. The only metal that had an R^2 greater than 0.8 was Na in summer and over all of the samples. This large R^2 indicates that Na is positively correlated with carbon. The following metals were observed to

have positive slopes associated with carbon and had an R^2 between 0.5 and 0.8 for winter, summer, and all samples; Mg, Ca, Ni, Se82, and Sr. Due to the majority of samples being collected in summer time, at almost 50% more, the all year's linear regressions mimic summer statistics. There are further metals that have statistical linear regressions however, their R^2 are not great enough to be considered a linear regression. Additionally, there are some negative linear correlations as well with R^2 values less than 0.5 for Cu, Mo, and Al. These linear results were verified by Pearson correlation where the majority of samples who saw minimal linear trends were correlated negatively to carbon (Figure 3.18).

The analysis of metal to metal correlation revealed a positive correlation between Fe and As (Figure 3.16). The highest total iron concentration was observed in GSL hypolimnion during the May 2018 sampling campaign at 4339.7 ppb, however only 3.7% of the iron was complexed to the organic matter (Table 3.25). Meanwhile, the highest complexation percentage observed for iron was observed in a stream, OCC, at 55.7% with only a total Fe concentration of 906.5 ppb.

3.4.4.4.2 Metal to Carbon Ratio Intra-Annual Variability:

Similarly to just the metal concentrations specific metals thermokarst lakes saw statistical differences between the epilimnion and hypolimnion (Table 3.26). GSL observed statistical differences with Mn and Fe, OCT observed statistical differences with Al, Mn, Co, and Ba, while DNL observed differences with V and As. For seasonality, OCT hypolimnion observed the most seasonal variability with winter having an increased metal – carbon ratio for the following metal relationships; Na, Mg, K, Ca, Ti, V, Cr, Mn, Fe, As, and Sr (Table 3.27). Meanwhile, OCT epilimnion had no seasonal variability for the carbon-metal ratios, GSL hypolimnion only observed a statistical increase in ratio for Ag. GSL epilimnion was the second sampling location

to have the most statistical seasonal variability with the following metal – carbon ratios observing an increase in winter; Mg, V, Cr, Mn, and Fe, while Mo and Cl observed an increase in ratio during the summer samples. DNL epilimnion and hypolimnion observed seasonal differences with an increase in wintertime for Fe and Ba, while epilimnion saw differences in Mg, Mn, and U as well. DNL hypolimnion saw statistical differences in Na, Ca, and Cr.

In order to determine if metal – carbon ratios are controlled by the permafrost degradation ANOVAs were conducted for all thermokarst lake epilimnion and hypolimnion to observe whether the metal – carbon ratios were statistically different between thermokarst lakes. OCT had the highest ratio for eight metal – carbon ratios while DNL had the lowest ratio for the following ratios; Al, Ti, V, Cr, Fe, Co, As, and Ba (Table 3.28). Secondly, GSL had the highest for seven metals but the lowest flipped between OCT and DNL. GSL had the highest ratio and OCT had the lowest ratio for the following; Cl, Na, Mg, Se 82, and U; while DNL had the lowest ratio for Ni and Mo. Finally, DNL had the highest ratio when GSL had the lowest for Ag. Meanwhile, the hypolimnion had more statistical differences between thermokarst lake based on metal – carbon ratio with the addition of 5 metals showing statistical differences between thermokarst lakes (Table 3.29). The most prominent highest ratio and lowest ratio group were observed with 8 metals with having OCT highest and GSL lowest, the metals with these ratios included; Ti, V, Cr, Mn, Fe, Co, Sr, and Mo. OCT remained the highest ratio but switched to DNL having the lowest ratio for Li, Al., K, Cu, As, and Ba. GSL remained the highest ratio for Na, Ni, U, and Cl, however the lowest ratio switched from OCT to DNL and vice versa. Sodium, Ni, and U had the highest ratio in GSL hypolimnion while the lowest ration in OCT hypolimnion, meanwhile Cl had the lowest ratio with DNL hypolimnion. Finally, GSL

hypolimnion had the lowest ratio for Se 82, which was observed in DNL hypolimnion with the highest ratio.

When comparing the metal – carbon ratio statistical differences between thermokarst lakes it is important to observe how the normalization changed the statistical differences for the metals without normalization. When comparing the epilimnion statistical differences of plain metals compared to carbon normalized similar patterns immerged of high to low comparisons. The following metals remained in the same groups of GSL high and OCT low; Na, Mg, K, and U, GSL high and DNL low; Ni and Mo, OCT high and DNL low; Al, V, Fe, and As. The following metals were statistically different between thermokarst lakes for plain metal concentrations and carbon normalized however the order of thermokarst lake values were different as plain concentrations observed Ti, Cr, Co, and Ba as highest in GSL and lowest in DNL. Carbon normalized introduced a statistical difference for Se 82 but removed statistical variance for the following metals; K, Ca, Sr, Sb, Se 78, and Cu

As for the similarity between the hypolimnion and epilimnion, thermokarst lake variability decreased after carbon normalization. However, the hypolimnion had decreased metal concentrations that continued with similar results as unnormalized metal concentrations for example when GSL was high and OCT was low only Na, Ni, and U remained that way for both true concentration and normalized ratio. Another example in this was when OCT was high and DNL was low only Al and As remained in this category. There were many overlapping metals with statistical differences between thermokarst lakes and only 4 metals that lost their variability between thermokarst lakes; Ca, Sb, Mg, and Se 78. The following metals had statistical difference but the pattern of high to low values were different; K, Se 82, and Sr were high in GSL and low in OCT, while; Ti, Cr, Mn, Co, Cu, Mo, and Ba were high in GSL and low in DNL

for metal concentration averages. Iron and V were the last two metals that continued to have statistical variability between thermokarst lake but switched to high values in OCT and low values in DNL.

Meanwhile, when observing metal – carbon relationships a seasonal clustering was not observed similar to the metal – chloride relationship discussed earlier. When all summer and winter carbon normalized ratios were statistically observed only Li, Ni, Se 82, Mo, and Pb were deemed statistically different between the two seasons with a p-value > 0.0500 through a t-test. All carbon normalized ratios in this case were higher in summer than winter with the exception of Se 82 (Table 3.31). These differences were also observed with the chloride normalized values with the exception of Ni (Table 3.14). Additionally, the following metals had a decrease in variability when normalized to carbon during the summer; Li, Ni, Zn, Mo, Ag, Pb, Bi, and Cl (Table 3.32). All other metals observed saw a decrease in variability during the winter months. Carbon concentrations in ground water is limited with only one well in the watershed exceeding 10 mg C L^{-1}.

3.5. Discussion:

3.5.1. Principal Component Analysis Discussion:

PCA modeling was utilized to observed correlation between samples through three models; O (optical indices only), M (trace metals only), and OM (all analyses included). Through this modeling water types were distinguishable through O and OM, indicating that the optical indices were important to the water chemistry and unique between wells, streams, and thermokarst lakes (Figure 3.8). This unique behavior was most prevalent in well samples, as the PCA models showed a complete separation in correlation, showcasing the difference in water

chemistry of ground water to surface water (Katz et al. 1998). Even though water types were distinct by the use of PCA models the difference between epilimnion and hypolimnion, within and between thermokarst lakes, as well as between stream water sampling locations were non-existent through PCA analysis (Figure 3.9/Figure 3.10). Thus, thermokarst lakes do not possess unique waters within the sampling water body, potentially due to the movement and flow within the thermokarst lakes during summer and fall turn over mixing the epilimnion and hypolimnion waters. Streams sampled in this study observed no differences within the PCA models, this could be due to the lack of stream variability in sampling locations as the surface hydrology goes through the same ecosystem and the two stream locations of GSBA and OCC converge together prior to sampling location GSSC. Additionally, this verifies the ANOVA statistics that metals were not statistically different between stream samples (Table 3.8). Thus, the hydrology of the watershed provides streams with the same water sources through surface flow, since the stream is for the majority underlain by permafrost, limiting the influx from groundwater.

As discussed previously, the sampling years were different in temperature and precipitation amounts in the form of both snow and rain (Figures 3.1 – 3.4). Due to these differences the PCA M model was able to distinguish between sampling years (Figure 3.11). Additionally, there was no seasonality determined through the use of PCA models (Figure 3.12). This lack of seasonality could be caused by the inability to collect the same magnitude of samples collected in summer as well as, streams not having winter samples under the ice affecting the results. Thus, these observed differences between years was not caused by seasonality differences. Based on PCA M being the only model to observe clear distinctions between the years through correlation optical indices were determined to have an increased stability between the years. While metals were affected by changes in temperatures, which

includes increases in soil temperatures and permafrost thaw, as well as increases in precipitation increasing surface flow hydrology.

Samples with varying amounts of permafrost degradation observed different clustering behavior with the OM and M PCAs, with the most prevalent separation occurring within the OM PCA (Figure 3.13). Thus, the combination of optical indices and metals provided the best ability to observe permafrost degradation when placed on this specific PCA model. Optical indices alone cannot determine permafrost degradation however, these indices exemplify the ability with the conjunction of metals data, as the clustering behavior of samples were more condensed in PCA OM compared to PCA M. This find would allow for thermokarst lake samples with unknown permafrost degradation in this area or potentially boreal, sub-Arctic watersheds could be analyzed using this PCA in order to determine a potential permafrost degradation beneath the thermokarst lake with scientific statistics to back up that assumption.

3.5.2. Major Metals Composition Discussion:

Literature has observed the major metals of Ca, Mg, K, and Na as having increased concentrations with increased permafrost degradation (Frey and McClelland 2009; Keller et al. 2007; Petrone et al. 2006, 2007; Stottlemyer 2001). These studies utilized samples collected from streams in the Arctic (Keller et al. 2007; Stottlemyer 2001) and sub-Arctic regions (Petrone et al. 2006, 2007) of Alaska and did not utilize under ice water samples during the winter. Additional studies conducted in sub-Arctic and Arctic Canadian streams affected by retrogressive thaw slumps observed statistically significant increased concentrations of Ca, K, Mg, and Na with influence from permafrost degradation (Kokelj et al. 2013; Lafrenière and Lamoureux 2013). Thus, the observation of the highest concentrations of these major metals (eg. Na, Mg, K, and

Ca) within the thermokarst lake with the most permafrost underlaying the water which, is actively thawing and releasing these solutes was consistent with literature based on Arctic streams (Table 3.5/Table 3.6)

3.5.3. Statistical Analysis Discussion:

3.5.3.1. Trace Metal Analysis Discussion:

3.5.3.1.1. Inter-Annual Variability Discussion:

The sampling year of 2016 was observed to have the most statistically different metals of Ag had an increased average, while Cd and Bi had a decreased in average concentration (Table 3.11). These differences could be caused by the increased temperatures causing more permafrost soil to thaw increasing active layer depth and surface area for complexation and leaching to occur. Additionally, the increase in active layer has the potential to not fully freeze and thus, flow patterns may continue throughout the winter. Precipitation was also observed to have a decreased amount during 2016 compared to the other years, this lack of precipitation would decrease the amount of surface lateral flow through vegetation and soils affecting the ability for these metals to complex of leach into the surface waters.

3.5.3.1.2. Effects of Thermokarst Lake Stratification Discussion:

Observations of individual sampling locations observed a statistical difference in epilimnion and hypolimnion, with the majority of those differences occurring in GSL (Table 3.9). GSL is the deepest thermokarst lake of this study and thus, has an increased ability to have a stratified water column. This stratified water column would cause specific metals to concentrate in epilimnion or hypolimnion waters. Additionally, the lack of statistical differences

observed in OCT and DNL for metal concentrations between epilimnion and hypolimnion could be caused by the influx of groundwater allowing for the influx to thoroughly mix the thermokarst lake water.

3.5.3.1.3. Intra-Annual Variability Discussion:

Seasonality variability was observed between winter and summer with the majority of metals increasing in concentration during winter (Table 3.10). These increases could be caused by the thermokarst lake being cut off from precipitation, which causes dilution of metals in summer and allow for the leaching of soils beneath the water levels into the thermokarst lake. This dilution can be considered by the normalization with chloride, as chloride is a tracer for precipitation (Lockwood et al. 1995; McNamara et al. 1997). The exception to the concentration increase was observed with Cu in GSL epilimnion (Table 3.10). Potential increases of Cu in this thermokarst lake could be anthropogenic sources, GSL is the closest thermokarst lake to a high traffic, paved road. Due to this proximity infiltration of Cu through water runoff from the road (Rice et al. 2002). Copper can accumulate on roads due to deposition from motor-vehicles as Cu is used in brake components, gasoline, oil, and tires (Nicholas Hewitt and Rashed 1990; Shaheen 1975; Ward 1990). Additionally, streams did not observe seasonal differences and this could be due to no under ice samples collected during this study and winter samples when ice had yet to cover the streams and there was still precipitation and surface flow occurring in the system. This is another prime example as why collection of winter stream samples is important in order to understand the geochemistry of waters in sub-Arctic Alaska.

3.5.3.1.4. Effect of Permafrost Extent Discussion:

Running ANOVAs allowed for the interpretation of how permafrost degradation may affect the geochemistry of the thermokarst lake waters (Table 3.5/Table 3.6). This interpretation can occur due to the unique ability of this study to observe three thermokarst lakes of varying permafrost degradation within the same watershed. Majority of the metals that observed differences in concentration based on thermokarst lake were at the highest concentration in GSL, with the lowest concentration changing between DNL and OCT, in both the epilimnion and hypolimnion. Similar results have been observed in west Siberia that observed an increase in micronutrients as a proxy for degrading permafrost as inorganic solutes such as Cu, Co, Fe, Mn, Mo, Ni, and Zn had higher concentrations during a degrading permafrost environment (Frey et al. 2007). This result is similar to this studies watershed with the exception of Fe and Zn. However, Fe concentrations in this watershed are extremely high which, could be influenced by gold deposits associated with this watershed. Additionally, Zn did not observe statistically significant differences between all three thermokarst lakes. This average is much higher than OCT and DNL which had an observed average less than 10 ppb for both thermokarst lakes in both the epilimnion and hypolimnion (Table 3.5/Table 3.6). In Arctic Alaska major ions were observe to increase in major ion concentrations due to near surface thawing of permafrost (Keller et al. 2010; Kokelj et al. 2013). This near surface thawing is occurring most readily around GSL as OCT and DNL both have areas of completely thawed permafrost, while GSL is surrounded by actively thawing permafrost. Due to limited metal concentrations observed in leachate experiments conducted on active layer and permafrost layer soils in near-by boreal forest sub-Arctic watershed conclusions regarding increased metal concentrations solely on permafrost influence is difficult to analyze (Gagné, Section 1.4.3.2.1.). However, the leachate studies were

conducted on only 60 g of soil and thus, the concentrations observed could be amplified through thawing of multiple magnitudes more soils actively thawing and in contact with surface water at the study sites. Soil samples collected within the watershed observed metal concentrations greater than 100 ppb for Na, Mg, Al, K, and Fe in the leachates analyzed, Ca saw greater concentrations of more than 1000 ppb (Table 1.9). All with the exception of Al and Fe had the highest concentration in the closed thermokarst lake of GSL. The only metals that observed a change in high concentration were Al, V, Fe, and As (Table 3.5/Table 3.6). These four metals increased in concentration in OCT, however there are plausible reasons as to why this increase occurred regardless of permafrost degradation. This residential valley has a gold mining history and has many pockets of gold beneath the surface (Brown et al. 1982) and has observed gold mining disturbances through dredging and placer mining (LaPerriere and Reynolds 1997; Spence 1994), which has altered stream location for GSBA (Lesh and Ridgway 2007). Gold is associated with high concentrations of arsenopyrite (FeAsS), which would increase the concentrations of Fe and As in the surface waters (Corkhill and Vaughan 2009). Aluminum on the other hand is one of the most abundant metals in the earth's crust that releases into the aquatic system when complexation occurs (Driscoll and Schecher 1990). OCT natural organic matter was observed to have a different functional group composition and thus, the potential for Al to complex to natural organic matter in the water may be different for OCT causing an increase in Al's solubility (Gagné, Section 1.4.3.2.1.). Finally, V concentrations were around 1 ppb in the thermokarst lakes and this low concentration could be determined statistically different with a small increase in concentration and source (Table 3.5/Table 3.6). As this watershed is residential there is the potential for anthropogenic sources to increase metal concentrations. Vanadium concentration increases in OCT could be caused by the contamination of diesel or steel into the water

(Moskalyk and Alfantazi 2003). Streams run through the entire watershed and thus, the statistical differences within the streams could also be anthropogenic in source.

3.5.3.2. Chloride Analysis Discussion:

3.5.3.2.1. Correlation of Metals to Chloride Concentrations Discussion:

Chloride was also observed to only show minor increases due to permafrost degradation in sub-Arctic Canada streams (Kokelj et al. 2013). Positive correlations with chloride is an indication that the metals were introduced to the thermokarst lake through the leaching of adjacent soils with the assistance of precipitation (Lockwood et al. 1995; McNamara et al. 1997). A negative correlation was only observed with Li (Figure 3.15), a highly reactive and soluble metal found in the earth's crust (Shahzad et al. 2016). Lithium has been used as an additional conservative tracer for hydrology work (Shahzad et al. 2016; Stewart et al. 1996; Tate et al. 1995.) However, Li is hydrologically conservative but not biologically conservative as plants and aquatic animals have been observed to present with toxicity levels from 150 – 500 ppb (Tate et al. 1995). Although, Li levels are a maximum of 5 pbb there is still the potential for plant uptake within the watershed as observed by the negative correlation with chloride. Positive correlations observed with Na, Ca, and Mg with chloride indicate a lateral surface flow source into the thermokarst lake, these metals have been observed to increase stream concentrations through the surface flow of active permafrost thaw slumps (Kokelj et al. 2013). Additionally, the positive correlation of Ba with chloride concur with a previous study that found Ba concentrations increased in Arctic streams during times of maximum active layer thaw depth (Barker et al. 2014). Barium is thus, being flushed into the thermokarst lakes through lateral flow from precipitation through the active layer soils and active permafrost thaw causing a positive

correlation with chloride. Permafrost underlain watersheds are known to have high carbonate concentrations (Frey and McClelland 2009; Keller et al. 2007) and Ca is commonly found as Ca-carbonate, which dissolves off of calcite rocks. Ca and Sr have been observed to have the strongest metal to metal correlation in this watershed. This correlation is consistent with the coprecipitation of Sr with calcite, that was previously observed in a European lake (Stabel 1989). Along with the metal to metal correlation between Ca and Sr both also observed a positive correlation with chloride. This correlation is caused by the weathering of calcite and carbonate minerals in active layer soils through lateral surface flow through active layers and deeply thawed soils (Keller et al. 2007).

3.5.3.2.2. Metal to Chloride Ratio Intra-Annual Variability Discussion:

This chloride normalization was employed to determine seasonality of metal concentrations without the concern of dilution from surface flow and precipitation. Normalizing to chloride limited the seasonality to just the metals that were being sourced within the thermokarst lake, which caused the high concentration metals in GSL to switch with high OCT chloride ratios for both the epilimnion and hypolimnion (Table 3.16/Table 3.17). This change in high values showcases that GSL has more influence from surface waters and leaching from actively thawing permafrost surrounding the thermokarst lake. Thus, further studies should be conducted on lateral flow the thermokarst lakes to better isolate the lake water geochemistry affected by permafrost degradation below the water body.

Due to the influx of chloride through precipitation chloride concentrations were compared to other metal concentrations to determine if metal – chloride relationships were distinguishable based off of season (Figure 3.17). Barker et al. 2014 observed as seasonal differences with metal

– chloride relationships between fall and summer in permafrost underlain streams, specifically with Ba, Fe, Mn, Al, Zn, and Ni. With all samples together collected from both streams and thermokarst lakes summer and winter samples did not observe different metal – chloride relationships (Table 3.14). This sentiment was consistent for all other metals observed in this study. When observing Fall (September and October) and Summer (June, July, and August) similarly to Barker et al. (2014) there was a lack of fall samples in comparison to summer and thus, a metal – chloride relationship seasonally was not observed as seen by Barker et al. (2014) even with the separation of lakes and streams. Thus, further interpretation on whether this was site specific was unable to be concluded due to the limited number of samples collected during fall. Overall, no specific metal – chloride relationships were observed between summer and winter for this watershed, with or without lakes and streams together. Although there were no distinct relationships between metal – chloride seasonality of overall water samples was observed to have a decrease in variability in the ratios during the winter for select metal – chloride relationships. This would conclude that during wintertime the thermokarst lakes and streams are cut off from lateral flow limiting the input of these metal inputs from lateral flow through the soils from precipitation.

3.5.3.3. Nitrogen Analysis Discussion:

Total dissolved nitrogen only had statistical differences in stream waters and not in thermokarst lake waters, with the highest concentration found in OCC had a 43 – 87% increase in nitrogen concentration compared to GSSC and GSBA respectively (Table 2.23). Permafrost thaw would not be influencing this increase in nitrogen content as nitrogen is statistically the same in all three thermokarst lakes and the stream locations are all underlined with 100%

permafrost. Nitrogen has a few sources in the aquatic system through the deposition from atmospheric aerosols (Wolfe et al. 2006), plant mineralization (Mary et al. 1996), manure, fertilizer (Schindler et al. 2006), and nitrogen fixation (Jones et al. 2005). Since the weather patterns and thus, the atmospheric deposition is the same for the watershed, atmospheric influences would not increase one water body and not the others. The same would occur for plant mineralization as the ecosystem and plants are the same, which would imply a consistent influx of nitrogen from plant material and subsequent soil leaching. Therefore, manure and fertilizer influence from residential farming may be the potential cause for increased nitrogen concentrations in one stream location. The meandering ability of the streams allows the streams to have increased contact with residential areas compared to the thermokarst lakes. Additionally, the sampling location was downstream from a small cow farm and thus, their manure is probably causing an increase in nitrogen content that is diluted by the time the water reached GSBA.

3.5.3.4. Carbon Analysis Discussion:

Leaching from the bottom of the lake introduces carbon and nitrogen which would limit the seasonality differences from surface flow introduction. This phenomenon can be observed by the consistent carbon concentrations at the hypolimnion level (Table 3.21). Seasonality was also observed in literature from sub-Arctic boreal forest headwater streams located in Whitehorse, Canada; however, number of winter samples and if the sample occurred under ice coverage was not disclosed (Shatilla and Carey 2019). The lack of statistical difference in carbon and nitrogen concentrations for streams during winter and summer in this study could be due to the limited samples collected associated with winter sampling skewing the statistical results.

The largest carbon concentration occurred in GSL, which may be caused by active thawing of high carbon yedoma permafrost leaching carbon into the surface water flow into the thermokarst lakes and underneath the thermokarst lakes (Table 3.22). Active permafrost thaw has shown increases in carbon concentration in west Siberia streams (Frey and Smith 2005) and high Arctic disturbances by thaw slumps (Grewer et al. 2016). This increase in carbon concentrations with decreased permafrost degradation is due to high carbon concentrations being observed when flow paths are shallow and do not flow deeper into the mineral soil where adsorption can occur (Carey 2003; Frey and McClelland 2009; Kawahigashi et al. 2004; Maclean et al. 1999; O'Donnell and Jones 2006; Prokushkin et al. 2007; Striegl et al. 2005, 2007). DNL did not observe the lowest carbon concentrations potentially due to suspected lateral flow into DNL through surface plant material and deeper lateral flow through soils could be causing an increase in carbon concentration as permafrost free zones facilitate increased ecological inorganic solute inputs (Frey et al. 2007). Thus, further studies on the area's hydrology is important to conduct to verify this working hypothesis. When BSP was added to the ANOVA the thermokarst lakes were still statistically different and BSP had the highest concentration of carbon. The difference between high carbon thermokarst lakes and low carbon thermokarst lakes is drastic as OCT and DNL had 50% less carbon compared to GSL and BSP (Table 3.22).

Due to the high carbon content of this watershed of upwards of 215 mg C L^{-1}, there is an increased propensity for trace metal complexation. Carbon concentrations are controlled and formed through the degradation of microbial and plant material which is then leached into the surface waters from plant material and soils. Due to the statistical variability of carbon based on permafrost degradation beneath the thermokarst lakes carbon normalization of metals was observed to allow interpretation of metal influence. Similar to the normalization with chloride

metal – carbon ratios were limited and locations with a sample value less than 3 interpretations on seasonality were lost or should be interpreted with the utmost care (Table 3.28/Table 3.29). Once normalized the seasonality differences had an overall decrease in seasonality, however not as much as chloride (Table 3.27). Similarly to the normalization of chloride carbon normalization also caused the high concentration metals in GSL to switch with high ratios of OCT for both the epilimnion and hypolimnion, as GSL had such high concentration of carbon. This high carbon concentration caused a decrease in values for GSL to make it the lowest between the three thermokarst lakes. This decrease in values may be due to complexation with carbon from either lateral flow or from permafrost degradation below GSL thermokarst lake.

3.5.3.4.1. Correlation of Metals to Carbon Concentrations Discussion:

Metals complexation to organic carbon and thus, a correlation was completed to observe any potential metal complexations that could explain the seasonality of the carbon normalized metals (Figure 3.18). Commonly transition metals complex to organic carbon ligands (Wan et al. 2019) and thus, many studies have been utilized to observe these complexation and correlations between organic carbon. The following studies include sampling locations all over the world and within different bodies of waters and verify the positive correlation observed in the current watershed; Mg, Ca, Mn (Pokrovsky and Schott 2002; Wan et al. 2019), Cr (Gu and Chen 2003; Wan et al. 2019), Ti, Sb, weakly Sr (Pokrovsky and Schott 2002), Co (Pokrovsky and Schott 2002; Qian et al. 1998), U (Gu and Chen 2003; Pokrovsky and Schott 2002; Porcelli et al. 1997), Ni (Sigg et al. 2000), and Se specifically in areas of high carbon content soils (Chagué-Goff and Fyfe 1997). Additionally, Ba saw a positive correlation with organic carbon but is not known for its strong binding ability to organic carbon. Barium however does share a similar source to

organic carbon through the leaching of soil as Ba was found to increase with increased active layer thaw depth (Barker et al. 2014). This increase in Ba with increased depth of surface water flow has also been observed in rivers draining from carbonate rocks. This watershed is underlain by carbonate rich schist (Schirrmeister et al. 2016). Furthermore, metals determined to be correlated with carbon concentrations include; Na and K, these metals were not found in current literature to be complexed with organic carbon and probably share a similar source like Ba does with carbonate rock. Al and Fe are commonly known to associate with organic carbon in literature, however this study observed no correlation between carbon and the two metals (Pokrovsky and Schott 2002). Additionally, Al saw a slight negative linear regression indicating Al and organic carbon are not complexed together, which was also observed by Pokrovsky and Schott (2002) as Al had a stronger association with Fe – colloids (Pokrovsky and Schott 2002). Similarly, As and Fe are associated together through high concentrations of arsenopyrite (FeAsS) associated with gold as observed in the metal to metal correlation from this watershed (Corkhill and Vaughan 2009) (Figure 3.16). Additionally, As did not observe a linear correlation with organic carbon, most likely due to the As requires Fe complexation too complex to organic matter and in the case of this watershed Fe does not correlate with organic carbon complexation (Mladenov et al. 2015). Iron's lack of positive correlation associated with organic matter complexation could be caused by the large concentration of iron overloading the organic matter and maxing out the complexation (Figure 3.19). Iron is potentially overloading the watershed and organic matter complexation site and thus, a metal that commonly is observed to have a linear relationship with carbon does not within the studied watershed (Oleinikova et al. 2019; Pokrovsky and Schott 2002; Wan et al. 2019). When the complexed Fe percentage was compared to the total Fe concentrations there was inconsistencies, thus verifying the possibility

for Fe overload in the watershed (Figure 3.19). Overall, the complexation of Fe was not dependent on carbon concentrations in this sub-Arctic boreal forest watershed as observed in the various percentages not dependent upon the initial total Fe concentration, which explains why Fe did not observe a linear relationship with carbon.

3.5.3.4.2. Metal to Carbon Ratio Intra-Annual Variability Discussion:

Seasonal variability for metals associated with organic carbon or co-leaching from soils observed an increase in wintertime samples. The increase of metal – carbon ratios during winter indicates an increase in metal leaching with carbon as carbon concentrations in the epilimnion also observed an increase in winter (Table 3.20). This increase in carbon concentration would affect the ratio in a negative way if the metals were not leaching along with the carbon into the surface waters. This increase is potentially due to deeper lateral flow through the bottom of the active layer since active layer freezes from the top down (Barker et al. 2014) or from the bottom of the thermokarst lake through active permafrost thaw or groundwater influx. All metal – carbon ratios that increased in the summer time were not known associates to organic matter and carried no linear correlation. These two metals Mo and Ag are thus, most likely associated with leaching from soil material and chloride is coming from the precipitation in the watershed. Bottom of the thermokarst lake soil sample collection could provide insight on whether these metals with increased ratios in the hypolimnion are leaching from the soil or from ground water influence. Additionally, when observing the overall metal – carbon ratio values within the watershed for summer and winter the majority of the metals fell into the category of decreased variability in winter (Table 3.19). This decrease was also similar to metal – carbon relationship

ratios, bolstering the idea the majority of the metals are surface sourced through surface flow into the thermokarst lake as carbon concentrations are soil and plant matter derived.

3.6. Conclusions:

This study was a case study to observe any changes in water geochemistry with the independent variable of known permafrost degradation and how summer and winter vary in water geochemistry in the watershed. The use of principal component analysis has allowed the input of optical indices and metal concentrations to observe a difference in water type and permafrost degradation. This tandem type sampling to cover all of the analysis is important as just optical indices and metal concentrations alone were not strong enough to resolved permafrost degradation and water type through a principal component analysis. Overall, the thermokarst lake water observed similar metal concentration relationships with permafrost degradation as sub-Arctic and Arctic streams, however as determined by the PCA analysis stream water and thermokarst lake waters are different. An increase in intensity of sampling thermokarst lake water is suggested for further studies of geochemistry related to permafrost degradation and seasonality, as the lack of sample numbers in sampling locations caused potential variability to not be observed.

Carbon concentrations within the watershed was extremely high compared to other water samples in lower latitudes. These high carbon concentrations peaked in the thermokarst lake with 100% permafrost underlying the water due to the initial permafrost thaw leaching the most organic carbon into the water. Carbon concentrations observed a seasonal difference with an increase in winter due to the leaching from the bottom of the thermokarst lake water column and lack of dilution from precipitation. While nitrogen concentrations were not affected by seasonal

changes or permafrost degradation. Iron concentrations in this watershed were also very high due to the influence from arsenopyrite due to the natural geology of the watershed. Due to the extremely high iron concentration there was no linear relationship observed between Fe and organic carbon for Fe complexation to organic carbon. In this sub-Arctic boreal forest watershed the complexation of Fe was not dependent on carbon concentrations as the percentage of Fe complexation varied with disregard to total Fe concentration. The high Fe affects the photo-Fenton photochemistry observed in isolated natural organic matter samples, however due to the oversaturation the rate of photolysis through the photo-Fenton reaction was not dependent upon the total iron concentration (Gagné, Section 2.4.3.).

Similarly seasonality was observed in most metal concentrations, with highest concentrations occurring in wintertime in the 100% permafrost underlain thermokarst lake. When metal concentrations were normalized by chloride and carbon to decipher metal source, seasonality trends occurred in less samples. Metal ratios also observed the highest values during winter, however the highest values were changed to being observed in the thermokarst lake with 50-75% permafrost underlying the water. Chloride removed the precipitation influence and carbon introduced complexed metals and metals associated with similar sourcing such as from soil leaching. The following metals were observed to increase through leaching of soil organic matter Na, Mg, K, Ca, Ti, V, Cr, Mn, Fe, As, Sr, Ba, and U as the metal – carbon relationship was positive. Variability within all samples observed decreased variability for the majority of metals analyzed showcasing the thermokarst lake water being cut off from lateral flow through the active layer. This decreased variability validates the importance of winter sampling to isolate the geochemistry within the thermokarst lake water column without lateral flow influence. The

amount of lateral flow introduced a complexity to the hydrology that was not initially hypothesized.

However, these observations of metal concentration and metal ratios did not occur in all thermokarst lakes and all water samples mostly likely due to the complexity of the hydrology associated with discontinuous permafrost regions and further information on the hydrology of the watershed would benefit the overall conclusions associated with permafrost degradation influence on geochemistry in thermokarst lake waters.

3.7. Acknowledgements:

Funding for portions of this project was supplied by the Alaska Space Grant and National Institutes for Water Resources Graduate Student-Lead Proposal through the Water & Environmental Research Center and the U.S. Department of Interior – Geological Survey. Access to residential lakes were obtained through permits supplied by NSF Grant 1500931, Methane release from thermokarst lakes: Thresholds and feedbacks in the lakes to watershed hydrology-permafrost systems. A sincere thank you to PI's on the NSF project for allowing access and providing intellectual support; Anna Liljedahl, David Barnes, Vladimir E Romanovsky, and Katey Walter Anthony. A special thanks to Karen Spaleta for assistance in running and obtaining ICP-MS data, Shane Billings for assistance in running and obtaining IC data, and Ronald Daanen for sampling and watershed expertise. Further thanks to the support or numerous students and collaborators for instrumentation assistance and sampling companionship; Bridget Eckhardt, Madison Ross, Emily Youcha, Nicole Ramos, Dallon Knight, Nina Ruckhaus, Ruth Osborne (Noratuk), Audrey Mutschlecner, Sara Ewers, Ragen Davey, Rachel Voight, Jef Spaleta and Tamara Harms.

3.8. References:

Albek, E.: Identification of the Different Sources of Chlorides in Streams by Regression Analysis Using Chloride-Discharge Relationships, Water Environ. Res., 71(7), 1310–1319, doi:10.2175/106143096x122384, 1999.

Bagard, M. L., Chabaux, F., Pokrovsky, O. S., Viers, J., Prokushkin, A. S., Stille, P., Rihs, S., Schmitt, A. D. and Dupré, B.: Seasonal variability of element fluxes in two Central Siberian rivers draining high latitude permafrost dominated areas, Geochim. Cosmochim. Acta, 75, 3335–3357, doi:10.1016/j.gca.2011.03.024, 2011.

Barker, A. J., Douglas, T. A., Jacobson, A. D., McClelland, J. W., Ilgen, A. G., Khosh, M. S., Lehn, G. O. and Trainor, T. P.: Late season mobilization of trace metals in two small Alaskan arctic watersheds as a proxy for landscape scale permafrost active layer dynamics, Chem. Geol., 381, 180–193, doi:10.1016/j.chemgeo.2014.05.012, 2014.

Brown, E. J., Luong, H. V and Forshaug, J. M.: The Occurrence of Thiobacillus ferrooxidans and Arsenic in Subarctic Streams Affected by Gold-Mine Drainage, Arct. Inst. North Am., 35(3), 417–421, doi:10.14430/arctic2344, 1982.

Callegary, J. B., Kikuchi, C. P., Koch, J. C., Lilly, M. R. and Leake, S. A.: Review: Groundwater in Alaska (USA), Hydrogeol. J., 21, 25–39, doi:10.1007/s10040-012-0940-5, 2013.

Carey, S. K.: Dissolved Organic Carbon Fluxes in a Discontinuous Permafrost Subarctic Alpine Catchment, Permafr. Periglac. Process., 14, 161–171, doi:10.1002/ppp.444, 2003.

Carey, S. K. and Woo, M. K.: The role of soil pipes as a slope runoff mechanism, Subarctic Yukon, Canada, J. Hydrol., 233, 206–222, doi:10.1016/S0022-1694(00)00234-1, 2000.

Chagué-Goff, C. and Fyfe, W. S.: Effect of permafrost on geochemistry in a Canadian peat plateau bog, Appl. Geochemistry, 12, 465–472, doi:10.1016/S0883-2927(97)00023-1, 1997.

Chapin, F. S., Sturm, M., Serreze, M. C., McFadden, J. P., Key, J. R., Lloyd, A. H., McGuire, A. D., Rupp, T. S., Lynch, A. H., Schimel, J. P., Beringer, J., Chapman, W. L., Epstein, H. E., Euskirchen, E. S., Hinzman, L. D., Jia, G., Ping, C. L., Tape, K. D., Thompson, C. D. C., Walker, D. A. and Welker, J. M.: Role of land-surface changes in arctic summer warming, Science (80-.)., 310, 657–660, doi:10.1126/science.1117368, 2005.

Chin, K. S., Lento, J., Culp, J. M., Lacelle, D. and Kokelj, S. V.: Permafrost thaw and intense thermokarst activity decreases abundance of stream benthic macroinvertebrates, Glob. Chang. Biol., 22, 2715–2728, doi:10.1111/gcb.13225, 2016.

Corkhill, C. L. and Vaughan, D. J.: Arsenopyrite oxidation - A review, Appl. Geochemistry, 24, 2342–2361, doi:10.1016/j.apgeochem.2009.09.008, 2009.

Cory, R. M., Ward, C. P., Crump, B. C. and Kling, G. W.: Sunlight controls water column processing of carbon in arctic frech waters, Science (80-.)., 345(6199), 925–928, doi:10.1126/science.1253119, 2014.

Dittmar, T., Koch, B., Hertkorn, N. and Kattner, G.: A simple and efficient method for the solid-phase extraction of dissolved organic matter (SPE-DOM) from seawater, Limnol. Oceanogr. Methods, 6, 230–235, doi:10.4319/lom.2008.6.230, 2008.

Drake, T. W., Wickland, K. P., Spencer, R. G. M., McKnight, D. M. and Striegl, R. G.: Ancient low-molecular-weight organic acids in permafrost fuel rapid carbon dioxide production upon thaw, Proc. Natl. Acad. Sci. U. S. A., 112(45), 13946–13951, doi:10.1073/pnas.1511705112, 2015.

Driscoll, C. T. and Schecher, W. D.: The chemistry of aluminum in the environment, Environ. Geochem. Health, 12, 28–49, doi:10.1007/BF01734046, 1990.

Elder, C. D., Schweiger, M., Lam, B., Crook, E. D., Xu, X., Walker, J., Walter Anthony, K. M. and Czimczik, C. I.: Seasonal Sources of Whole-Lake CH 4 and CO 2 Emissions From Interior Alaskan Thermokarst Lakes, J. Geophys. Res. Biogeosciences, 124(5), 1209–1229, doi:10.1029/2018JG004735, 2019.

Emond, A. M., Daanen, R. P., Graham, G. R. C., Anthony, K. W., Liljedahl, A. K., Minsley, B. J., Barnes, D. L. and Romanovsky, V. E.: Airborne electromagnetic and magnetic survey, Goldstream Creek watershed, interior Alaska, Fairbanks., 2018.

Frey, K. E. and McClelland, J. W.: Impacts of permafrost degradation on arctic river biogeochemistry, Hydrol. Process., 23(1), 169–182, doi:10.1002/hyp.7196, 2009.

Frey, K. E. and Smith, L. C.: Amplified carbon release from vast West Siberian peatlands by 2100, Geophys. Res. Lett., 32, L09401, doi:10.1029/2004GL022025, 2005.

Frey, K. E., McClelland, J. W., Holmes, R. M. and Smith, L. G.: Impacts of climate warming and permafrost thaw on the riverine transport of nitrogen and phosphorus to the Kara Sea, J. Geophys. Res. Biogeosciences, 112, G04S58, doi:10.1029/2006JG000369, 2007.

Giesler, R., Lyon, S. W., Mörth, C. M., Karlsson, J., Karlsson, E. M., Jantze, E. J., Destouni, G. and Humborg, C.: Catchment-scale dissolved carbon concentrations and export estimates across six subarctic streams in northern Sweden, Biogeosciences, 11, 525–537, doi:10.5194/bg-11-525-2014, 2014.

Grant, R. F., Mekonnen, Z. A., Riley, W. J., Wainwright, H. M., Graham, D. and Torn, M. S.: Mathematical Modelling of Arctic Polygonal Tundra with Ecosys: 1. Microtopography Determines How Active Layer Depths Respond to Changes in Temperature and Precipitation, J. Geophys. Res. Biogeosciences, 122, 3161–3173, doi:10.1002/2017JG004035, 2017.

Grewer, D. M., M. J. Lafrenière, S. F. Lamoureux, and M. J. Simpson. Redistribution of soil organic matter by permafrost disturbance in the Canadian High Arctic, Biogeochemistry, 128, 397–415, doi:10.1007/s10533-016-0215-7, 2016.

Gu, B. and Chen, J.: Enhanced microbial reduction of Cr(VI) and U(VI) by different natural organic matter fractions, Geochim. Cosmochim. Acta, 67(19), 3575–3582, doi:10.1016/S0016-7037(03)00162-5, 2003.

Heslop, J. K., Chandra, S., Sobzcak, W. V., Davydov, S. P., Davydova, A. I., Spektor, V. V. and Walter Anthony, K. M.: Variable respiration rates of incubated permafrost soil extracts from the Kolyma River lowlands, north-east Siberia, Polar Res., 37(1), doi:10.1080/17518369.2017.1305157, 2017.

Holmes, R. M., Peterson, B. J., Gordeev, V. V., Zhulidov, A. V., Meybeck, M., Lammers, R. B. and Vörösmarty, C. J.: Flux of nutrients from Russian rives to the Arctic Ocean: Can we establish a baseline against which to judge future changes?, Water Resour. Res., 36(8), 2309–2320, doi:10.1029/2000WR900099, 2000.

Iijima, Y., Ohta, T., Kotani, A., Fedorov, A. N., Kodama, Y. and Maximov, T. C.: Sap flow changes in relation to permafrost degradation under increasing precipitation in an eastern Siberian larch forest, Ecohydrology, 7(2), 177–187, doi:10.1002/eco.1366, 2014.

Jones, J. B., Petrone, K. C., Finlay, J. C., Hinzman, L. D. and Bolton, W. R.: Nitrogen loss from watersheds of interior Alaska underlain with discontinuous permafrost, Geophys. Res. Lett., 32, L02401, doi:10.1029/2004GL021734, 2005.

Jorgenson, M. T., Shur, Y. L. and Pullman, E. R.: Abrupt increase in permafrost degradation in Arctic Alaska, Geophys. Res. Lett., 33, L02503, doi:10.1029/2005GL024960, 2006.

Katz, B. G., Catches, J. S., Bullen, T. D. and Michel, R. L.: Changes in the isotopic and chemical composition of ground water resulting from a recharge pulse from a sinking stream, J. Hydrol., 211, 178–207, doi:10.1016/S0022-1694(98)00236-4, 1998.

Kawahigashi, M., Kaiser, K., Kalbitz, K., Rodionov, A. and Guggenberger, G.: Dissolved organic matter in small streams along a gradient from discontinuous to continuous permafrost, Glob. Chang. Biol., 10, 1576–1586, doi:10.1111/j.1365-2486.2004.00827.x, 2004.

Keller, K., Blum, J. D. and Kling, G. W.: Geochemistry of soils and streams on surfaces of varying ages in arctic Alaska, in Arctic, Antarctic, and Alpine Research, vol. 39, pp. 84–98., 2007.

Keller, K., Blum, J. D. and Kling, G. W.: Stream geochemistry as an indicator of increasing permafrost thaw depth in an arctic watershed, Chem. Geol., 273, 76–81, doi:10.1016/j.chemgeo.2010.02.013, 2010.

Keuper, F., van Bodegom, P. M., Dorrepaal, E., Weedon, J. T., van Hal, J., van Logtestijn, R. S. P. and Aerts, R.: A frozen feast: Thawing permafrost increases plant-available nitrogen in subarctic peatlands, Glob. Chang. Biol., 18, 1998–2007, doi:10.1111/j.1365-2486.2012.02663.x, 2012.

Kling, G. W., Brien, W. J. O., Miller, M. C. and Hershey, A. E.: The biogeochemistry and zoogeography of lakes and rivers in arctic Alaska. Hydrobiologia **240**: 1–14. doi:10.1007/BF00013447, 1992.

Kokelj, S. V., Lacelle, D., Lantz, T. C., Tunnicliffe, J., Malone, L., Clark, I. D. and Chin, K. S.: Thawing of massive ground ice in mega slumps drives increases in stream sediment and solute flux across a range of watershed scales, J. Geophys. Res. Earth Surf., 118, 681–692, doi:10.1002/jgrf.20063, 2013.

Lafrenière, M. J. and Lamoureux, S. F.: Thermal perturbation and rainfall runoff have greater impact on seasonal solute loads than physical disturbance of the active layer, Permafr. Periglac. Process., 24, 241–251, doi:10.1002/ppp.1784, 2013.

LaPerriere, J. D. and Reynolds, J. B.: Gold Placer Mining and Stream Ecosystems of Interior Alaska, in Freshwaters of Alaska, edited by A. M. Milner, pp. 265–280, Springer, New York, NY., 1997.

Larouche, J. R., Abbott, B. W., Bowden, W. B. and Jones, J. B.: The role of watershed characteristics, permafrost thaw, and wildfire on dissolved organic carbon biodegradability and water chemistry in Arctic headwater streams, Biogeosciences, 12, 4221–4233, doi:10.5194/bg-12-4221-2015, 2015.

Lesh, M. E. and Ridgway, K. D.: Geomorphic evidence of active transpressional deformation in the tanana foreland basin, south-central alaska, Spec. Pap. Geol. Soc. Am., 431(22), 573–592, doi:10.1130/2007.2431(22), 2007.

Liljedahl, A.: Climate Data from the Goldstream Creek Watershed Study of Mathane Release from Thermokarst Lakes, [online] Available from: http://ine.uaf.edu/werc/werc-projects/goldstream/, Fairbanks, Alaska, variously paged. [11/3/19].

Lockwood, P. V., McGarity, J. W. and Charley, J. L.: Measurement of chemical weathering rates using natural chloride as a tracer, Geoderma, 64, 215–232, doi:10.1016/0016-7061(94)00010-8, 1995.

Maclean, R., Oswood, M. W., Irons, J. G. and Mcdowell, W. H.: The effect of permafrost on stream biogeochemistry: A case study of two streams in the Alaskan (U.S.A.) taiga, Biogeochemistry, 47, 239–267, doi:10.1007/BF00992909, 1999.

Mary, B., Recous, S., Darwis, D. and Robin, D.: Interactions between decomposition of plant residues and nitrogen cycling in soil, Plant Soil, 181, 71–82, doi:10.1007/BF00011294, 1996.

Mcadams, B. C., Aiken, G. R., Mcknight, D. M., Arnold, W. A. and Chin, Y. P.: High Pressure Size Exclusion Chromatography (HPSEC) Determination of Dissolved Organic Matter Molecular Weight Revisited: Accounting for Changes in Stationary Phases, Analytical Standards, and Isolation Methods, , doi:10.1021/acs.est.7b04401, 2017.

McNamara, J. P., Kane, D. L. and Hinzman, L. D.: Hydrograph separations in an Arctic watershed using mixing model and graphical techniques, Water Resour. Res., 33(7), 1707–1719, doi:10.1029/97WR01033, 1997.

Mladenov, N., Miller, M. P., Nemergut, D. R., Legg, T., Simone, B., Hageman, C., Mcknight, D. M., Zheng, Y., Rahman, M. M. and Ahmed, K. M.: Dissolved organic matter sources and consequences for iron and arsenic mobilization in Bangladesh aquifers, Environ. Sci. Technol., 44(1), 123–128, doi:10.1021/es901472g, 2010.

Moskalyk, R. R. and Alfantazi, A. M.: Processing of vanadium: A review, Miner. Eng., 16, 793–805, doi:10.1016/S0892-6875(03)00213-9, 2003.

Muhs, D. R. and Budahn, J. R.: Geochemical evidence for the origin of late Quaternary loess in central Alaska, Can. J. Earth Sci., 43, 323–337, doi:10.1139/E05-115, 2006.

Neumann, R. B., Moorberg, C. J., Lundquist, J. D., Turner, J. C., Waldrop, M. P., McFarland, J. W., Euskirchen, E. S., Edgar, C. W. and Turetsky, M. R.: Warming Effects of Spring Rainfall Increase Methane Emissions From Thawing Permafrost, Geophys. Res. Lett., 46, 1393–1401, doi:10.1029/2018GL081274, 2019.

Nicholas Hewitt, C. and Rashed, M. B.: An integrated budget for selected pollutants for a major rural highway, Sci. Total Environ., 93, 375–384, doi:10.1016/0048-9697(90)90128-H, 1990.

O'Donnell, J. A. and Jones, J. B.: Nitrogen retention in the riparian zone of catchments underlain by discontinuous permafrost, Freshw. Biol., 51, 854–864, doi:10.1111/j.1365-2427.2006.01535.x, 2006.

Olefeldt, D., Goswami, S., Grosse, G., Hayes, D., Hugelius, G., Kuhry, P., Mcguire, A. D., Romanovsky, V. E., Sannel, A. B. K., Schuur, E. A. G. and Turetsky, M. R.: Circumpolar distribution and carbon storage of thermokarst landscapes, Nat. Commun., 7, 1–11, doi:10.1038/ncomms13043, 2016.

Oleinikova, O. V., Poitrasson, F., Drozdova, O. Y., Shirokova, L. S., Lapitskiy, S. A. and Pokrovsky, O. S.: Iron isotope fractionation during bio- And photodegradation of organoferric colloids in boreal humic waters, Environ. Sci. Technol., 53, 11183–11194, doi:10.1021/acs.est.9b02797, 2019.

Petrone, K. C., Jones, J. B., Hinzman, L. D. and Boone, R. D.: Seasonal export of carbon, nitrogen, and major solutes from Alaskan catchments with discontinuous permafrost, J. Geophys. Res. Biogeosciences, 111, 1–13, doi:10.1029/2005JG000055, 2006.

Petrone, K. C., Hinzman, L. D., Shibata, H., Jones, J. B. and Boone, R. D.: The influence of fire and permafrost on sub-arctic stream chemistry during storms, Hydrol. Process., 21, 423–434, doi:10.1002/hyp.6247, 2007.

Pokrovsky, O. S. and Schott, J.: Iron colloids/organic matter associated transport of major and trace elements in small boreal rivers and their estuaries (NW Russia), Chem. Geol., 190, 141–179, doi:10.1016/S0009-2541(02)00115-8, 2002.

Pokrovsky, O. S., Bueno, M., Manasypov, R. M., Shirokova, L. S., Karlsson, J. and Amouroux, D.: Dissolved Organic Matter Controls Seasonal and Spatial Selenium Concentration Variability in Thaw Lakes across a Permafrost Gradient, Environ. Sci. Technol., 52, 10254–10262, doi:10.1021/acs.est.8b00918, 2018a.

Pokrovsky, O. S., Karlsson, J. and Giesler, R.: Freeze-thaw cycles of Arctic thaw ponds remove colloidal metals and generate low-molecular-weight organic matter, Biogeochemistry, 137, 321–336, doi:10.1007/s10533-018-0421-6, 2018b.

Porcelli, D., Andersson, P. S., Wasserburg, G. J., Ingri, J. and Baskaran, M.: The importance of colloids and mires for the transport of uranium isotopes through the Kalix River watershed and Baltic Sea, Geochim. Cosmochim. Acta, 61(19), 4095–4113, doi:10.1016/S0016-7037(97)00235-4, 1997.

Prokushkin, A. S., Gleixner, G., McDowell, W. H., Ruehlow, S. and Schulze, E. D.: Source- and substrate-specific export of dissolved organic matter from permafrost-dominated forested watershed in central Siberia, Global Biogeochem. Cycles, 21, GB4003, doi:10.1029/2007GB002938, 2007.

Qian, J., Xue, H. Bin, Sigg, L. and Albrecht, A.: Complexation of cobalt by natural ligands in freshwater, Environ. Sci. Technol., 32(14), 2043–2050, doi:10.1021/es971018l, 1998.

Rember, R. D. and Trefry, J. H.: Increased concentrations of dissolved trace metals and organic carbon during snowmelt in rivers of the alaskan arctic, Geochim. Cosmochim. Acta, 68(3), 477–489, doi:10.1016/S0016-7037(03)00458-7, 2004.

Rice, K. C., Conko, K. M. and Hornberger, G. M.: Anthropogenic sources of arsenic and copper to sediments in a Suburban Lake, Northern Virginia, Environ. Sci. Technol., 36(23), 4962–4967, doi:10.1021/es025727x, 2002.

Savenko, A. V., Demidenko, N. A. and Pokrovsky, O. S.: Spatial and temporal variability of the transformation of dissolved matter runoff in the Mezen' River estuary, Oceanography, 59(2), 199–207, doi:10.31857/s0030-1574592216-226, 2019.

Schädel, C., Mcguire, A. D. and Schuur, E. A. G.: Permafrost Carbon Network : 5-Year Synthesis Report., 2015.

Schindler, D. W., Dillon, P. J. and Schreier, H.: A review of anthropogenic sources of nitrogen and their effects on Canadian aquatic ecosystems, Biogeochemistry, 79, 25–44, doi:10.1007/s10533-006-9001-2, 2006.

Schirrmeister, L., Meyer, H., Andreev, A., Wetterich, S., Kienast, F., Bobrov, A., Fuchs, M., Sierralta, M. and Herzschuh, U.: Late Quaternary paleoenvironmental records from the Chatanika River valley near Fairbanks (Alaska), Quat. Sci. Rev., 147, 259–278, doi:10.1016/j.quascirev.2016.02.009, 2016.

Schuur, E. A. G., McGuire, A. D., Schädel, C., Grosse, G., Harden, J. W., Hayes, D. J., Hugelius, G., Koven, C. D., Kuhry, P., Lawrence, D. M., Natali, S. M., Olefeldt, D., Romanovsky, V. E., Schaefer, K., Turetsky, M. R., Treat, C. C. and Vonk, J. E.: Climate change and the permafrost carbon feedback, Nature, 520, 171–179, doi:10.1038/nature14338, 2015.

Shaheen, D. G.: Document Display | NEPIS | US EPA. [online] (Accessed 9 November 2019), 1975.

Shahzad, B., Tanveer, M., Hassan, W., Shah, A. N., Anjum, S. A., Cheema, S. A. and Ali, I.: Lithium toxicity in plants: Reasons, mechanisms and remediation possibilities – A review, Plant Physiol. Biochem., 107, 104–115, doi:10.1016/j.plaphy.2016.05.034, 2016.

Shatilla, N. J. and Carey, S.: Assessing inter-annual and seasonal patterns of DOC and DOM quality across a complex alpine watershed underlain by discontinuous permafrost in Yukon, Canada, Hydrol. Earth Syst. Sci., 23, 3571–3591, doi:10.5194/hess-23-3571-2019, 2019.

Sigg, L., Xue, H., Kistler, D. and Sshönenberger, R.: Size fractionation (dissolved, colloidal and particulate) of trace metals in the Thur river, Switzerland, Aquat. Geochemistry, 6, 413–434, doi:10.1023/A:1009692919804, 2000.

Spence, C. C.: Alaska Gold Dredging, Min. Hist. Assoc., 109–118, 1994.

Stabel, H. H.: Coupling of strontium and calcium cycles in Lake Constance, Hydrobiologia, 176/177, 323–329, doi:10.1007/978-94-009-2376-8_30, 1989.

Stewart, A. J. and Kszos, L. A.: Caution on using lithium (Li+) as a conservative tracer in hydrological studies, Limnol. Oceanogr., 41(1), 190–191, doi:10.4319/lo.1996.41.1.0190, 1996.

Stocker, T. F., Qin, D., Plattner, G. K., Tignor, M. M. B., Allen, S. K., Boschung, J., Nauels, A., Xia, Y., Bex, V. and Midgley, P. M.: Climate change 2013 the physical science basis: Working Group I contribution to the fifth assessment report of the intergovernmental panel on climate change, edited by T. F. Stocker, D. Qin, G. K. Plattner, M. M. B. Tignor, S. K. Allen, J. Boschung, A. Nauels, Y. Xia, V. Bex, and P. M. Midgley, Cambridge University Press., 2013.

Stolpe, B., Guo, L. and Shiller, A. M.: Binding and transport of rare earth elements by organic and iron-rich nanocolloids in alaskan rivers, as revealed by field-flow fractionation and ICP-MS, Geochim. Cosmochim. Acta, 106, 446–462, doi:10.1016/j.gca.2012.12.033, 2013.

Stottlemyer, R.: Biogeochemistry of a treeline watershed, northwestern Alaska, J. Environ. Qual., 30, 1990–1998, doi:10.2134/jeq2001.1990, 2001.

Strauss, J., Schirrmeister, L., Grosse, G., Fortier, D., Hugelius, G., Knoblauch, C., Romanovsky, V., Schädel, C., Schneider von Deimling, T., Schuur, E. A. G., Shmelev, D., Ulrich, M. and Veremeeva, A.: Deep Yedoma permafrost: A synthesis of depositional characteristics and carbon vulnerability, Earth-Science Rev., 172, 75–86, doi:10.1016/j.earscirev.2017.07.007, 2017.

Striegl, R. G., Aiken, G. R., Dornblaser, M. M., Raymond, P. A. and Wickland, K. P.: A decrease in discharge-normalized DOC export by the Yukon River during summer through autumn, Geophys. Res. Lett., 32, L21413, doi:10.1029/2005GL024413, 2005.

Striegl, R. G., Dornblaser, M. M., Aiken, G. R., Wickland, K. P. and Raymond, P. A.: Carbon export and cycling by the Yukon, Tanana, and Porcupine rivers, Alaska, 2001-2005, Water Resour. Res., 43, W02411, doi:10.1029/2006WR005201, 2007.

Tate, C. M., Broshears, R. E. and McKnight, D. M.: Phosphate dynamics in an acidic mountain stream: Interactions involving algal uptake, sorption by iron oxide, and photoreduction, Limnol. Oceanogr., 40(5), 938–946, doi:10.4319/lo.1995.40.5.0938, 1995.

Thienpont, J. R., Rühland, K. M., Pisaric, M. F. J., Kokelj, S. V., Kimpe, L. E., Blais, J. M. and Smol, J. P.: Biological responses to permafrost thaw slumping in Canadian Arctic lakes, Freshw. Biol., 58, 337–353, doi:10.1111/fwb.12061, 2013.

Toohey, R. C., Herman-Mercer, N. M., Schuster, P. F., Mutter, E. A. and Koch, J. C.: Multidecadal increases in the Yukon River Basin of chemical fluxes as indicators of changing flowpaths, groundwater, and permafrost, Geophys. Res. Lett., 43, 12,120-12,130, doi:10.1002/2016GL070817, 2016.

Walter Anthony, K., Schneider Von Deimling, T., Nitze, I., Frolking, S., Emond, A., Daanen, R., Anthony, P., Lindgren, P., Jones, B., Grosse, G., Walter Anthony, K., Schneider Von Deimling, T., Nitze, I., Frolking, S., Emond, A., Daanen, R., Anthony, P., Lindgren, P., Jones, B. and Grosse, G.: 21st-century modeled permafrost carbon emissions accelerated by abrupt thaw beneath lakes, Nat. Commun., 9, 1–11, doi:10.1038/s41467-018-05738-9, 2018.

Walter Anthony, K. M., Zimov, S. A., Grosse, G., Jones, M. C., Anthony, P. M., Iii, F. S. C., Finlay, J. C., Mack, M. C., Davydov, S., Frenzel, P. and Frolking, S.: A shift of thermokarst lakes from carbon sources to sinks during the Holocene epoch, Nature, 511, 452–456, doi:10.1038/nature13560, 2014.

Wan, D., Sharma, V. K., Liu, L., Zuo, Y. and Chen, Y.: Mechanistic Insight into the Effect of Metal Ions on Photogeneration of Reactive Species from Dissolved Organic Matter, Environ. Sci. Technol., 53, 5778–5786, doi:10.1021/acs.est.9b00538, 2019.

Ward, N. I.: Multielement contamination of British motorway environments, Sci. Total Environ., 93, 393–401, doi:10.1016/0048-9697(90)90130-M, 1990.

Weyhenmeyer, G. A., Prairie, Y. T. and Tranvik, L. J.: Browning of boreal freshwaters coupled to carbon-iron interactions along the aquatic continuum, PLoS One, 9(2), e88104, doi:10.1371/journal.pone.0088104, 2014.

Wickland, K. P., Neff, J. C. and Aiken, G. R.: Dissolved organic carbon in Alaskan boreal forest: Sources, chemical characteristics, and biodegradability, Ecosystems, 10, 1323–1340, doi:10.1007/s10021-007-9101-4, 2007.

Winkel, M., Sepulveda-Jauregui, A., Martinez-Cruz, K., Heslop, J. K., Rijkers, R., Horn, F., Liebner, S., Anthony, W., Walter Anthony, K. M. and Anthony, W.: First evidence for cold-adapted anaerobic oxidation of methane in deep sediments of thermokarst lakes, Environ. Res. Commun., 1, 021002, doi:10.1088/2515-7620/ab1042, 2019.

Wolfe, A. P., Cooke, C. A. and Hobbs, W. O.: Are current rates of atmospheric nitrogen deposition influencing lakes in the eastern Canadian Arctic?, Arctic, Antarct. Alp. Res., 38(3), 465–476, doi:10.1657/1523-0430(2006)38[465:ACROAN]2.0.CO;2, 2006.

Yoshikawa, K. and Hinzman, L. D.: Shrinking thermokarst ponds and groundwater dynamics in discontinuous permafrost near Council, Alaska, Permafr. Periglac. Process., 14, 151–160, doi:10.1002/ppp.451, 2003.

3.9. Figures:

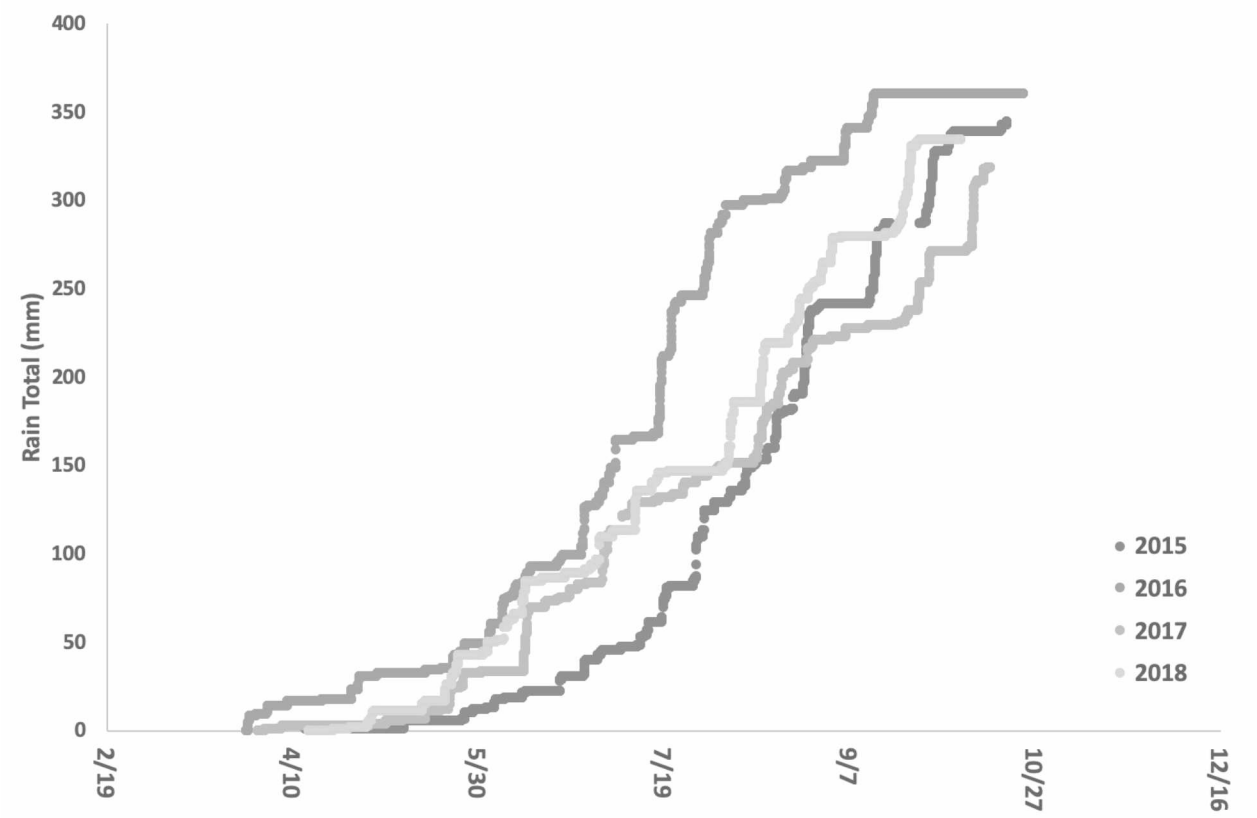

Figure 3.1: Cumulative Rainfall in Sampling Watershed

Cumulative rainfall values were determined post collected after value errors were determined through the collection of watershed specific weather station installed and operated by Lijledahl, A. (Liljedahl, A., 2019).

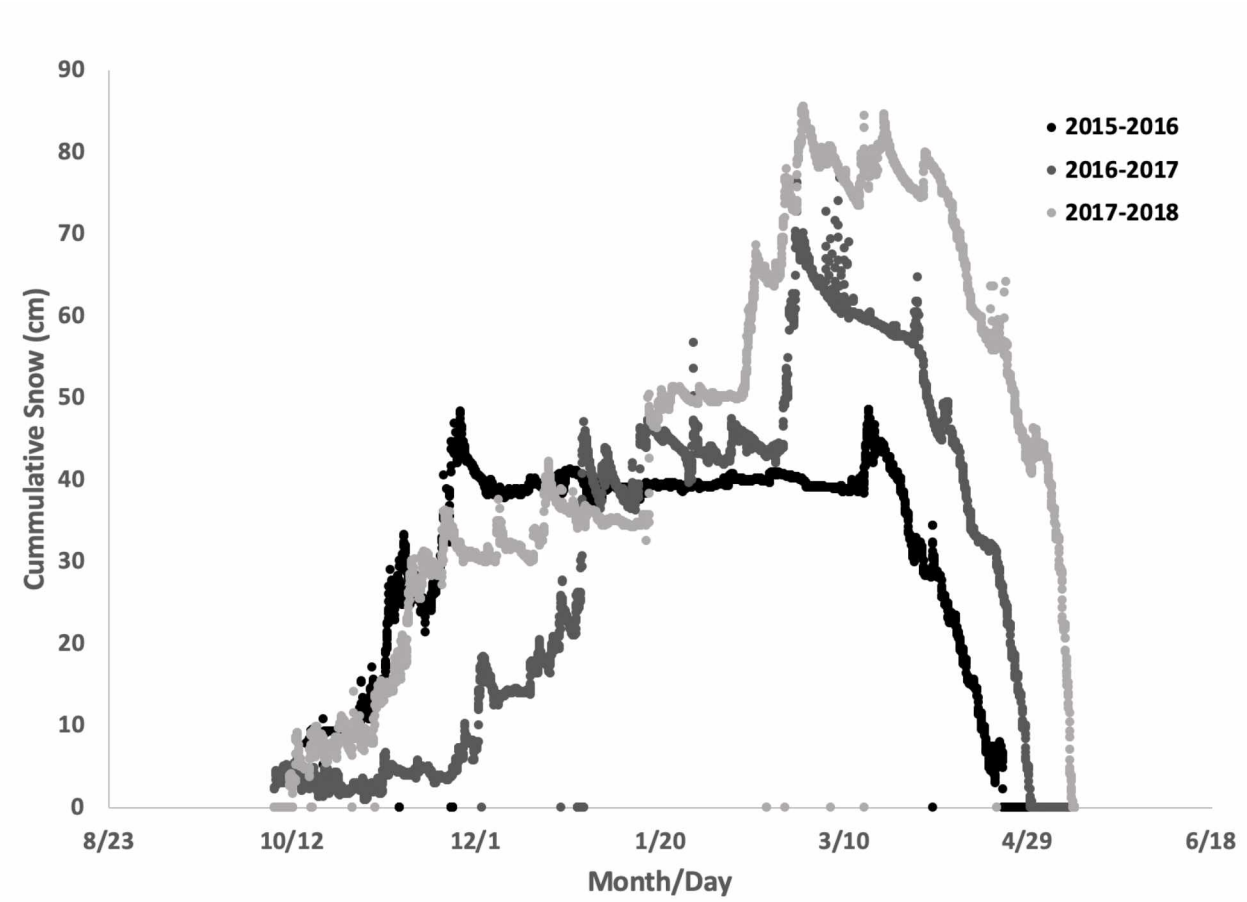

Figure 3.2: Cumulative Snow Accumulation for Sampling Watershed

Cumulative snow accumulation values were determined post collected after value errors were determined through the collection of watershed specific weather station installed and operated by Liljedahl, A. (Liljedahl, A., 2019).

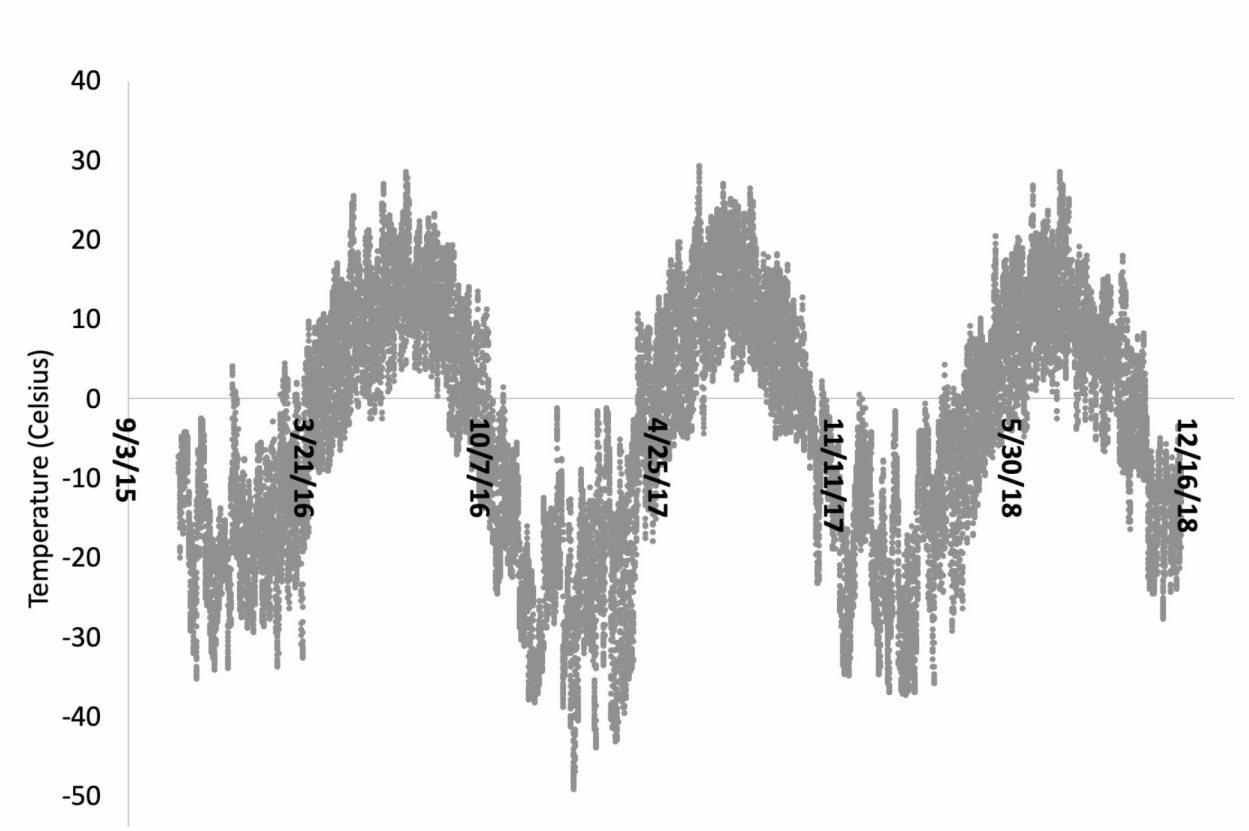

Figure 3.3: Air Temperatures for Sampling Watershed

Temperatures were determined post collected after value errors were determined through the collection of watershed specific weather station installed and operated by Liljedahl, A. (Liljedahl, A., 2019).

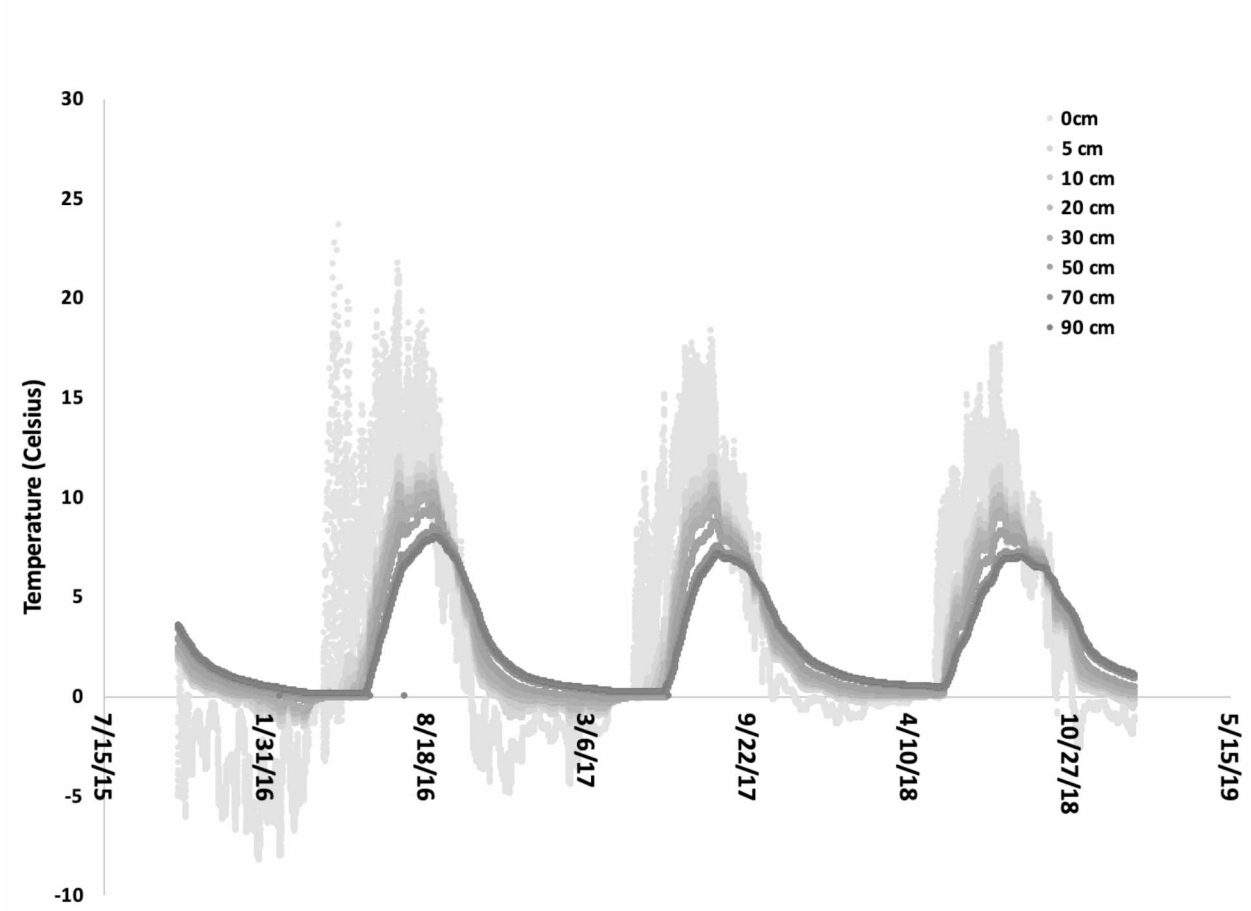

Figure 3.4: Soil Temperatures of Active Layer in Sampling Watershed

Temperatures were determined post collected after value errors were determined through the collection of watershed specific weather station installed and operated by Liljedahl, A. through the installation by Romanovsky. (Liljedahl, A., 2019).

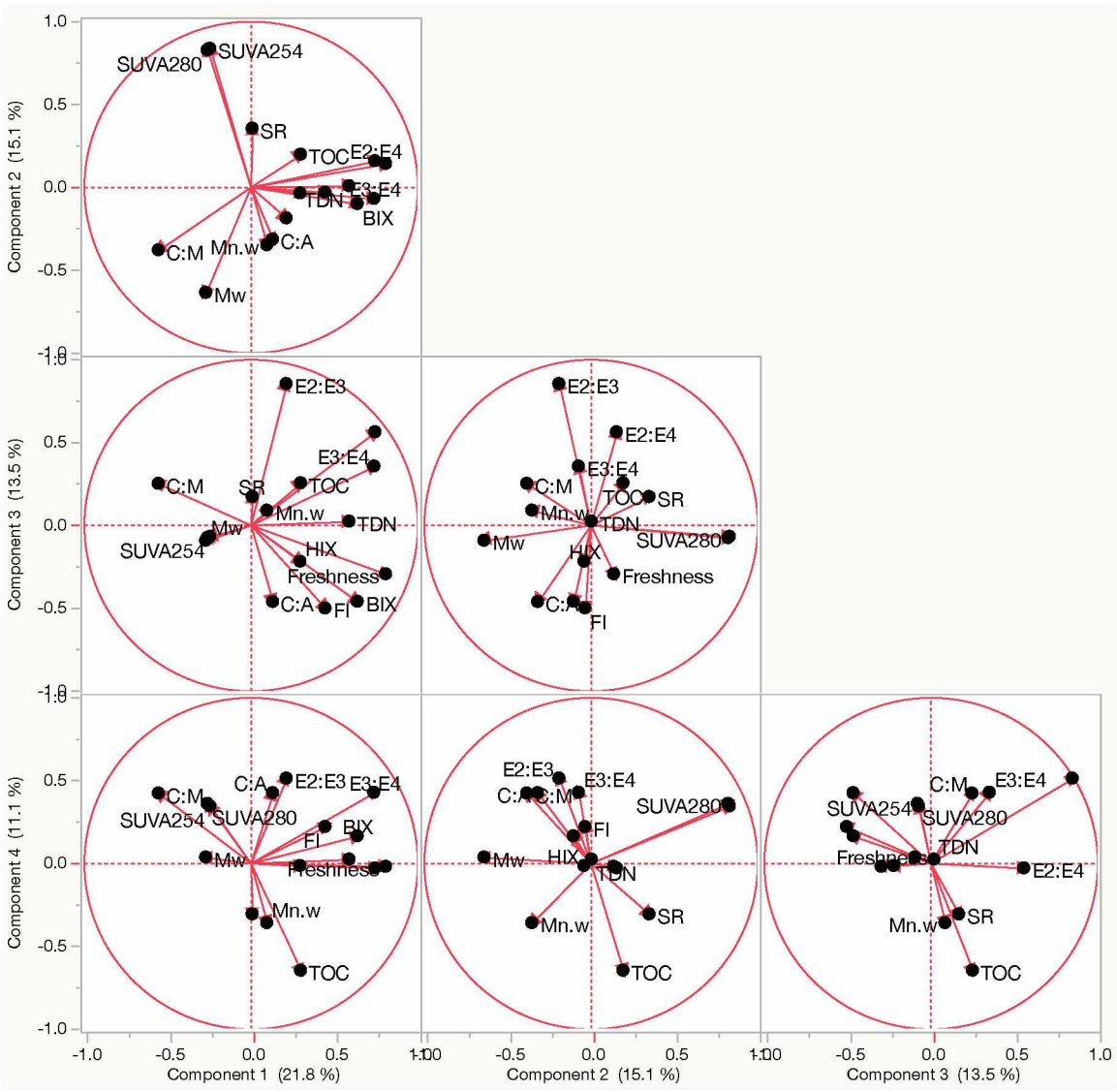

Figure 3.5: Principal Component Loading Plots for PCA O

Principal component analysis loading matrix for optical indices normalized using a z-score. Principal components 1 through 4 are represented as they explain at least 50% of the sample scores and Eigenvalues were determined significant through a Bartlett Test. Loading Matrix showcases which optical indices correlate with each other to represent each quadrant in the plots produced by principal component analysis. Variables utilized in PCA O can be observed in Table 3.3. Abbreviations defined in Table 2.1 and 2.2.

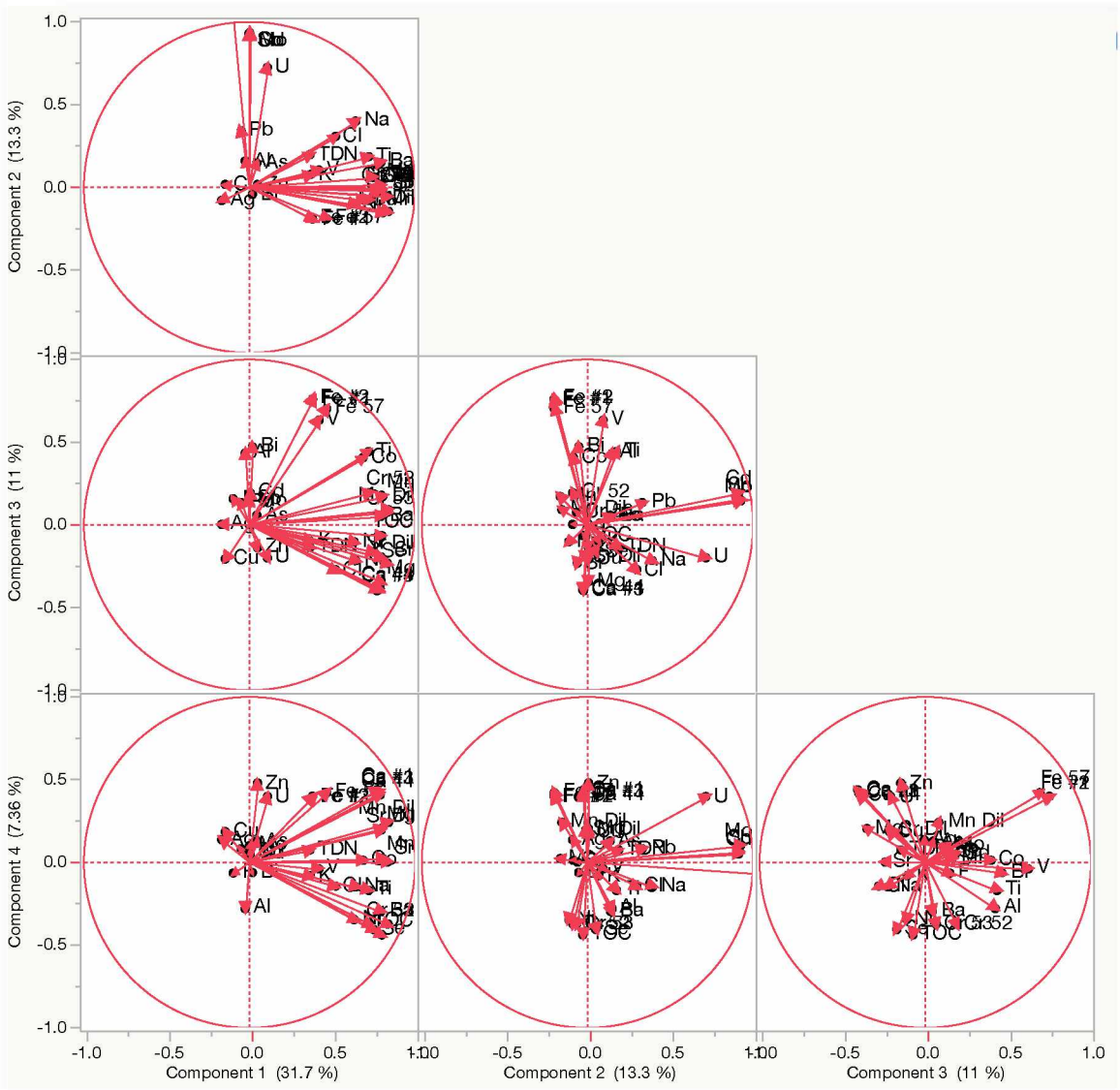

Figure 3.6: Principal Component Loading Plots PCA M

Principal component analysis loading matrix for metal concentrations normalized using a z-score. Principal components 1 through 4 are represented as they explain at least 50% of the sample scores and Eigenvalues were determined significant through a Bartlett Test. Loading Matrix showcases which metals correlate with each other through principal component analysis to represent each quadrant in the plots. Variables utilized in PCA M can be observed in Table 3.3

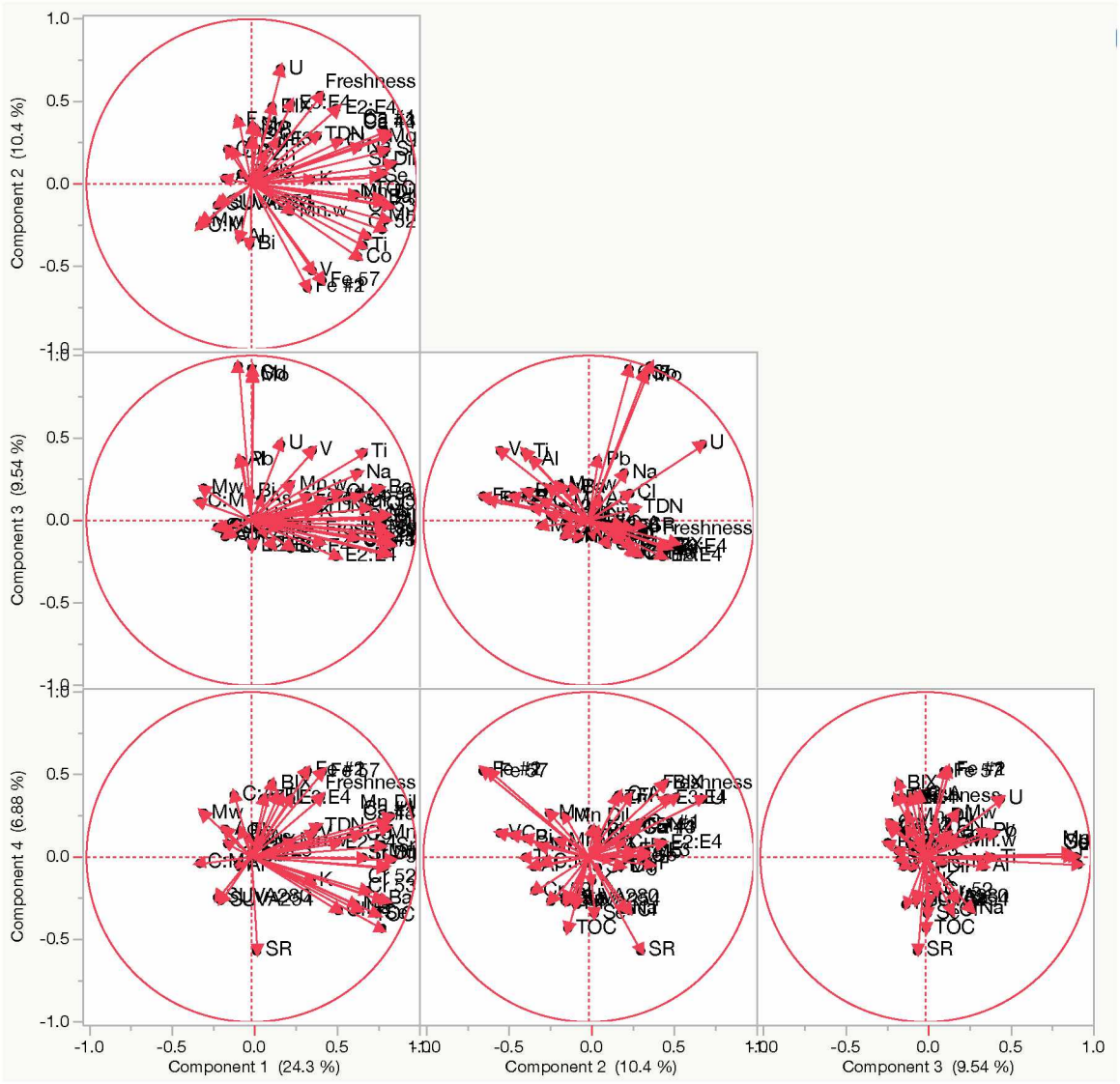

Figure 3.7: Principal Component Loading Plot for PCA OM

Principal component analysis loading matrix for metal concentrations and optical indices normalized using a z-score. A combination of PCA O and PCA M. Principal components 1 through 4 are represented as they explain at least 50% of the sample scores and Eigenvalues were determined significant through a Bartlett Test. Loading Matrix showcases which metals and optical indices correlate with each other through principal component analysis to represent each quadrant in the plots. Variables utilized in PCA M can be observed in Table 3.3. Abbreviations defined in Table 2.1 and 2.2.

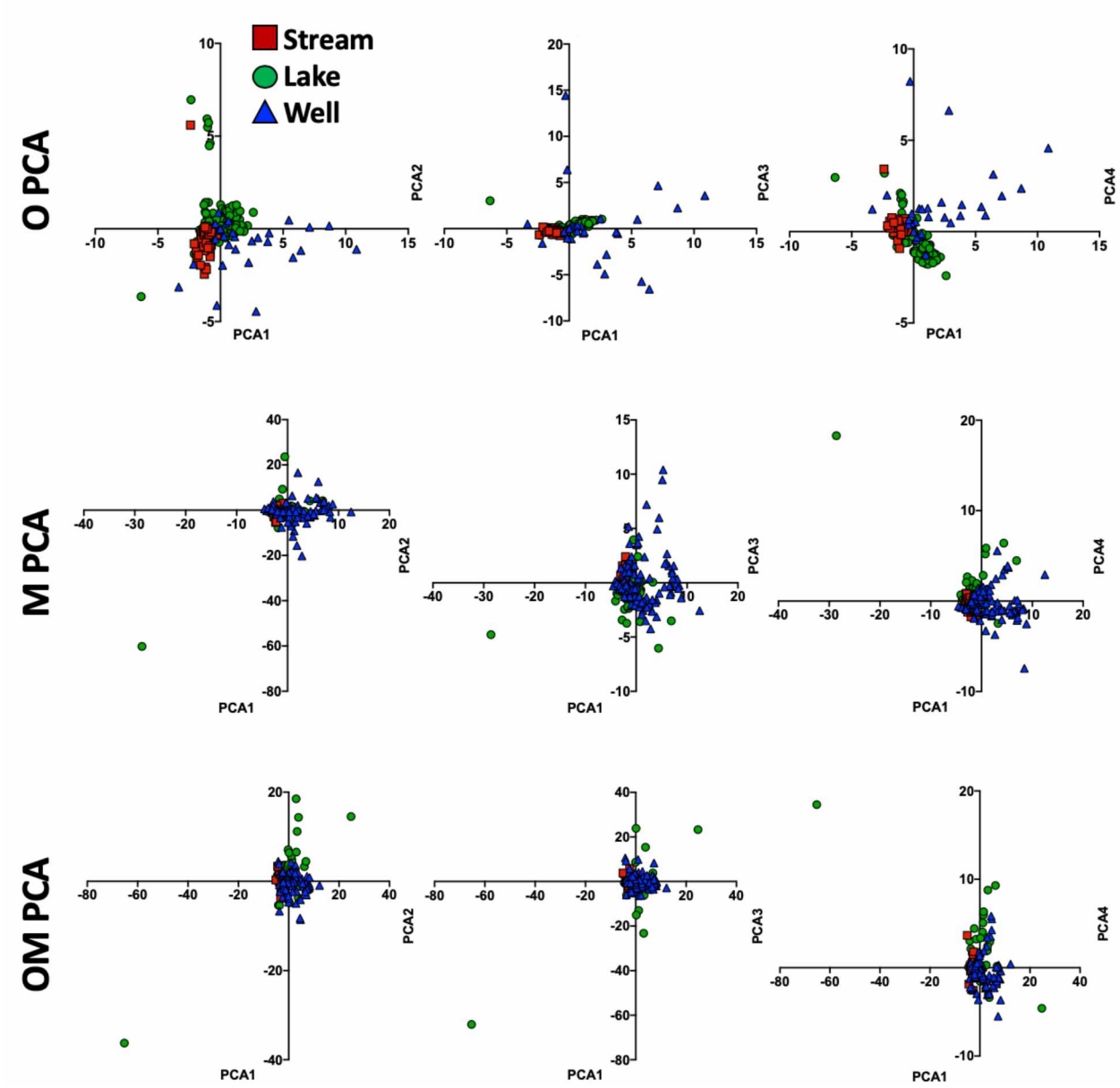

Figure 3.8: Principal Component Analysis Comparison of Water Type

Principal component matrix with water types denoted with different symbols from normalized data utilizing a z-score. All three PCA models are represented using component 1 as the x variable versus the additional components to represent all 4 components within a three-plot matrix.

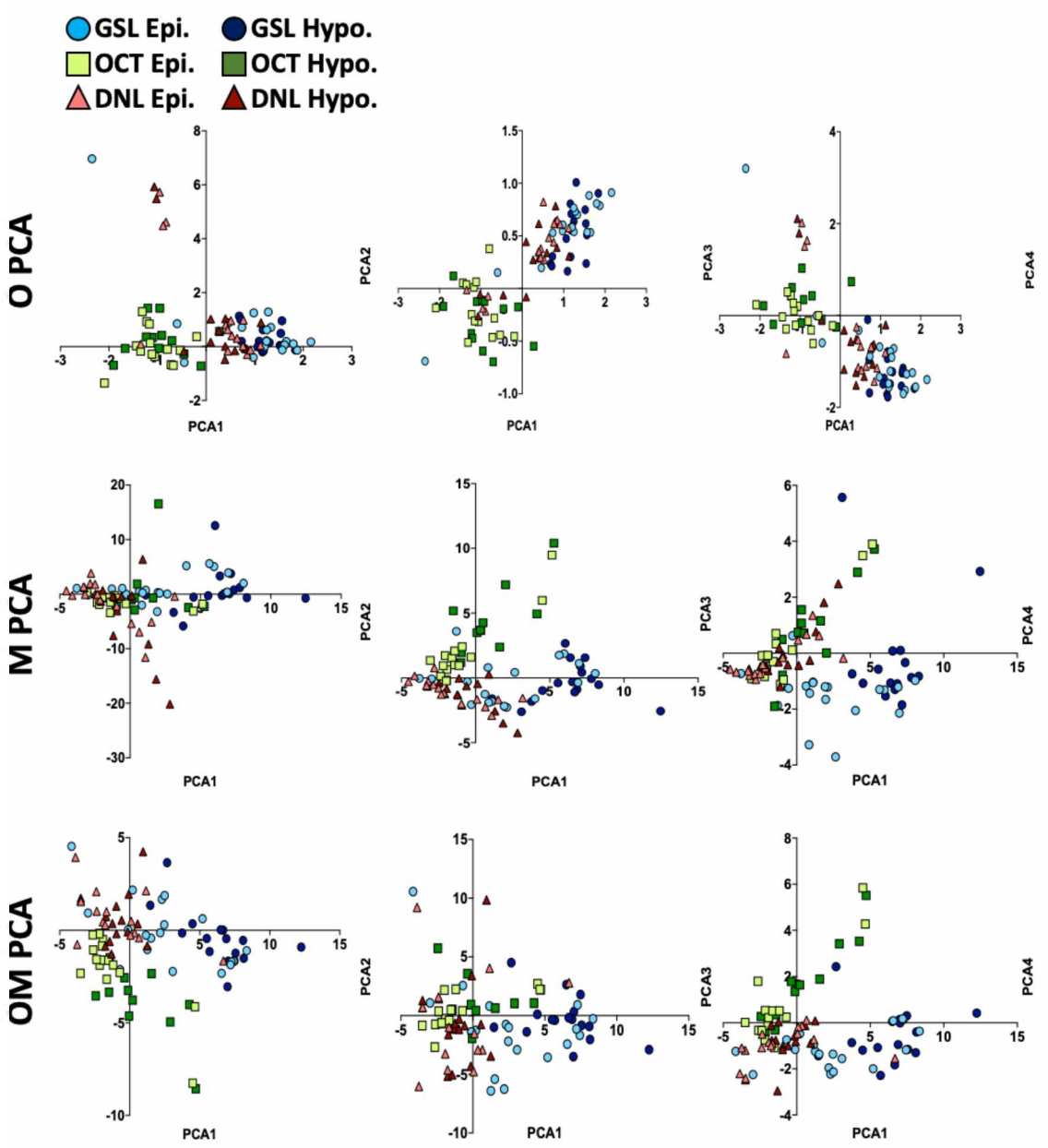

Figure 3.9: Principal Component Analysis Comparison of Thermokarst Lake Epilimnion and Hypolimnion

Principal component matrix thermokarst lake samples from epilimnion and hypolimnion from normalized data utilizing a z-score. All three PCA models are represented using component 1 as the x variable versus the additional components to represent all 4 components within a three-plot matrix. Abbreviations denoted in Table 3.1.

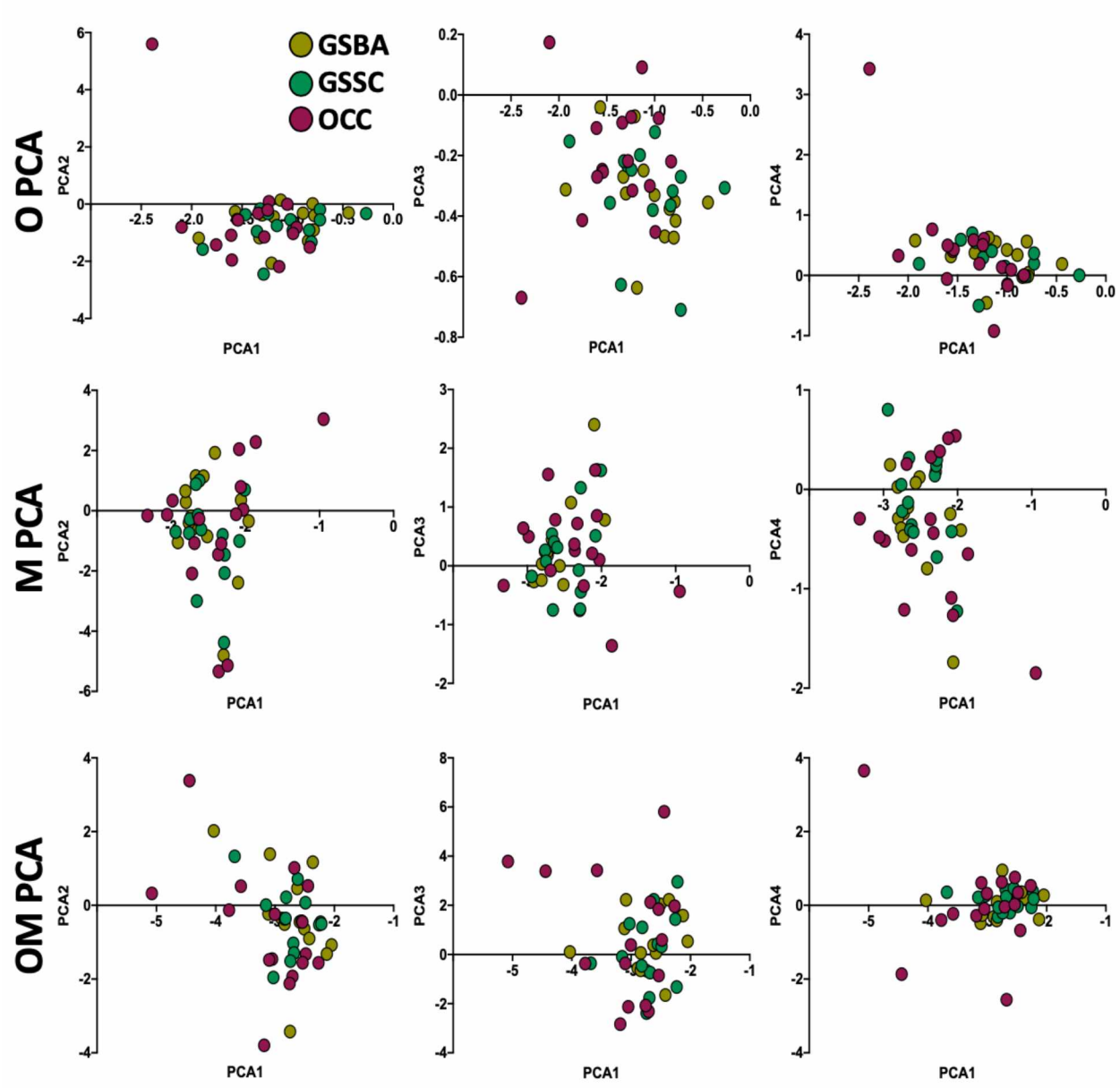

Figure 3.10: Principal Component Analysis Comparison of Streams

Principal component matrix with streams collected from 2016 to 2018 from normalized data utilizing a z-score. All three PCA models are represented using component 1 as the x variable versus the additional components to represent all 4 components within a three-plot matrix. Abbreviations are denoted in table 3.1.

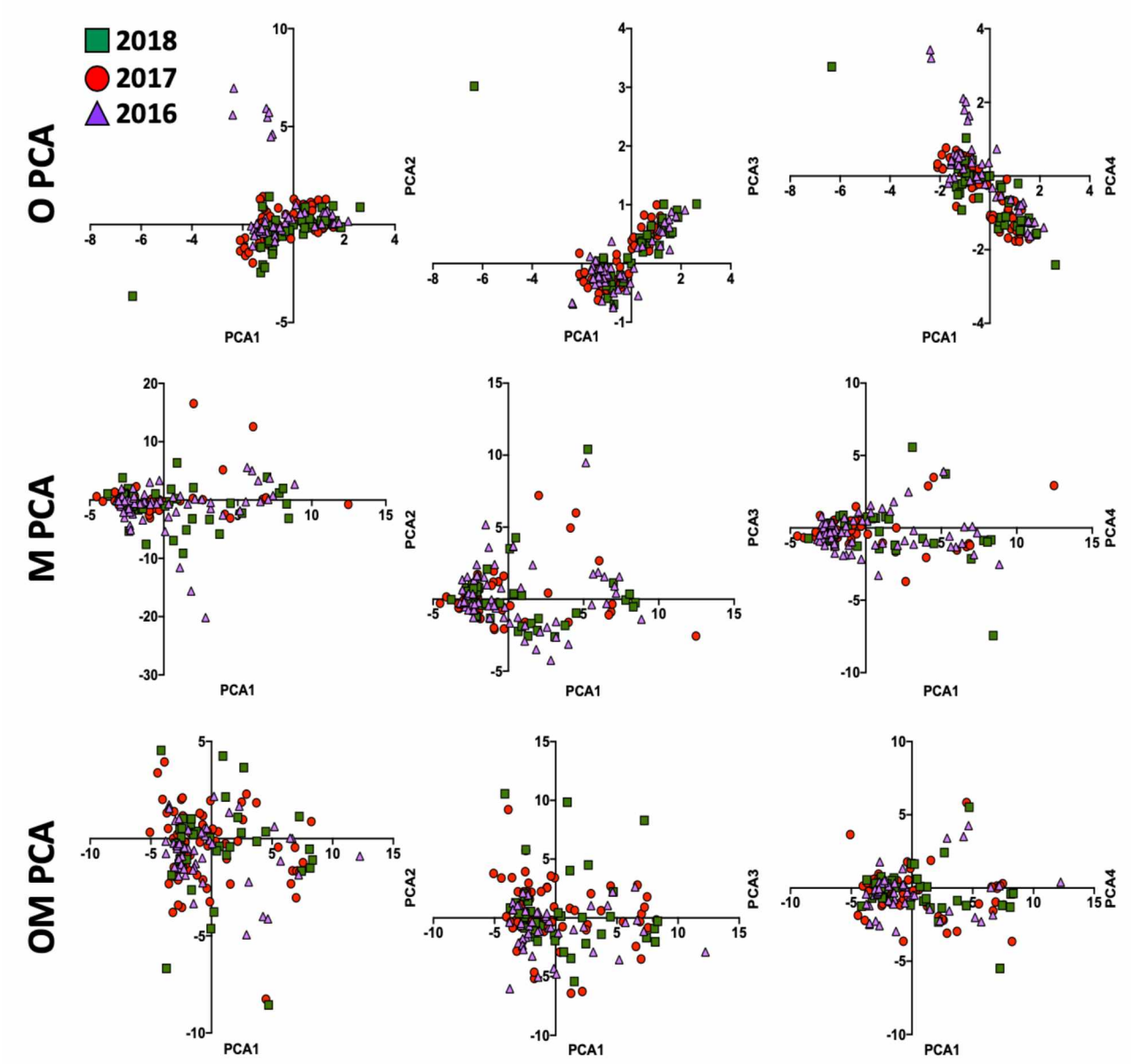

Figure 3.11: Principal Component Analysis Comparison of Years

Principal component matrix with all thermokarst lake and stream waters compiled and separated by years from normalized data utilizing a z-score. Wells were included in the initial PCA modeling but excluded from these loading matrices figures. All three PCA models are represented using component 1 as the x variable versus the additional components to represent all 4 components within a three-plot matrix.

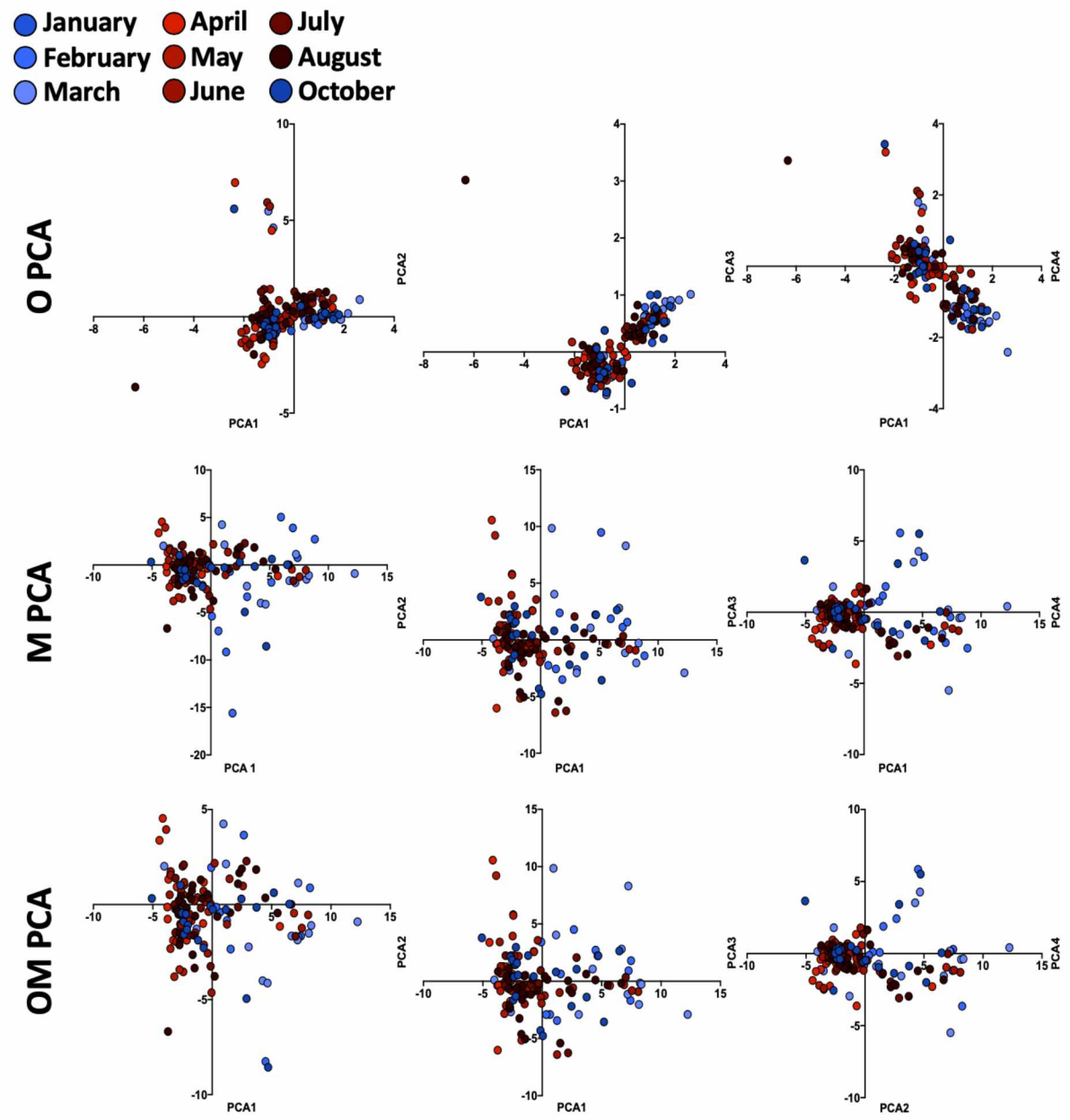

Figure 3.12: Principal Component Analysis Comparison of Months for Seasonality

Principal component matrix with thermokarst lake water samples from normalized data utilizing a z-score. All months included 2016, 2017, and 2018 years where applicable. Wells were included in the initial PCA modeling but excluded from these loading matrices figures All three PCA models are represented using component 1 as the x variable versus the additional components to represent all 4 components within a three-plot matrix.

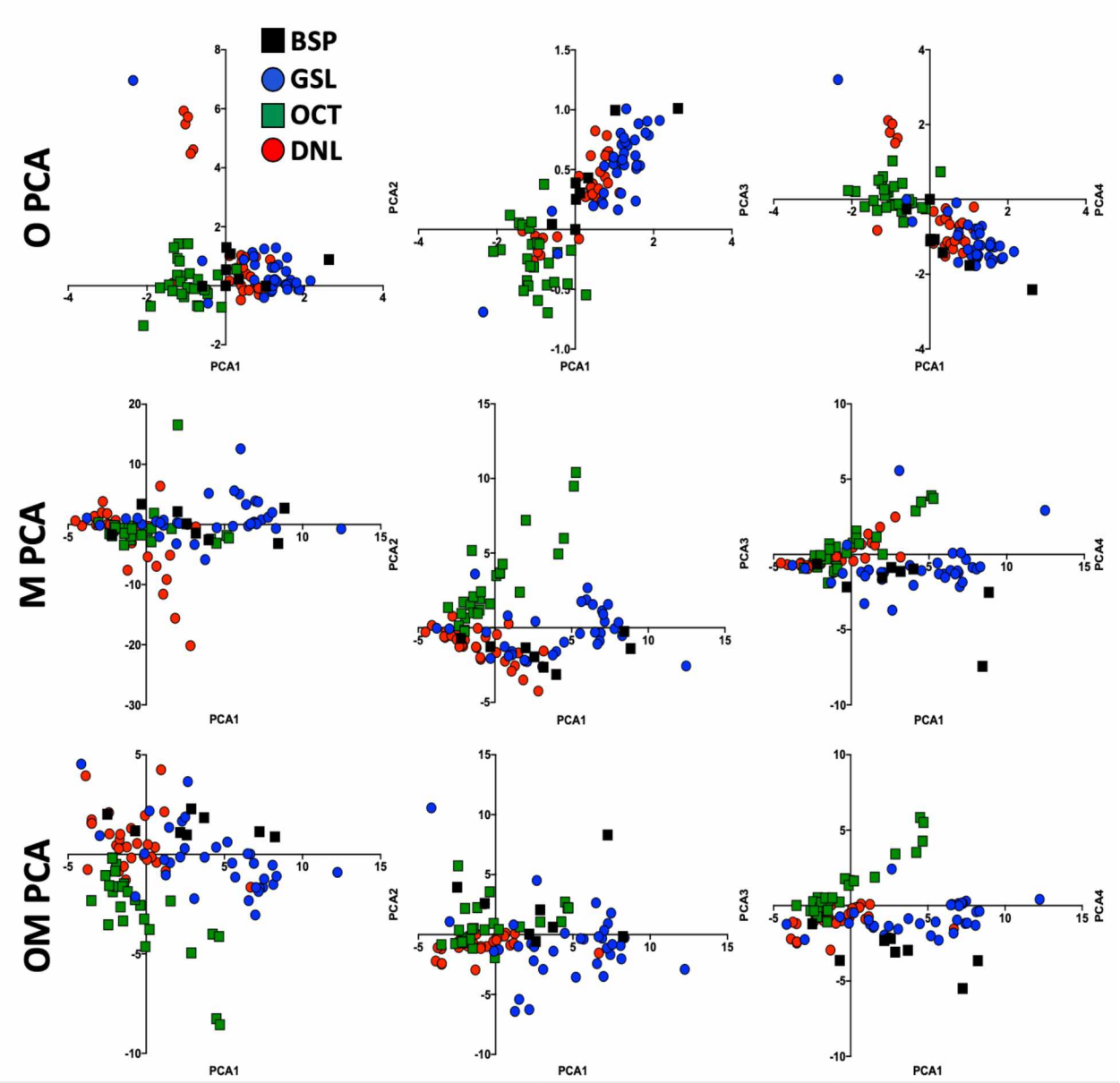

Figure 3.13: Principal Component Analysis Comparison of Permafrost Degradation

Principal component matrix with thermokarst lake samples separated based on permafrost degradation from normalized data using z-scores. All three PCA models are represented using component 1 as the x variable versus the additional components to represent all 4 components within a three-plot matrix. BSP was added to verify correlation observed in clustering of permafrost degradation types.

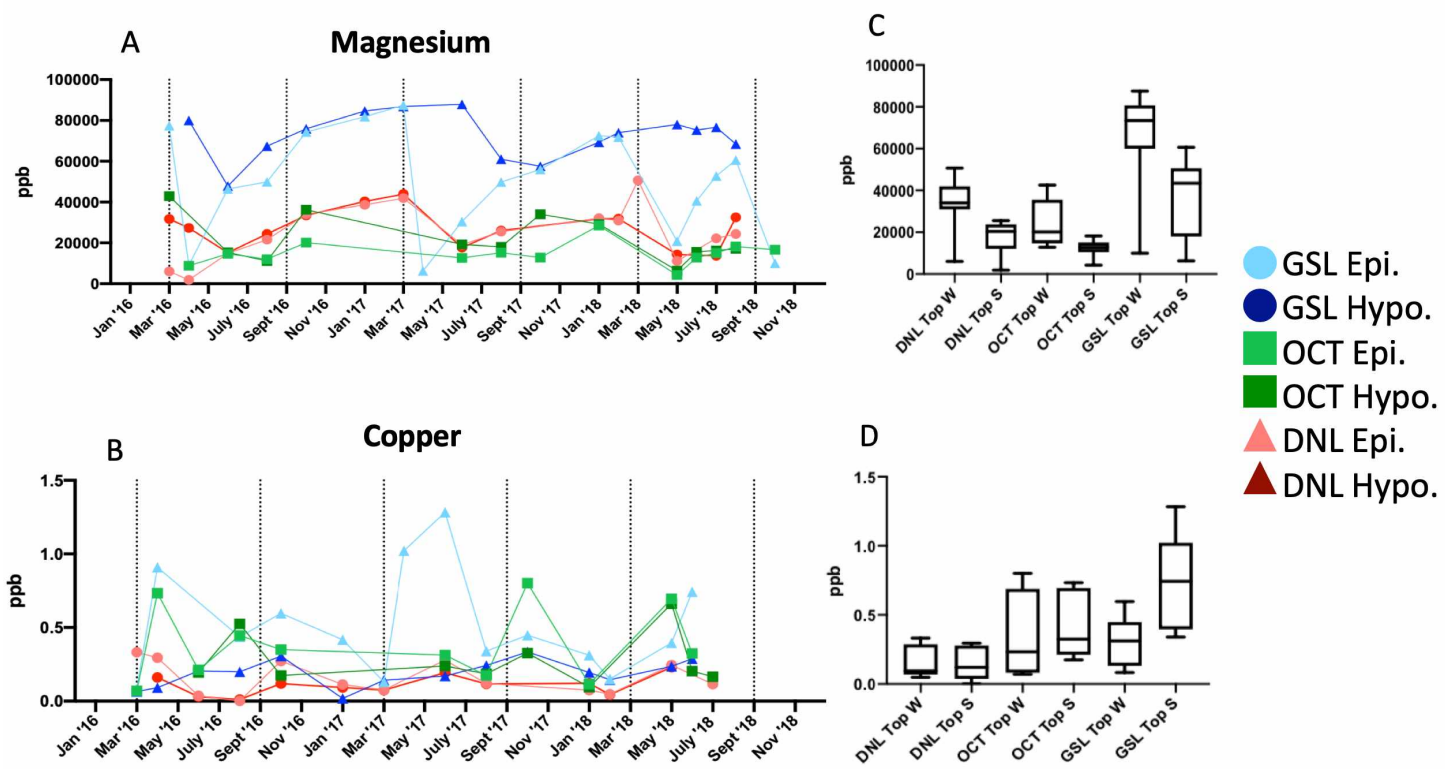

Figure 3.14: Seasonality Plots of Magnesium and Copper

Metal concentration seasonality graphs and associated box and whisker graphs for two select metals. Outliers were removed through a ROUT outliers test. Magnesium (A and C) is representative of metals that have a statistical increase in wintertime samples. Copper (B and D) is representative of metals that observe no statistical differences between winter and summer and are thus, classified as steady in concentration, with the exception of GSL epilimnion (top). Abbreviations for samples are denoted in Table 3.1, summer (S), and winter (W).

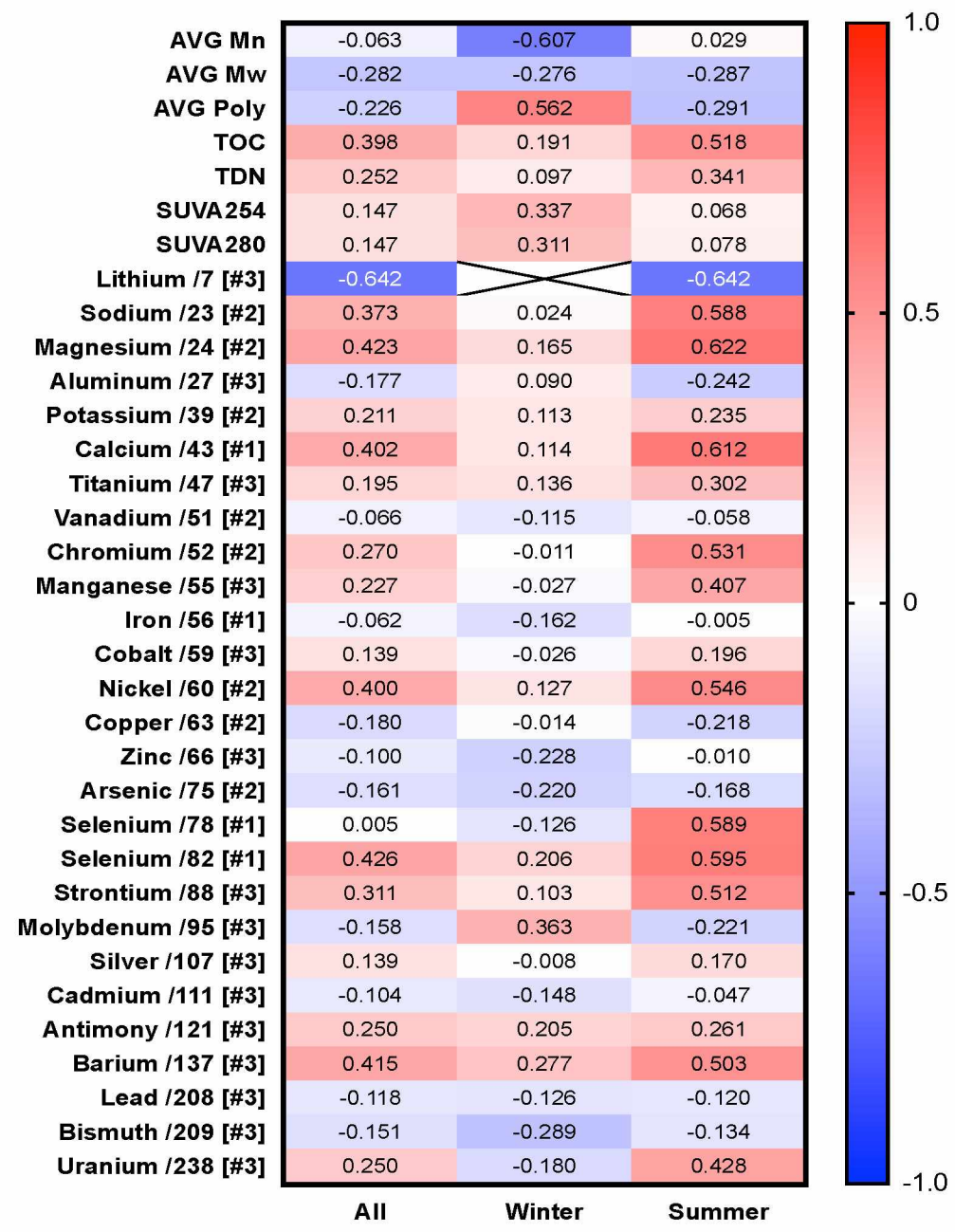

Figure 3.15: Pearson Linear Correlation Matrix for Chloride Relationships

Statistical positive and negative correlations observed between metals and chloride for summer, winter, and in total. Strong negative correlations are denoted by dark blue, while strong positive correlations are denoted by a dark red. These Pearson correlation values are denoted within each box with not enough samples marked with an X. Data utilized were obtained for number average molecular weight (AVG Mn), weight average molecular weight (Mw), polydispersity (Poly), total organic carbon (TOC), total dissolved nitrogen (TDN), specific UV absorbance values ($SUVA_{254}/SUVA_{280}$) equation found in Table 1.1, and metals numbers are associated with ICP-MS mode utilized for analysis.

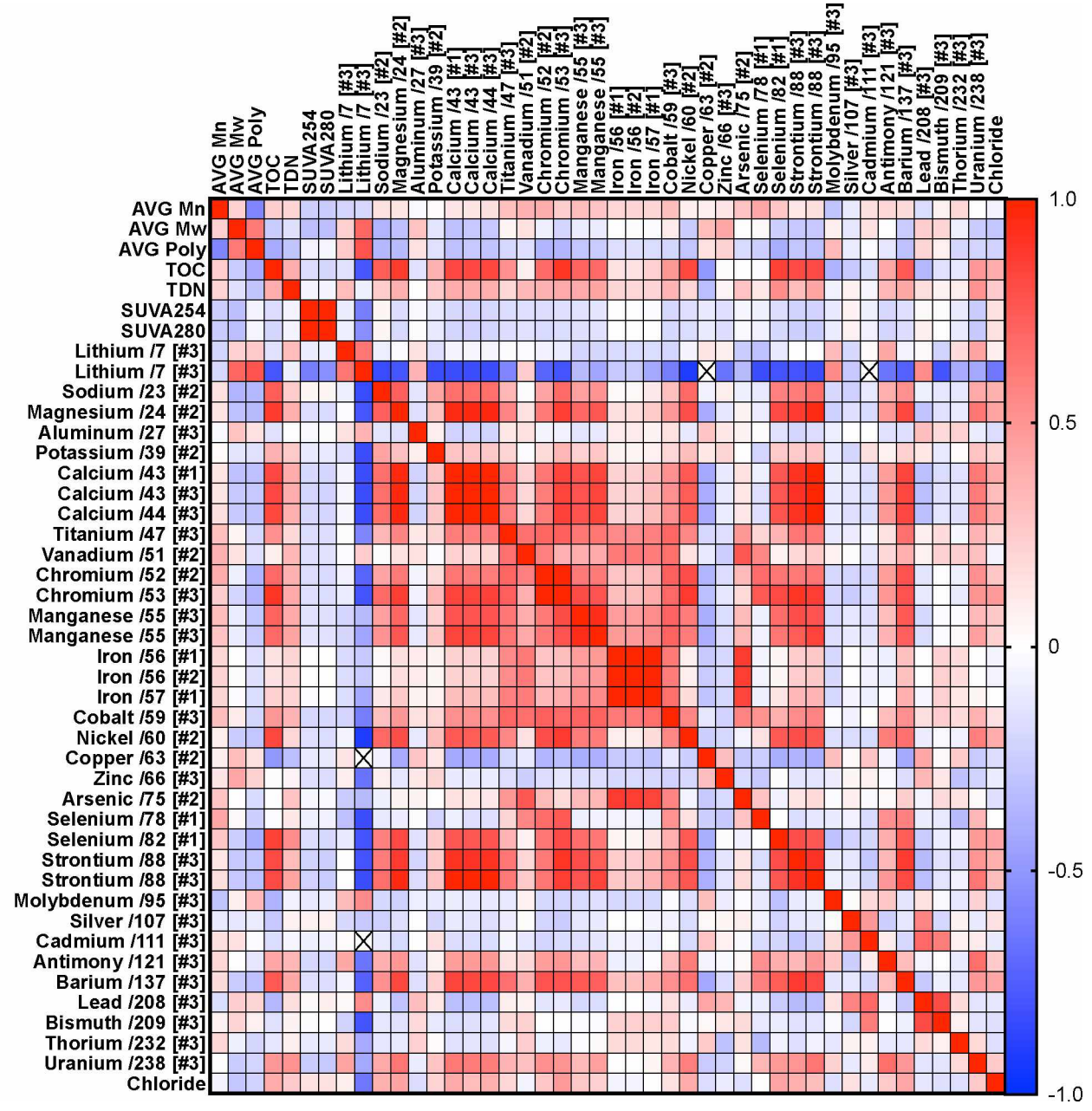

Figure 3.16: Pearson Correlation Matrix for all Metal to Metal Relationships

Statistical positive and negative correlations observed between metals within the cumulative sampling campaign. Strong negative correlations are denoted by dark blue, while strong positive correlations are denoted by a dark. These Pearson correlation values are denoted within each box with not enough samples marked with an X. Data utilized were obtained for number average molecular weight (Mn), weight average molecular weight (Mw), polydispersity (Poly), total organic carbon (TOC), total dissolved nitrogen (TDN), specific UV absorbance values ($SUVA_{254}/SUVA_{280}$) equation found in Table 1.1, and metals numbers are associated with ICP-MS mode utilized for analysis.

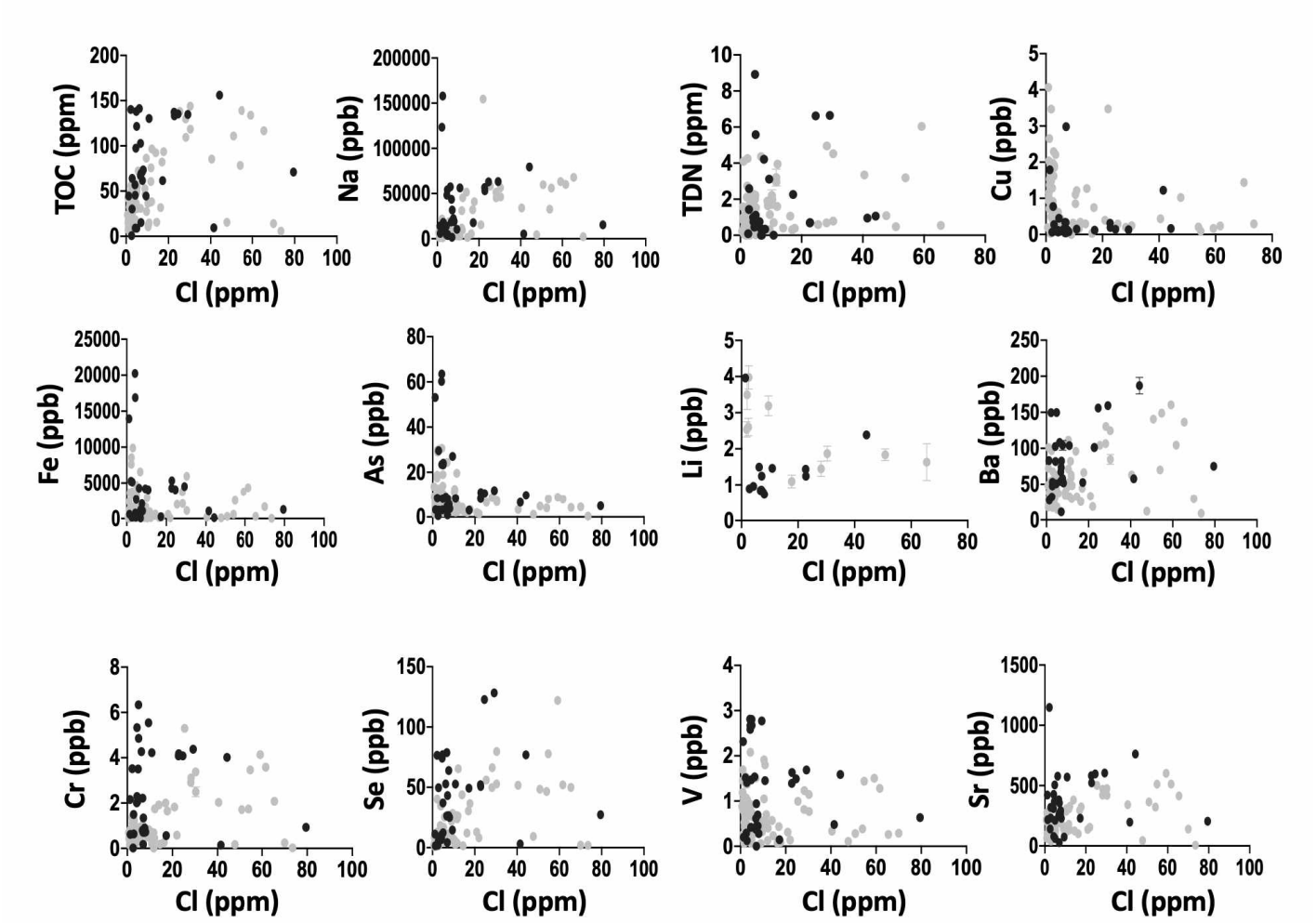

Figure 3.17: Metal – Chloride Relationship Graphs of Select Metals

Metal – chloride relationships determined by graphing all of the thermokarst lake and stream samples on an XY graph with the independent variable being Chloride. Black dots represent winter samples and grey dots represent summer samples. Abbreviations: total organic carbon (TOC) and total dissolved nitrogen (TDN).

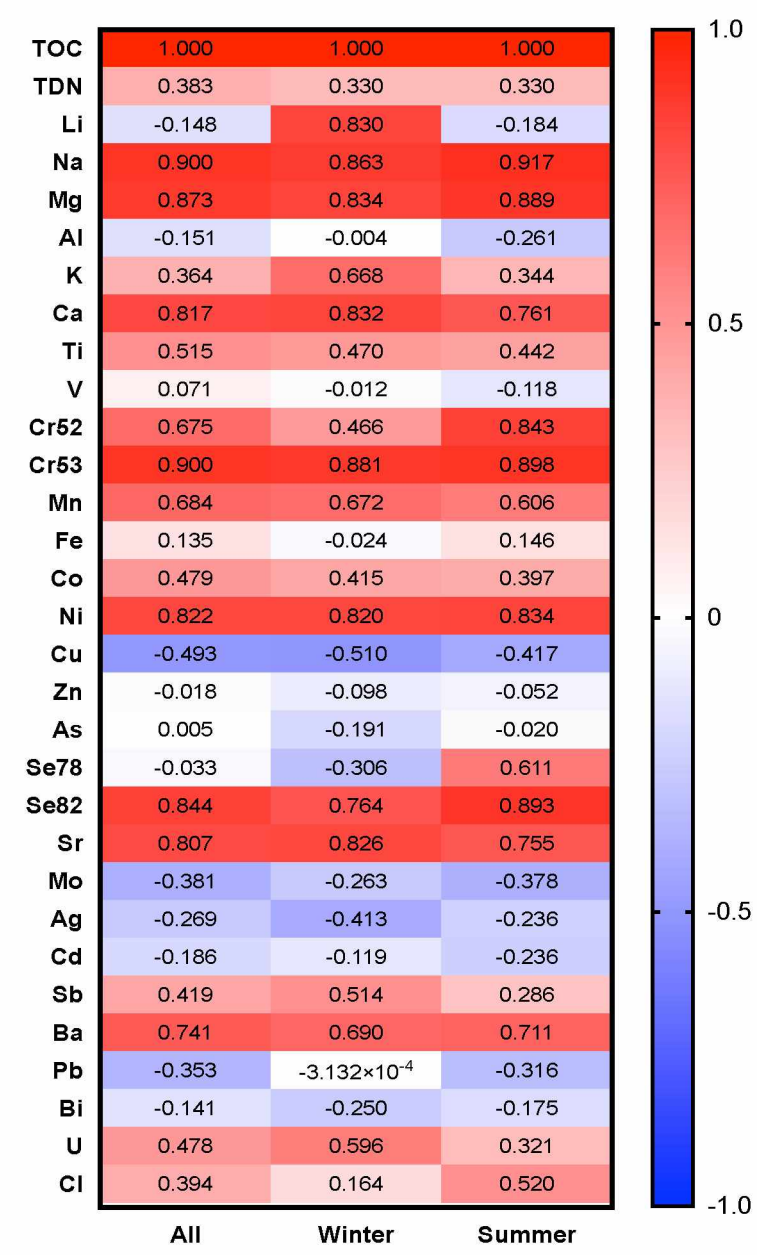

Figure 3.18: Pearson Correlation Matrix for Carbon Relationships

Statistical positive and negative correlations observed between metals and carbon for summer, winter, and in total. Strong negative correlations are denoted by dark blue, while strong positive correlations are denoted by a dark. These Pearson correlation values are denoted within each box. Data utilized were obtained from total organic carbon (TOC) and total dissolved nitrogen (TDN).

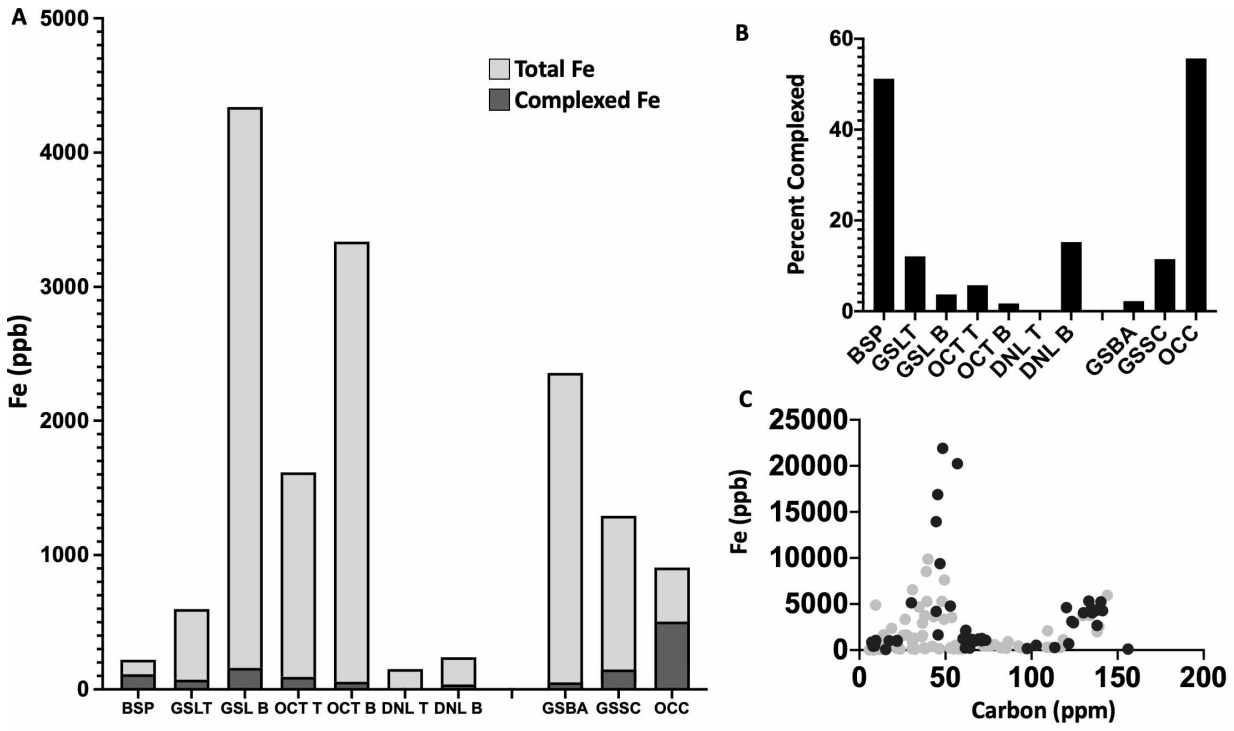

Figure 3.19: Iron to Carbon Relationship Graph and Complexation Percentage

(A) Represents the complexation concentration compared to the total iron concentration obtained using Field Flow Fractionation for complexed concentration and running on an ICP-MS for concentration values. (B) Represents the percentage of iron complexed to organic carbon and (C) is a depiction of the iron – carbon relationship using an XY scatterplot. Sample abbreviations found in table 3.1.

3.10. Tables:

Table 3.1: Sampling Site Location Details

General information about sampling locations and permafrost underlain percentage based on AEM data discussed in detail in Section 3.3.1. Map of sampling location is located in Figure 2.1.

Name	Condensed Name	Latitude (ºN)	Longitude (ºW)	Surface Area (m^2)	Max Depth (m)	Permafrost Degradation (%)
Goldstream Lake	GSL	64.916	-147.847	10,000	4.7	75-100%
Octopus Lake	OCT	64.907	-147.860	22,000	2	25-75%
Doughnut Lake	DNL	64.899	-147.908	34,000	3.8	0-25%
Blacksheep Pond	BSP	64.888	-147.920	540	0.5	100%
Goldstream Creek	GSBA	64.912	-147.832	N/A	N/A	50%
	GSSC	64.909	-147.948	N/A	N/A	50-75%
O'Connor Creek	OCC	64.915	-147.899	N/A	N/A	100%

Table 3.2: YSI Probe Data Compiled Averages

General water chemistry obtained through the use of a YSI probe. Averages were compiled on samples (Table 3.1) that utilized the probe, as some weather conditions limited the ability to measure. Average daily temperature was obtained at a weather station adjacent to GSL (Liljedahl, A., 2019). Error for each measurement was obtained from the standard deviation of probe measurements and denoted as ± values.

Summer	pH	+/-	Water Temperature (ºC)	+/-	Average Daily Temp (ºC)	+/-	Specific Conductivity ($\mu S\ cm^{-3}ºC^{-1}$)	+/-	Conductivity ($\mu S\ cm^{-1}$)	+/-	DO ($mg\ L^{-1}$)	+/-	DO (%)	+/-
GSL Epi.	7.70	0.85	14.49	5.89	8.97	4.17	281.88	426.08	208.59	315.05	6.09	2.43	61%	26%
GSL Hypo.	7.10	0.45	8.35	3.24	10.54	2.84	318.48	587.42	221.28	410.28	1.46	2.53	5%	7%
OCT Epi.	7.34	1.02	13.69	6.62	9.72	3.64	77.05	117.12	58.80	94.57	5.47	1.67	53%	19%
OCT Hypo.	7.01	0.29	11.33	4.11	10.54	2.84	117.47	229.66	87.26	169.08	0.61	0.61	5%	6%
DNL Epi.	7.74	1.07	14.91	5.99	9.66	3.31	149.71	219.35	111.42	156.69	5.40	2.51	54%	28%
DNL Hypo.	6.98	0.53	13.41	5.56	9.66	3.31	170.66	240.02	124.88	174.22	2.66	5.67	5%	5%
BSP	7.62	0.07	15.80	3.54	8.30	6.07	1.02	0.36	0.84	0.31	2.31	1.88	22%	17%
GSBA	7.71	0.34	11.21	3.96	11.07	3.41	168.08	393.35	127.25	296.51	9.41	2.03	89%	6%
GSSC	7.10	0.49	9.71	5.94	8.28	6.16	181.93	390.14	133.22	295.20	10.00	2.23	85%	10%
OCC	7.71	0.25	4.86	3.10	9.15	5.37	186.42	444.53	129.69	269.33	11.28	3.15	96%	1%
Winter														
GSL Epi.	6.76	0.92	1.14	1.10	-12.53	11.28	513.59	640.97	360.67	399.89	14.82	17.78	28%	30%
GSL Hypo.	6.65	0.76	2.73	1.99	-11.95	12.02	595.89	663.09	433.00	423.64	7.08	12.79	13%	13%
OCT Epi.	7.31	0.34	1.27	1.05	-6.35	6.52	14.73	28.84	145.00	306.09	5.70	5.08	34%	26%
OCT Hypo.	7.19	0.18	3.03	2.19	-7.55	6.86	284.39	491.56	296.31	346.73	2.09	2.06	16%	16%
DNL Epi.	6.69	0.91	0.77	0.73	-14.37	10.53	367.13	337.35	177.43	166.70	21.53	23.25	9%	3%
DNL Hypo.	6.80	0.48	2.08	1.26	-14.73	11.49	367.73	338.43	239.36	188.44	16.12	16.98	21%	37%
BSP	7.14	N/A	-0.10	N/A	-17.64	N/A	0.08	N/A	0.15	N/A	1.76	N/A	13%	N/A
GSBA	6.75	1.71	1.21	1.33	-6.94	6.16	76.83	132.65	39.76	68.63	49.50	52.60	78%	15%
GSSC	7.01	0.62	0.77	0.97	-7.12	7.53	5.51	9.09	2.84	4.47	13.33	N/A	94%	N/A
OCC	7.06	0.93	-0.13	0.15	-7.12	7.53	19.19	32.74	9.77	16.66	13.40	N/A	92%	N/A

Table 3.3: Principal Component Analysis Data Points Analyzed

Data obtained through instrumentation that was utilized in each Principal Component Analysis model after obtaining z-scores for all concentrations and values Equation 1. Number Average Molecular Weight (Mn.w),Weight Average Molecular Weight (Mw), total organic carbon (TOC), total dissolved nitrogen (TDN), metals denoted with Dil were diluted 100 times, and the rest of abbreviations are found in Table 1.1 and Table 1.2. Numbers are associated with ICP-MS mode utilized for metal analysis.

PCA O	PCA OM			PCA M	
Mn.w	Mn.w	Mg	Cu	TOC	Co
Mw	Mw	Al	Zn	TDN	Ni
TOC	TOC	K	As	Na	Cu
TDN	TDN	Ca #1	Se	Mg	Zn
SR	SR	Ca #3	Sr	Al	As
E2:E3	E2:E3	Ca 44	Sr Dil	K	Se
E2:E4	E2:E4	Ti	Mo	Ca #1	Sr
E3:E4	E3:E4	V	Ag	Ca #3	Sr Dil
BIX	BIX	Cr 52	Cd	Ca 44	Mo
C:A	C:A	Cr 53	Sb	Ti	Ag
C:M	C:M	Mn	Ba	V	Cd
FI	FI	Mn Dil	Pb	Cr 52	Sb
Freshness	Freshness	Fe #1	Bi	Cr 53	Ba
HIX	HIX	Fe #2	U	Mn	Pb
SUVA254	SUVA254	Fe 57	F	Mn Dil	Bi
SUVA280	SUVA280	Co	Cl	Fe #1	U
	Na	Ni		Fe #2	F
				Fe 57	Cl

Table 3.4: Principal Component Eigenvalues

The percentage of how much of the data is explained by each component in each individual PCA model. All components listed were deemed statistically significant through a Barlett Test run by JMP statistical software. The first 4 principal components were used to observed close to 50% data explained.

Component	PCA O	PCA OM	PCA M
1	21.8%	24.3%	31.7%
2	15.1%	10.4%	13.3%
3	13.5%	9.5%	11.0%
4	11.1%	6.9%	7.4%

Table 3.5: ANOVA Results and Epilimnion Averages

Statistical comparison of metals with comparison to thermokarst lake permafrost degradation in the epilimnions through an ANOVA statistical test. With a p-value of <0.0500 as statistically significant with the average metal concentrations denoted in ppb for each metal. Colors determines which thermokarst lake has the highest (red), medium (yellow), and low (green) concentration for metals that observed statistical difference between thermokarst lake epilimnion. Asterisk (*) denotes Welch ANOVA p-values used, when Brown-Forsythe test determined the standard deviation variance between samples were different requiring the use of a Welch ANOVA. Sample average was determined for metal concentrations over three-year period from 2016 – 2018. Where error in the average was determined through standard deviation of all sample values averaged and is denoted with ±. Sample abbreviations are denoted in Table 3.1.

Sample	Na ppb	+/-	Mg ppb	+/-	Al ppb	+/-	K ppb	+/-	Ca ppb	+/-	Ti ppb	+/-
N	45*		47*		35*		43		45		46	
GSL Epi.	37485.5	19982.3	49905.9	25917.3	36.2	62.6	5080.3	5012.8	61264.7	29877.5	4.1	2.8
OCT Epi.	8425.4	3314.9	16729.6	9263.3	46.2	29.6	4141.5	8342.5	27291.3	16932.3	3.7	2.9
DNL Epi.	14521.4	8018.8	25001.6	13478.8	9.2	10.0	2694.6	1580.2	38440.7	20235.8	1.1	0.9

	V ppb	+/-	Cr ppb	+/-	Mn ppb	+/-	Fe ppb	+/-	Co ppb	+/-	Ni ppb	+/-
N	43		47*		46		47*		43		43*	
GSL Epi.	0.8	0.8	2.5	1.7	602.5	722.3	1255.7	1616.4	0.6	0.3	7.2	3.9
OCT Epi.	1.1	0.9	1.3	1.3	380.2	515.7	5478.1	5737.8	0.6	0.3	1.9	0.5
DNL Epi.	0.2	0.2	0.6	0.3	325.9	439.5	513.4	612.7	0.2	0.1	1.5	1.0

	Cu ppb	+/-	Zn ppb	+/-	As ppb	+/-	Se78 ppb	+/-	Se82 ppb	+/-	Sr ppb	+/-
N	38		22		47*		33*		40*		46*	
GSL Epi.	0.5	0.4	127.6	395.0	6.0	5.3	0.8	1.5	52.6	37.2	323.2	164.6
OCT Epi.	0.4	0.3	3.0	4.0	19.2	19.2	0.9	1.9	8.5	4.3	155.1	101.6
DNL Epi.	0.4	0.8	7.8	9.5	3.1	1.5	0.2	0.1	27.3	19.0	165.0	100.7

	Mo ppb	+/-	Ag ppb	+/-	Cd ppb	+/-	Sb ppb	+/-	Ba ppb	+/-	Pb ppb	+/-
N	40*		24		25		39*		45		17	
GSL Epi.	0.4	0.2	0.1	0.1	0.0	0.0	0.5	0.2	74.3	42.5	0.1	0.3
OCT Epi.	0.2	0.1	0.1	0.1	0.0	0.0	0.2	0.1	48.3	23.2	0.1	0.0
DNL Epi.	0.1	0.1	0.1	0.1	0.0	0.0	0.2	0.1	41.6	28.7	0.1	0.2

	Bi ppb	+/-	U ppb	+/-
N	30		28*	
GSL Epi.	0.2	0.3	0.7	0.3
OCT Epi.	0.1	0.2	0.1	0.0
DNL Epi.	0.2	0.2	0.1	0.1

P-Value	Concentration
<0.0001	High
<0.0010	Medium
<0.0100	Low
<0.0500	

Table 3.6: ANOVA Results and Hypolimnion Averages

Statistical comparison of metals with comparison to thermokarst lake permafrost degradation in the hypolimnions through an ANOVA statistical test. With a p-value of <0.0500 as statistically significant with the average metal concentrations denoted in ppb for each metal. Colors determines which thermokarst lake has the highest (red), medium (yellow), and low (green) concentration for metals that observed statistical difference between thermokarst lake hypolimnion. Asterisk (*) denotes Welch ANOVA p-values used, when Brown-Forsythe test determined the standard deviation variance between samples were different requiring the use of a Welch ANOVA. Sample average was determined for metal concentrations over three-year period from 2016 – 2018. Where error in the average was determined through standard deviation of all sample values averaged and is denoted with ±. Sample abbreviations are denoted in Table 3.1.

Sample	Na ppb	+/-	Mg ppb	+/-	Al ppb	+/-	K ppb	+/-	Ca ppb	+/-	Ti ppb	+/-
N	41		41		35		41		40		42	
GSL Hypo.	57823.5	19306.2	79102.4	27650.3	9.9	10.9	7408.3	7206.7	95851.6	29036.7	5.7	2.4
OCT Hypo.	9680.3	4543.6	21814.4	11132.6	57.0	98.0	2999.5	2211.6	35120.2	17137.7	5.1	2.4
DNL Hypo.	14141.8	6196.6	27452.8	9512.7	7.7	7.2	2771.3	1108.1	40799.6	13776.2	1.6	1.1

	V ppb	+/-	Cr ppb	+/-	Mn ppb	+/-	Fe ppb	+/-	Co ppb	+/-	Ni ppb	+/-
N	39		41*		40*		42*		42*		40	
GSL Hypo.	1.2	0.4	3.5	0.9	1870.8	701.8	3331.5	1696.0	1.0	0.2	9.8	1.4
OCT Hypo.	1.6	1.0	1.4	0.7	769.3	435.9	8011.5	5549.6	1.0	0.3	2.2	1.4
DNL Hypo.	0.5	0.3	0.6	0.2	493.7	393.3	739.6	589.6	0.3	0.1	1.9	0.9

	Cu ppb	+/-	Zn ppb	+/-	As ppb	+/-	Se78 ppb	+/-	Se82 ppb	+/-	Sr ppb	+/-
N	32		28		40*		31*		39*		41	
GSL Hypo.	0.2	0.1	595.0	2050.7	9.5	6.0	0.6	0.2	69.5	29.8	532.6	187.5
OCT Hypo.	0.3	0.2	1.7	2.1	29.3	17.3	0.2	0.2	9.7	5.8	212.5	107.2
DNL Hypo.	0.1	0.1	4.0	4.6	5.8	4.2	0.2	0.1	31.6	16.0	180.1	67.8

	Mo ppb	+/-	Ag ppb	+/-	Cd ppb	+/-	Sb ppb	+/-	Ba ppb	+/-	Pb ppb	+/-
N	36		21		21		38		42		16	
GSL Hypo.	0.5	0.3	0.0	0.0	0.0	0.0	0.8	0.5	104.5	41.8	0.1	0.1
OCT Hypo.	0.3	0.2	0.1	0.2	0.0	0.0	0.2	0.1	62.0	19.6	0.2	0.2
DNL Hypo.	0.2	0.2	0.1	0.1	0.0	0.0	0.4	0.4	58.7	24.1	0.0	0.0

	Bi ppb	+/-	U ppb	+/-
N	25*		30	
GSL Hypo.	0.1	0.1	0.8	0.4
OCT Hypo.	0.3	0.3	0.2	0.3
DNL Hypo.	0.1	0.1	0.1	0.1

P-Value	Concentration
<0.0001	High
<0.0010	Medium
<0.0100	Low
<0.0500	

Table 3.7: ANOVA Results and Epilimnion Averages with BSP

Statistical comparison of metals with comparison to thermokarst lake permafrost degradation in the hypolimnions and BSP added to observe another 100% thermokarst lake through an ANOVA statistical test. With a p-value of <0.0500 as statistically significant with the average metal concentrations denoted in ppb for each metal. Colors determines which thermokarst lake has the highest (red), medium (yellow), low (green), lowest (blue) concentration for metals that observed statistical difference between thermokarst lake epilimnion including BSP. Asterisk (*) denotes Welch ANOVA p-values used, when Brown-Forsythe test determined the standard deviation variance between samples were different requiring the use of a Welch ANOVA. Sample average was determined for metal concentrations over three-year period from 2016 – 2018. Where error in the average was determined through standard deviation of all sample values averaged and is denoted with ±. Sample abbreviations are denoted in Table 3.1.

Sample	Na ppb	+/-	Mg ppb	+/-	Al ppb	+/-	K ppb	+/-	Ca ppb	+/-	Ti ppb	+/-
N	53*		55*		43*		50		53*		54	
BSP	70617.4	39592.0	66911.1	44908.0	34.4	33.9	6675.0	6914.3	59292.1	35739.7	6.1	5.1
GSL Epi.	37485.5	19982.3	49905.9	25917.3	36.2	62.6	5080.3	5012.8	61264.7	29877.5	4.1	2.8
OCT Epi.	8425.4	3314.9	16729.6	9263.3	46.2	29.6	4141.5	8342.5	27291.3	16932.3	3.7	2.9
DNL Epi.	14521.4	8018.8	25001.6	13478.8	9.2	10.0	2694.6	1580.2	38440.7	20235.8	1.1	0.9

	V ppb	+/-	Cr ppb	+/-	Mn ppb	+/-	Fe ppb	+/-	Co ppb	+/-	Ni ppb	+/-
N	51		55		54		55*		51		51*	
BSP	0.7	0.6	2.1	1.4	222.8	219.0	216.1	128.3	0.6	0.4	6.0	3.1
GSL Epi.	0.8	0.8	2.5	1.7	602.5	722.3	1255.7	1616.4	0.6	0.3	7.2	3.9
OCT Epi.	1.1	0.9	1.3	1.3	380.2	515.7	5478.1	5737.8	0.6	0.3	1.9	0.5
DNL Epi.	0.2	0.2	0.6	0.3	325.9	439.5	513.4	612.7	0.2	0.1	1.5	1.0

	Cu ppb	+/-	Zn ppb	+/-	As ppb	+/-	Se78 ppb	+/-	Se82 ppb	+/-	Sr ppb	+/-
N	44		28		55*		41		52*		54	
BSP	0.8	1.3	6.2	8.0	5.2	3.1	0.5	0.3	67.7	67.8	271.1	140.3
GSL Epi.	0.5	0.4	127.6	395.0	6.0	5.3	0.8	1.5	52.6	37.2	323.2	164.6
OCT Epi.	0.4	0.3	3.0	4.0	19.2	19.2	0.9	1.9	8.5	4.3	155.1	101.6
DNL Epi.	0.4	0.8	7.8	9.5	3.1	1.5	0.2	0.1	27.3	19.0	165.0	100.7

	Mo ppb	+/-	Ag ppb	+/-	Cd ppb	+/-	Sb ppb	+/-	Ba ppb	+/-	Pb ppb	+/-
N	48		24		30		47*		53*		23	
BSP	0.2	0.2	0.0	N/A	0.0	0.0	0.7	0.4	133.1	114.7	0.1	0.1
GSL Epi.	0.4	0.2	0.1	0.1	0.0	0.0	0.5	0.2	74.3	42.5	0.1	0.3
OCT Epi.	0.2	0.1	0.1	0.1	0.0	0.0	0.2	0.1	48.3	23.2	0.1	0.0
DNL Epi.	0.1	0.1	0.1	0.1	0.0	0.0	0.2	0.1	41.6	28.7	0.1	0.2

	Bi ppb	+/-	U ppb	+/-
N	34		36*	
BSP	0.1	0.1	0.6	0.3
GSL Epi.	0.2	0.3	0.7	0.3
OCT Epi.	0.1	0.2	0.1	0.0
DNL Epi.	0.2	0.2	0.1	0.1

P-Value	Concentration
<0.0001	High
<0.0010	Medium
<0.0100	Low
<0.0500	Lowest

Table 3.8: ANOVA Results and Stream Averages

Statistical comparison of metals with comparison to stream sampling locations through an ANOVA statistical test. With a p-value of <0.0500 as statistically significant with the average metal concentrations denoted in ppb for each metal. Colors determines which thermokarst lake has the highest (red), medium (yellow), and low (green) concentration for metals that observed statistical difference between streams. Asterisk (*) denotes Welch ANOVA p-values used, when Brown-Forsythe test determined the standard deviation variance between samples were different requiring the use of a Welch ANOVA. Sample average was determined for metal concentrations over three-year period from 2016 – 2018. Where error in the average was determined through standard deviation of all sample values averaged and is denoted with ±. Sample abbreviations are denoted in Table 3.1.

Sample	Na ppb	+/-	Mg ppb	+/-	Al ppb	+/-	K ppb	+/-	Ca ppb	+/-	Ti ppb	+/-
N	40		42		38		38		42		42	
GSBA	4527.8	2939.1	8265.9	2825.6	28.8	23.8	1754.5	679.8	23135.2	4831.9	2.1	0.9
GSSC	5152.9	2970.4	10062.3	2100.1	28.4	28.4	2126.6	2026.2	24154.8	5517.9	2.3	0.9
OCC	21813.2	46891.2	22014.3	6321.2	39.1	34.0	3035.4	5417.3	19992.4	5784.2	2.9	1.1

	V ppb	+/-	Cr ppb	+/-	Mn ppb	+/-	Fe ppb	+/-	Co ppb	+/-	Ni ppb	+/-
N	42		40		42		41		38		37	
GSBA	0.7	0.6	0.8	1.4	113.6	52.1	889.7	454.6	0.5	0.3	2.2	1.2
GSSC	0.9	0.6	0.7	1.4	109.9	59.3	1055.6	241.0	0.4	0.2	1.8	1.2
OCC	1.2	0.6	0.7	1.2	80.5	34.4	621.1	297.4	0.4	0.2	1.7	0.9

	Cu ppb	+/-	Zn ppb	+/-	As ppb	+/-	Se78 ppb	+/-	Se82 ppb	+/-	Sr ppb	+/-
N	36		17		40		21		45		40	
GSBA	1.7	0.6	4.0	5.9	5.7	5.0	1.0	2.1	2.5	1.4	146.8	38.3
GSSC	1.6	0.6	2.7	2.4	6.6	5.0	1.0	2.1	2.9	1.7	149.0	42.5
OCC	1.9	1.1	7.4	7.9	3.9	6.1	0.6	1.7	3.6	3.4	95.7	30.4

	Mo ppb	+/-	Ag ppb	+/-	Cd ppb	+/-	Sb ppb	+/-	Ba ppb	+/-	Pb ppb	+/-
N	39		22		24		39		39		16	
GSBA	1.2	0.3	0.1	0.3	0.0	0.0	0.4	0.1	31.5	5.6	0.2	0.2
GSSC	1.0	0.3	0.1	0.2	0.0	0.0	0.4	0.1	31.8	9.1	0.2	0.1
OCC	0.3	0.2	0.1	0.1	0.0	0.0	0.4	0.2	24.0	4.9	0.2	0.1

	Bi ppb	+/-	U ppb	+/-
N	18		32	
GSBA	0.2	0.3	0.3	0.2
GSSC	0.1	0.1	0.3	0.3
OCC	0.2	0.2	0.4	0.3

P-Value	Concentration
<0.0001	High
<0.0010	Medium
<0.0100	Low
<0.0500	

Table 3.9: T-Test to Determine Differences Between Epilimnion and Hypolimnion for Trace Metals

Statistical T-Test to determine which metals observed concentration differences between the epilimnion (epi.) and hypolimnion (hypo.) over three years of sample collection; 2016 – 2018. P-Values < 0.0500 were deemed statistically different, observing stratification of metal concentrations as observed in gradient coloration, the darker the color the increase in statistical difference observed in metal concentrations between epilimnion and hypolimnion. Numbers within the table denote the number of samples observed in the epilimnion and hypolimnion (epi./hypo.). Asterisk (*) denotes Welch t-test p-values used, when the standard deviation variance between samples were statistically different through an F-test to compare variance. Sample abbreviations are denoted in Table 3.1.

	Na	Mg	Al	K	Ca	Ti	V	Cr	Mn	Fe	Co	Ni	Cu
DNL Epi. Vs. Hypo.	14/14	14/15	12/11	14/14	14/14	14/15	13/13	14/15	14/15	14/15	14/15	13/14	11/13
GSL Epi. Vs. Hypo.	15/17*	15/18*	13/11	15/16*	15/17*	16/17	14/17*	15/18*	14/17*	16/18	16/17	15/17*	13/14*
OCT Epi. Vs. Hypo.	12/14	12/14	10/13*	12/13*	11/14	12/14	12/13	12/14*	12/14	12/14	12/11	12/12*	8/11*
GSL Epi. Vs. BSP	17/8*	18/8	11/8*	16/7	17/8	17/8*	17/8	18/8	17/8*	18/8*	17/8	17/8*	14/6*

	Zn	As	Se	Sr	Mo	Ag	Cd	Sb	Ba	Pb	Bi	U	Legend
DNL Epi. Vs. Hypo.	8/7	13/15	9/10	14/15	9/11	4/6	5/7	12/12	14/15	5/6*	8/8	7/7	<0.0001
GSL Epi. Vs. Hypo.	10/9*	15/18*	13/14	15/17*	15/17	9/9	8/11*	15/16	16/17	6/6*	9/13	16/14	<0.0010
OCT Epi. Vs. Hypo.	10/6*	12/14	9/9	12/14	12/12	8/9*	8/7*	11/11	12/13	5/5*	8/9	7/7	<0.0100
GSL Epi. v BSP	9/6*	18/8	14/8	17/8	17/8	N/A	11/5	16/8	17/8*	6/6*	13/4	14/8	<0.0500

Table 3.10: T-Test Results Comparing Summer and Winter Metal Concentrations Thermokarst Lakes

Statistical T-Test to observe seasonal differences in individual thermokarst lake samples for metal concentrations between winter and summer over three years of sample collection; 2016 – 2018. Color gradient indicates p-value, with the lightest representing the maximum cut off for statistical differences of p-value > 0.05000. Blue gradient indicates the average was higher in winter time. Orange gradient indicates the average was higher in summer time. Numbers within the table denote the number of samples observed in summer and winter (summer/winter). Asterisk (*) denotes Welch t-test p-values used, when the standard deviation variance between samples were statistically different through an F-test to compare variance. Numbers in italics and red are samples were the sample number is less than or equal to 3, and interpretations should be made with caution. Sample abbreviations are denoted in Table 3.1.

Table Analyzed	Na	Mg	Al	K	Ca	Ti	V	Cr	Mn	Fe	Co	Ni	Cu
GSL Top	10/7	10/8	6/5	9/7	10/7	9/8*	9/8*	10/8	9/8*	10/8*	10/7	10/7	7/7
GSL Bottom	9/6	9/6	8/5	8/7*	9/6	9/7	9/5*	9/6	8/6	9/7	9/7	9/6	7/6
OCT Top	9/5	9/5*	9/4	8/5*	9/5*	9/5*	8/5*	9/5*	9/5*	9/5*	7/4*	8/4	7/4
OCT Bottom	8/4	8/4	6/4	8/4*	7/4*	8/4	8/4	8/4*	8/4	8/4*	8/4	8/4	*5/3**
DNL Top	7/7	8/7	4/7	7/7	7/7*	8/7*	6/7	8/7	8/7*	8/7*	8/7	7/7	7/6
DNL Bottom	8/6	8/6	6/6	8/6	8/6	8/6	7/6	8/6	8/6	8/6	8/6	7/6	6/5

	Zn	As	Se	Sr	Mo	Ag	Cd	Sb	Ba	Pb	Bi	U	Legend
GSL Top	4/5	10/8*	6/6	10/7	10/7	*7/2*	5/6*	9/7	10/7	*4/2*	7/6*	7/7	<0.0001
GSL Bottom	5/5	9/6	6/5	9/6	8/7*	*6/3**	4/4*	9/6	9/7	*4/2*	4/5*	9/7	<0.0010
OCT Top	*4/2*	9/5*	*4/3*	9/5*	8/4	*6/3**	*4/3*	7/4	9/4*	*4/1*	*6/3**	*5/2*	<0.0100
OCT Bottom	6/4	8/4*	*5/3*	8/4	8/4	*5/3*	*5/3*	7/4	8/4	*4/1*	*5/3*	*5/2*	<0.0500
DNL Top	*2/5*	8/7	*3/6*	8/7	5/6*	*5/1*	*3/4**	6/6	8/7*	*3/3*	4/4	*4/3*	
DNL Bottom	*3/5*	7/6	*3/5**	8/6	4/5	*3/1*	*2/3*	6/6	8/6	*3/2*	*5/3**	*4/3**	

Table 3.11: Determination of Year to Year Statistical Differences

An overall ANOVA for determining statistical differences between sampling seasons of 2016, 2017, and 2018. Underneath the ANOVA denoted by the years utilized are the T-test to determine which year was significantly different. The grey gradation is an indicator of p-value strength with the lightest grey representing the maximum p-value considered statistically different at a p-value > 0.0500. Sample number are found within the cells as an overall in the ANOVA or for each year in the T-Tests (early year/later year). Additionally, asterisks (*) denoted sample numbers are for those statistical tests that utilized the Welch's version, after determining the standard deviation variance between samples was statistically different through Brown-Forsythe test for ANOVA and the F-Test for T-Tests. Underneath statistical tests results are the averages and standard deviation (±) for each metal concentration throughout that sample year are found. Colored boxes indicate which year was statistically different overall with blue being 2016, orange being 2017, and purple being 2018. Samples without values did not have enough samples above detection limits or were not run. Sample abbreviations are denoted in Table 3.1.

	C		N		Li		Na		Mg		Al		K		Ca	
	#/#		#/#		#/#		#/#		#/#		#/#		#/#		#/#	
3 Year ANOVA	137		127*				148		149		122		147		165	
T-Test 2016 Vs. 2017	44/40		32/41				44/42*		45/42		34/35*		43/42*		61/42	
T-Test 2016 Vs. 2018	44/53		32/54*				44/62		45/62		34/53		43/62*		61/62	
T-Test 2017 Vs.2018	40/53		41/54*				42/62		42/62		35/53		42/62*		42/62	
	ppm	+/-	ppm	+/-	ppb	+/-	ppb	+/-	ppb	+/-	ppb	+/-	ppb	+/-	ppb	+/-
2016 Avg. Concentration	46.3	39.6	2.6	2.7			19729.0	31443.0	29802.0	30616.0	22.1	21.2	4492.0	7582.0	47629.0	32504.0
2017 Avg. Concentration	59.0	48.1	2.6	3.0			23173.0	21893.0	32140.0	26273.0	26.6	32.8	3497.0	2277.0	42039.0	26567.0
2018 Avg. Concentration	58.8	45.9	0.6	0.9	1.6	1.2	23762.0	29058.0	31091.0	28921.0	21.6	24.7	3443.0	3649.0	44414.0	29286.0

	Ti		V		Cr		Mn		Fe		Co		Ni		Cu	
	#/#		#/#		#/#		#/#		#/#		#/#		#/#		#/#	
3 Year ANOVA	149		143		146*		149		149		143		139		124	
T-Test 2016 Vs. 2017	45/42		43/41		45/41		45/42		45/42		45/42		44/37		42/42*	
T-Test 2016 Vs. 2018	45/62		43/59		45/60*		45/62		45/62		45/56		44/58		41/41*	
T-Test 2017 Vs.2018	42/62		41/59		41/60		42/62		42/62		42/56		37/58		42/41	
	ppb	+/-	ppb	+/-	ppb	+/-	ppb	+/-	ppb	+/-	ppb	+/-	ppb	+/-	ppb	+/-
2016 Avg. Concentration	3.1	2.4	0.8	0.7	1.1	1.1	522.6	763.9	2236.0	3496.0	0.5	0.3	3.4	3.4	0.7	0.6
2017 Avg. Concentration	2.7	2.2	0.9	0.6	1.2	1.3	571.1	650.9	2022.0	3617.0	0.6	0.4	3.4	3.5	0.9	1.0
2018 Avg. Concentration	4.1	2.8	1.0	0.8	1.7	1.7	495.2	619.0	2027.0	3158.0	0.5	0.3	4.0	3.4	0.8	1.0

	Zn		As		Se78		Se82		Sr		Mo		Ag		Cd	
	#/#		#/#		#/#		#/#		#/#		#/#		#/#		#/#	
3 Year ANOVA	80		149		91*		149*		148		135		78*		83*	
T-Test 2016 Vs. 2017	17/26*		45/42		7/22		45/41*		45/42		36/42*		34/13*		9/42*	
T-Test 2016 Vs. 2018	17/37*		45/62		7/62*		45/62*		45/61		36/57*		34/31*		9/32	
T-Test 2017 Vs.2018	26/37		42/62		22/62*		42/62*		42/61		42/57		13/31		42/32	
	ppb	+/-	ppb	+/-	ppb	+/-	ppb	+/-	ppb	+/-	ppb	+/-	ppb	+/-	ppb	+/-
2016 Avg. Concentration	77.0	302.8	9.6	13.0	0.2	0.2	22.1	29.5	239.0	196.4	0.6	0.8	0.19	0.21	0.01	0.00
2017 Avg. Concentration	3.9	4.9	9.9	11.6	0.3	0.3	39.7	48.3	247.8	157.0	0.5	0.4	0.02	0.02	0.02	0.01
2018 Avg. Concentration	3.6	4.4	9.1	10.2	0.7	1.4	19.3	20.2	234.7	163.4	0.5	0.5	0.02	0.04	0.01	0.01

	Sb		Ba		Pb		Bi		U		Cl		Legend	
	#/#		#/#		#/#		#/#		#/#		#/#			
3 Year ANOVA	135		144				89*		105*		123		2016 Different	<0.0001
T-Test 2016 Vs. 2017	36/42*		45/42*				27/32*		22/26*		32/39*		2017 Different	<0.0010
T-Test 2016 Vs. 2018	36/57		45/57				27/30		22/57		32/52		2018 Different	<0.0100
T-Test 2017 Vs.2018	42/57*		42/57*		3/56		32/30		26/57*		39/52*			<0.0500
	ppb	+/-	ppb	+/-	ppb	+/-	ppb	+/-	ppb	+/-	ppb	+/-		
2016 Avg. Concentration	0.3	0.2	55.8	35.0			0.0	0.1	0.6	0.6	12.2	16.0		
2017 Avg. Concentration	0.6	0.4	66.0	64.4	0.2	0.1	0.2	0.2	0.6	0.3	9.6	10.5		
2018 Avg. Concentration	0.4	0.2	57.6	38.4	0.1	0.2	0.2	0.3	0.3	0.2	15.2	21.6	*Welch ANOVA or T-Test utilized	

Table 3.12: T-Test Results Comparing Summer and Winter Metal Concentrations in Streams

Statistical T-Test to observe seasonal differences in metal concentrations for individual stream samples between winter and summer over three-year water collection; 2016 – 2018. Color gradient indicates p-value, with the lightest representing the maximum cut off for statistical differences of p-value > 0.05000. Blue gradient indicates the average was higher in winter time. Numbers in the cells are those of the sample number (summer/winter) and asterisks (*) indicates Welch's T-Test was utilized, when the standard deviation variance was determined to be statistically different between samples using an F-Test. Red italicized cells are samples with a sample number less than or equal to 3 and thus, care should be taken when observing the statistics. Sample abbreviations denoted in Table 3.1.

Sample Location	Na	Mg	Al	K	Ca	Ti	V	Cr	Mn	Fe	Co	Ni	Cu
GSSC	*11/3*	*11/3*	*10/2*	*10/3*	*11/3*	*11/3**	*11/3**	*10/3**	*11/3*	*11/3*	*10/2*	*11/2*	*10/2*
GSBA	10/4	10/4*	*10/3*	10/4	10/4*	10/4*	10/4*	9/4*	10/4	9/4	*10/3*	*10/3*	*9/3*
OCC	*9/3**	*11/3*	*11/2*	*8/3*	*11/3*	*11/3*	*11/3**	*11/3**	*11/3*	*11/3*	*11/2*	*10/1*	*10/2*

Sample Location	Zn	As	Se	Sr	Mo	Ag	Cd	Sb	Ba	Pb	Bi	U	Legend
GSSC	*6/1*	*11/3**	*4/3**	*9/3**	*11/2*	n/a	*6/2*	*11/2*	*11/2*	n/a	*7/1*	*9/2*	<0.0001
GSBA	*4/3**	10/4*	4/4*	*10/4*	*10/3*	n/a	*5/3*	*10/3*	*10/3*	*4/1*	*4/1*	*7/2*	<0.0010
OCC	n/a	*9/3**	*7/3**	*11/3*	*11/2*	*8/1*	*6/2*	*11/2*	*11/2*	n/a	*4/1*	*10/2*	<0.0100
													<0.0500

Table 3.13: Seasonality of Metal to Chloride Ratio Values for Individual Thermokarst Lakes

Statistical T-Test to observe seasonal differences in individual thermokarst lake samples for metal to chloride ratio values between winter and summer for a three-year period from 2016 – 2018. Color gradient indicates p-value, with the lightest representing the maximum cut off for statistical differences of p-value > 0.05000. Blue gradient indicates the average was higher in winter time. Numbers in the cells are those of the sample number (summer/winter) and asterisks (*) indicates Welch's T-Test was utilized when F-Test determined the standard deviation variance of samples were statistically different. Red italicized cells are samples with a sample number less than or equal to 3 and thus, care should be taken when observing the statistics. Sample abbreviations are denoted in Table 3.1.

Sample Location	C/Cl ppm/ppm	Li/Cl ppb/ppm	Na/Cl ppb/ppm	Mg/Cl ppb/ppm	Al/Cl ppb/ppm	K/Cl ppb/ppm	Ca/Cl ppb/ppm	Ti/Cl ppb/ppm	V/Cl ppb/ppm	Cr/Cl ppb/ppm	Mn/Cl ppb/ppm	Fe/Cl ppb/ppm	Co/Cl ppb/ppm	Ni/Cl ppb/ppm	N/Cl ppb/ppm
GSL Epi.	8/6*	*3/2*	9/6*	9/6*	5/4	8/6*	9/6*	8/6*	8/6*	9/6*	7/6*	9/6*	9/5*	9/6*	7/5
GSL Hypo.	8/5*	*4/2*	9/5*	9/5*	*4/3*	8/5*	9/5*	9/5*	9/4*	9/4*	9/5*	8/5*	9/5*	9/4*	7/5*
OCT Epi.	*9/3*	*4/1*	*9/3*	*9/3*	*8/2*	*8/3*	*9/3*	*9/3*	*8/3*	*9/3*	*9/3**	*9/3*	*8/2*	*8/2*	*8/3*
OCT Hypo.	*8/2*	*4/1*	*8/2*	*8/2*	*6/2*	*8/2*	*8/2*	*8/2*	*8/2*	*8/2*	*8/2*	*8/2*	*8/2*	*8/2*	*7/2*
DNL Epi.	8/5	*3/2*	7/4*	8/5	4/5	7/5	7/4*	8/5	6/5	8/5	7/4*	8/5*	8/5	6/5*	7/4
DNL Hypo.	7/4	*3/2*	8/4	7/4	6/4	8/4	8/4	7/4	6/4	8/4	7/4*	7/4*	8/4	6/4*	*7/3*

Sample Location	Cu/Cl ppb/ppm	Zn/Cl ppb/ppm	As/Cl ppb/ppm	Se/Cl ppb/ppm	Sr/Cl ppb/ppm	Mo/Cl ppb/ppm	Ag/Cl ppb/ppm	Cd/Cl ppb/ppm	Sb/Cl ppb/ppm	Ba/Cl ppb/ppm	Pb/Cl ppb/ppm	Bi/Cl ppb/ppm	U/Cl ppb/ppm	Legend
GSL Epi.	6/5	*4/3*	9/6*	5/6*	9/6*	8/5	*6/1*	5/5*	8/5*	9/5*	*3/2*	7/4	6/5*	<0.0001
GSL Hypo.	7/5*	5/4*	9/5*	6/4*	9/5*	9/5*	*6/2*	4/5	9/5*	9/5*	*4/2*	4/4*	9/5*	<0.0010
OCT Epi.	*7/2*	*4/1*	*9/3*	*4/2*	*9/3*	*8/2*	*6/2*	*4/2*	*7/2*	*9/2*	*4/1*	*6/2**	*5/2*	<0.0100
OCT Hypo.	*6/2*	*6/2*	*8/2*	*5/2*	*8/2*	*8/2*	*5/2*	*4/2*	*7/2*	*8/2*	*4/1*	*5/2*	*5/2*	<0.0500
DNL Epi.	7/4*	*2/3*	8/5	*3/4**	8/4*	5/4*	*5/1*	*3/2*	6/4	8/5	*3/2*	4/4	*4/2*	
DNL Hypo.	*6/3*	*3/3**	7/4	*3/3**	6/4*	*4/3*	*3/1*	*2/1*	6/4	7/4	*3/2*	*5/2*	*4/3*	

Table 3.14: Seasonality of Metal to Chloride Ratio Values of Overall Ratio Values

Statistical T-Test to observe seasonal differences in total watershed (thermokarst lake and stream samples) compilation for metal to chloride ratio values between winter and summer for three-years from 2016 – 2018, to observe overall seasonality observed for chloride normalized metal concentrations. Color gradient indicates p-value, with the lightest representing the maximum cut off for statistical differences of p-value > 0.05000. Blue gradient indicates the average was higher in winter time. Orange gradient indicates the average was higher in summer time. Numbers in the cells are those of the sample number (summer/winter) and asterisks (*) indicates Welch's T-Test was utilized when F-test determined the standard deviation variance between samples was statistically different.

C/Cl ppm/ppm	N/Cl ppm/ppm	Li/Cl ppb/ppm	Na/Cl ppb/ppm	Mg/Cl ppb/ppm	Al/Cl ppb/ppm	K/Cl ppb/ppm	Ca/Cl ppb/ppm	Ti/Cl ppb/ppm	V/Cl ppb/ppm
86/33	77/31*	36/11*	87/32*	85/33	70/25*	86/33*	88/32*	88/33	84/32
Cr/Cl ppb/ppm	**Mn/Cl ppb/ppm**	**Fe/Cl ppb/ppm**	**Co/Cl ppb/ppm**	**Ni/Cl ppb/ppm**	**Cu/Cl ppb/ppm**	**Zn/Cl ppb/ppm**	**As/Cl ppb/ppm**	**Se78/Cl ppb/ppm**	**Se82/Cl ppb/ppm**
88/32*	86/32*	86/33*	89/28	85/28	74/26*	41/19*	86/33*	44/27*	82/33*
Sr/Cl ppb/ppm	**Mo/Cl ppb/ppm**	**Ag/Cl ppb/ppm**	**Cd/Cl ppb/ppm**	**Sb/Cl** ppb/ppm	**Ba/Cl ppb/ppm**	**Pb/Cl ppb/ppm**	**Bi/Cl ppb/ppm**	**U/Cl ppb/ppm**	
85/32*	80/26*	54/10*	40/22	81/27*	87/28*	37/11*	54/22*	62/24*	**Legend**
									<0.0100
									<0.0500

Table 3.15: Seasonal Variability in Metal to Chloride Ratio Values

Variability between metal – chloride relationships was determined based on the magnitude of standard deviation from the average of all the samples during the winter or summer. The maximum and minimum for a certain sample number is represented for each ratio. The samples denoted with a triple asterisks (***) represent the metals that were determined to have a seasonal difference through a T-Test, results found in Table 3.14. Yellow indicates a decreased standard deviation or variance and thus, variability in summer time samples. Meanwhile, green indicates a decreased standard deviation or variance and thus, variability in winter samples.

	C/Cl				N/Cl				Li/Cl***				Na/Cl***			
	n	Minimum ppm/ppm	Maximum ppm/ppm	Variance +/-	n	Minimum ppm/ppm	Maximum ppm/ppm	Variance +/-	n	Minimum ppb/ppm	Maximum ppb/ppm	Variance +/-	n	Minimum ppb/ppm	Maximum ppb/ppm	Variance +/-
Summer	86	0.9	31.8	5.9	77	0.0	3.8	0.6	36	0.0	2.9	0.7	87	367.0	23022.0	2635.0
Winter	33	2.0	29.6	7.6	31	0.0	1.5	0.3	11	0.0	0.3	0.1	32	115.8	13796.0	3548.0

	Mg/Cl				Al/Cl				K/Cl				Ca/Cl			
	n	Minimum ppb/ppm	Maximum ppb/ppm	Variance +/-	n	Minimum ppb/ppm	Maximum ppb/ppm	Variance +/-	n	Minimum ppb/ppm	Maximum ppb/ppm	Variance +/-	n	Minimum ppb/ppm	Maximum ppb/ppm	Variance +/-
Summer	85	773.8	41537.0	6218.0	70	0.0	142.8	19.3	86	30.4	5129.0	736.7	88	1017.0	88718.0	14089.0
Winter	33	102.7	19106.0	4899.0	25	0.1	22.5	5.7	33	18.0	1728.0	409.5	32	417.7	22084.0	6461.0

	Ti/Cl				V/Cl				Cr/Cl***				Mn/Cl			
	n	Minimum ppb/ppm	Maximum ppb/ppm	Variance +/-	n	Minimum ppb/ppm	Maximum ppb/ppm	Variance +/-	n	Minimum ppb/ppm	Maximum ppb/ppm	Variance +/-	n	Minimum ppb/ppm	Maximum ppb/ppm	Variance +/-
Summer	88	0.0	5.3	1.0	84	0.0	3.4	0.5	88	0.0	1.5	0.2	86	0.4	1579.0	188.3
Winter	33	0.0	4.0	0.9	32	0.0	2.2	0.5	32	0.1	4.1	0.9	32	0.7	480.6	131.7

	Fe/Cl				Co/Cl				Ni/Cl				Cu/Cl***			
	n	Minimum ppb/ppm	Maximum ppb/ppm	Variance +/-	n	Minimum ppb/ppm	Maximum ppb/ppm	Variance +/-	n	Minimum ppb/ppm	Maximum ppb/ppm	Variance +/-	n	Minimum ppb/ppm	Maximum ppb/ppm	Variance +/-
Summer	86	4.1	4138.0	728.3	89	0.0	1.4	0.2	85	0.0	3.2	0.6	74	0.0	2.8	0.6
Winter	33	1.4	7778.0	1363.0	28	0.0	0.7	0.2	28	0.0	2.8	0.8	26	0.0	1.8	0.4

	Zn/Cl				As/Cl				Se78/Cl				Se82/Cl***			
	n	Minimum ppb/ppm	Maximum ppb/ppm	Variance +/-	n	Minimum ppb/ppm	Maximum ppb/ppm	Variance +/-	n	Minimum ppb/ppm	Maximum ppb/ppm	Variance +/-	n	Minimum ppb/ppm	Maximum ppb/ppm	Variance +/-
Summer	41	0.0	4.1	0.9	86	0.1	12.6	3.1	44	0.0	0.5	0.1	82	0.1	7.5	1.6
Winter	19	0.0	1.6	0.4	33	0.1	23.0	5.4	27	0.0	4.5	1.0	33	0.6	28.0	5.7

	Sr/Cl				Mo/Cl***				Ag/Cl				Cd/Cl***			
	n	Minimum ppb/ppm	Maximum ppb/ppm	Variance +/-	n	Minimum ppb/ppm	Maximum ppb/ppm	Variance +/-	n	Minimum ppb/ppm	Maximum ppb/ppm	Variance +/-	n	Minimum ppb/ppm	Maximum ppb/ppm	Variance +/-
Summer	85	3.6	500.9	74.4	80	0.0	4.0	0.6	54	0.0	0.7	0.1	40	0.0	0.0	0.0
Winter	32	2.3	131.8	37.2	26	0.0	0.7	0.1	10	0.0	0.1	0.0	22	0.0	0.0	0.0

	Sb/Cl***				Ba/Cl				Pb/Cl***				Bi/Cl			
	n	Minimum ppb/ppm	Maximum ppb/ppm	Variance +/-	n	Minimum ppb/ppm	Maximum ppb/ppm	Variance +/-	n	Minimum ppb/ppm	Maximum ppb/ppm	Variance +/-	n	Minimum ppb/ppm	Maximum ppb/ppm	Variance +/-
Summer	81	0.0	1.0	0.2	87	1.3	94.6	16.4	37	0.0	0.3	0.1	54	0.0	0.5	0.1
Winter	27	0.0	0.3	0.1	28	0.4	34.8	8.7	11	0.0	0.0	0.0	22	0.0	0.2	0.1

	U/Cl				Cl			
	n	Minimum ppb/ppm	Maximum ppb/ppm	Variance +/-	n	Minimum ppb/ppm	Maximum ppb/ppm	Variance +/-
Summer	62	0.0	1.4	0.2	90	0.6	73.5	17.9
Winter	24	0.0	0.4	0.1	33	1.2	79.5	16.1

Variablity Decreased in Summer

Variability Decreased in Winter

***Statisitically Different See Table 3.14

Table 3.16: ANOVA Results of Metal to Chloride Ratio in Thermokarst lake Epilimnion

Statistical comparison of metal to chloride ratio with comparison to thermokarst lake permafrost degradation in the epilimnion (epi.) through an ANOVA statistical test. With a p-value of <0.0500 as statistically significant with the average metal to chloride ratio values for each location, with the number of samples found in the box denoted N for which the color gradient determines the p-value obtained. Colors determines which thermokarst lake epilimnion has the highest (red), medium (yellow), and low (green) concentration for metal chloride ratio values that observed statistical difference between streams. Asterisk (*) denotes Welch ANOVA p-values used, when Brown-Forsythe test determined the standard deviation variance between samples were different requiring the use of a Welch ANOVA. Sample average was determined for ratio values over three-year period from 2016 – 2018. Where error in the average was determined through standard deviation of all sample values averaged and is denoted with ±. Sample abbreviations are denoted in Table 3.1.

Sample	C/Cl ppm/ppm	+/-	N/Cl ppm/ppm	+/-	Li/Cl ppb/ppm	+/-	Na/Cl ppb/ppm	+/-	Mg/Cl ppb/ppm	+/-	Al/Cl ppb/ppm	+/-	K/Cl ppb/ppm	+/-	Ca/Cl ppb/ppm	+/-
N	39		31		15		38		40		28		37		36	
GSL Epi.	4.44	8.96	0.07	0.14	0.05	0.11	1807.00	4055.00	2384.00	5435.00	1.19	2.53	210.90	343.30	2871.00	6491.00
OCT Epi.	8.67	5.69	0.11	0.24	0.24	0.20	1690.00	1264.00	3041.00	2261.00	6.78	4.72	371.40	393.30	7659.00	4974.00
DNL Epi.	7.65	3.54	0.09	0.21	0.11	0.04	2605.00	1001.00	4331.00	1726.00	0.53	2.41	417.20	226.20	5992.00	2352.00

	Ti/Cl ppb/ppm	+/-	V/Cl ppb/ppm	+/-	Cr/Cl ppb/ppm	+/-	Mn/Cl ppb/ppm	+/-	Fe/Cl ppb/ppm	+/-	Co/Cl ppb/ppm	+/-	Ni/Cl ppb/ppm	+/-	Cu/Cl ppb/ppm	+/-
N	39		36		40		36		40*		37*		36		31	
GSL Epi.	0.03	0.53	0.11	0.11	8.34	0.29	17.41	137.10	0.03	314.70	0.34	0.07	0.03	0.63	0.23	0.03
OCT Epi.	0.23	0.40	0.22	0.11	34.66	0.16	601.20	46.67	0.11	870.40	0.39	0.07	0.07	0.34	0.15	0.09
DNL Epi.	0.04	0.13	0.10	0.02	4.37	0.04	33.20	54.41	0.03	79.63	0.17	0.02	0.01	0.08	0.15	0.05

	Zn/Cl ppb/ppm	+/-	As/Cl ppb/ppm	+/-	Se78/Cl ppb/ppm	+/-	Se82/Cl ppb/ppm	+/-	Sr/Cl ppb/ppm	+/-	Mo/Cl ppb/ppm	+/-	Ag/Cl ppb/ppm	+/-	Cd/Cl ppb/ppm	+/-
N	17		40*		24		40		39		32*		21		21	
GSL Epi.	0.18	0.23	0.02	0.70	3.13	0.05	3.13	7.02	16.16	39.82	0.02	0.02	0.00	0.00	0.00	0.00
OCT Epi.	2.29	1.78	0.07	2.83	1.25	0.17	1.25	1.23	30.46	24.00	0.05	0.05	0.01	0.01	0.00	0.00
DNL Epi.	0.56	0.66	0.02	0.23	3.68	0.03	3.68	2.61	33.65	12.54	0.01	0.02	0.02	0.04	0.00	0.01

	Sb/Cl ppb/ppm	+/-	Ba/Cl ppb/ppm	+/-	Pb/Cl ppb/ppm	+/-	Bi/Cl ppb/ppm	+/-	U/Cl ppb/ppm	+/-
N	32		38		15		27		24	
GSL Epi.	0.03	0.05	2.40	9.57	0.00	0.02	0.01	0.01	0.03	0.04
OCT Epi.	0.05	0.03	10.21	8.00	0.02	0.02	0.01	0.02	0.02	0.01
DNL Epi.	0.04	0.02	5.73	3.22	0.00	0.02	0.02	0.06	0.02	0.01

P-Value	Concentration
<0.0001	High
<0.0010	Medium
<0.0100	Low
<0.0500	

Table 3.17: ANOVA Results of Metal to Chloride Ratio in Thermokarst lake Hypolimnion

Statistical comparison of metal to chloride ratio with comparison to thermokarst lake permafrost degradation in the hypolimnion (hypo.) through an ANOVA statistical test. With a p-value of <0.0500 as statistically significant with the average metal to chloride ratio values for each location, with the number of samples found in the box denoted N for which the color gradient determines the p-value obtained. Colors determines which thermokarst lake hypolimnion has the highest (red), medium (yellow), and low (green) concentration for metal chloride ratio values that observed statistical difference between streams. Asterisk (*) denotes Welch ANOVA p-values used, when Brown-Forsythe test determined the standard deviation variance between samples were different requiring the use of a Welch ANOVA. Sample average was determined for ratio values over three-year period from 2016 – 2018. Where error in the average was determined through standard deviation of all sample values averaged and is denoted with ±. Sample abbreviations are denoted in Table 3.1.

Sample	C/Cl ppm/ppm	+/-	N/Cl ppm/ppm	+/-	Li/Cl ppb/ppm	+/-	Na/Cl ppb/ppm	+/-	Mg/Cl ppb/ppm	+/-	Al/Cl ppb/ppm	+/-	K/Cl ppb/ppm	+/-	Ca/Cl ppb/ppm	+/-
N	34		28		16		36		35		29*		35		32	
GSL Hypo.	4.55	9.02	0.11	0.28	0.06	0.12	1916.00	3683.00	2504.00	4828.00	0.18	0.51	183.10	375.80	2656.00	4504.00
OCT Hypo.	8.41	4.39	0.24	0.46	0.21	0.06	2279.00	1878.00	4818.00	3228.00	5.68	3.40	699.90	431.10	6078.00	5947.00
DNL Hypo.	8.12	3.99	0.12	0.26	0.11	0.06	1102.00	1050.00	2245.00	1509.00	0.92	0.54	305.60	207.30	3998.00	19397.00

	Ti/Cl ppb/ppm	+/-	V/Cl ppb/ppm	+/-	Cr/Cl ppb/ppm	+/-	Mn/Cl ppb/ppm	+/-	Fe/Cl ppb/ppm	+/-	Co/Cl ppb/ppm	+/-	Ni/Cl ppb/ppm	+/-	Cu/Cl ppb/ppm	+/-
N	35*		33*		35		35		34*		36*		33		29*	
GSL Hypo.	0.13	0.58	0.03	0.11	0.10	0.29	69.24	118.80	61.97	324.40	0.04	0.07	0.31	0.75	0.01	0.01
OCT Hypo.	1.23	0.84	0.39	0.35	0.33	0.27	183.30	143.30	1501.00	2248.00	0.24	0.15	0.50	0.51	0.07	0.06
DNL Hypo.	0.17	0.13	0.05	0.04	0.06	0.04	33.25	56.96	53.52	82.81	0.03	0.02	0.16	0.10	0.01	0.01

	Zn/Cl ppb/ppm	+/-	As/Cl ppb/ppm	+/-	Se78/Cl ppb/ppm	+/-	Se82/Cl ppb/ppm	+/-	Sr/Cl ppb/ppm	+/-	Mo/Cl ppb/ppm	+/-	Ag/Cl ppb/ppm	+/-	Cd/Cl ppb/ppm	+/-
N	23		35*		23		34		34		31*		19		18	
GSL Hypo.	0.10	0.16	0.24	0.68	0.02	0.04	1.86	5.02	16.64	36.81	0.02	0.03	0.00	0.00	0.00	0.00
OCT Hypo.	0.24	0.14	6.61	6.50	0.05	0.06	1.36	2.16	48.10	30.53	0.08	0.05	0.00	0.02	0.00	0.00
DNL Hypo.	0.09	0.46	0.46	0.35	0.02	0.01	2.99	2.63	13.63	12.75	0.02	0.01	0.01	0.01	0.00	0.01

	Sb/Cl ppb/ppm	+/-	Ba/Cl ppb/ppm	+/-	Pb/Cl ppb/ppm	+/-	Bi/Cl ppb/ppm	+/-	U/Cl ppb/ppm	+/-
N	33		35		16		22*		28	
GSL Hypo.	0.03	0.04	3.15	7.83	0.00	0.01	0.00	0.01	0.03	0.04
OCT Hypo.	0.05	0.04	15.15	8.97	0.03	0.08	0.11	0.12	0.02	0.10
DNL Hypo.	0.03	0.02	4.36	3.55	0.00	0.00	0.01	0.03	0.02	0.01

P-Value	Concentration
<0.0001	High
<0.0010	Medium
<0.0100	Low
<0.0500	

Table 3.18: ANOVA Results of Metal to Chloride Ratio in Streams

Statistical comparison of metal to chloride ratio with comparison to stream sampling location through an ANOVA statistical test. With a p-value of <0.0500 as statistically significant with the average metal to chloride ratio values for each location, with the number of samples found in the box denoted N for which the color gradient determines the p-value obtained. Colors determines which stream has the highest (red), medium (yellow), and low (green) concentration for metal – chloride ratio that observed statistical difference between streams. Asterisk (*) denotes Welch ANOVA p-values used, when Brown-Forsythe test determined the standard deviation variance between sample ratios were different requiring the use of a Welch ANOVA. Sample average was determined for ratios over three-year period from 2016 – 2018. Where error in the average was determined through standard deviation of all ratio values averaged and is denoted with ±. Sample abbreviations are denoted in Table 3.1.

Sample	C/Cl ppm/ppm	+/-	N/Cl ppm/ppm	+/-	Li/Cl ppb/ppm	+/-	Na/Cl ppb/ppm	+/-	Mg/Cl ppb/ppm	+/-	Al/Cl ppb/ppm	+/-	K/Cl ppb/ppm	+/-	Ca/Cl ppb/ppm	+/-
N	31*		25*		9		29		28*		28*		30		36	
GSBA	6.80	2.65	0.24	0.18	0.05	0.52	1643.00	1919.00	3744.00	1983.00	9.90	10.52	894.50	545.60	9187.00	4524.00
GSSC	5.45	2.35	0.24	0.17	0.24	0.27	1689.00	787.80	3210.00	501.90	6.43	4.88	646.10	772.40	8021.00	6236.00
OCC	9.66	9.78	0.81	0.45	0.11	1.36	1598.00	871.50	6955.00	5255.00	25.39	49.94	548.30	485.30	8988.00	7644.00

	Ti/Cl ppb/ppm	+/-	V/Cl ppb/ppm	+/-	Cr/Cl ppb/ppm	+/-	Mn/Cl ppb/ppm	+/-	Fe/Cl ppb/ppm	+/-	Co/Cl ppb/ppm	+/-	Ni/Cl ppb/ppm	+/-	Cu/Cl ppb/ppm	+/-
N	31*		31*		29		31		30		28		28*		26	
GSBA	1.01	0.41	0.38	0.31	0.16	0.68	58.32	34.77	377.20	212.80	0.24	0.19	1.13	0.70	0.81	0.54
GSSC	0.81	0.38	0.27	0.32	0.14	0.62	35.36	19.24	333.60	238.20	0.14	0.05	0.81	0.35	0.58	0.41
OCC	2.44	1.47	0.85	0.76	0.32	1.36	32.27	48.03	459.60	423.00	0.20	0.23	1.52	1.17	0.46	1.07

	Zn/Cl ppb/ppm	+/-	As/Cl ppb/ppm	+/-	Se78/Cl ppb/ppm	+/-	Se82/Cl ppb/ppm	+/-	Sr/Cl ppb/ppm	+/-	Mo/Cl ppb/ppm	+/-	Ag/Cl ppb/ppm	+/-	Cd/Cl ppb/ppm	+/-
N	10		29		13		27		28		28		18		14	
GSBA	1.31	0.54	2.26	2.53	0.04	1.02	0.83	0.87	59.04	27.67	0.68	0.27	0.00	0.01	0.01	0.00
GSSC	0.44	0.31	1.84	2.51	0.03	0.99	0.82	0.76	46.10	10.25	0.38	0.29	0.01	0.08	0.01	0.01
OCC	1.50	0.00	1.27	6.76	0.23	2.19	1.14	3.26	45.15	36.68	0.09	0.08	0.01	0.12	0.00	0.00

	Sb/Cl ppb/ppm	+/-	Ba/Cl ppb/ppm	+/-	Pb/Cl ppb/ppm	+/-	Bi/Cl ppb/ppm	+/-	U/Cl ppb/ppm	+/-
N	28		26*		9		17		21	
GSBA	0.20	0.13	15.21	5.77	0.09	0.10	0.05	0.18	0.14	0.18
GSSC	0.15	0.13	10.30	2.50	0.05	0.01	0.01	0.05	0.11	0.06
OCC	0.22	0.10	16.01	12.13	0.09	0.03	0.06	0.04	0.15	0.06

P-Value	Concentration
<0.0001	High
<0.0010	Medium
<0.0100	Low
<0.0500	

Table 3.19: Overall Carbon and Nitrogen Seasonal Variability

Variability between carbon and nitrogen concentrations in summer and winter samples based on the magnitude of standard deviation from the average of all the samples during the winter or summer for a three-year study from 2016 – 2018. The samples denoted with an asterisk (*) represent that carbon and nitrogen required a Welch's T-test to determine the p-value showcased within the table that denotes seasonal differences, due to the standard deviation between winter and summer having a statistically different variance through an F-Test. Yellow indicates a decreased standard deviation (±) or variance and thus, variability in summer time samples.

	Carbon				Nitrogen			
	n	Minimum ppm	Maximum ppm	Variance +/-	n	Minimum ppm	Maximum ppm	Variance +/-
Summer	92	5.7	143.9	36.1	83	0.0	6.0	1.3
Winter	47	0.7	215.8	50.6	42	0.0	16.6	3.6
P-Value	<0.0001*				0.0158*			

Table 3.20: Carbon and Nitrogen Seasonal Variability in Individual Samples

Statistical T-Test to observe seasonal differences in individual samples for carbon and nitrogen concentrations between winter and summer from 2016 – 2018 sample collection for epilimnion (epi.) and hypolimnion (hypo.) separated. Color gradient indicates p-value, with the lightest representing the maximum cut off for statistical differences of p-value > 0.05000. Blue gradient indicates the average was higher in winter time. Numbers in the cells are those of the sample number (summer/winter) and asterisks (*) indicates Welch's T-Test was utilized for when the standard deviation or variance was deemed statistically different through an F-Test. Red italicized cells are samples with a sample number less than or equal to 3 and thus, care should be taken when observing the statistics. Averages and the associated standard deviations (±) were included for summer and winter. Samples highlighted in green are samples with a decreased variability in wintertime, while samples highlighted in yellow were samples with a decreased variability in summertime. Sample abbreviations are denoted in Table 3.1.

	C		N	
	ppm	+/-	ppm	+/-
n	9/8*		8/8	
GSL Epi. Summer	70.6	32.9	1.9	1.5
GSL Epi. Winter	124.6	13.8	4.1	3.3
n	8/7		7/6	
GSL Hypo. Summer	123.9	21.6	3.0	2.3
GSL Hypo. Winter	128.1	13.7	3.4	3.2
n	8/4		8/4	
OCT Epi. Summer	38.1	8.1	0.9	0.9
OCT Epi. Winter	49.1	5.5	1.8	1.4
n	8/4		8/3*	
OCT Hypo. Summer	38.8	9.0	1.8	1.8
OCT Hypo. Winter	42.5	8.3	5.3	7.0
n	8/5*		7/5	
DNL Epi. Summer	40.8	18.1	1.0	0.9
DNL Epi. Winter	65.3	5.2	2.1	1.7
n	7/6		7/5	
DNL Hypo. Summer	57.3	18.9	1.7	1.2
DNL Hypo. Winter	66.8	4.4	1.8	1.6
n	5/2		4/2	
BSP Summer	92.7	32.2	0.4	0.2
BSP Winter	185.9	42.2	8.8	11.0
n	10/3		10/3	
GSBA Summer	13.7	3.4	0.4	0.3
GSBA Winter	10.8	5.6	0.4	0.3
n	9/3		9/3	
GSSC Summer	14.8	2.7	0.6	0.3
GSSC Winter	13.5	7.3	0.6	0.5
n	9/3		9/3*	
OCC Summer	15.5	6.7	0.9	0.3
OCC Winter	10.5	10.8	0.4	0.6
	P-Value	<0.0010	<0.0100	<0.0500

Table 3.21: T-Test to Determine Differences Epilimnion and Hypolimnion for Carbon and Nitrogen

Statistical T-Test to determine Carbon and Nitrogen concentration differences between the epilimnion (epi.) and hypolimnion (hypo.). P-Values < 0.0500 were deemed statistically different, observing stratification of carbon and nitrogen concentrations for those samples with grey coloration. Numbers in the cells are those of the sample number (Epi./Hypo.) and asterisks (*) indicates Welch's T-Test was utilized for when the standard deviation or variance was deemed statistically different through an F-Test. Sample abbreviations were denoted in Table 3.1.

	C	N
GSL Epi. Vs. Hypo.	15/17*	12/15
OCT Epi. Vs. Hypo.	12/14	10/11*
DNL Epi. Vs. Hypo.	13/13	11/12
GSL Epi. Vs. BSP	17/7	15/5*
	P-Value	<0.0100

Table 3.22: ANOVA Results for Carbon and Nitrogen for Thermokarst Lake

Statistical comparison of carbon and nitrogen with comparison to thermokarst lake permafrost degradation in the epilimnion (epi.) and hypolimnion (hypo.) through an ANOVA statistical test. With a p-value of <0.0500 as statistically significant with the average concentrations for each location, with the number of samples found in the box denoted N for which the color gradient determines the p-value obtained. Colors determines which thermokarst lake epilimnion and hypolimnion has the highest (red), medium (yellow), and low (green) concentration that observed statistical difference between thermokarst lake epilimnion and hypolimnion. Asterisk (*) denotes Welch ANOVA p-values used, when Brown-Forsythe test determined the standard deviation variance between sample ratios were different requiring the use of a Welch ANOVA. Sample average was determined for ratios over three-year period from 2016 – 2018. Where error in the average was determined through standard deviation of all ratio values averaged and is denoted with ±. Sample abbreviations are denoted in Table 3.1.

	C ppm	+/-	N ppm	+/-	P-Value	Legend
N	44*		38*		<0.0001	High
GSL Epi.	96.0	37.4	2.6	2.3	<0.0010	Medium
OCT Epi.	42.1	8.9	1.1	1.1	<0.0100	Low
DNL Epi.	50.2	18.8	1.4	1.3	<0.0500	
N	40		33			
GSL Hypo.	125.8	17.9	3.1	2.7		
OCT Hypo.	40.0	8.6	2.8	4.0		
DNL Hypo.	61.7	14.5	1.6	1.3		

Table 3.23: ANOVA Results for Carbon and Nitrogen for Streams

Statistical comparison of stream location concentration in nitrogen and carbon through an ANOVA statistical test. With a p-value of <0.0500 as statistically significant with the average concentrations for each location, with the number of samples found in the box denoted N for which the color gradient determines the p-value obtained. Colors determines which stream has the highest (red), medium (yellow), and low (green) concentration that observed statistical difference between streams. Asterisk (*) denotes Welch ANOVA p-values used, when Brown-Forsythe test determined the standard deviation variance between sample ratios were different requiring the use of a Welch ANOVA. Sample average was determined for ratios over three-year period from 2016 – 2018. Where error in the average was determined through standard deviation of all ratio values averaged and is denoted with ±. Sample abbreviations are denoted in Table 3.1.

	C ppm	+/-	N ppm	+/-	P-Value	Legend
N	37		33		<0.0001	High
GSBA	13.0	3.9	0.3	0.3	<0.0010	Medium
GSSC	14.5	4.0	0.6	0.3	<0.0100	Low
OCC	14.2	7.7	0.9	0.4	<0.0500	

Table 3.24: Linear Regression for Metal – Carbon Relationship

Linear regression statistics for metal – carbon relationship with the carbon concentration represented on the independent variable axis. The number within the box represents the total number of samples from 2016 – 2018 that was used to conduct the linear regression with carbon. Which was split between summer, winter, and overall linear regression. Coloration gradient provides information on the strength of the p-value and fitness of the line (R^2). The darker the color the stronger the fitness to the line with a cut off of any linear regressions with an $R^2 > 0.8$; Orange gradation indicates a statistically positive linear slope with a P-value between 0.0500 and 0.001, Yellow gradation indicates a statistically positive linear slope with a P-value < 0.0001, Blue gradation indicates a statistically negative linear slope with a P-value between 0.0500 and 0.001, Green gradation indicates a statistically negative linear slope with a P-value < 0.0001. Dark yellow and dark green are the strongest linear regressions.

Winter	C	N	Li	Na	Mg	Al	K	Ca
N	45	40	13	47	47	39	47	47
	Ti	V	Cr	Mn	Fe	Co	Ni	Cu
N	47	46	46	47	47	42	42	40
	Zn	As	Se78	Se82	Sr	Mo	Ag	Cd
N	31	47	35	47	47	40	16	32
	Sb	Ba	Pb	Bi	U	Cl		
N	41	42	13	28	30	32		

Summer	C	N	Li	Na	Mg	Al	K	Ca
N	92	84	44	98	99	80	97	98
	Ti	V	Cr	Mn	Fe	Co	Ni	Cu
N	99	94	97	99	99	98	95	81
	Zn	As	Se78	Se82	Sr	Mo	Ag	Cd
N	47	99	53	99	99	92	62	48
	Sb	Ba	Pb	Bi	U	Cl		
N	91	99	46	60	72	90		

Overall	C	N	Li	Na	Mg	Al	K	Ca
N	137	124	57	145	146	119	144	145
	Ti	V	Cr	Mn	Fe	Co	Ni	Cu
N	146	140	143	146	146	140	137	121
	Zn	As	Se78	Se82	Sr	Mo	Ag	Cd
N	78	146	88	146	146	132	78	80
	Sb	Ba	Pb	Bi	U	Cl		
N	132	141	59	88	102	122		

Positive Slope		Negative Slope	
p-Value <0.05	p-Value <0.001	p-Value <0.05	p-Value <0.001
<0.5	<0.5	<0.5	<0.5
0.5 to 0.8	0.5 to 0.8	0.5 to 0.8	0.5 to 0.8
>0.8	>0.8	>0.8	>0.8

Table 3.25: Percentage of Iron Complexed to the Organic Carbon

Iron concentrations of individual samples from thermokarst lake and stream samples collected in May through whole water analysis and fractions taken from field-flow fractionation analysis. Field-flow fractionation fractions were obtained when organic matter passed through the membrane and through the detector, thus samples are considered complexed to the organic matter. A percentage was determined for the percentage of iron complexed to the organic matter sample for each individual sample. Sample abbreviations denoted in Table 3.1, epilimnion (epi.), and hypolimnion (hypo.).

	Total Fe Leached ppb	Total Fe Complexed ppb	Percent Fe Complexed (ppb/ppb)%
GSL Epi.	597.4	72.2	12.1%
GSL Hypo.	4339.7	160.6	3.7%
OCT Epi.	1615.9	92.6	5.7%
OCT Hypo.	3337.0	57.1	1.7%
DNL Epi.	151.5	BDL	N/A
DNL Hypo.	239.8	36.6	15.2%
BSP	220.6	113.0	51.2%
GSBA	2356.3	52.7	2.2%
GSSC	1292.3	148.4	11.5%
OCC	906.5	504.8	55.7%

Table 3.26: T-Test to Determine Differences Between Epilimnion and Hypolimnion for Metal to Carbon Ratio

Statistical T-Test to determine which metal to carbon ratios observed concentration differences between the epilimnion (epi.) and hypolimnion (hypo.) over three years of sample collection; 2016 – 2018. P-Values < 0.0500 were deemed statistically different, observing stratification of metal concentrations as observed in gradient coloration, the darker the color the increase in statistical difference observed in metal concentrations between epilimnion and hypolimnion. Numbers within the table denote the number of samples observed in the epilimnion and hypolimnion (epi./hypo.). Asterisk (*) denotes Welch t-test p-values used, when the standard deviation variance between samples were statistically different through an F-test to compare variance. Sample abbreviations are denoted in Table 3.1.

	N/C ppm/ppm	Li/C ppb/ppm	Na/C ppb/ppm	Mg/C ppb/ppm	Al/C ppb/ppm	K/C ppb/ppm	Ca/C ppb/ppm	Ti/C ppb/ppm	V/C ppb/ppm	Cr/C ppb/ppm	Mn/C ppb/ppm	Fe/C ppb/ppm	Co/C ppb/ppm	Ni/C ppb/ppm	Cu/C ppb/ppm
GSL Epi. Vs. Hypo.	13/16	5/5	14/16*	14/16	12/11*	12/15*	13/16	14/17	14/16*	14/17*	14/15	14/17	15/16*	14/17*	12/13*
OCT Epi. Vs. Hypo.	11/12*	5/5	12/14	12/14	10/13*	12/13*	12/14	11/14	12/13	12/14*	12/14	12/14	12/13	12/12*	9/11*
DNL Epi. Vs. Hypo.	12/12	4/5*	13/13	12/14	11/9*	13/13	13/13	13/14	12/12*	13/14*	13/13	13/14	13/13*	12/13	10/11
GSL Epi. Vs. BSP	16/6	5/5	16/7	16/7*	11/7*	15/6*	16/7*	17/7	16/7	17/7*	15/7*	17/7*	16/7*	17/7*	13/5*

	Zn/C ppb/ppm	As/C ppb/ppm	Se78/C ppb/ppm	Se82/C ppb/ppm	Sr/C ppb/ppm	Mo/C ppb/ppm	Ag/C ppb/ppm	Cd/C ppb/ppm	Sb/C ppb/ppm	Ba/C ppb/ppm	Pb/C ppb/ppm	Bi/C ppb/ppm	U/C ppb/ppm	Cl/C ppm/ppm	Legend
GSL Epi. Vs. Hypo.	10/8	14/17*	10/11	14/17	12/15	15/15	7/8*	8/10*	14/15*	14/16	5/5	9/13	15/13	13/14	<0.0001
OCT Epi. Vs. Hypo.	10/6*	12/14	8/7*	12/14	12/14	12/12	8/9*	7/7	11/11	12/13	5/5*	8/10*	7/7*	10/12*	<0.0010
DNL Epi. Vs. Hypo.	8/6	12/14	7/8*	13/14	11/13	8/10*	4/6	5/6	11/11	12/13	4/5*	7/7	6/6*	11/13	<0.0100
GSL Epi. Vs. BSP	8/5	17/7	11/6	17/7	15/6	15/6*	N/A	10/4*	15/7*	16/7	5/5	13/4	13/7	14/7	<0.0500

Table 3.27: Seasonality of Metal to Carbon Ratios for Individual Thermokarst Lake Samples

Statistical T-Test to observe seasonal differences in individual thermokarst lake samples for metal to carbon ratio values between winter and summer for a three-year period from 2016 – 2018. Color gradient indicates p-value, with the lightest representing the maximum cut off for statistical differences of p-value > 0.0500. Blue gradient indicates the average was higher in winter time. Numbers in the cells are those of the sample number (summer/winter) and asterisks (*) indicates Welch's T-Test was utilized when F-Test determined the standard deviation variance of samples were statistically different. Red italicized cells are samples with a sample number less than or equal to 3 and thus, care should be taken when observing the statistics. Sample abbreviations are denoted in Table 3.1, epilimnion (epi.), and hypolimnion (hypo.).

Sample Location	N/C ppm/ppm	Li/C ppb/ppm	Na/C ppb/ppm	Mg/C ppb/ppm	Al/C ppb/ppm	K/C ppb/ppm	Ca/C ppb/ppm	Ti/C ppb/ppm	V/C ppb/ppm	Cr/C ppb/ppm	Mn/C ppb/ppm	Fe/C ppb/ppm	Co/C ppb/ppm	Ni/C ppb/ppm	Cu/C ppb/ppm
GSL Epi.	8/8	*3/2*	9/7	9/7	6/5*	8/7*	9/7	9/8	8/8	9/8	7/8*	9/8*	9/7*	9/8	6/7*
GSL Hypo.	7/6	*3/2*	7/7	7/7	6/6	6/6	7/6	7/7	7/7	7/7	7/7*	7/7	7/8	7/7	5/7
OCT Epi.	8/4	*4/1*	9/5	9/5*	9/4	8/5	9/5	9/5*	8/5*	9/5*	9/5*	9/5*	9/4	8/4	7/4
OCT Hypo.	*8/3**	*4/1*	8/4	8/4	6/4	8/4	8/4	7/4	8/4	8/4	8/4	8/4	8/4	8/4	*6/3*
DNL Epi.	7/5	*3/2*	7/6*	8/6	4/5*	7/6*	7/6*	8/6	6/6	8/6*	7/6*	8/6*	7/6*	7/6	6/5
DNL Hypo.	7/5	*2/2*	7/6	6/6	5/6	7/6*	7/6	7/6	6/6	7/6	7/6	7/6	7/6	6/6	5/5*

	Zn/C ppb/ppm	As/C ppb/ppm	Se78/C ppb/ppm	Se82/C ppb/ppm	Sr/C ppb/ppm	Mo/C ppb/ppm	Ag/C ppb/ppm	Cd/C ppb/ppm	Sb/C ppb/ppm	Ba/C ppb/ppm	Pb/C ppb/ppm	Bi/C ppb/ppm	U/C ppb/ppm	Cl/C ppm/ppm	Legend
GSL Epi.	*3/5*	9/8*	5/6	9/8	9/6*	8/7	*6/2*	4/6*	8/7	9/7	*3/2*	7/6	6/7	8/6	
GSL Hypo.	4/6	7/7	5/5	7/7	7/5	7/8	*3/4*	*3/5**	7/7	7/7	*3/2*	*3/6*	7/8	7/6	<0.0001
OCT Epi.	*4/2*	9/5*	*4/3**	9/5	9/5*	8/4*	*6/3**	*4/3*	7/4	9/4	*4/1*	*7/3*	*5/2*	*9/3*	<0.0010
OCT Hypo.	6/4	8/4	*5/3**	8/4	8/4	8/4	*5/3*	*4/3*	7/4	8/4	*4/1*	*5/3*	*5/2*	*8/2*	<0.0100
DNL Epi.	*2/4*	8/6	*3/5**	8/6	8/5	5/5*	*5/1*	*3/3**	6/5	7/6	*3/2*	*4/3**	*4/2*	8/5	<0.0500
DNL Hypo.	*3/5*	6/6	*2/5*	7/6	7/4	*3/5*	*3/1*	*2/3*	5/6	6/6	*2/2*	*4/3**	*3/3**	7/4	

Table 3.28: ANOVA Results for Metal to Carbon Ratio for Thermokarst Lake Epilimnion

Statistical comparison of metal to carbon ratio with comparison to thermokarst lake permafrost degradation in the epilimnions (epi.) through an ANOVA statistical test. With a p-value of <0.0500 as statistically significant with the average metal to carbon ratio values for each location, with the number of samples found in the box denoted N for which the color gradient determines the p-value obtained. Colors determines which thermokarst lake epilimnion has the highest (red), medium (yellow), and low (green) concentration for metal to carbon ratio values that observed statistical difference between streams. Asterisk (*) denotes Welch ANOVA p-values used, when Brown-Forsythe test determined the standard deviation variance between samples were different requiring the use of a Welch ANOVA. Sample average was determined for ratio values over three-year period from 2016 – 2018. Where error in the average was determined through standard deviation of all sample values averaged and is denoted with ±. Sample abbreviations are denoted in Table 3.1.

Sample	Cl/C ppm/ppm	+/-	Li/C ppb/ppm	+/-	Na/C ppb/ppm	+/-	Mg/C ppb/ppm	+/-	Al/C ppb/ppm	+/-	K/C ppb/ppm	+/-	Ca/C ppb/ppm	+/-	Ti/C ppb/ppm	+/-
N	39*		15		43		44		33*		41		43*		45	
GSL Epi.	0.28	0.19	0.01	0.00	411.90	74.69	539.20	83.98	0.30	0.50	54.60	36.37	671.80	83.61	0.04	0.02
OCT Epi.	0.13	0.07	0.02	0.01	197.10	57.37	374.00	187.30	1.14	0.87	48.19	26.63	637.30	340.40	0.08	0.05
DNL Epi.	0.16	0.07	0.01	0.00	241.90	70.53	465.60	97.57	0.16	0.24	49.25	28.23	659.10	179.00	0.02	0.01

	V/C ppb/ppm	+/-	Cr/C ppb/ppm	+/-	Mn/C ppb/ppm	+/-	Fe/C ppb/ppm	+/-	Co/C ppb/ppm	+/-	Ni/C ppb/ppm	+/-	Cu/C ppb/ppm	+/-	Zn/C ppb/ppm	+/-
N	41*		45		42		45*		42*		42		35		20	
GSL Epi.	0.01	0.01	0.02	0.01	5.53	5.52	11.27	11.63	0.01	0.00	0.08	0.04	0.01	0.02	0.03	0.03
OCT Epi.	0.03	0.02	0.03	0.03	8.43	9.98	120.50	106.20	0.01	0.01	0.04	0.01	0.01	0.01	0.10	0.16
DNL Epi.	0.00	0.00	0.01	0.00	4.64	5.81	8.51	9.22	0.00	0.00	0.03	0.01	0.00	0.00	0.14	0.15

	As/C ppb/ppm	+/-	Se78/C ppb/ppm	+/-	Se82/C ppb/ppm	+/-	Sr/C ppb/ppm	+/-	Mo/C ppb/ppm	+/-	Ag/C ppb/ppm	+/-	Cd/C ppb/ppm	+/-	Sb/C ppb/ppm	+/-
N	45*		26		45*		42*		37		23		23		37	
GSL Epi.	0.06	0.04	0.00	0.00	0.55	0.26	3.62	0.72	0.00	0.00	0.00	0.00	0.00	0.00	0.01	0.00
OCT Epi.	0.42	0.37	0.02	0.04	0.20	0.08	3.63	2.07	0.00	0.00	0.00	0.00	0.00	0.00	0.00	0.00
DNL Epi.	0.06	0.01	0.00	0.00	0.51	0.26	2.97	1.00	0.00	0.00	0.01	0.01	0.00	0.00	0.00	0.00

	Ba/C ppb/ppm	+/-	Pb/C ppb/ppm	+/-	Bi/C ppb/ppm	+/-	U/C ppb/ppm	+/-	N/C ppm/ppm	+/-
N	42		15		30		26*		40	
GSL Epi.	0.81	0.22	0.00	0.00	0.00	0.00	0.01	0.00	0.03	0.02
OCT Epi.	1.15	0.44	0.00	0.00	0.00	0.00	0.00	0.00	0.03	0.02
DNL Epi.	0.78	0.37	0.00	0.00	0.00	0.01	0.00	0.00	0.03	0.02

P-Value	Legend
<0.0001	High
<0.0010	Medium
<0.0100	Low
<0.0500	

Table 3.29: ANOVA Results for Metal to Carbon Ratios for Thermokarst Lake Hypolimnion

Statistical comparison of metal to carbon ratio with comparison to thermokarst lake permafrost degradation in the hypolimnion (hypo.) through an ANOVA statistical test. With a p-value of <0.0500 as statistically significant with the average metal to carbon ratio values for each location, with the number of samples found in the box denoted N for which the color gradient determines the p-value obtained. Colors determines which thermokarst lake hypolimnion has the highest (red), medium (yellow), and low (green) concentration for metal to carbon ratio values that observed statistical difference between streams. Asterisk (*) denotes Welch ANOVA p-values used, when Brown-Forsythe test determined the standard deviation variance between samples were different requiring the use of a Welch ANOVA. Sample average was determined for ratio values over three-year period from 2016 – 2018. Where error in the average was determined through standard deviation of all sample values averaged and is denoted with ±. Sample abbreviations are denoted in Table 3.1.

Sample	Cl/C ppm/ppm	+/-	Li/C ppb/ppm	+/-	Na/C ppb/ppm	+/-	Mg/C ppb/ppm	+/-	Al/C ppb/ppm	+/-	K/C ppb/ppm	+/-	Ca/C ppb/ppm	+/-	Ti/C ppb/ppm	+/-
N	34*		14		39		38*		33*		37*		38*		38*	
GSL Hypo.	0.24	0.16	0.01	0.00	424.60	33.40	562.20	88.90	0.05	0.04	40.44	3.41	710.70	68.01	0.04	0.02
OCT Hypo.	0.10	0.04	0.02	0.01	242.30	96.30	547.60	258.10	0.54	0.22	77.94	52.74	896.80	444.80	0.12	0.06
DNL Hypo.	0.16	0.08	0.01	0.00	239.50	83.52	481.70	108.50	0.11	0.11	45.61	19.33	695.90	181.30	0.02	0.01

Sample	V/C ppb/ppm	+/-	Cr/C ppb/ppm	+/-	Mn/C ppb/ppm	+/-	Fe/C ppb/ppm	+/-	Co/C ppb/ppm	+/-	Ni/C ppb/ppm	+/-	Cu/C ppb/ppm	+/-	Zn/C ppb/ppm	+/-
N	38*		39*		39*		39*		40*		38		31		28*	
GSL Hypo.	0.01	0.00	0.03	0.01	13.66	3.67	25.37	12.35	0.01	0.00	0.08	0.02	0.00	0.00	0.03	0.03
OCT Hypo.	0.04	0.02	0.03	0.01	19.23	10.65	195.10	110.70	0.02	0.01	0.05	0.03	0.01	0.00	0.03	0.01
DNL Hypo.	0.01	0.00	0.01	0.00	8.22	6.60	11.98	8.90	0.00	0.00	0.03	0.01	0.00	0.00	0.07	0.08

Sample	As/C ppb/ppm	+/-	Se78/C ppb/ppm	+/-	Se82/C ppb/ppm	+/-	Sr/C ppb/ppm	+/-	Mo/C ppb/ppm	+/-	Ag/C ppb/ppm	+/-	Cd/C ppb/ppm	+/-	Sb/C ppb/ppm	+/-
N	38*		25		39		35*		35*		19		20		36*	
GSL Hypo.	0.06	0.01	0.00	0.00	0.57	0.25	3.98	0.49	0.00	0.00	0.00	0.00	0.00	0.00	0.01	0.00
OCT Hypo.	0.72	0.36	0.01	0.01	0.24	0.11	5.38	2.66	0.01	0.00	0.00	0.00	0.00	0.00	0.00	0.00
DNL Hypo.	0.08	0.02	0.00	0.00	0.55	0.24	3.22	1.00	0.00	0.00	0.00	0.00	0.00	0.00	0.00	0.00

Sample	Ba/C ppb/ppm	+/-	Pb/C ppb/ppm	+/-	Bi/C ppb/ppm	+/-	U/C ppb/ppm	+/-	N/C ppm/ppm	+/-
N	38		14		24*		28		36	
GSL Hypo.	0.81	0.31	0.00	0.00	0.00	0.00	0.01	0.00	0.03	0.02
OCT Hypo.	1.58	0.52	0.01	0.01	0.01	0.01	0.00	0.01	0.07	0.08
DNL Hypo.	0.92	0.36	0.00	0.00	0.00	0.00	0.00	0.00	0.03	0.03

P-Value	Legend
<0.0001	High
<0.0010	Medium
<0.0100	Low
<0.0500	

Table 3.30: ANOVA Results for Metal to Carbon Ratios for Streams

Statistical comparison of metal to carbon ratio with comparison between streams through an ANOVA statistical test. With a p-value of <0.0500 as statistically significant with the average metal to carbon ratio values for each location, with the number of samples found in the box denoted N for which the color gradient determines the p-value obtained. Colors determines which stream has the highest (red), medium (yellow), and low (green) concentration for metal to carbon ratio values that observed statistical difference between streams. Asterisk (*) denotes Welch ANOVA p-values used, when Brown-Forsythe test determined the standard deviation variance between samples were different requiring the use of a Welch ANOVA. Sample average was determined for ratio values over three-year period from 2016 – 2018. Where error in the average was determined through standard deviation of all sample values averaged and is denoted with ±. Sample abbreviations are denoted in Table 3.1.

Sample	Cl/C ppm/ppm	+/-	Li/C ppb/ppm	+/-	Na/C ppb/ppm	+/-	Mg/C ppb/ppm	+/-	Al/C ppb/ppm	+/-	K/C ppb/ppm	+/-	Ca/C ppb/ppm	+/-	Ti/C ppb/ppm	+/-
N	31		12		37		39		36		37		39		39	
GSBA	0.15	0.06	0.22	0.12	361.40	261.50	606.30	349.70	1.92	1.48	134.80	62.58	1896.00	777.10	0.18	0.14
GSSC	0.19	0.06	0.21	0.16	314.50	166.40	650.80	314.70	1.46	0.95	108.60	55.52	1719.00	790.10	0.16	0.11
OCC	0.13	0.09	0.31	0.22	19768.00	67763.00	2831.00	7134.00	2.98	2.37	193.60	392.40	4498.00	10994.00	0.32	0.39

	V/C ppb/ppm	+/-	Cr/C ppb/ppm	+/-	Mn/C ppb/ppm	+/-	Fe/C ppb/ppm	+/-	Co/C ppb/ppm	+/-	Ni/C ppb/ppm	+/-	Cu/C ppb/ppm	+/-	Zn/C ppb/ppm	+/-
N	39		36		39		39		36		34		33		14	
GSBA	0.07	0.08	0.08	0.19	9.28	4.92	72.12	27.60	0.04	0.02	0.16	0.07	0.13	0.05	0.14	0.09
GSSC	0.07	0.07	0.07	0.16	7.13	3.61	72.19	24.43	0.02	0.01	0.12	0.07	0.10	0.03	0.11	0.07
OCC	0.12	0.12	0.06	0.15	13.06	28.59	61.48	63.94	0.05	0.09	0.09	0.05	0.19	0.32	0.26	0.17

	As/C ppb/ppm	+/-	Se78/C ppb/ppm	+/-	Se82/C ppb/ppm	+/-	Sr/C ppb/ppm	+/-	Mo/C ppb/ppm	+/-	Ag/C ppb/ppm	+/-	Cd/C ppb/ppm	+/-	Sb/C ppb/ppm	+/-
N	39		19		39		39		36		19		20		36	
GSBA	0.56	0.71	0.14	0.29	0.23	0.20	12.10	5.66	0.10	0.05	0.00	0.00	0.00	0.00	0.03	0.02
GSSC	0.54	0.64	0.12	0.25	0.23	0.20	10.33	4.79	0.08	0.04	0.01	0.01	0.00	0.00	0.03	0.02
OCC	0.38	0.73	0.08	0.20	0.46	0.88	22.07	56.11	0.03	0.05	0.01	0.01	0.00	0.00	0.07	0.15

	Ba/C ppb/ppm	+/-	Pb/C ppb/ppm	+/-	Bi/C ppb/ppm	+/-	U/C ppb/ppm	+/-	N/C ppm/ppm	+/-
N	36		13		20		29		32	
GSBA	2.62	1.17	0.02	0.01	0.01	0.02	0.03	0.02	0.04	0.02
GSSC	2.32	1.40	0.01	0.00	0.00	0.00	0.02	0.02	0.04	0.03
OCC	5.43	13.35	0.01	0.01	0.01	0.01	0.06	0.10	0.06	0.04

P-Value	Legend
<0.0001	High
<0.0010	Medium
<0.0100	Low
<0.0500	

Table 3.31: Seasonality of Metal to Chloride Ratio Values of Overall Ratio Values

Statistical T-Test to observe seasonal differences in total watershed (thermokarst and stream samples) compilation for metal to carbon ratio values between winter and summer for three-years from 2016 – 2018, to observe overall seasonality observed for chloride normalized metal concentrations. Color gradient indicates p-value, with the lightest representing the maximum cut off for statistical differences of p-value > 0.05000. Blue gradient indicates the average was higher in winter time. Orange gradient indicates the average was higher in summer time. Numbers in the cells are those of the sample number (summer/winter) and asterisks (*) indicates Welch's T-Test was utilized when F-test determined the standard deviation variance between samples was statistically different.

N/C	Li/C	Na/C	Mg/C	Al/C	K/C	Ca/C	Ti/C	V/C	Cr/C
ppm/ppm	ppb/ppm	ppb/ppm	ppb/ppm	ppb/ppm	ppb/ppm	ppb/ppm	ppb/ppm	ppb/ppm	ppb/ppm
82/52*	39/11*	91/46*	93/46*	76/38	87/46*	93/46*	93/48*	89/47*	91/47*
Mn/C	**Fe/C**	**Co/C**	**Ni/C**	**Cu/C**	**Zn/C**	**As/C**	**Se78/C**	**Se82/C**	**Sr/C**
ppb/ppm	ppb/ppm	ppb/ppm	ppb/ppm	ppb/ppm	ppb/ppm	ppb/ppm	ppb/ppm	ppb/ppm	ppb/ppm
91/47	94/48	93/43*	89/42*	75/40*	41/31	93/47*	48/35*	94/48*	94/40*
Mo/C	**Ag/C**	**Cd/C**	**Sb/C**	**Ba/C**	**Pb/C**	**Bi/C**	**U/C**	**Cl/C**	
ppb/ppm	ppb/ppm	ppb/ppm	ppb/ppm	ppb/ppm	ppb/ppm	ppb/ppm	ppb/ppm	ppb/ppm	
84/41*	53/15*	43/31*	85/41*	92/43*	41/11*	57/28*	68/31*	85/34	

Legend
<0.0001
<0.0010
<0.0100
<0.0500

Table 3.32: Overall Metal – Carbon Relationship Seasonal Variability

Variability between metal – carbon relationships was determined based on the magnitude of standard deviation from the average of all the samples during the winter or summer from 2016 – 2018. The maximum and minimum for a certain sample number is represented for each ratio. The samples denoted with a triple asterisks (***) represent the metals that were determined to have a seasonal difference through a T-Test, results found in Table 3.31. Yellow indicates a decreased standard deviation or variance and thus, variability in summer time samples. Meanwhile, green indicates a decreased standard deviation or variance and thus, variability in winter samples.

	N/C				Li/C***				Na/C				Mg/C			
	n	Minimum ppm/ppm	Maximum ppm/ppm	Variance +/-	n	Minimum ppm/ppm	Maximum ppm/ppm	Variance +/-	n	Minimum ppb/ppm	Maximum ppb/ppm	Variance +/-	n	Minimum ppb/ppm	Maximum ppb/ppm	Variance +/-
Summer	82	0.00	0.51	0.07	39	0.01	0.52	0.14	91	34.97	1037.00	196.00	93	123.90	2742.00	521.50
Winter	52	0.00	0.84	0.13	11	0.01	0.03	0.01	46	99.62	234944.00	34585.00	46	28.43	26518.00	3828.00

	Al/C				K/C				Ca/C				Ti/C			
	n	Minimum ppm/ppm	Maximum ppm/ppm	Variance +/-	n	Minimum ppm/ppm	Maximum ppm/ppm	Variance +/-	n	Minimum ppb/ppm	Maximum ppb/ppm	Variance +/-	n	Minimum ppb/ppm	Maximum ppb/ppm	Variance +/-
Summer	76	0.00	6.40	1.31	87	1.47	289.50	61.58	93	200.500	6328.000	1335.000	93	0.00	0.46	0.10
Winter	38	0.01	8.42	1.41	46	7.58	1414.00	205.20	46	85.600	41001.000	5938.000	48	0.01	1.53	0.24

	V/C				Cr/C				Mn/C				Fe/C			
	n	Minimum ppm/ppm	Maximum ppm/ppm	Variance +/-	n	Minimum ppm/ppm	Maximum ppm/ppm	Variance +/-	n	Minimum ppb/ppm	Maximum ppb/ppm	Variance +/-	n	Minimum ppb/ppm	Maximum ppb/ppm	Variance +/-
Summer	89	0.00	0.21	0.05	91	0.00	0.09	0.02	91	0.10	65.95	13.48	94	1.37	666.10	96.58
Winter	47	0.00	0.44	0.09	47	0.01	0.67	0.14	47	0.15	108.00	16.55	48	0.33	453.30	106.60

	Co/C				Ni/C***				Cu/C				Zn/C			
	n	Minimum ppm/ppm	Maximum ppm/ppm	Variance +/-	n	Minimum ppm/ppm	Maximum ppm/ppm	Variance +/-	n	Minimum ppb/ppm	Maximum ppb/ppm	Variance +/-	n	Minimum ppb/ppm	Maximum ppb/ppm	Variance +/-
Summer	93	0.00	0.07	0.02	89	0.00	0.25	0.06	75	0.00	0.19	0.05	41	0.00	0.42	0.10
Winter	43	0.00	0.35	0.05	42	0.00	0.22	0.04	40	0.00	1.15	0.18	31	0.00	0.40	0.09

	As/C				Se78/C				Se83/C**				Sr/C			
	n	Minimum ppm/ppm	Maximum ppm/ppm	Variance +/-	n	Minimum ppm/ppm	Maximum ppm/ppm	Variance +/-	n	Minimum ppb/ppm	Maximum ppb/ppm	Variance +/-	n	Minimum ppb/ppm	Maximum ppb/ppm	Variance +/-
Summer	93	0.03	2.53	0.43	48	0.00	0.04	0.01	94	0.04	0.91	0.19	94	1.00	29.85	6.83
Winter	47	0.02	2.85	0.71	35	0.00	0.65	0.17	48	0.11	3.15	0.49	40	0.47	208.60	32.40

	Mo/C***				Ag/C				Cd/C				Sb/C			
	n	Minimum ppm/ppm	Maximum ppm/ppm	Variance +/-	n	Minimum ppm/ppm	Maximum ppm/ppm	Variance +/-	n	Minimum ppb/ppm	Maximum ppb/ppm	Variance +/-	n	Minimum ppb/ppm	Maximum ppb/ppm	Variance +/-
Summer	84	0.00	0.53	0.07	53	0.00	0.07	0.01	43	0.00	0.00	0.00	85	0.00	0.10	0.02
Winter	41	0.00	0.22	0.05	15	0.00	0.02	0.01	31	0.00	0.01	0.00	41	0.00	0.53	0.08

	Ba/C				Pb/C***				Bi/C				U/C			
	n	Minimum ppm/ppm	Maximum ppm/ppm	Variance +/-	n	Minimum ppm/ppm	Maximum ppm/ppm	Variance +/-	n	Minimum ppb/ppm	Maximum ppb/ppm	Variance +/-	n	Minimum ppb/ppm	Maximum ppb/ppm	Variance +/-
Summer	92	0.26	12.50	1.84	41	0.00	0.03	0.01	57	0.00	0.05	0.01	68	0.00	0.19	0.03
Winter	43	0.07	47.75	7.17	11	0.00	0.00	0.00	28	0.00	0.01	0.00	31	0.00	0.35	0.06

	Cl/C			
	n	Minimum ppm/ppm	Maximum ppm/ppm	Variance +/-
Summer	85	0.03	0.63	0.14
Winter	34	0.03	0.51	0.11

Variability Decreased in Summer

Variability Decreased in Winter

***Statistically Different See Table 3.31

3.11. Abbreviations:

+/-	Standard Deviation of Error
AEM	Airborne Electromagnetic
BIX	Biological Index (Equation in Table 1.2)
BSP	Blacksheep Pond
C:A	EEMs Ratio
C:M	EEMs Ratio
DNL	Doughnut Lake
DO	Dissolved Oxygen
E2:E3	Absorbance250/Absorbance 365 (Equation in Table 1.1)
E2:E4	Absorbance254/Absorbance 436 (Equation in Table 1.1)
E3:E4	Absorbance300/Absorbance 400
Epi.	Epilimnion
FFF	Field Flow Fractionation
GSBA	Goldstream Stream at Ballaine Road
GSL	Goldstream Lake
GSSC	Goldstream Stream at Sheep Creek Road
HIX	Humification Index (Equation in Table 1.2)
Hypo.	Hypolimnion
ICP-MS	Inductively Coupled Plasma Mass Spectrometry
M PCA	Metals only Principal Component Analysis
Mn or Mn.w	Number Average Molecular Weight
Mw	Weight Average Molecular Weight
NOM	Natural Organic Matter
O PCA	Optical Indices only Principal Component Analysis
OCC	O'Connor Creek
OCT	Octopus Lake
OM PCA	Optical Indices and Metals Principal Component Analysis
PCA	Principal Component Analysis
PLFA	Pony Lake Fulvic Acid
Poly.	Polydispersity
SRFA	Suwannee River Fulvic Acid
$SUVA_{254}/SUVA_{280}$	Specific Ultraviolet Absorbance (Equation in Table 1.1)
TDN	Total Dissolved Nitrogen
TOC	Total Organic Carbon
UV-Vis	Ultraviolet-Visible Spectrometry

General Conclusions:

The goal of this study was to observe how permafrost thaw influences surface waters functional group composition, photoreactivity, and metal geochemical cycling. Additionally, seasonal differences were determined in surface waters through under-the-ice winter sampling in sub-Arctic Alaska. Furthermore, this study was utilized as a case study to observe statistical differences between different surface waters with a known extent of permafrost degradation. In order to complete this goal, permafrost soils were obtained from three separate watersheds and leached in water, a basic solution, and a high ionic strength solution. The organic matter from the leaching samples were isolated along with surface water organic matter to determine the photoreactivity, functional group composition, and metal leachability within permafrost and active layer samples collected in various sub-Arctic watersheds. In addition to collecting soils, waters were collected over a three-year period from specific areas within the main watershed. This watershed is unique in that it allowed for the observation of various thermokarst lake formations within the same ecosystem and overall water source. The permafrost degradation beneath the thermokarst lake was previously determined through an airborne electromagnetic survey conducted in conjunction with the Alaska Division of Geological & Geophysical Surveys as 0 – 25%, 25 – 75%, and 75 – 100% frozen permafrost.

Permafrost soils were determined to be heterogeneous in functional group composition and photo reactivity both intra-watershed and inter-watershed. There were no statistically significant trends observed within the permafrost soils based on radiocarbon dating of the soil material. Leachability of organic matter and metals depends primarily on the pH and ionic strength of the leaching material, however aliphatic functional groups remained for the majority absorbed onto the soil matrix and did not release into the leaching media.

This study was also able to observe seasonal variability within thermokarst lakes during winter during periods with ice coverage. It was determined that during winter there was a significant difference in functional group composition, photoreactivity, and metal composition. Winter isolated organic matter showed differences in functional group composition through the decrease in aromatic content and photoreactivity was increased for reactive oxygen species during the winter isolation experimentation. Winter also observed statistical differences in metal concentrations through an increase in Na, Mg, K, Ca, Ti, V, Cr, Mn, Fe, Co, Ni, As, Sr, Ag, Sb, Ba, Bi, and U in select thermokarst lake waters. Metal sources were observed to be majority from lateral flow through active layer and thawing permafrost layers as normalizing to chloride and carbon decreased the variability of values observed in wintertime. Conditions underneath of the ice were deemed to be an important piece to the geochemical cycling through the observation of statistical differences in the metal concentrations and sourced material.

Overall, the presence of various permafrost degradation influenced photoreactivity, functional group composition, and metal concentrations. When the isolated organic matter from surface waters was most similar to permafrost isolated organic matter, these samples showed similar photoreactive ability to for reactive oxygen species and functional group composition. In addition to observing metal concentrations including optical indices allowed for the determination of permafrost influence on surface waters through the use of statistical analysis to observe correlations between permafrost degradation and these analyses. Additionally, metal concentrations were observed to have the highest concentrations in the 75 – 100% frozen permafrost underlain thermokarst lake due to the potential of high metal concentrations leaching in from lateral flow through actively thawing permafrost.

Future studies would improve the overall understanding of permafrost influence on surface water functional group composition and photoreactivity. These studies should start with utilizing simulated rain water to leach and isolate permafrost NOM for photoreactivity studies, which should be expanded to observe other reactive oxygen species such as but not limited to; peroxides, superoxides, and singlet oxygen. Utilizing isolated PENOM from all three watersheds in incubation studies would help determine PENOM greenhouse gas potential that could be utilized in future atmospheric modeling to determine the global impact of permafrost thaw. Finally, future and increased duration of surface water sampling analysis in this discontinuous permafrost watershed would aid in the understanding of water sources. It is suggested to obtain lateral surface water flow through the soils to determine how much each thermokarst lake is obtaining from lateral flow compared to upward ground alter flow or active thawing at the bottom of the hypolimnion. Additionally, increasing the duration of sampling to more than once a month or every other month would benefit the determination of seasonality trends and include sampling under-ice stream winter. These studies should be assessed and conducted prior to permafrost thawing completely and irreparably affects the sub-Arctic environment.

References:

Aguer, J. P., Tétégan, D. and Richard, C.: Humic substances mediated phototransformation of 2,4,6-trimethylphenol: A catalytic reaction, Photochem. Photobiol. Sci., 4, 451–453, doi:10.1039/b416925e, 2005.

Battin, T. J., Kaplan, L. A., Findlay, S., Hopkinson, C. S., Marti, E., Packman, A. I., Newbold, J. D. and Sabater, F.: Biophysical controls on organic carbon fluxes in fluvial networks, Nat. Geosci., 1, 95–100, doi:10.1038/ngeo101, 2008.

Binet, D. J., Goldberg, E. L. and Forster, L. S.: Energy transfer and quenching of triplet states by chromium(III) complexes, J. Phys. Chem., 72(8), 3017–3020, doi:10.1021/j100854a059, 1968.

Blough, N. V. and Zepp, R. G.: Reactive Oxygen Species in Natural Waters, in Active Oxygen in Chemistry, edited by C. S. Foote, J. S. Valentine, A. Greenberg, and J. F. Liebman, pp. 280–333, Chapman & Hall, London., 1995.

Boreen, A. L., Arnold, W. A. and McNeill, K.: Photodegradation of pharmaceuticals in the aquatic environment: A review, Aquat. Sci., 65, 320–341, doi:10.1007/s00027-003-0672-7, 2003.

Brinkmann, T., Hörsch, P., Sartorius, D. and Frimmel, F. H.: Photoformation of low-molecular-weight organic acids from brown water dissolved organic matter, Environ. Sci. Technol., 37(18), 4190–4198, doi:10.1021/es0263339, 2003.

Buschmann, J. and Sigg, L.: Antimony(III) binding to humic substances: Influence of pH and type of humic acid, Environ. Sci. Technol., 38(17), 4535–4541, doi:10.1021/es049901o, 2004.

Buxton, G. V., Greenstock, C. L., Helman, W. P. and Ross, A. B.: Critical Review of rate constants for reactions of hydrated electrons, hydrogen atoms and hydroxyl radicals (·OH/·O⁻ in Aqueous Solution, J. Phys. Chem. Ref. Data, 17(2), 513–886, doi:10.1063/1.555805, 1988.

Canonica, S. and Freiburghaus, M.: Electron-rich phenols for probing the photochemical reactivity of freshwaters., Environ. Sci. Technol., 35(4), 690–5, doi:10.1021/es0011360, 2001.

Canonica, S. and Hoigné, J.: Enhanced oxidation of methoxy phenols at micromolar concentration photosensitized by dissolved natural organic material, Chemosphere, 30(12), 2365–2374, doi:10.1016/0045-6535(95)00108-K, 1995.

Canonica, S., Jans, U., Stemmler, K. and Hoigné, J.: Transformation Kinetics of Phenols in Water: Photosensitization by Dissolved Natural Organic Material and Aromatic Ketones, Environ. Sci. Technol., 29(7), 1822–1831, doi:10.1021/es00007a020, 1995.

Cavani, L., Halladja, S., Ter Halle, A., Guyot, G., Corrado, G., Ciavatta, C., Boulkamh, a. and Richard, C.: Relationship between photosensitizing and emission properties of peat humic acid fractions obtained by tangential ultrafiltration, Environ. Sci. Technol., 43(12), 4348–4354, doi:10.1021/es802964m, 2009.

Cawley, K. M., Hakala, J. A. and Chin, Y. P.: Evaluating the triplet state photoreactivity of dissolved organic matter isolated by chromatography and ultrafiltration using an alkylphenol probe molecule, Limnol. Oceanogr. Methods, 7, 391–398, doi:10.4319/lom.2009.7.391, 2009.

Challis, J. K., Hanson, M. L., Friesen, K. J. and Wong, C. S.: A critical assessment of the photodegradation of pharmaceuticals in aquatic environments: Defining our current understanding and identifying knowledge gaps, Environ. Sci. Process. Impacts, 16, 672–696, doi:10.1039/c3em00615h, 2014.

Chin, Y. P., Alken, G. and O'Loughlin, E.: Molecular Weight, Polydispersity, and Spectroscopic Properties of Aquatic Humic Substances, Environ. Sci. Technol., 28(11), 1853–1858, doi:10.1021/es00060a015, 1994.

Chin, Y. P., Miller, P. L., Zeng, L., Cawley, K. M. and Weavers, L. K.: Photosensitized degradation of bisphenol A by dissolved organic matter, Environ. Sci. Technol., 38(22), 5888–5894, doi:10.1021/es0496569, 2004.

Choi, J. H., Kim, Y. G., Lee, Y. K., Pack, S. P., Jung, J. Y. and Jang, K. S.: Chemical characterization of dissolved organic matter in moist acidic tussock tundra soil using ultra-high resolution 15T FT-ICR mass spectrometry, Biotechnol. Bioprocess Eng., 22, 637–646, doi:10.1007/s12257-017-0121-4, 2017.

Cieśla, P., Kocot, P., Mytych, P. and Stasicka, Z.: Homogeneous photocatalysis by transition metal complexes in the environment, J. Mol. Catal. A Chem., 224, 17–33, doi:10.1016/j.molcata.2004.08.043, 2004.

Claret, F., Schäfer, T., Bauer, A. and Buckau, G.: Generation of humic and fulvic acid from Callovo-Oxfordian clay under high alkaline conditions, Sci. Total Environ., 317, 189–200, doi:10.1016/S0048-9697(03)00337-1, 2003.

Cory, R. M. and McKnight, D. M.: Fluorescence spectroscopy reveals ubiquitous presence of oxidized and reduced quinones in dissolved organic matter, Environ. Sci. Technol., 39(21), 8142–8149, doi:10.1021/es0506962, 2005.

Cory, R. M., McNeill, K., Cotner, J. P., Amado, A., Purcell, J. M. and Marshall, A. G.: Singlet Oxygen in the Coupled Photochemical and Biochemical Oxidation of Dissolved Organic Matter, Environ. Sci. Technol., 44(10), 3683–3689, doi:10.1021/es902989y, 2010.

Cory, R. M., Crump, B. C., Dobkowski, J. A. and Kling, G. W.: Surface exposure to sunlight stimulates CO 2 release from permafrost soil carbon in the Arctic, PNAS, 110(9), 3429–3434, doi:10.1073/pnas.1214104110, 2013.

Cory, R. M., Ward, C. P., Crump, B. C. and Kling, G. W.: Sunlight controls water column processing of carbon in arctic frech waters, Science (80-.)., 345(6199), 925–928, doi:10.1126/science.1253119, 2014.

Croot, P. L., Streu, P., Peeken, I., Lochte, K. and Baker, A. R.: Influence of the ITCZ on H2O2 in near surface waters in the equatorial Atlantic Ocean, Geophys. Res. Lett., 31, L23S04, doi:10.1029/2004GL020154, 2004.

Diehl, B.: Molecular Dynamics, in NMR Spectroscopy in Pharmaceutical Analysis, edited by U. Holzgrabe, I. Wawer, and B. Diehl, pp. 24–25, Elsevier B.V, Amsterdam. [online] (Accessed 13 November 2019), 2008.

Dimou, A. D., Sakkas, V. A. and Albanis, T. A.: Metolachlor photodegradation study in aqueous media under natural and simulated solar irradiation, J. Agric. Food Chem., 53, 694–701, doi:10.1021/jf048766w, 2005.

Drake, T. W., Wickland, K. P., Spencer, R. G. M., McKnight, D. M. and Striegl, R. G.: Ancient low-molecular-weight organic acids in permafrost fuel rapid carbon dioxide production upon thaw, Proc. Natl. Acad. Sci. U. S. A., 112(45), 13946–13951, doi:10.1073/pnas.1511705112, 2015.

Frey, K. E. and McClelland, J. W.: Impacts of permafrost degradation on arctic river biogeochemistry, Hydrol. Process., 23(1), 169–182, doi:10.1002/hyp.7196, 2009.

Gabor, R. S., Burns, M. A., Lee, R. H., Elg, J. B., Kemper, C. J., Barnard, H. R. and McKnight, D. M.: Influence of leaching solution and catchment location on the fluorescence of water-soluble organic matter, Environ. Sci. Technol., 49, 4425–4432, doi:10.1021/es504881t, 2015.

Grannas, A. M., Martin, C. B., Chin, Y. P. and Platz, M.: Hydroxyl radical production from irradiated Arctic dissolved organic matter, Biogeochemistry, 78(1), 51–66, doi:10.1007/s10533-005-2342-4, 2006.

Grosse, G., Harden, J., Turetsky, M., McGuire, a. D., Camill, P., Tarnocai, C., Frolking, S., Schuur, E. a G., Jorgenson, T., Marchenko, S., Romanovsky, V., Wickland, K. P., French, N., Waldrop, M., Bourgeau-Chavez, L. and Striegl, R. G.: Vulnerability of high-latitude soil organic carbon in North America to disturbance, J. Geophys. Res. Biogeosciences, 116, G00K06, doi:10.1029/2010JG001507, 2011.

Guo, M. and Chorover, J.: Transport and fractionation of dissolved organic matter in soil columns, Soil Sci., 168(2), 108–118, doi:10.1097/00010694-200302000-00005, 2003.

Halladja, S., Ter Halle, A., Aguer, J. P., Boulkamh, A. and Richard, C.: Inhibition of humic substances mediated photooxygenation of furfuryl alcohol by 2,4,6-trimethylphenol. Evidence for reactivity of the phenol with humic triplet excited states, Environ. Sci. Technol., 41(17), 6066–6073, doi:10.1021/es070656t, 2007.

Hansen, A. M., Kraus, T. E. C., Pellerin, B. A., Fleck, J. A., Downing, B. D. and Bergamaschi, B. A.: Optical properties of dissolved organic matter (DOM): Effects of biological and photolytic degradation, Limnol. Oceanogr., 61, 1015–1032, doi:10.1002/lno.10270, 2016.

Helms, J. R., Stubbins, A., Ritchie, J. D., Minor, E. C., Kieber, D. J. and Mopper, K.: Absorption spectral slopes and slope ratios as indicators of molecular weight, source, and photobleaching of chromophoric dissolved organic matter, Limonology Oceanogr., 53(3), 955–969, 2008.

Hertkorn, N., Harir, M., Koch, B. P., Michalke, B. and Schmitt-kopplin, P.: High field NMR Spectroscopy and FTICR Mass Spectrometry: Powerful Discovery Tools for the Molecular Level Characterization of Marine Dissolved Organic Matter - Supplemental, Supplemental, 1–25, 2007.

Heslop, J. K., Chandra, S., Sobzcak, W. V., Davydov, S. P., Davydova, A. I., Spektor, V. V. and Walter Anthony, K. M.: Variable respiration rates of incubated permafrost soil extracts from the Kolyma River lowlands, north-east Siberia, Polar Res., 37(1), doi:10.1080/17518369.2017.1305157, 2017.

Heslop, J. K., Winkel, M., Walter Anthony, K. M., Spencer, R. G. M., Podgorski, D. C., Zito, P., Kholodov, A., Zhang, M. and Liebner, S.: Increasing organic carbon biolability with depth in yedoma permafrost: ramifications for future climate change, J. Geophys. Res. Biogeosciences, 124, 1–18, doi:10.1029/2018jg004712, 2019.

Huguet, A., Vacher, L., Relexans, S., Saubusse, S., Froidefond, J. M. and Parlanti, E.: Properties of fluorescent dissolved organic matter in the Gironde Estuary, Org. Geochem., 40, 706–719, doi:10.1016/j.orggeochem.2009.03.002, 2009.

Humphries, C.: A sleeping giant, Nat. Reports Clim. Chang., 3, 46–49, doi:10.1038/502S14a, 2013.

Imai, A., Fukushima, T., Matsushige, K., Kim, Y. H. and Choi, K.: Characterization of dissolved organic matter in effluents from wastewater treatment plants, Water Res., 36, 859–870, doi:10.1016/S0043-1354(01)00283-4, 2002.

Kim, S., Kaplan, L. A. and Hatcher, P. G.: Biodegradable dissolved organic matter in a temperate and a tropical stream determined from ultra-high resolution mass spectrometry, Limnol. Oceanogr., 51(2), 1054–1063, doi:10.4319/lo.2006.51.2.1054, 2006.

Lam, B. and Simpson, A. J.: Direct 1H NMR spectroscopy of dissolved organic matter in natural waters, Analyst, 133, 263–269, doi:10.1039/B713457F, 2008.

Lang, K., Wagnerová, D. M., Klementová, Š. and Kubát, P.: Humic substances - Excited states, quenching by metal ions, and photosensitized degradation of chlorophenols, Collect. Czechoslov. Chem. Commun., 62, 1159–1168, doi:10.1135/cccc19971159, 1997.

Larouche, J. R., Abbott, B. W., Bowden, W. B. and Jones, J. B.: The role of watershed characteristics, permafrost thaw, and wildfire on dissolved organic carbon biodegradability and water chemistry in Arctic headwater streams, Biogeosciences, 12, 4221–4233, doi:10.5194/bg-12-4221-2015, 2015.

Leenheer, J. A., Nanny, M. A. and McIntyre, C.: Terpenoids as major precursors of dissolved organic matter in landfill leachates, surface water, and groundwater, Environ. Sci. Technol., 37(11), 2323–2331, doi:10.1021/es0264089, 2003.

Li, P. and Hur, J.: Utilization of UV-Vis spectroscopy and related data analyses for dissolved organic matter (DOM) studies: A review, Crit. Rev. Environ. Sci. Technol., 47(3), 131–154, doi:10.1080/10643389.2017.1309186, 2017.

Linschitz, H. and Pekkarinen, L.: The Quenching of Triplet States of Anthracene and Porphyrins by Heavy Metal Ions, J. Am. Chem. Soc., 82, 2411–2416, doi:10.1021/ja01495a002, 1960.

Maloney, K. O., Morris, D. P., Moses, C. O. and Osburn, C. L.: The role of iron and dissolved organic carbon in the absorption of ultraviolet radiation in humic lake water, Biogeochemistry, 75, 393–407, doi:10.1007/s10533-005-1675-3, 2005.

Mann, P. J., Sobczak, W. V., LaRue, M. M., Bulygina, E., Davydova, A., Vonk, J. E., Schade, J., Davydov, S., Zimov, N., Holmes, R. M. and Spencer, R. G. M.: Evidence for key enzymatic controls on metabolism of Arctic river organic matter, Glob. Chang. Biol., 20(4), 1089–1100, doi:10.1111/gcb.12416, 2014.

Mao, J., Chen, N. and Cao, X.: Characterization of humic substances by advanced solid state NMR spectroscopy: Demonstration of a systematic approach, Org. Geochem., 42, 891–902, doi:10.1016/j.orggeochem.2011.03.023, 2011.

McKnight, D. M., Boyer, E. W., Westerhoff, P. K., Doran, P. T., Kulbe, T. and Andersen, D. T.: Spectrofluorometric characterization of dissolved organic matter for indication of precursor organic material and aromaticity, Limnol. Oceanogr., 46(1), 38–48, doi:10.4319/lo.2001.46.1.0038, 2001.

McNeill, K. and Canonica, S.: Triplet state dissolved organic matter in aquatic photochemistry: Reaction mechanisms, substrate scope, and photophysical properties, Environ. Sci. Process. Impacts, 18, 1381–1399, doi:10.1039/c6em00408c, 2016.

Meunier, L., Laubscher, H., Hug, S. J. and Sulzberger, B.: Effects of size and origin of natural dissolved organic matter compounds on the redox cycling of iron in sunlit surface waters, Aquat. Sci., 67, 292–307, doi:10.1007/s00027-005-0779-0, 2005.

Moran, M. A., Sheldon, W. M. and Zepp, R. G.: Carbon loss and optical property changes during long-term photochemical and biological degradation of estuarine dissolved organic matter, Limnol. Oceanogr., 45(6), 1254–1264, doi:10.4319/lo.2000.45.6.1254, 2000.

Nebbioso, A. and Piccolo, A.: Molecular characterization of dissolved organic matter (DOM): A critical review, Anal. Bioanal. Chem., 405, 109–124, doi:10.1007/s00216-012-6363-2, 2013.

Neff, J. C., Finlay, J. C., Zimov, S. A., Davydov, S. P., Carrasco, J. J., Schuur, E. A. G. and Davydova, A. I.: Seasonal changes in the age and structure of dissolved organic carbon in Siberian rivers and streams, Geophys. Res. Lett., 33, L23401, doi:10.1029/2006GL028222, 2006.

Ogawa, K., Guo, F. and Schanze, K. S.: Phosphorescence quenching of a platinum acetylide polymer by transition metal ions, J. Photochem. Photobiol. A Chem., 207, 79–85, doi:10.1016/j.jphotochem.2009.04.013, 2009.

Ohno, T.: Fluorescence inner-filtering correction for determining the humification index of dissolved organic matter, Environ. Sci. Technol., 36(4), 742–746, doi:10.1021/es0155276, 2002.

Packer, J. L., Werner, J. J., Latch, D. E., McNeill, K. and Arnold, W. A.: Photochemical fate of pharmaceuticals in the environment: Naproxen, diclofenac, clofibric acid, and ibuprofen, Aquat. Sci., 65, 342–351, doi:10.1007/s00027-003-0671-8, 2003.

Page, S. E., Arnold, W. A. and McNeill, K.: Assessing the contribution of free hydroxyl radical in organic matter-sensitized photohydroxylation reactions, Environ. Sci. Technol., 45, 2818–2825, doi:10.1021/es2000694, 2011.

Parlanti, E., Wörz, K., Geoffroy, L. and Lamotte, M.: Dissolved organic matter fluorescence spectroscopy as a tool to estimate biological activity in a coastal zone submitted to anthropogenic inputs, Org. Geochem., 31, 1765–1781, doi:10.1016/S0146-6380(00)00124-8, 2000.

Pérez, M., Torrades, F., García-Hortal, J. A., Domènech, X. and Peral, J.: Removal of organic contaminants in paper pulp treatment effluents under Fenton and photo-Fenton conditions, Appl. Catal. B Environ., 36, 63–74, doi:10.1016/S0926-3373(01)00281-8, 2002.

Pernet-Coudrier, B., Varrault, G., Saad, M., Croue, J. P., Dignac, M. F. and Mouchel, J. M.: Characterisation of dissolved organic matter in Parisian urban aquatic systems: Predominance of hydrophilic and proteinaceous structures, Biogeochemistry, 106, 89–106, doi:10.1007/s10533-010-9480-z, 2011.

Peuravuori, J. and Pihlaja, K.: Molecular size distribution and spectroscopic properties of aquatic humic substances, Anal. Chim. Acta, 337, 133–149, doi:10.1016/S0003-2670(96)00412-6, 1997.

Poulin, B. A., Ryan, J. N. and Aiken, G. R.: Effects of iron on optical properties of dissolved organic matter, Environ. Sci. Technol., 48, 10098–10106, doi:10.1021/es502670r, 2014.

Raudina, T. V., Loiko, S. V., Lim, A., Manasypov, R. M., Shirokova, L. S., Istigechev, G. I., Kuzmina, D. M., Kulizhsky, S. P., Vorobyev, S. N. and Pokrovsky, O. S.: Permafrost thaw and climate warming may decrease the CO2, carbon, and metal concentration in peat soil waters of the Western Siberia Lowland, Sci. Total Environ., 634, 1004–1023, doi:10.1016/j.scitotenv.2018.04.059, 2018.

Redfield, A. G. and Gupta, R. K.: Pulsed fourier-transform NMR spectrometer for use with H 2 O solutions, J. Chem. Phys., 54, 1418–1419, doi:10.1063/1.1674990, 1971.

Rodríguez, F. J., Schlenger, P. and García-Valverde, M.: Monitoring changes in the structure and properties of humic substances following ozonation using UV-Vis, FTIR and 1H NMR techniques, Sci. Total Environ., 541, 623–637, doi:10.1016/j.scitotenv.2015.09.127, 2016.

Romanovsky, V. E., Gruber, S., Jin, H., Marchenko, S. S., Smith, S. L., Trombotto, D. and Walter, K. M.: Frozen Ground, in Global Outlook for Ice & Snow, pp. 411–419, Elsevier B.V., 2011.

Santos, L., Pinto, A., Filipe, O., Cunha, Â., Santos, E. B. H. and Almeida, A.: Insights on the optical properties of estuarine DOM - Hydrological and biological influences, edited by C.-L. Lee, PLoS One, 11(5), e0154519, doi:10.1371/journal.pone.0154519, 2016.

Scully, N. M., Cooper, W. J. and Tranvik, L. J.: Photochemical effects on microbial activity in natural waters: The interaction of reactive oxygen species and dissolved organic matter, FEMS Microbiol. Ecol., 46, 353–357, doi:10.1016/S0168-6496(03)00198-3, 2003.

Southworth, B. A. and Voelker, B. M.: Hydroxyl radical production via the photo-fenton reaction in the presence of fulvic acid, Environ. Sci. Technol., 37(6), 1130–1136, doi:10.1021/es020757l, 2003.

Spencer, R. G. M., Mann, P. J., Dittmar, T., Eglinton, T. I., McIntyre, C., Holmes, R. M., Zimov, N. and Stubbins, A.: Detecting the signature of permafrost thaw in Arctic rivers, Geophys. Res. Lett., 42, 2830–2835, doi:10.1002/2015GL063498.Received, 2015.

Stocker, T. F., Qin, D., Plattner, G. K., Tignor, M. M. B., Allen, S. K., Boschung, J., Nauels, A., Xia, Y., Bex, V. and Midgley, P. M.: Climate change 2013 the physical science basis: Working Group I contribution to the fifth assessment report of the intergovernmental panel on climate change, edited by T. F. Stocker, D. Qin, G. K. Plattner, M. M. B. Tignor, S. K. Allen, J. Boschung, A. Nauels, Y. Xia, V. Bex, and P. M. Midgley, Cambridge University Press., 2013.

Strauss, J., Schirrmeister, L., Grosse, G., Wetterich, S., Ulrich, M., Herzschuh, U. and Hubberten, H. W.: The deep permafrost carbon pool of the Yedoma region in Siberia and Alaska, Geophys. Res. Lett., 40, 6165–6170, doi:10.1002/2013GL058088, 2013.

Strauss, J., Schirrmeister, L., Mangelsdorf, K., Eichhorn, L., Wetterich, S. and Herzschuh, U.: Organic-matter quality of deep permafrost carbon - a study from Arctic Siberia, Biogeosciences, 12, 2227–2245, doi:10.5194/bg-15-6033-2018, 2015.

Strauss, J., Schirrmeister, L., Grosse, G., Fortier, D., Hugelius, G., Knoblauch, C., Romanovsky, V., Schädel, C., Schneider von Deimling, T., Schuur, E. A. G., Shmelev, D., Ulrich, M. and Veremeeva, A.: Deep Yedoma permafrost: A synthesis of depositional characteristics and carbon vulnerability, Earth-Science Rev., 172, 75–86, doi:10.1016/j.earscirev.2017.07.007, 2017.

Striegl, R. G., Aiken, G. R., Dornblaser, M. M., Raymond, P. A. and Wickland, K. P.: A decrease in discharge-normalized DOC export by the Yukon River during summer through autumn, Geophys. Res. Lett., 32, L21413, doi:10.1029/2005GL024413, 2005.

Świetlik, J. and Sikorska, E.: Characterization of natural organic matter fractions by high pressure size-exclusion chromatography, specific UV absorbance and total luminescence spectroscopy, Polish J. Environ. Stud., 15(1), 145–153, 2006.

Tixier, C., Singer, H. P., Canonica, S. and Müller, S. R.: Phototransformation of triclosan in surface waters: A relevant elimination process for this widely used biocide - Laboratory studies, field measurements, and modeling, Environ. Sci. Technol., 36(16), 3482–3489, doi:10.1021/es025647t, 2002.

Ulrich, M., Grosse, G., Strauss, J. and Schirrmeister, L.: Quantifying Wedge-ice volumes in Yedoma and thermokarst basin deposits, Permafr. Periglac. Process., 25, 151–161, doi:10.1002/ppp.1810, 2014.

Uyguner, C. S. and Bekbolet, M.: Evaluation of humic acid photocatalytic degradation by UV-vis and fluorescence spectroscopy, Catal. Today, 101, 267–274, doi:10.1016/j.cattod.2005.03.011, 2005.

Vaughan, P. P. and Blough, N. V.: Photochemical formation of hydroxyl radical by constituents of natural waters, Environ. Sci. Technol., 32, 2947–2953, doi:10.1021/es9710417, 1998.

Del Vecchio, R. and Blough, N. V.: On the origin of the optical properties of humic substances, Environ. Sci. Technol. Technol., 38(14), 3885–3891, doi:10.1021/es049912h, 2004.

Vione, D., Minella, M., Maurino, V. and Minero, C.: Indirect photochemistry in sunlit surface waters: Photoinduced production of reactive transient species, Chem. - A Eur. J. Rev., 20, 10590–10606, doi:10.1002/chem.201400413, 2014.

Voelker, B. M. and Sulzberger, B.: Effects of fulvic acid on Fe(II) oxidation by hydrogen peroxide, Environ. Sci. Technol., 30(4), 1106–1114, doi:10.1021/es9502132, 1996.

Voelker, B. M., Sedlak, D. L. and Zafiriou, O. C.: Chemistry of Superoxide Radical in Seawater: Reactions with Organic Cu Complexes, Environ. Sci. Technol., 34(6), 1036–1042, doi:10.1021/es990545x, 2000.

Vonk, J. E., Mann, P. J., Dowdy, K. L., Davydova, A., Davydov, S. P., Zimov, N., Spencer, R. G. M., Bulygina, E. B., Eglinton, T. I. and Holmes, R. M.: Dissolved organic carbon loss from Yedoma permafrost amplified by ice wedge thaw, Environ. Res. Lett., 8, doi:10.1088/1748-9326/8/3/035023, 2013.

Walter Anthony, K. M., Zimov, S. A., Grosse, G., Jones, M. C., Anthony, P. M., Iii, F. S. C., Finlay, J. C., Mack, M. C., Davydov, S., Frenzel, P. and Frolking, S.: A shift of thermokarst lakes from carbon sources to sinks during the Holocene epoch, Nature, 511, 452–456, doi:10.1038/nature13560, 2014.

Wan, D., Sharma, V. K., Liu, L., Zuo, Y. and Chen, Y.: Mechanistic Insight into the Effect of Metal Ions on Photogeneration of Reactive Species from Dissolved Organic Matter, Environ. Sci. Technol., 53, 5778–5786, doi:10.1021/acs.est.9b00538, 2019.

Weishaar, J. L., Aiken, G. R., Bergamaschi, B. A., Fram, M. S., Fujii, R. and Mopper, K.: Evaluation of specific ultraviolet absorbance as an indicator of the chemical composition and reactivity of dissolved organic carbon, Environ. Sci. Technol., 37, 4702–4708, doi:10.1021/es030360x, 2003.

Werner, J. J., McNeill, K. and Arnold, W. A.: Environmental photodegradation of mefenamic acid, Chemosphere, 58(10), 1339–1346, doi:10.1016/j.chemosphere.2004.10.004, 2005.

Wilson, H. F. and Xenopoulos, M. A.: Effects of agricultural land use on the composition of fluvial dissolved organic matter, Nat. Geosci., 2, 37–41, doi:10.1038/ngeo391, 2009.

Wolf, R., Thrane, J. E., Hessen, D. O. and Andersen, T.: Modelling ROS formation in boreal lakes from interactions between dissolved organic matter and absorbed solar photon flux, Water Res., 132, 331–339, doi:10.1016/j.watres.2018.01.025, 2018.

Yan, M., Wang, D., Korshin, G. V. and Benedetti, M. F.: Quantifying metal ions binding onto dissolved organic matter using log-transformed absorbance spectra, Water Res., 47, 2603–2611, doi:10.1016/j.watres.2013.02.044, 2013a.

Yan, M., Benedetti, M. F. and Korshin, G. V.: Study of iron and aluminum binding to Suwannee River fulvic acid using absorbance and fluorescence spectroscopy: Comparison of data interpretation based on NICA-Donnan and Stockholm humic models, Water Res., 47, 5439–5446, doi:10.1016/j.watres.2013.06.022, 2013b.

Yan, M., Ma, J. and Ji, G.: Examination of effects of Cu(II) and Cr(III) on Al(III) binding by dissolved organic matter using absorbance spectroscopy, Water Res., 93, 84–90, doi:10.1016/j.watres.2016.02.017, 2016.

Yan, S. and Song, W.: Photo-transformation of pharmaceutically active compounds in the aqueous environment: A review, Environ. Sci. Process. Impacts, 16(4), 697–720, doi:10.1039/c3em00502j, 2014.

Yuan, C., Chin, Y. P. and Weavers, L. K.: Photochemical acetochlor degradation induced by hydroxyl radical in Fe-amended wetland waters: Impact of pH and dissolved organic matter, Water Res., 132, 52–60, doi:10.1016/j.watres.2017.11.056, 2018.

Zepp, R. G., Faust, B. C., Jürg, H. and Holgné, J.: Hydroxyl Radical Formation in Aqueous Reactions (pH 3-8) of Iron(II) with Hydrogen Peroxide: The Photo-Fenton Reaction, Environ. Sci. Technol., 26, 313–319, doi:10.1021/es00026a011, 1992.

Zhou, Z., Hua, B., Cao, X., Yang, J., Olk, D. C., Deng, B., Liu, F., Li, R. and Mao, J.: Chemical composition of dissolved organic matter from various sources as characterized by solid-state NMR, Aquat. Sci., 77, 595–607, doi:10.1007/s00027-015-0405-8, 2015.

Zimov, S. A., Davydov, S. P., Zimova, G. M., Davydova, A. I., Schuur, E. A. G., Dutta, K. and Chapin, I. S.: Permafrost carbon: Stock and decomposability of a globally significant carbon pool, Geophys. Res. Lett., 33, L20502, doi:10.1029/2006GL027484, 2006.